MARTIN MARIETTA ENERGY SYSTEMS LIBRARIES
3 4456 0361431 9

180

CENTRAL RESEARCH LIBRARY
DOCUMENT COLLECTION

ORNL-2888
UC-81 - Reactors-Power

GAS-COOLED REACTOR PROJECT

QUARTERLY PROGRESS REPORT

FOR PERIOD ENDING DECEMBER 31, 1959

OAK RIDGE NATIONAL LABORATORY
CENTRAL RESEARCH LIBRARY
CIRCULATION SECTION
4500N ROOM 175
LIBRARY LOAN COPY
DO NOT TRANSFER TO ANOTHER PERSON
If you wish someone else to see this report, send in name with report and the library will arrange a loan.
UCN-7969 (3 9-77)

OAK RIDGE NATIONAL LABORATORY
operated by
UNION CARBIDE CORPORATION
for the
U.S. ATOMIC ENERGY COMMISSION

Printed in USA. Price $3.50. Available from the

Office of Technical Services
Department of Commerce
Washington 25, D.C.

LEGAL NOTICE

This report was prepared as an account of Government sponsored work. Neither the United States, nor the Commission, nor any person acting on behalf of the Commission:

A. Makes any warranty or representation, expressed or implied, with respect to the accuracy, completeness, or usefulness of the information contained in this report, or that the use of any information, apparatus, method, or process disclosed in this report may not infringe privately owned rights; or

B. Assumes any liabilities with respect to the use of, or for damages resulting from the use of any information, apparatus, method, or process disclosed in this report.

As used in the above, "person acting on behalf of the Commission" includes any employee or contractor of the Commission, or employee of such contractor, to the extent that such employee or contractor of the Commission, or employee of such contractor prepares, disseminates, or provides access to, any information pursuant to his employment or contract with the Commission, or his employment with such contractor.

ORNL-2888

Reactors – Power
TID-4500 (15th ed.)

Contract No. W-7405-eng-26

GAS-COOLED REACTOR PROJECT
QUARTERLY PROGRESS REPORT
For Period Ending December 31, 1959

Staff
Oak Ridge National Laboratory

DATE ISSUED

FEB 9 1960

OAK RIDGE NATIONAL LABORATORY
Oak Ridge, Tennessee
operated by
UNION CARBIDE CORPORATION
for the
U. S. ATOMIC ENERGY COMMISSION

MARTIN MARIETTA ENERGY SYSTEMS LIBRARIES

3 4456 0361431 9

CONTENTS

SUMMARY vii

PART 1. DESIGN INVESTIGATIONS

1. REACTOR PHYSICS 3

Comparison of EGCR Heterogeneous and Homogeneous Calculations 3

Effects of Experiments on EGCR Radial Power Distributions .. 4

Analysis of Measurements To Be Made at Hanford of the Neutron Fluxes Near an EGCR Experimental Tube and the Reactivity Effect of the Tube 8

Control Rod Worth in EGCR 9

Effects of Cladding EGCR Dummy Assemblies with Stainless Steel 11

Graphite Damage Resulting from the Moderation of Fast Neutrons 15

Activity in the EGCR Experimental Loops 18

EGCR Experimental Cell Shielding 20

Effect of Reflector on Exposure of Pressure Vessel to Fast Neutrons 22

Thermal and Resonance Absorption Cross Sections of the U^{233}, U^{235}, and Pu^{239} Fission Products 24

2. REACTOR DESIGN STUDIES 27

EGCR Fuel Assemblies 27

Mechanical Design 27

Heat Transfer and Pressure Drop 27

Fuel Handling and Flow Control 29

Temperature Cycling 31

Thermal Analyses 32

Structural Investigations 33

Study of Fuel Cladding Behavior Under Arbitrary Temperature Distributions 33

Tests of Metal-Clad Graphite Bodies 39

Coolant Channel Flow Adjustment and Pneumatic Load Sensing by EGCR Charge Machine 43

Procedures for Decontamination of Charge and Service Machines 44

EGCR Hazards Evaluations 45

Core Levitation in the EGCR in Case of Main Coolant Pipe Failure 45

Pressure and Temperature in the EGCR Experimental Loop Cell in Case of Accidental Release of Main Reactor Coolant 46

3. EXPERIMENTAL INVESTIGATIONS OF HEAT TRANSFER AND FLUID FLOW 48

Resistance-Heated-Tube Heat-Transfer Experiment 48

Mass-Transfer Measurements 51

Velocity Distribution in Septafoil Channels 60

PART 2. MATERIALS RESEARCH AND TESTING

4. METALLURGY 65

Fuel Materials Development 65

Fabrication of UO_2 65

Thermal Conductivity of UO_2 65

High-Temperature Compression Testing of UO_2 67

Mechanical Behavior of Encapsulated UO_2 67

Fission-Product-Release Studies 68

Structural Materials Evaluation 72

Gas-Metal Reaction Studies 72

Mechanical Properties of Structural Materials 77

Manufacturing and Inspection Methods 84

Fabrication of Title I EGCR Fuel Elements 84

Welding of Ferritic Steels to Austenitic Stainless Steels 90

Reactor Vessel Penetrations 91

Inspection of Pressure Vessel Welds 92

Beryllium Investigation 93

Reactions of Beryllium with Gases 93

Evaluation of Beryllium Tubing 94
Joining of Beryllium 94

5. IN-PILE TESTING OF COMPONENTS AND MATERIALS 99

Fuel Element Irradiation Program 99
Full-Diameter Prototype Fuel Capsules 99
Reduced-Size Prototype Capsules 103
Miniature Capsule Fission-Gas-Release Experiments 104
Advanced Fuel Elements 107
Instantaneous Fission-Gas-Release Experiment 109
Neutron Flux Measurements 111
UO_2 Thermal Conductivity Determinations 112
Examinations of Irradiated Capsules 114
Miniature Capsules 114
GETR Capsules 121
ORR Capsules 122
Closed-Cycle-Loop Irradiation Facility in ORR 125
Radiation Effects on Structural Metals 127
Beryllium 127
Steel 133

6. OUT-OF-PILE TESTING OF MATERIALS AND COMPONENTS 141

Materials Compatibility Tests 141
Static Helium Tests 141
Low-Pressure Thermal-Convection Loop Tests 145
High-Pressure Thermal-Convection Loop Tests 151
Forced-Circulation Loop Tests 152
Evolution of Gases from Graphite 153
Transport of Gases Through Graphite 158
Cesium in EGCR Fuel Capsules 162
Measurement of High Temperatures 164
Attachment of Thermocouples for Measurement of Surface Temperatures in High-Velocity Cooling Gas 164
Equipment and Techniques for High-Temperature Thermocouple Studies 165

Stability of Rhenium-Tungsten Thermocouples 166
Effects of Radiation on Thermocouples 167
Purification of Cooling Gases 168
Measurement of Fission Gas Retention by Adsorbers 168
Removal of Coolant Impurities by Oxidation with Copper Oxide 170
Analyses of UO_2 Fuel Pellets 176
Oxygen-to-Uranium Ratio 176
Carbon 178
Fluorine, Iron, and Nitrogen 178
Automatic Continuous Analysis of Helium from Test Loops 178

7. DEVELOPMENT OF TEST LOOPS AND COMPONENTS 185

ORR-Gas-Cooled In-Pile Loops 185
GCR-ORR Loop No. 1 185
GCR-ORR Loop No. 2 186
EGCR Experimental Loops 186
Mechanical Joint Service Testing 192
Special Gas Compressors 196
Grease-Lubricated Centrifugal Compressors 196
Regenerative Compressors 196
Compressors with Gas-Lubricated Bearings 198
Compressor for High-Temperature Electric-Motor Test System 199
Compressors for ORR In-Pile Loop No. 2 200
Compressors for EGCR Experimental Loops 200
Study of Back-Diffusion Through Labyrinth Seals 202

GAS-COOLED REACTOR PROJECT QUARTERLY PROGRESS REPORT

SUMMARY

Part 1. Design Investigations

1. Reactor Physics

A series of calculations has been performed which indicate that a two-group, two-dimensional calculation based on a homogeneous representation of the EGCR core yields interpretable results for neutron flux and power distributions that are sufficiently close to the four-group heterogeneous core results to permit valid analyses of the effects of experimental loops on the core.

The effects on radial power distribution in the EGCR core of various experimental fuel assemblies in the experimental loops have been studied. Calculations have also been made of the power production capabilities of the loops containing the various experimental assemblies. It was found that it would be possible to load one or more selected loops with highly reactive assemblies if the contents of the other loops, the positions of the control rods, or the core loading pattern were adjusted to give acceptable excess reactivities and power distributions. Measurements to be made at Hanford with the Physical Constants Test Reactor (PCTR) will provide a partial check of the physics analysis of the EGCR loops.

Preliminary experimental results for a modified EGCR core rod lattice have been obtained with the PCTR. A review of the calculations of the control rod worth, which was prompted by the availability of experimental data, gave a value that was essentially identical to the previously calculated value and which was in excellent agreement with the preliminary analysis of the experimental results.

Since the problems of joining graphite and stainless steel in the EGCR Title I dummay fuel assemblies have not been resolved, the effect of stainless steel cladding on the graphite plugs and sleeves of the dummy assemblies has been studied. Calculations indicate that for the

mode of operation currently planned for the EGCR, complete cladding of the dummy fuel assembly can be considered to produce no significant effects on the axial power distribution or on reactivity.

Preliminary calculations have been made of the graphite damage that will occur in the EGCR as a result of moderation of fast neutrons. Results have been obtained in terms of neutron energy, the extent to which the damage is proportional to the integrated flux, and the spatial distribution of the predicted damage.

As part of an over-all study of the EGCR experimental loops, it was found that for the "worst" experimental fuel element being studied the circulating fission-product activity to be expected at equilibrium in a 1.5-Mw loop was 7.53×10^3 curies. Also, the shielding requirements for the EGCR loops were specified. Assumptions were made that led to the most stringent shielding requirement for each component because of uncertainty regarding the deposition of fission products on loop surfaces in contact with the coolant gas.

Calculations have been made to determine the effect of reflector thickness and composition on exposure of the pressure vessel to fast neutrons. It was found that 6 in. of lithium hydroxide would be as effective as 18 in. of graphite in protecting the vessel. With a beryllium oxide reflector it would be possible to further reduce the reflector thickness, but the thickness advantage would be offset by the higher cost of the beryllium oxide.

A study was completed of the absorption properties, both thermal and resonance, of the U^{233}, U^{235}, and Pu^{239} fission products as a function of the relative burnup of the fuel and the degree of flux thermalization. The results of this study will be valuable in reactor poisoning calculations, which require an accurate knowledge of the fission-product absorption cross sections.

2. Reactor Design Studies

A modification has been made to the Title I EGCR fuel assembly which eliminates the need for making the final bottom weld with the cluster

in the graphite sleeve and also gives the operator a means of removing the fuel-bearing part of the assembly in case the sleeve becomes "jammed" in the channel. Alternate designs for rod spacers are being considered in an effort to reduce the total core pressure drop. Extrapolations of heat transfer results to reactor conditions have shown a sharp change in the heat transfer coefficient near a spacer, but the configuration of the spacer appears to have little effect on the heat transfer coefficient at the exit of an assembly.

Fuel handling and coolant flow control provisions were studied to assess the effect of the lifting force of the gas stream on the fuel assemblies. It was found that when only one fuel assembly is left in a channel the seal between the lower plenum and the charge machine chute must be sufficient to maintain the pressure in the chute about 5.8 psi below that in the surrounding lower plenum of the reactor.

Analyses of preliminary EGCR analog studies have indicated that the rate of change of temperature of the fuel elements, even for very fast startups and scrams, will not cause severe strains in the cladding due to the relative thermal expansion of the cladding and the UO_2. The analog studies show that in no case will it be desirable to have a startup in which the rate of change of the fuel cladding temperature exceeds 150°F/min. Data are being obtained in order to estimate the allowable number of temperature cycles. Analyses have been made of the temperature variations of the fuel elements.

Studies are being made of deflections and stresses in the fuel element cladding under arbitrary temperature distributions. Relations have been formulated with which to predict the plane of bowing, the displacements and stresses caused by the central spacer, and the maximum stresses corresponding to the temperature functions.

The first test of a metal-clad graphite body was completed. The stainless steel clad body was heated from room temperature to 600°F at one end and 1300°F at the other. After one thermal cycle it was found that the matched helical grooves in the graphite and cladding had not adequately accommodated the different dimensional changes of the two materials.

Studies of the coolant channel flow adjustments required for the EGCR have led to a new concept of flow adjustment. A bottom dummy fuel assembly fitted with an adjustable nozzle and a new ram head for the flexible fuel ram of the charge machine have been designed which will provide for the adjustment of the coolant flow control nozzle in place in a fuel channel. The new design also incorporates in the fuel ram head a pneumatic load-sensing device to replace the much more cumbersome fuel-column weighing device presently proposed.

The amount and nature of the contamination to be expected in the charge and service machines are being studied. Following these determinations, methods for decontaminating these machines are to be devised.

An analysis was made of the possibility of core levitation in the EGCR in case of single-ended or double-ended failures of the main exit coolant pipes. It was found that levitation could occur, and therefore means for preventing it are being considered. Studies of the pressure and temperature that would exist in the EGCR experimental loop cell in the case of accidental release of the main reactor coolant revealed the need for blowout disks to vent the experimental cell atmosphere into the containment shell if the cell pressure exceeds the design limit of 12 psig.

3. Experimental Investigations of Heat Transfer and Fluid Flow

The study of heat transfer in the septafoil geometry was continued using an inlet plenum chamber screen arrangement designed to reduce the rotational component of the flow at the channel entrance. Initial data with this modified entrance were in reasonable agreement with earlier results. Circumferential temperature profiles appeared more nearly like those theoretically anticipated; evidences of some cross flow were still present. Heat-transfer coefficients, estimated from an axial traverse of a single peripheral tube, varied from 45 $Btu/hr.ft^2.°F$ immediately downstream of the mid-cluster spacer to 26 $Btu/hr\cdot ft^2\cdot °F$ at the channel exit; the value of the heat-transfer coefficient at the channel entrance is in doubt because of some uncertainty in the tube temperature at the inlet.

A series of tests using cotton threads to visualize the flow in the channel entrance indicated that a set of three coaxial screens in the inlet plenum region was most effective in reducing the rotational flow observed in earlier studies. The optimum width of a baffle contiguous with the outermost screen (located diametrically opposite the flow inlet) was established through a systematic study. Mass-transfer tests with this modified entrance configuration showed that some cross flow (or rotation) still existed; little consistency was observed between the results of three runs with the apparent rotation varying from clockwise to counterclockwise. The circumferential mass-removal patterns have been interpreted on the basis of a laminar-to-turbulent transition in the boundary flow and a flow separation. An apparatus for studying heat transfer downstream of the mid-cluster spacer by mass-transfer techniques is being assembled.

Measurement of velocity profiles in the septafoil channel for a $\gamma = 2$ tube spacing was completed at five additional L/d_e levels ranging from the channel inlet to the outlet. The patterns observed are consistent with those previously reported at the $L/d_e = 50$ position. Uncertainties and scatter associated with these data have indicated the need for more accurate spacing of the tubes in the cluster and more precise knowledge of the Pitot-tube position; velocity profiles will be redetermined at the six axial positions following correction of these defects.

4. Metallurgy

The continuous process for the conversion of UF_6 to UO_2 has been refined to the point that satisfactory reproducibility is being obtained. The process has been used for the production of numerous small batches of oxide for use in experimental programs. In another fuel materials development program, an apparatus for measuring the thermal conductivity of UO_2 has been constructed and is being tested with a suitable standard. Also, a series of compression tests of UO_2 at high temperatures has been completed. The results indicate that fuel pellets of UO_2 will support substantial loads at 1500°C with only slight deformation.

Equipment has been designed and built for observing the mechanical behavior of encapsulated UO_2 by radiography. The capsule is heated internally with a tantalum resistor to temperatures of approximately 3000°F. In a preliminary run, the radial gap was measured to within 0.001 in., and the temperature drop through the annular pellets at central temperatures up to 2000°F was determined.

An apparatus has been built for collecting and measuring the fission gases released from heated specimens of irradiated UO_2. Suitable samples of UO_2 are induction heated in a tantalum susceptor. Data are being obtained at temperatures up to 1650°C.

Experiments on gas-metal reactions carried out at pressures as low as 10 μ have shown that the concentration of CO_2 has little effect on the reaction rate of CO_2 with type 304 stainless steel at temperatures of about 1400°F. The rate of carburization of stainless steel in CO is also being studied. Preliminary data indicate little, if any, change in the total amount of carbon absorbed on unstressed specimens in environments ranging from 1 to 5% of 1 atm of CO. However, analyses of specimens from creep-rupture tests in CO indicate much greater absorption of carbon on the highly stressed gage length. Additional data from analysis of layers taken from a strain-cycled specimen of stainless steel show variations of carbon content from 1.3% on the surface to 0.36% across the thickness of the 0.060-in.-wall tubular specimen.

In some cases the results from laboratory tests have been reproduced in the materials compatibility testing of engineering components. Installation of a purification system to control the composition of the gas may minimize the unexplained scatter of results from these tests. There are significant variations in the constituents outgassed from graphite. A recent series of failures by catastrophic oxidation of engineering-test loops constructed of type 316 stainless steel has emphasized the need for proper selection of materials and environmental conditions and for further study of this phenomenon.

An extensive series of tube-burst tests of type 304 stainless steel in various environments is being run. Tests in air have been completed,

and the data have been summarized. Data from a limited number of in-pile tube-burst tests agree substantially with base-line data under normal conditions.

A thermal cycling test of a fuel capsule collapsed around UO_2 pellets has been conducted that consisted of 75 cycles from 1000 to 1600°F at a rate of 100°F/min. The specimen length was found to have increased by only 0.07% and the diameter by 0.13%. Buckling experiments on specimens with brazed spacers have shown that finned spacers will collapse uniformly and completely at 1800°F. Criteria for failure of loop materials by creep buckling are being studied.

Interim data on the effect of gaseous environments on the creep rate of type 304 stainless steel indicate that hydrogen is the only environment which adversely affects the creep properties as compared with the properties observed in argon. Results of creep tests in helium and argon demonstrated that the effects of the two environments are practically identical.

The brittle fracture characteristics of various pressure vessel steels are being determined. Charpy V-notch impact specimens oriented both transversely and parallel to the rolling direction of type SA-212, grade B plate showed similar curves of absorbed energy below -20°F. However, the curves diverged somewhat at higher temperatures. Similar specimens were thermally cycled to duplicate conditions in the weld heat-affected zone. Cycling to 1400°F improved the impact properties, but cycling to 2400°F drastically reduced the maximum absorbed energy.

The procurement of components and fabrication of Title I fuel elements are being carried out on a pilot plant scale. Components are being inspected and evaluated before assembly, and fuel capsule loading and closure welding are being conducted in an inert-atmosphere chamber.

Techniques for welding of dissimilar metals for cyclic service at high temperatures were studied. Results indicate that the development electrode BP-85 (INCO) is quite satisfactory. A tentative specification for joining type 1020 carbon steel to austenitic stainless steel was prepared. Welding procedures and variations in design for assembly of the

burst-slug-detection (BSD) tubes and thermocouples into the pressure vessel nozzles are being studied. Mockups of the BSD tube assembly have been prepared.

Several feet of weldment of 4-in.-thick, type SA-212, grade B steel were inspected by ultrasound, both for evaluation of the welds and development of the inspection techniques. The validity of the inspection results is being determined by metallographic examination of selected sections.

Experiments on the reaction of CO_2 with beryllium at 700°C have indicated that the only reaction products are BeO and CO. Removal of surface inclusions in beryllium tubing by selective etching is necessary to eliminate interference with inspection techniques.

Successful joining of beryllium to itself and to stainless steel by brazing has been demonstrated. A brazing alloy consisting of titanium, copper, and beryllium appears to be most promising. Leaktight end closures of beryllium tubing have been successfully prepared by diffusion bonding at 1000 to 1100°C.

5. In-Pile Testing of Components and Materials

Fuel element irradiation studies have continued, and a total of 18 capsules are now being irradiated. Eight full-size (diameter only) capsules are in the ORR and ten are in the ETR. Eight were removed from the ORR during the quarter and one from ETR. The five fuel stringers irradiated in the GETR loop were removed, and all were found to be defective because of faulty installation or improper loop operation. Use of the GETR loop has been discontinued.

Irradiation of UO_2 pellets in fission-gas-release experiments has been extended to temperatures up to 3400°F. A new capsule has been designed with test capability in excess of 4000°F. Efforts are being made to extend the thermometry to this range. The absence of increases in central fuel temperatures at thermal neutron doses between 3×10^{16} and 3×10^{20} neutrons/cm^2 has indicated that the thermal conductivity of UO_2 does not change significantly with irradiation over this range of exposures.

A series of irradiation experiments has been initiated to evaluate graphite-clad fuel elements consisting of UC_2 in a graphite matrix.

Instantaneous fission-gas-release experiments have continued. An experimental assembly is being irradiated that contains two thin plates of high-density UO_2 with thermocouples sandwiched between them, as well as thermocouples on the outer surfaces. It has been found that a single channel is not adequate for studying the complex spectrum being obtained, and therefore a 200-channel spectrometer is being installed. An argon-activation method has been devised for determining the neutron flux in the fuel assembly. Preliminary flux measurements have been reproducible to within 10%. Determinations of the thermal conductivity of the UO_2 based on temperature measurements have indicated no change in a two-month period.

Comparisons of UO_2 specimens before and after irradiation in miniature capsules have shown a correlation between initial bulk density and changes in structure and dimensions. The changes decrease with increasing bulk density. In order to check the validity of neutron fluxes determined by flux monitors for these specimens, mass analyses were made of the uranium isotopes and plutonium. The agreement of the measured fluxes and the fluxes calculated from the analytical results was fairly good. In comparing the analyses, it was found that peak-height ratio measurements were more precise than absolute atomic fraction determinations.

A capsule containing two ThO_2-UO_2 cylinders encased in siliconized silicon carbide-coated graphite was tested in the closed-cycle-loop irradiation facility in the ORR. The capsule had been irradiated for 440 hr at 1500°F when high gas activity indicated a broken sample. Fission gas leakage was evident from the onset of the test, and gas samples indicated that all the fission gas that escaped from the fuel was emitted into the coolant gas. Radioactive materials plated out on the loop exit leg and were especially concentrated at the main tube-to-pipe tee joint.

Since beryllium is being considered as a material for fuel element cladding, studies have been initiated to determine the effects of fast

neutrons on the high-temperature strength of the material. Data from annealing experiments have shown that the volume increase of beryllium may be significant at temperatures above 600°C, and other effects on the mechanical properties are probable. Calculations of the swelling expected under given conditions were made using the restraint resulting from the yield strength of the metal in one case and the restraint from the surface tension in a second case. Comparison of these calculated data with observed volume increases indicate that the first method yields values comparable to available experimental data. Irradiation experiments have been planned in which the amounts of gas formed by the (n,α) and $(n,2n)$ reactions and the high-temperature mobility of the gas will be studied further experimentally; void formation during irradiation will be related to crystal orientation, grain size, and section thickness; and the effect of neutron irradiation on creep strength and permeability will be studied. Apparatus has been designed for these investigations and is being fabricated.

Methods for removing irradiation-induced property changes in pressure vessel steels by periodic annealing are being studied. The effects of annealing are being determined by making hardness measurements and by conducting notched-bar impact and tensile tests on irradiated specimens annealed at several temperatures.

6. Out-of-Pile Testing of Materials and Components

Additional test results have been obtained from out-of-pile tests designed to evaluate the corrosion behavior and structural stability of the EGCR fuel element assembly. Four static-helium tests of heated elements at 1500, 1600, 1700, and 1800°F were completed during the quarter, and two tests of heated elements at 1700 and 1800°F were started. A 5000-hr low-pressure thermal-convection loop test at 1400°F was completed. High-pressure thermal-convection loop test 3 was completed after 500 hr of operation with a test section temperature of 1225°F. Test 2, scheduled for 5000 hr, completed 500 hr of operation at 1225°F. Forced-circulation loop test 3 was completed upon 1000 hr of operation at a

test temperature of 1400°F. Analyses of the results of the completed tests are presented, as well as correlations with the results of previous tests, where possible. A small-scale gas-purification system of the type proposed for use at the EGCR has been designed and is currently being fabricated for evaluation in conjunction with forced-circulation loop test 4.

Studies of the degassing behavior of various types of graphite have continued, and data obtained during the quarter are presented and discussed in relation to data obtained previously. Modifications of the equipment are planned that will permit a systematic study of the rates of evolution of gases by graphite.

A series of experiments has been designed for determining the apparent interdiffusion coefficients of noble gases in reactor-grade graphites. Initial experiments gave results that were much lower than anticipated from preliminary calculations, possibly because of mass-transfer films at the graphite surfaces. Attempts are being made to eliminate experimental difficulties.

Investigations of the chemistry of cesium have shown that cesium metal is the most likely form of the cesium fission product in the EGCR. Estimates have been made of the vapor pressures to be expected in the fuel rods. Initial studies of the effect of cesium metal on stainless steel have indicated the need for definitive studies of the compatibility of cesium with stainless steel.

Studies of factors influencing the accuracy of thermocouples attached to metal surfaces in high-velocity cooling gas were continued. Calculations are being made of the heat transfer in a thermocouple junction used as a cooling fin, and an attempt will be made to correlate the results with experimentally determined corrections for thermocouples attached in coolant streams. Work is continuing on equipment and techniques for high-temperature thermocouple studies. A computing program has been established for analyzing thermocouple calibration data. Another computing program is being designed for determining the amounts of impurities produced by transmutation reactions in thermocouple alloys as a function

of neutron exposure time and flux. A standard is being sought for use in calibration studies of thermocouples during irradiation.

Methods of removing impurities, particularly fission gases, from the coolants of gas-cooled reactors are being studied. In one phase of this study, measurements are being made of the fission gas retention of various absorbers. Of the various materials tested thus far, no material has been found that is better than Columbia G activated carbon for krypton adsorption under the test conditions being used. Mechanisms for the removal of coolant impurities by oxidation with copper oxide have been studied, and simple-continuous and cyclic-continuous operation schemes are to be tested at reactor temperature and pressure.

A study of the reliability of analyses of UO_2 fuel pellets has been initiated in an effort to establish methods of analysis that will serve as standards in the evaluation of chemical tests for the acceptability of UO_2 fuel pellets for reactor use. The determinations of most importance at present are the oxygen-to-uranium ratio and the carbon, fluorine, iron, and nitrogen contents.

A system for the automatic continuous analysis of helium from test loops has been put into service. The chromatograph used in this system gives analytical values for H_2, CO_2, O_2, N_2, CH_4, and CO.

7. Development of Test Loops and Components

Construction is under way on a gas-cooled loop for operation in the ORR (GCR-ORR loop No. 1) to test advanced clad fuel elements. Design studies continued on a similar gas-cooled loop (GCR-ORR loop No. 2) in which unclad fuel elements would be tested. A flow diagram of the loop system and a plan view of the installation in the ORR have been prepared. Design criteria have been established for the eight permanently installed experimental loops that are to be constructed as an integral part of the EGCR.

Equipment has been set up for service tests of the commerically available mechanical joints specified for the EGCR experimental tubes and the double-gasketed, gas-buffered, mechanical joints being considered

for other applications. Tests will be initiated when the joints now on order are received from the vendors.

The endurance test of a grease-lubricated centrifugal compressor was continued with the compressor operating at 12,000 rpm in helium at 590°F and 400 psig suction pressure. The accumulated operating time is more than 2500 hr. High-temperature tests of a prototype regenerative compressor were initiated. A test of a gas-lubricated bearing was started in the recently completed gas-bearing tester, and design work continued on the loop for testing a compressor with gas-lubricated bearings. The compressor, which is being obtained from Bristol-Siddeley Engines, Ltd., should be shipped early in 1960.

The low bid was accepted for the fabrication of the compressor (GABE-1) designed for use in the high-temperature electric-motor test system. A specification was prepared for the purchase of helium compressors having self-acting gas bearings; these compressors are required for GCR-ORR in-pile loop No. 2. Studies were initiated to determine criteria for the compressors to be installed in the EGCR experimental loops.

Part 1. Design Investigations

1. REACTOR PHYSICS

Comparison of EGCR Heterogeneous and Homogeneous Calculations

Prior to an analysis of the effects of experiments in the EGCR loops on the radial power distribution, a series of calculations was performed to determine whether a two-group, two-dimensional, homogeneized core model could be employed to obtain accurate flux distributions. The basic motivation for the study was the prohibitive cost of more exact calculations. In order to provide an accurate reference point, a calculation had previously been done which explicitly included the heterogeneous character of the reactor lattice and the two-dimensional nature of the EGCR core in the horizontal plane.[1] This calculation required the use of an IBM-704 with a 32,000-word core storage unit, which was not available at ORNL. As a result of the much larger numerical mesh required for the problem and the use of a four-group model, the calculation was more expensive by a factor of 32 than a two-dimensional, two-group, homogeneous core calculation. The first step of the study was a comparison of the results of the four-group heterogeneous core calculation with results for two four-group homogeneous models. In one case the core was homogeneized over the entire area outside the experimental loop tubes, while in the second case it was considered that the actual experimental loop cell (the graphite block containing the loop tube) was surrounded by a homogeneous core.

Heterogeneous and homogeneous core flux distributions for the EGCR with empty experimental loops are presented in Fig. 1.1. Only slight differences were noted in the over-all flux distributions obtained from the two four-group homogeneous models, but the detailed flux distribution in the vicinity of the experimental loop tubes was more reliable in the model containing the complete experimental cell. Ratios of thermal flux in the homogeneous model to the peak value of the moderator flux between

---

[1] GCR Quar. Prog. Rep. Sept. 30, 1959, ORNL-2835, p 3.

each fuel element in the heterogeneous model were found to be nearly constant, except for locations adjacent to the reflector. Similar behavior was noted for the ratio of thermal flux in the homogeneous case to the flux in the center of the fuel elements in the heterogeneous case.

An examination of the thermal flux gradients in the homogeneous core at locations where fuel elements actually exist revealed remarkable agreement with the flux gradients across fuel elements obtained from the heterogeneous core model. Most of the gradients calculated from the homogeneous flux distributions were within 1% of the corresponding heterogeneous values, but there were areas, particularly near the reflector, where the gradients had a 3% variation.

Flux distributions resulting from four-group and two-group homogeneous core calculations are presented in Fig. 1.2. For these calculations it was assumed that each of the eight experimental loops contained an experimental homogeneous fuel element having a carbon-to-U^{235} atom ratio of 200. In the four-group model, a void zone was located outside the experimental tubes, but in the two-group case the void was eliminated and filled with graphite; this accounts for the difference in the flux distributions near the loops. Thermal fluxes were in good agreement throughout the remainder of the core.

It is concluded that a two-group, two-dimensional calculation based on a homogeneous representation of the core yields interpretable results for neutron flux and power distributions that are sufficiently close to the four-group heterogeneous core results to premit valid analyses of the effects of experimental loops on the EGCR core.

Effects of Experiments on EGCR Radial Power Distributions

In order to determine the effect of various loop experiments on the radial power distribution in the EGCR core and to estimate the power production capabilities of the loops, a series of two-group, two-dimensional, homogeneous core calculations were performed using the PDQ code on the IBM-704 digital computer. A summary of the cases analyzed

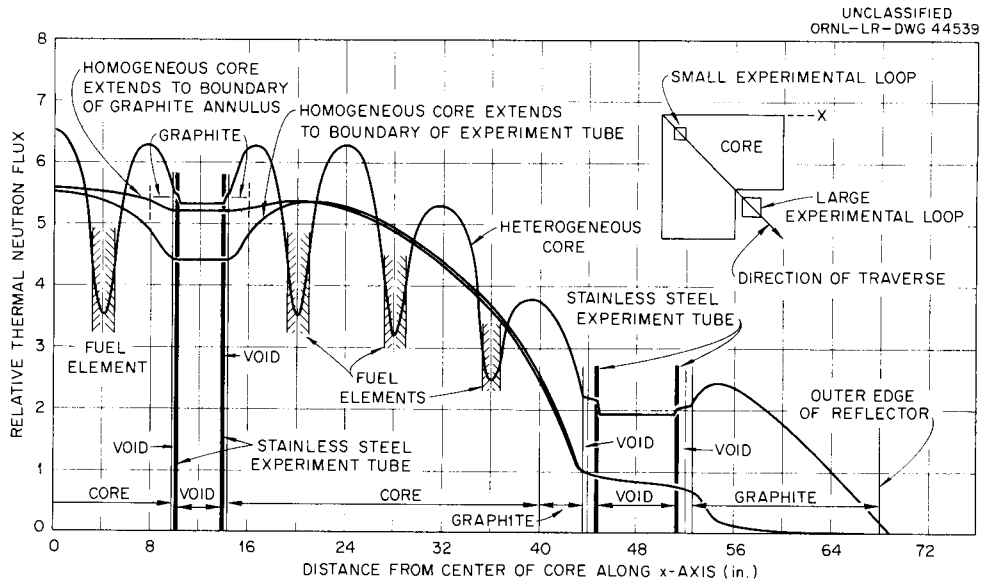

Fig. 1.1. Comparison of EGCR Thermal-Neutron Flux Distributions Obtained from Four-Group Heterogeneous and Homogeneous Core Calculations.

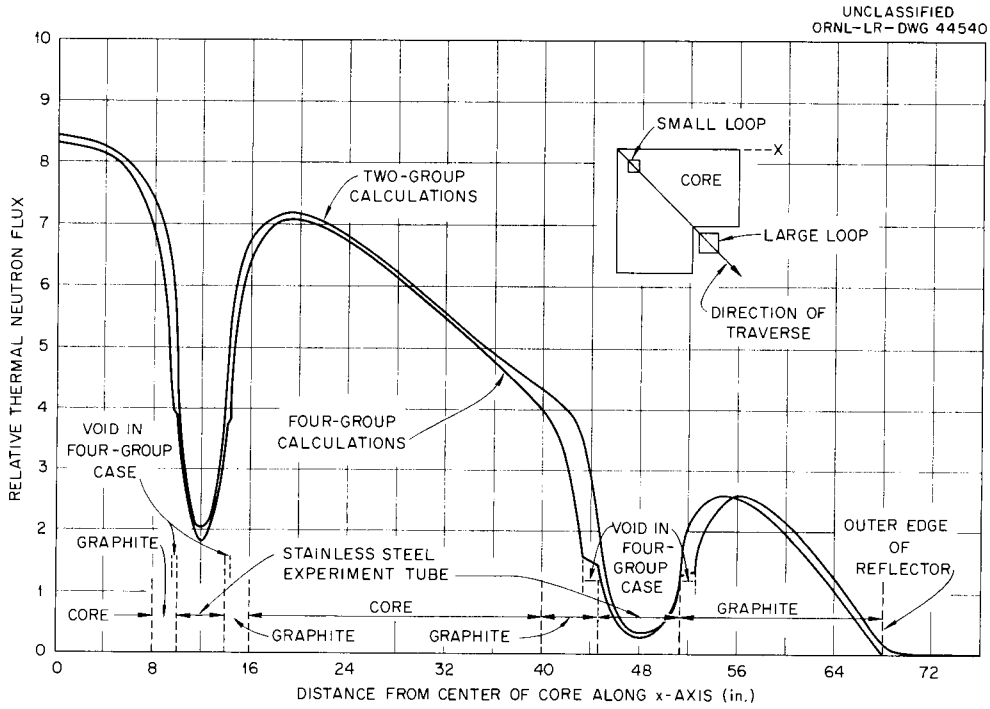

Fig. 1.2. Comparison of EGCR Thermal-Neutron Flux Distributions Obtained from Two-Group and Four-Group Homogeneous Core Calculations. Experimental loops assumed to contain homogeneous fuel elements with carbon-to-U^{235} atom ratios of 200.

and the effects of various experiments on the EGCR power distribution is presented in Table 1.1.

Experimental homogeneous fuel elements having carbon-to-U^{235} atom ratios of 50, 100, 200, 500, 1000, and 5000 were considered, and in each case the fuel assembly and 25% void volume were homogeneized to fill the experimental loop tube. The insertion of homogeneous assemblies having a carbon-to-uranium ratio of 5000 into eight formerly empty loops failed to alter the 1.254 radial peak-to-average power ratio of 1.254 in the core; however, assemblies with carbon-to-U^{235} ratios of 200 and 50 raised this value to 1.569 and 1.778, respectively.

There are numerous methods available for flattening the power distribution in the EGCR core, but only three were considered in this study. The insertion of one control rod in the center of the core, where the specific power was the greatest, decreased the radial peak-to-average power ratio for a core containing homogeneous assemblies (C/U = 200) from 1.569 to 1.200. A second case employing an outer row of core fuel elements enriched to 3.3% near the outer experimental loops yielded a radial peak-to-average power ratio of 1.380 for the same loop experiment. Flattening of the power distribution can also be effected by inserting experimental assemblies containing a higher fuel concentration in the large outer loops than in small inner loops. For example, a core containing homogeneous assemblies with a carbon-to-U^{235} atom ratio of 200 in the large facilities and 1000 in the small loops was found to have a peak-to-average power ratio of 1.212. During operation of the EGCR, it is likely that each experimental tube will contain an assembly which is different from all others, and the power distribution in the core will be greatly influenced by the loop assignment for each experiment.

The effect of concentrating the U^{235} into one rod in the center of a graphite block was investigated for assemblies containing carbon-to-U^{235} ratios of 200 and 1000. The area of the fuel rod was assumed to be equal to the fuel area of the seven rods in the EGCR cluster, and the uranium density (kg/ft of length) in each loop was identical to that used

Table 1.1. Effects of Experiments on EGCR Radial Power Distribution

	Small Loops		Large Loops		Experiment Reactivity, δk (8 loops)	Radial Peak-to-Average Power Ratio
	U^{235} Concentration (kg/ft)	Power (Mw)	U^{235} Concentration (kg/ft)	Power (Mw)		
Carbon-to-U^{235} Atom Ratio in Homogeneous Experimental Assembly[a]						
All loops empty						1.254
50	1.32	3.41	3.692	4.52	0.1210	1.778
100	0.660	2.14	1.846	1.99	0.0783	1.702
200	0.330	1.31	0.923	1.08	0.0502	1.569
500	0.132	0.636	0.369	0.521	0.0257	1.404
1000	0.066	0.347	0.185	0.291	0.0144	1.317
5000	0.0132	0.0753	0.0369	0.0661	0.0031	1.254
200 in large loops; 1000 in small loops	0.066	0.323	0.923	1.25	0.0248	1.212
200 (with control rod)[b]	0.330	0.945	0.923	1.23	0.0235	1.200
200 (with row of enriched fuel elements)[c]	0.330	1.17	0.923	1.21	0.0617	1.380
Enrichment of Heterogeneous Fuel in Experimental Assembly						
Experiment 1[d]						
8.5% in small loops; 24% in large loops	0.330	0.930	0.923	0.474	0.0300	1.485
Experiment 2[e]						
1.7% in small loops; 4.8% in large loops	0.066	0.241	0.185	0.174	0.0031	1.244

[a]Homogeneized experimental assemblies with same carbon-to-uranium ratios in all eight loops unless otherwise stated.

[b]Control rod inserted in center of core.

[c]Outer row of core fuel elements near outer experimental loops enriched to 3.3%.

[d]Fuel area same as fuel area in EGCR cluster; carbon-to-U^{235} ratio = 200.

[e]Fuel area same as fuel area in EGCR cluster; carbon-to-U^{235} ratio = 1000.

in the homogeneous experiments for the same carbon-to-U^{235} ratios. The radial peak-to-average core power ratios for both heterogeneous models were approximately 5% lower than the corresponding values obtained when employing homogeneous assemblies, but the power output of the experiments suffered a marked decrease. The power generated in heterogeneous experiments was approximately 30% less than that generated in homogeneous assemblies in the small loops and 40 to 60% less than the power obtained from homogeneous assemblies in the large loops. It was observed that the power outputs of homogeneous assemblies in the small and large loops

and the heterogeneous assemblies in the small loops varied almost linearly with uranium concentration over most of the range of concentrations considered, while the power output of heterogeneous assemblies in the large loops appeared to be near saturation. For heavily loaded experiments in the large loops, local reactivity effects resulted in a power increase of more than a factor of 2 when the U^{235} concentration was doubled.

It should be pointed out that several of the cases described in Table 1.1 represent configurations which could not be allowed in the reactor. For example, because of the large amount of excess reactivity, the control system would be unable to shut the reactor down with all eight loops filled with assemblies containing carbon-to-U^{235} ratios of 50 and 100. In addition, the specified limitation of the radial peak-to-average power ratio to a maximum value of about 1.35 in order to prevent excessive core pressure drop eliminates many of the cases listed as possible configurations in the loops. This merely requires, however, that all loops not be loaded with these assemblies without taking corrective action. It would be possible to load one or more selected loops with highly reactive assemblies if the contents of the other loops, the positions of the control rods, or the core loading pattern were adjusted to give acceptable excess reactivities and power distributions.

Analysis of Measurements to be Made at Hanford of the Neutron Fluxes Near an EGCR Experimental Tube and the Reactivity Effect of the Tube

A partial check of the physics analysis of the EGCR loops will be provided by measurements to be made at Hanford with the Physical Constants Test Reactor (PCTR). The neutron flux distributions and multiplication factor will be measured for a cell consisting of a three by three array of EGCR lattice cells with a 4.5-in.-OD steel tube in the fuel channel of the central cell. Measurements will be made both with the tube empty and containing an EGCR fuel element.

In order to select a fuel enrichment for the experiment which would result in a supercritical system, a calculation was done to determine the reactivity effect of the steel tube. A two-dimensional representation of

the system was used in which the fuel assemblies were approximated with an equivalent square cross section having the same area as the fuel. This geometrical representation is shown in Fig. 1.3a and b, together with the thermal flux distributions along two axes of the system for a fuel enrichment of 1.8%. The reactivity decrease due to the substitution of a type 304 stainless steel tube with an outside diameter of 4.5 in. and an inside diameter of 4.2 in. for the central fuel element was calculated to be $\delta k = 0.0947$. This results in a value of 1.0521 for the multiplication factor if the experiment is performed with the 1.8% enriched fuel, as is currently planned.

Control Rod Worth in EGCR

Although previously reported calculations of control rod worth in the EGCR[2] were considered to be accurate, the importance of these results to the reactor design and the availability of preliminary results from experiments at Hanford with a modified EGCR control rod lattice prompted a review of the calculations. A careful re-evaluation of cross sections has been made, and new four-group calculations of the rod worth in the Hanford experiment have been completed. The result is essentially identical to the previous result and is in excellent agreement with the preliminary analysis of the experimental results.

The calculations were chosen in such a way that several common approximations could be examined for their effect on the calculated control rod worth. The basic calculation of the set was a two-dimensional representation of the Hanford experiment that explicitly included the heterogeneity of the lattice. Both the fuel assemblies and the control rod were represented by regions with an equivalent square cross section. In the case of the fuel assemblies the area of the square was taken to be the same as the actual area of the fuel, whereas the size of the square control rod was chosen such that it had the same effective

[2]GCR Semiann. Prog. Rep. June 30, 1959, ORNL-2767, p 40.

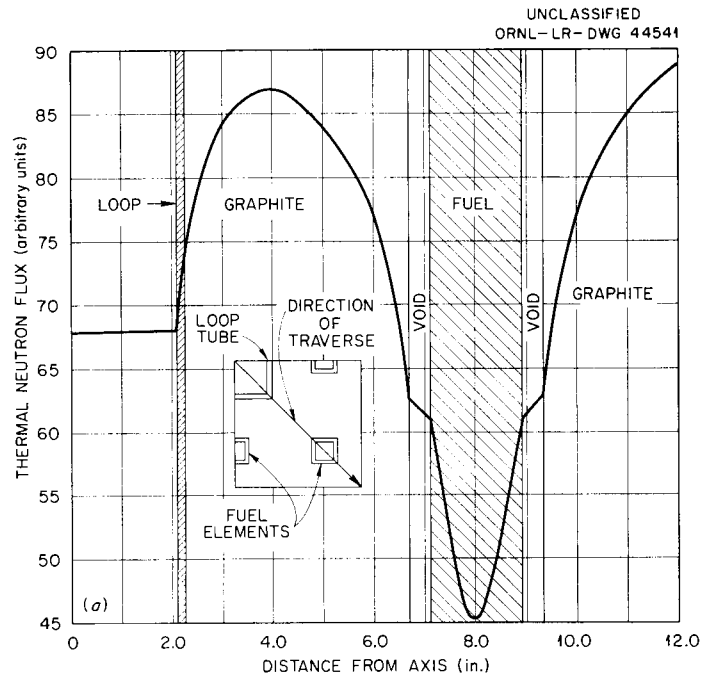

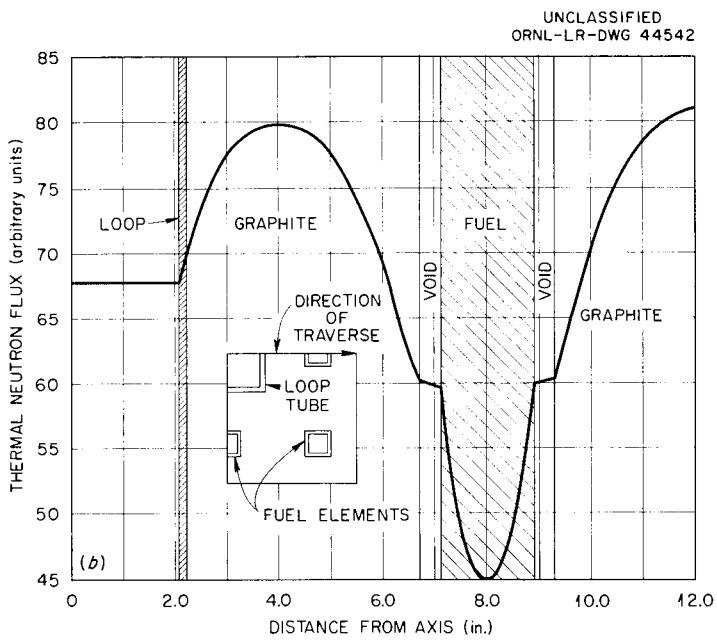

Fig. 1.3. Calculated Thermal-Neutron Flux Distributions Along Two Axes in the Nine-Channel Loop Supercell To Be Used in the PCTR at Hanford in Measuring the Reactivity Effect of the Steel Tube and the Thermal-Neutron Flux Distributions in Fuel Channels Adjacent to the Tube.

absorption area as the actual rod, according to the definition of Hurwitz and Roe.[3] The effect of a homogeneous approximation for the core material was examined by comparing the calculation with an identical one in which the fuel and graphite regions were homogeneized by flux- and volume-weighting in each energy group. The control rod worth given by this calculation was essentially identical to that with the heterogeneous lattice representation. The effects of the square approximation for the control rod and a cylindrical approximation to the control rod supercell were determined together by comparing the above results with those obtained using a cylindrical control rod and a homogeneous cylindrical supercell. Again, the results were essentially identical to those with the other representations.

On the basis of the above comparisons it can be concluded that a one-dimensional supercell model with a homogeneous core region extending to the control rod surface gives sufficient accuracy for the calculation of the worth of a regular array of control rods in an infinite reactor lattice. It should be noted that, in the thermal and lowest epithermal neutron groups, a transport-theoretical boundary condition is applied at the surface of the control rod; in the upper two groups diffusion theory is employed throughout, including the interior of the control rod.

The detailed agreement between the calculations and the experimental measurements is shown by a comparison of the rod worths in Table 1.2 and the thermal flux spatial distributions in Fig. 1.4a and b.

Effects of Cladding EGCR Dummy Assemblies with Stainless Steel

The problems of joining graphite and stainless steel in the EGCR Title I dummy fuel elements have not been resolved and, as a possible solution, the use of stainless steel cladding on the graphite dummy plugs and sleeves is being considered. Effects of the addition of stainless steel cladding in the dummy assemblies on the core axial power distribution

---

[3] H. Hurwitz, Jr., and G. M. Roe, J. Nuclear Energy 2, 85 (1955).

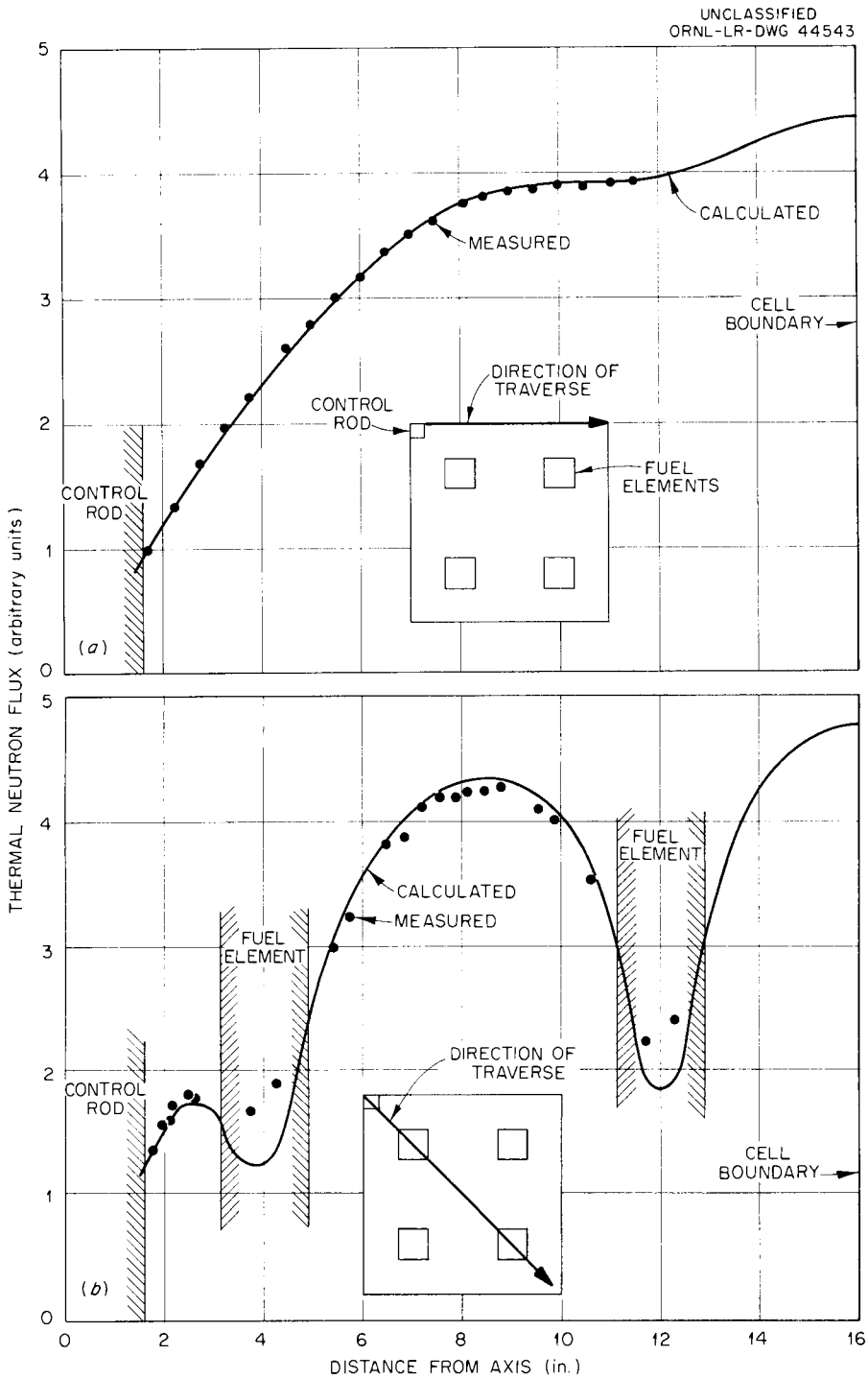

Fig. 1.4. Comparison of Measured and Calculated Thermal-Neutron Flux Distributions Along Two Axes in an EGCR Control Rod Supercell Containing 16 Fuel Channels. One quadrant of system is shown.

Table 1.2. Comparison of the Control Rod Worth Measured in the PCTR with Calculated Values Based on Three Different Models with 16 Fuel Channels per Control Rod

Description			K_∞	Control Rod δk
Control Rod	Core Region	Control Rod Supercell		
None	Heterogeneous	Square	1.1346	
Square	Heterogeneous	Square	0.9822	0.1524
None	Homogeneous	Square	1.1365	
Square	Homogeneous	Square	0.9828	0.1537
None	Homogeneous	Cylindrical	1.1347	
Cylindrical	Homogeneous	Cylindrical	0.9847	0.1500
PCTR experimental value (preliminary)				0.153

and excess reactivity have been investigated for the following three cases: (1) graphite plugs and sleeves clad with 1/8-in.-thick stainless steel, (2) graphite plugs and sleeves clad with 1/16-in.-thick stainless steel, and (3) graphite plugs clad with 1/8-in.-thick stainless steel and graphite sleeves clad with 1/8-in.-thick stainless steel on the outer surfaces only. In all cases the core was considered to have a uniform axial loading. The analysis showed the reactivity effect of the cladding to be small but revealed a pronounced detrimental effect on the axial core power distribution, as shown in Table 1.3.

Table 1.3. Effect of Stainless Steel Cladding on Plugs and Sleeves of Dummy Fuel Assemblies

Description	δk	Axial Peak-to-Average Power Ratio
Unclad plugs and sleeves		1.3821
1/8-in.-thick cladding on plugs and sleeves	0.0023	1.4546
1/16-in.-thick cladding on plugs and sleeves	0.0015	1.4454
1/8-in.-thick cladding on plugs and outer surfaces of sleeves	0.0019	1.4460

The results presented above apply only to the use of stainless steel cladding in the Title I dummy assemblies.[4] In this design the upper 10 in. of the unclad bottom dummy contains approximately 6 vol % stainless steel, whereas the lower 10 in. of the top dummy contains no stainless steel. Axial power distribution effects are shown in Fig. 1.5 and are observed to be primarily due to a reduction in the effectiveness of the top reflector when stainless steel is introduced.

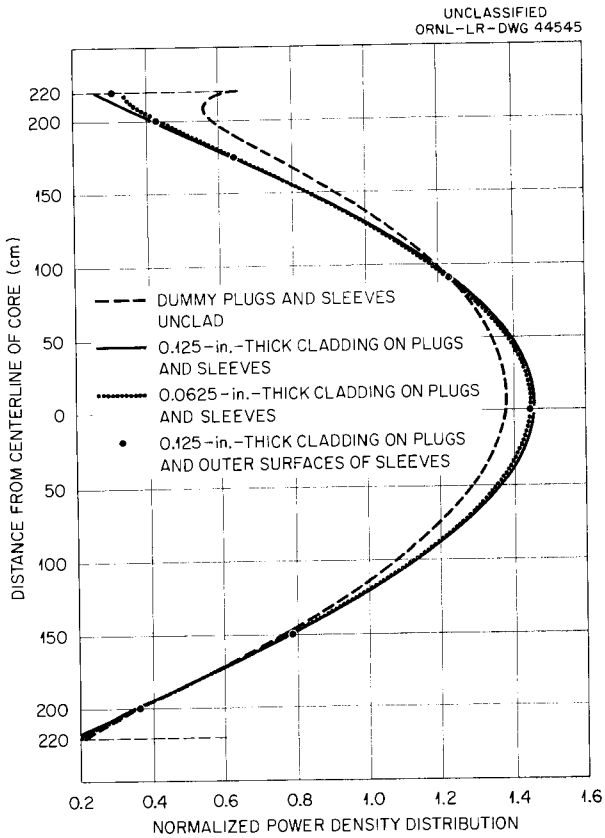

Fig. 1.5. Axial Power Density Distribution (Normalized to Average Axial Power of 1.0) Showing Effect of Stainless Steel Cladding on EGCR Dummy Assemblies.

All control rods were assumed to be fully withdrawn from the core and reflector in the cases studied. If the control rods were to extend to the interface of the upper reflector and core in the withdrawn position, flux peaking in the top reflector in the unclad case would be

[4]Allis-Chalmers Drawing 5917-EGCR-MS-3, Rev. 3 (Aug. 21, 1959).

decreased to the point where the addition of stainless steel cladding would produce very slight changes in the power distribution. Since this is the mode of operation currently planned for EGCR, complete cladding of the present dummy fuel assembly can be considered to produce no significant effects on the axial power distribution.

Graphite Damage Resulting from the Moderation of Fast Neutrons

Preliminary calculations have been made to determine the amount of damage to the graphite in EGCR as a result of collisions of fast neutrons with the graphite atoms. An approximate conversion factor has been obtained from Hanford, and the results have been converted from the natural unit of integrated neutron dose into equivalent megawatt days of exposure per adjacent tonne of fuel in the Hanford reactors (Mwd/AT). This allows a more direct calculation of the graphite shrinkage from the experimental data available at Hanford.

The graphite damage is calculated from a model which assumes it to be related to the energy lost by the neutrons to the graphite. The damage at a point x caused by all neutrons whose energy is greater than E_0 is obtained from the following relation:

$$D(E_0,x) = \int_{E_0}^{\infty} \phi(E,x)\ \Sigma_s(E,x)\ \gamma E\ w(E)\ dE \quad . \tag{1}$$

The term $D(E,x)$ is frequently referred to as the damage function. The definitions of the quantities appearing in Eq. 1 follow:

$\phi(E,x)$ = neutron flux per unit energy at point x,

$\Sigma_s(E,x)$ = scattering cross section at point x for neutrons of energy E,

γ = average fractional energy loss resulting from elastic collisions of neutrons with graphite atoms (this quantity is independent of energy),

$w(E)$ = weighting function which accounts for the fact that neutrons of different energies may produce different amounts of damage per unit of energy lost.

The details of the collosion are accounted for by w(E), which, in general, is not accurately known. It should be noted that if w(E) = 1 for all energies, then Eq. 1 says that the graphite damage per collision is proportional to the energy lost by the neutron in the collision. This implies that the kinetic energy gained by the graphite atom is dissipated by secondary collisions with other graphite atoms.

The weighting function w(E) is usually assumed to decrease with increasing energy; however, the variation of D(E,x) with E and x was found to be insensitive to the form of w(E) for the two cases which were studied. In one case, w(E) = 1 was assumed, and, in the other case, w(E) = 1 was assumed for energies less than 1.0 Mev and w(E) = 1/E was assumed for energies greater than 1.0 Mev. The second form of w(E) describes an extreme saturation condition in which the damage per neutron collision is constant above 1 Mev.

In order to evaluate the damage function over a lattice cell of the EGCR, a multigroup cell calculation was done with a cylindrical approximation to the cell. The resulting flux spectra at three points in the cell are shown in Fig. 1.6.

The manner in which the damage is distributed over the neutron energy spectrum is shown in Fig. 1.7. The ratio D(E)/D(0) is the fraction of the total damage caused by neutrons whose energies are greater than E. It may be seen that this model predicts that essentially all the damage is done by neutrons of energy greater than 10 kev and that only about 10% of the damage is caused by neutrons whose energies lie below 200 kev. The above conclusion is valid for both forms of w(E) which were considered.

It was of interest to determine the extent to which the damage function is proportional to the integrated flux above an appropriate threshold. At the cell boundary and at a radius of 3.0 in. (3/8 in. outside the channel boundary), the total damage integral was calculated. The ratio of the damage functions at these two points is compared with the ratio of the integrated flux in Fig. 1.8 for both forms of w(E). In Fig. 1.8 the integrated flux is written as

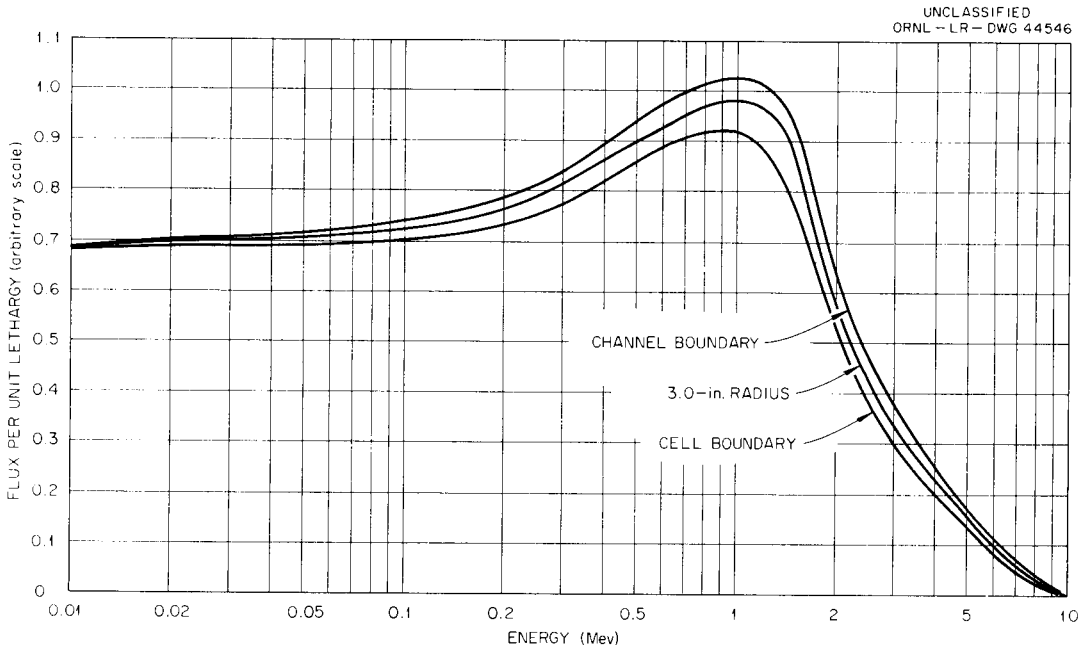

Fig. 1.6. Neutron Flux Spectra at Three Points in the EGCR Lattice Cell.

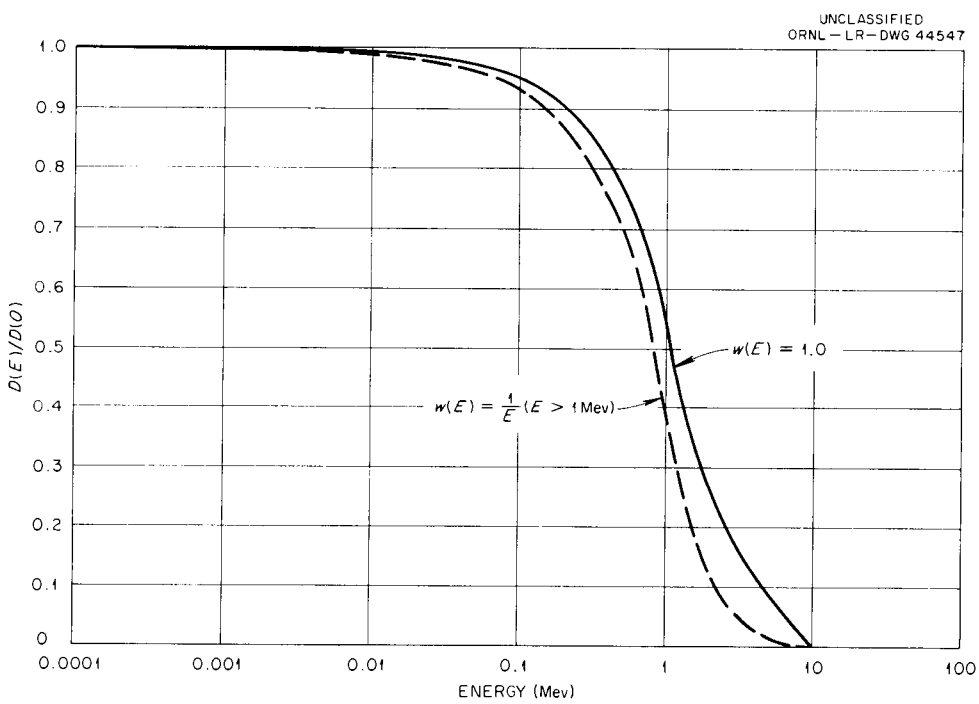

Fig. 1.7. Distribution of Graphite Damage Over the Neutron Spectrum at the Boundary of an EGCR Lattice Cell.

$$I(E_0,x) = \int_{E_0}^{\infty} \phi(E,x)\, dE \quad .$$

The spatial distribution of the predicted graphite damage may be seen from Fig. 1.8 to be very nearly the same as the spatial distribution of the neutron flux integrated above an energy of approximately 170 kev. It is important to note that this conclusion is valid for both of the quite different forms of w(E) studied. Thus, the large uncertainty in the form of w(E) does not affect the final results.

With the preliminary conversion factor provided by Hanford[5] to convert integrated neutron dose into megawatt days of exposure per adjacent tonne of fuel in the Hanford reactors, the 20-year exposure in Mwd/AT versus radial position in a cylindrical EGCR lattice cell was calculated. The conversion factor states that a dose of 10^{20} neutrons/cm^2 above 1 Mev is equivalent to 2300 Mwd/AT. The results of the calculation are presented in Fig. 1.9.

Activity in the EGCR Experimental Loops

A calculation of the amount of circulating, equilibrium, fission-product activity expected in the EGCR experimental loops was undertaken as a first step in the over-all loop study. The method used was an extension of the method followed in ORNL-2653.[6] The same element, that for the HGCR-1, was chosen as being representative of the "worst" element of those anticipated in the experimental program. The argument here is that in the HGCR-1 fuel element, no provisions are made to limit fission gas release from the element other than sizing the UO_2 particles to minimize fission-fragment recoils. Since graphites are available with

---

[5]Personal communication from D. R. de Halas (Hanford) to C. A. Preskitt (ORNL), October 1959.

[6]W. B. Cottrell *et al.*, The HGCR-1, A Design Study of a Nuclear Power Station Employing a High-Temperature Gas-Cooled Reactor with Graphite-UO_2 Fuel Elements, ORNL-2653 (July 14, 1959).

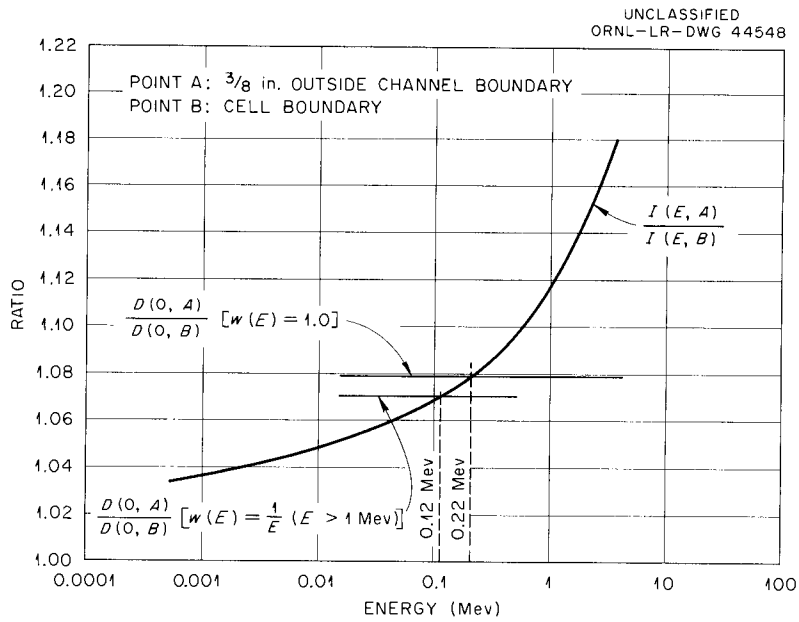

Fig. 1.8. Comparison of the Ratio of the Damage Integral at Two Points in the EGCR Lattice Cell with the Ratio of the Integrated Flux Above a Variable Lower Cutoff Energy. Both forms of the weighting function are illustrated.

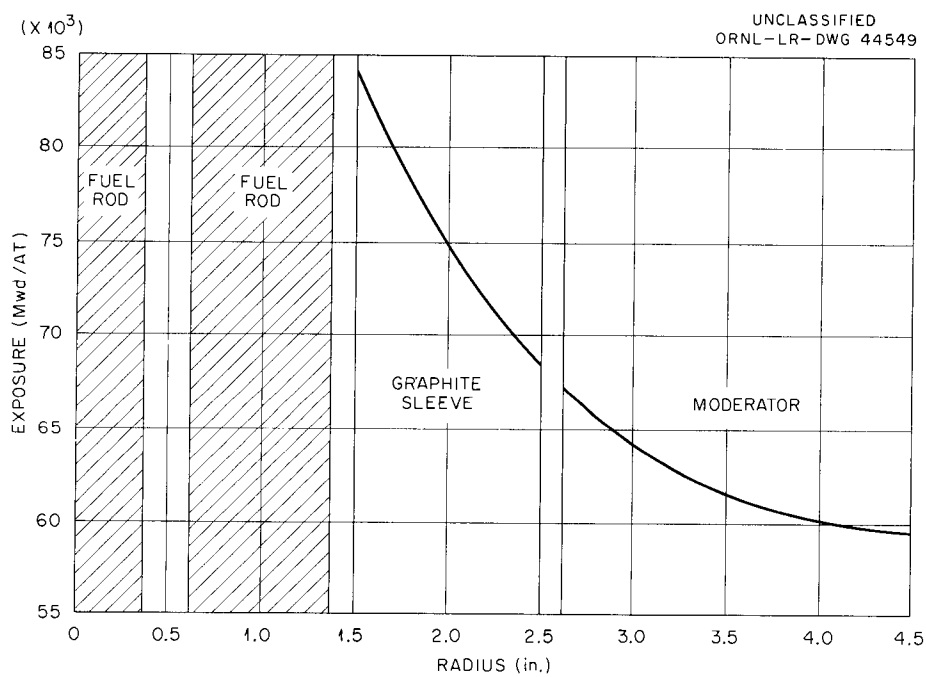

Fig. 1.9. Variation of the Graphite Exposure Over an EGCR Lattice Cell. A 20-yr exposure is given in terms of Hanford equivalent megawatt days per adjacent tonne of fuel. The normalization is to a power density in the fuel equal to the average power density in the core.

permeabilities of 10^{-6} or less times the permeability of the AGOT graphite used in the HGCR-1 element, it seemed reasonable to suppose that the elements surviving preliminary screening tests and reaching the full-scale test stage in the EGCR loops would, in general, have no greater fission product release rates than those calculated for the HGCR-1 fuel.

The temperature distribution for the HGCR-1 hot channel element was taken from a report by Fontana.[7] All assumptions related to Fontana's report and ORNL-2653 were used in the calculations. The circulating fission-product activity at equilibrium for a 1.5-Mw loop was found to be 7.53×10^3 curies.

EGCR Experimental Cell Shielding

Using available design information, the shielding requirements for the EGCR loop cells were specified. Concrete thicknesses for roof slabs, utility tunnel, and inter-cell walls were calculated which gave a dose rate at the surface of the concrete of 7.5 mr/hr or less. Calculations were based on a cell containing four blowers, valves, a pre-heater, main stream filters, a charcoal bed, holdup tanks, and some 50 to 100 ft of 6-in. loop piping.

The principal difficulty in carrying out calculations to determine adequate shield thicknesses for the experimental cells is the uncertainty regarding the deposition of fission products on loop surfaces in contact with the coolant gas. At the present time it does not appear to be possible to predict the detailed distribution of fission products, and a number of assumptions must be made:

1. Fission products will be removed by the bypass filtering arrangement.

2. Fission products will be uniformly deposited according to surface area of the loop components.

3. Fission products will be preferentially deposited in the cooler

---

[7]M. H. Fontana, Fuel Element Temperature Distribution in the HGCR-1, ORNL CF 58-12-3 (Dec. 3, 1958).

portions of the loop, that is, the bottom half of the heat exchanger, the cold-leg piping, the blowers, etc.

None of these assumptions is likely to be rigourously correct, but in view of the lack of experimental evidence supporting any particular assumption, it seems prudent to make the assumption that leads to the most stringent shielding requirement for each component. The conditions that were assumed are given below:

Component	Assumed Condition
Main-stream filter	100% fission product deposition
Charcoal bed	100% fission product deposition
Cool equipment	100% fission product deposition on surface area of half of cooler, cold-leg piping, and blowers

As a result of these assumptions, the concrete thicknesses required are as follows: (1) cell roof and inter-cell wall: 3 ft, with activity distributed in cool equipment; 3 ft, if determined by filter or charcoal bed alone, with 4 in. of lead around each; (2) utility tunnel wall: 3 1/2 ft, if determined by charcoal bed and filter alone with no lead shielding, or 2 ft with 4 in. of lead.

It should be noted that a factor of 2 in source strength of one of the components (when that component is controlling the dose rate) corresponds to 3 in. of concrete, or 3/4 in. of lead; a factor of 10 corresponds to 10.5 in. of concrete or 2 in. of lead. The assumed sources would have to be changed by large factors to alter radically the apparent concrete shielding requirements. All calculations were based on the assumed worst case, described above, for activity released from unclad elements in a 1.5-Mw loop. When viewed through 3 ft of concrete, the sources appear to decrease by a factor of 3.7 in one day, and by a factor of 45 in one week. Conversely, it follows that after startup of a fresh unclad-fuel experiment, the activity will be practically saturated in one day.

Effect of Reflector on Exposure of Pressure Vessel to Fast Neutrons

In a gas-cooled reactor operating at very high power density the thickness of the reflector may be determined by the requirement that the steel pressure vessel be protected from an excessive dose of fast neutrons, rather than by the usual requirements of neutron economy and power distribution. It is important that the reflector not be made thicker than necessary, since an increase in pressure vessel diameter can result in a marked increase in cost, as well as a decrease in the permissible gas pressure level. In designs for reactors with small cores, for instance, the reflector may take a large fraction of the volume within the pressure vessel. The suggestion has been made that a reduction in pressure vessel diameter could be achieved by substituting a thin layer of lithium hydroxide for the outer portion of the reflector. Lithium hydroxide is inexpensive and can be used at a relatively high temperature. It is effective in reducing the fast flux through the high slowing-down power ($\xi\Sigma_s$) of the hydrogen and also of the lithium and oxygen.

In order to determine the effectiveness of lithium hydroxide, a series of multigroup calculations was made using the Oracle Cornpone code (a consistent P_1 approximation to the transport equation). A preliminary comparison of the Cornpone results with calculations by the moments method[8] indicated that the Cornpone fluxes in a graphite matrix at points distant from the core are low by a factor of 2. Hence all subsequent results were multiplied by this factor. The allowable power density in each case was computed by assuming that the maximum fast flux to which any part of the pressure vessel could be subjected should give a dose of 4.0×10^{18} neutrons/cm^2 of neutrons at energies above 0.1 Mev in 20 years. The results of the calculations are given in Fig. 1.10 for a graphite reflector and in Fig. 1.11 for a beryllium oxide reflector. In the case of the graphite reflector, it may be seen that 6 in. of lithium hydroxide is as effective as 18 in. of graphite in protecting the pressure

[8]T. K. DeBoer, Estimation of the Fast Neutron Flux in the GCPR Prototype Pressure Vessel, ORNL CF 58-12-132 (Dec. 16, 1958).

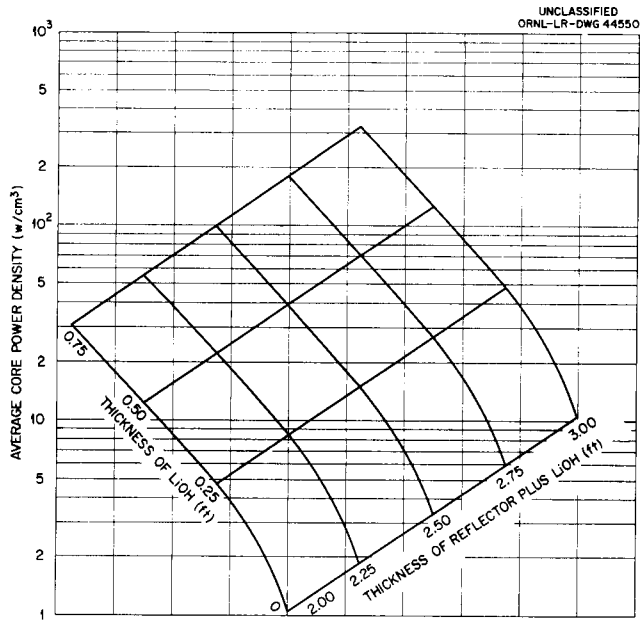

Fig. 1.10. Thickness of Graphite Reflector Plus LiOH Shield Required to Protect Pressure Vessel from Fast Flux.

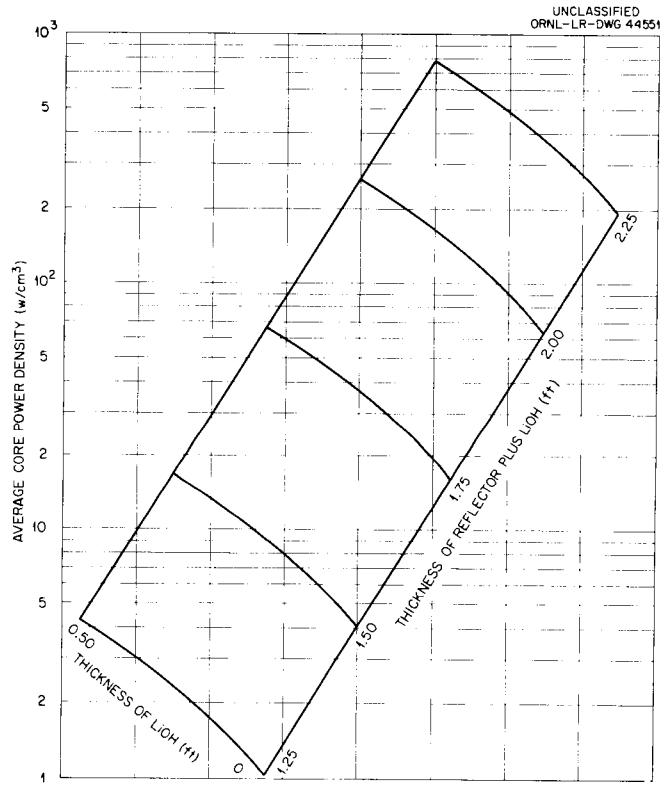

Fig. 1.11. Thickness of Beryllium Oxide Reflector Plus LiOH Shield Required to Protect Pressure Vessel from Fast Flux.

vessel. The calculations also indicated that the thickness of the graphite could not be reduced below about 2 ft (for an 8-ft-dia core) without seriously affecting the power distribution. With a beryllium oxide reflector it is possible to reduce the thickness further. However, this reduction does not appear to be sufficient, in any case, to compensate for the higher cost of the beryllium oxide.

Thermal and Resonance Absorption Cross Sections of the U^{233}, U^{235}, and Pu^{239} Fission Products

Reactor poisoning calculations require an accurate knowledge of the fission product absorption cross sections. For rough estimates the thermal cross sections are sufficient, particularly for thermal reactors, and have been the primary data used in the past. However, at the present time not only is it desirable to design reactors that operate at temperatures much higher than thermal, but, even for thermal reactors, the effects of absorption resonances should be included in the fission product cross sections. The great improvement in the past few years in both the amount and scope of cross section data available makes it possible to take the effects of neutron resonances into account. Therefore a study was undertaken to determine the absorption properties, both thermal and resonance, of the U^{233}, U^{235}, and Pu^{239} fission products as a function of the relative burnup of the fuel and the degree of flux thermalization. The results of this study are reported in ORNL-2869.[9]

The excess resonance absorption integrals of the low cross section stable and long-lived fission products are shown in Table 1.4, together with the yields and thermal cross sections. The high cross section fission products, Xe^{135}, Sm^{149}, Sm^{151}, Gd^{155}, Eu^{155}, Cd^{113}, and Gd^{157}, are not included, since they are to be treated explicitly in reactor calculations. Yield-weighted thermal cross sections and excess resonance integrals for the over-all low cross section fission product aggregates

[9]E. A. Nephew, Thermal and Resonance Absorption Cross Sections of the U^{233}, U^{235}, and Pu^{239} Fission Products, ORNL-2869 (to be issued).

of U^{233}, U^{235}, and Pu^{239} were found to be 37, 43, and 54 barns per fission, respectively, for the thermal cross section, and 134, 172, and 266 barns per fission, respectively, for the resonance integral. These

Table 1.4. Low Cross Section Fission Products

Fission Product	Thermal Cross Section, σ_o (barns)	Excess Resonance Integral, I_T (barns)	Excess Resonance Integral Below 100 ev, $I_{<100}$ (barns)	Yield (%)		
				U^{233}	U^{235}	Pu^{239}
Pm^{147}	60 ± 20	2050 ± 400	1950	1.71	2.70	2.92
Rh^{103}	156 ± 7	1000 ± 20	980	1.6	3.0	5.80
Cs^{133}	29 ± 1	375 ± 71	345.2	6.18	6.59	5.27
Xe^{131}	120 ± 15	768 ± 170	687.7	3.74	2.93	2.87
Sm^{152}	224 ± 7	2850 ± 300	2850	0.43	0.735	2.00
Tc^{99}	22 ± 3	168 ± 20	108.2	4.8	6.06	5.9
Nd^{145}	60 ± 6	310 ± 60	243.5	3.00	3.95	4.24
Mo^{95}	13.9 ± 4	101 ± 15	96.4	6.1	6.27	6.27
Ru^{101}	2.46	131 ± 131	116.8	3.00	5.00	5.0
Eu^{153}	450 ± 20	1512 ± 88	1121	0.095	0.150	0.41
Nd^{143}	324 ± 10	37.4 ± 2.2	13.5	5.20	5.98	6.31
La^{139}	8.2 ± 0.8	24.7 ± 1.5	8.7	5.91	6.55	5.70
Ag^{109}	87 ± 7	1396 ± 60	1358	0.04	0.03	1.50
Mo^{97}	2.2 ± 0.7	12.2 ± 2	6.6	5.35	6.09	6.09
In^{115}	207	3202 ± 90	3166	0.02	0.0104	0.041
I^{127}	7 ± 0.6	167 ± 20	117	0.25	0.25	0.39
Pr^{141}	11.6 ± 0.6	16 ± 8	2.4	5.57	6.00	6.02
I^{129}	11 ± 0.4	25 ± 1	6.4	0.90	0.90	5.5×10^{-4}
Nd^{146}	10 ± 1			2.3	3.07	3.53
Nd^{144}	5 ± 0.6			4.0	5.67	5.29
Zr^{93}	<4			7.10	6.45	6.45
Cs^{137}	<2			7.16	6.15	5.24
Zr^{91}	1.58 ± 0.12			6.53	5.84	5.84
Y^{89}	1.31 ± 0.08			6.5	4.79	1.90
Sr^{90}	1 ± 0.6			5.80	5.77	2.31
Mo^{98}	0.40 ± 0.40			5.18	5.78	5.78
Xe^{134}	0.2 ± 0.1			6.54	8.06	5.69
Kr^{83}	220 ± 40			1.14	0.544	0.29
Sm^{150}	3.0 ± 1.5			0.48	0.67	1.38

cross section values are for the fission product aggregates at zero fractional burnup of the fuel, and the resonance integrals in excess of 1/v are from 0.43 to 100 ev. Above 100 ev, the resonance integrals of the three fission-product-aggregates are taken as approximately 20 to 25 barns per fission, after the results of Gordeev and Pupko[10] and of Greebler, Hurwitz, and Storm.[11]

The relative concentration of a nuclide in the fission product aggregate begins to decrease as the nuclide approaches saturation in the reactor. If the neutron flux has an appreciable epithermal component, the absorption integral may be the decisive factor in controlling the saturation of the nuclide. Using an effective cross section representing both thermal and resonance absorptions, the thermal cross section and the excess resonance integral of the fission products were calculated as a function of relative burnup and flux by summing over the individual products. For convenience in reactor calculations, however, it is useful to reduce the number of fission products which must be treated separately. To this end four pseudoelements have been formulated which when taken together effectively represent the actual dependence of the fission product aggregate on burnup and epithermal flux. A different set of four pseudoelements has been obtained for each of the three fission product aggregates considered, that is, for each of the three fissile nuclides. Within a set, each pseudoelement is characterized by a distinct yield, its thermal cross section, and an energy-distributed resonance integral. Multigroup cross sections for use in a 32-group code have been computed for the pseudoelements and are listed in ORNL-2869,[9] together with the thermal group cross sections (69 to 2704°F).

---

[10] I. V. Gordeev and V. Ya. Pupko, Evaluation of the Absorption Cross Section of U^{235} Fission Fragments in the 0.025 – 10^6 ev Energy Range and Calculation of Fragment Effects in Intermediate Reactors, Second International Conference on Peaceful Uses of Atomic Energy, A/Conf.15/P/233 (1958).

[11] P. Greebler, H. Hurwitz, Jr., and M. L. Storm, Nuc. Sci. Eng. 2, 334–351 (1957).

2. REACTOR DESIGN STUDIES

EGCR Fuel Assemblies

Mechanical Design

A number of modifications of the Title I design are being considered, one of which is shown in Fig. 2.1. In this assembly the teeth on the spacers are parallel to the flow so that the pressure drop should be less than for spacers with helical teeth. The design of the top and bottom spiders has also been modified so that the cluster of elements can be fabricated and inserted into the sleeve and then fastened to the sleeve by means of shear pins at the top. This design eliminates the necessity of making the final bottom weld with the cluster in the graphite sleeve and also gives the operator a means of removing the fuel bearing part of the assembly in case the sleeve becomes "jammed" in the channel. The operator could latch onto the top spider and shear off the pin by lifting with the service machine and not applying any load to the stainless steel cladding. After removing this part of the assembly, cutting tools or other special equipment could be inserted to remove the sleeve.

Heat Transfer and Pressure Drop

Since the Title I design of the EGCR fuel assembly was completed, much information on pressure drop and heat transfer has been obtained. The pressure drop data have been analyzed[1] and the losses associated with various components of the design determined. An extrapolation of the results of these tests to reactor operating conditions is presented below. For the case considered, the flow rate was 2400 lb/hr across the elements and the temperature rise was from 510 to 1050°F. The extrapolated pressure drop data for a stacked column of six assemblies are as follows:

---

[1]Unpublished – Allis-Chalmers report.

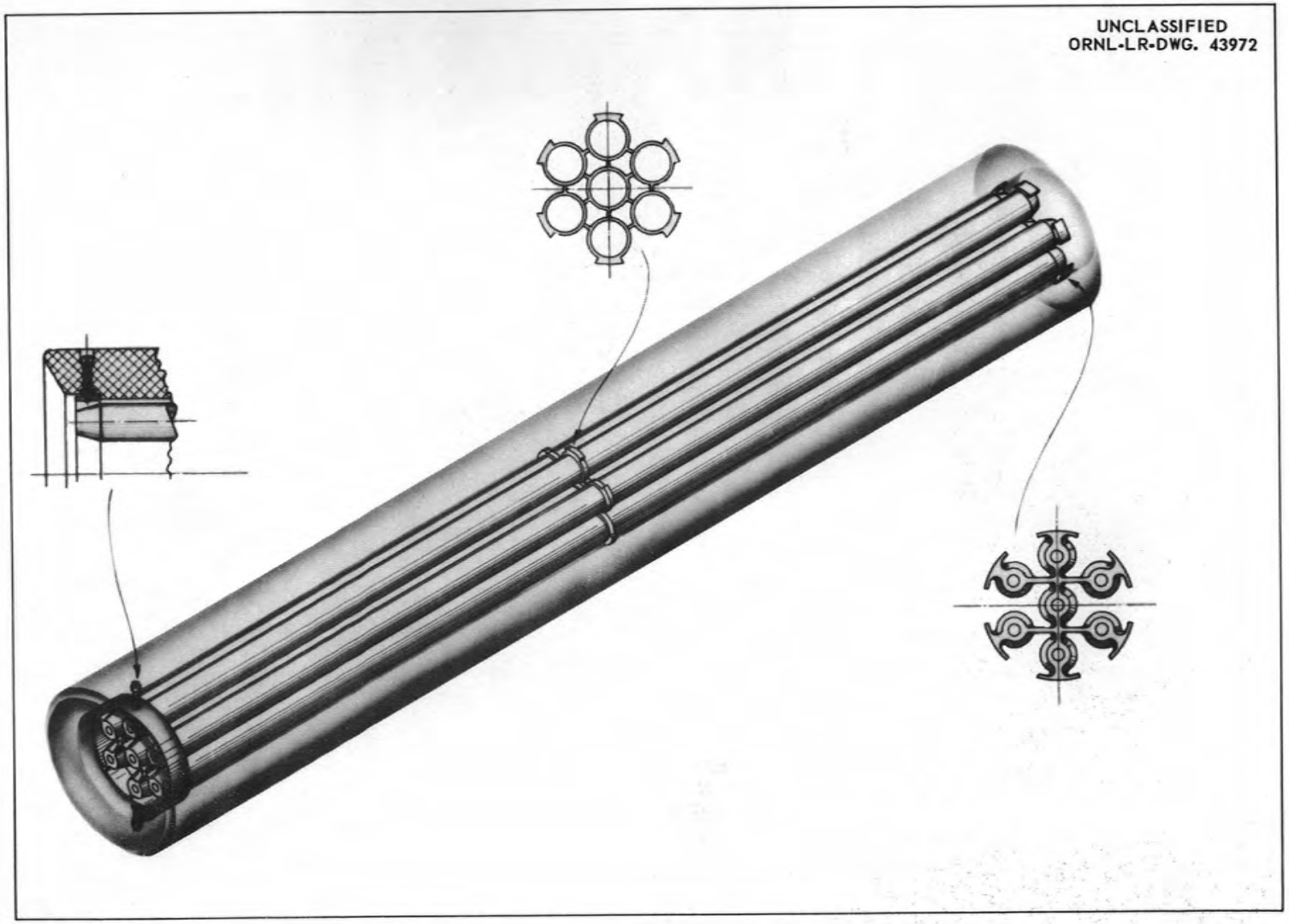

Fig. 2.1. EGCR Fuel Assembly, Modification I.

Friction loss	5.0 psi
Spacer loss	1.9 psi
Expansion and contraction loss between assemblies	1.2 psi
Entrance and exit loss to stacked assembly	0.5 psi
Total	8.6 psi

It may be seen from these data that the loss due to the spacers is a large part of the total core pressure drop. The teeth on the spacers in this case had a helix angle of 45°.

Two alternate designs are now being considered. The first is identical to the Title I design with the exception that the helix angle is reduced to 30°. Also, a small pad has been added to the tooth which is in contact with the graphite sleeve to minimize the possibility of small vibrations causing the tooth to wear or drill its ways into the sleeve. The second design is that shown in Fig. 2.1. In this design no attempt is made to mix the flow by the use of helical teeth on the spacers. The results of some preliminary heat transfer analyses of the helical spacers indicated that the helix did not aid in mixing the flow in the cluster and that these spacers reduced the flow in the central part of the cluster because of their high pressure drop.

The heat transfer test results presented previously[2] were also extrapolated to reactor conditions. These results indicate a heat transfer coefficient of approximately 300 at the exit of an assembly. One interesting part of these results is the very sharp change in heat transfer coefficient near the spacer. Although the dimensions of the assembly and the configuration of the spacers used in the tests to date have been different, preliminary results show similar heat transfer coefficients at the exit.

Fuel Handling and Coolant Flow Control

Another problem that is related to the pressure drop is the lifting force of the gas stream on the fuel assemblies. With the assemblies

[2]GCR Quar. Prog. Rep. Sept. 30, 1959, ORNL-2835, p 54.

in their normal operating positions, there is no problem. Difficulties may arise, however, during fuel charging or discharging operations when the number of assemblies in the channel is changing. The coolant flow through the core is divided into two parallel passages: (1) a small bleed flow of about 6% in the annulus between the fuel assembly sleeves and the channels through the core blocks and (2) the main flow passage through the sleeves. The bleed flow is controlled by orifices in the top dummy assembly at the top of the core. When a column of fuel assemblies is being lowered, there is no control of this flow, and the pressure drops in the passages equalize. The total flow must therefore be increased by about 30% to maintain the proper flow around the fuel elements. During this fuel-handling operation the charge machine must control the flow to the fuel channel so that sufficient coolant is supplied to prevent overheating of the elements and yet limit the flow so that the assemblies will not be lifted by the gas flow. These considerations limit the range of coolant flow to between 3000 and 4100 lb/hr.

To remove the assemblies from the channel, the charge machine inserts a jointed chute into the lower plenum, which is indexed to the desired channel. This arrangement necessitates the use of seals or close-fitting joints to prevent excess leakage between the lower plenum and the chute. The pressure drops across the core as a function of the number of assemblies in a channel are given below:

Number of Assemblies in Channel Plus the Top Dummy	Pressure Drop Across a Fuel Channel (psi)
6	14.5
5	12.3
4	10.2
3	8.0
2	5.8
1	3.6

These data are for a gas flow of 4100 lb/hr, which is the rate required to lift an assembly. The pressure drop across the top dummy is assumed

to be 0.5 psi for normal flow. As may be seen from these data, when only one assembly is left in the channel, the seals must be sufficient to maintain the pressure in the chute about 5.8 psi below that in the surrounding lower plenum of the reactor.

Temperature Cycling

Preliminary analog studies have been carried out to determine the relative temperature changes of the UO_2 fuel pellets and the stainless steel cladding during reactor power changes. Analyses of these studies indicate that the rate of change of temperature of the elements, even for very fast startups and scrams, will not cause severe strains in the cladding due to the relative thermal expansion of the cladding and the UO_2.

As mentioned previously,[3] tests have been completed in which short stainless steel specimens (without UO_2) with various end closures were cycled from 1400°F to room temperature for 1000 times with no appreciable change in dimensions or damage to the welds. The maximum heating and cooling rates of the cycles were in excess of 2000 and 1000°F/min, respectively. In another series of tests in which 6-in.-long specimens with and without UO_2 were cycled (see Chap. 4) some growth was noted, but this is believed to be due to cycling the cladding through the recrystallization temperature and not to the rate of change of the temperature.

Although the effect of the rate of change of the temperature does not appear to place rigid restrictions on reactor operations, the magnitude and number of cycles may be very important. This is due to strain cycling of the stainless steel cladding by the UO_2 during large temperature changes. The amount of strain will depend on the expansion of the UO_2 caused by the large temperature change. Tests are under way in which the expansion of the UO_2 will be measured for temperature changes similar to those expected in the reactor. A prediction of the allowable number of cycles can be based on the results of these tests.

---

[3]GCR Quar. Prog. Rep. Sept. 30, 1959, ORNL-2835, p 86.

Another result of the analog studies is that the kinetics of the system are such that in no case is it desirable to have a startup in which the rate of change of the fuel cladding temperature exceeds 150°F/min. As a corollary of this analysis, it has been concluded that the design limit for the rate of change of fuel element temperature for normal operating conditions will be 150°F/min. In the case of a reactor scram, it appears to be more important to protect the fuel elements from overheating than to limit the rate of cooling.

Thermal Analyses

An investigation was made of the temperature to be expected under a spacer if the brazed bond between the spacer and the cladding is poor. For this case the thermal conductivity of the UO_2 was neglected. The heat transfer coefficient was assumed to be 260 Btu/hr·ft^2·°F; the nominal clad surface temperature at each end of the spacer was taken to be 1500°F; and the heat flux used was 143,000 Btu/hr·ft^2. The results of the calculations are presented in Table 2.1.

Table 2.1. Cladding Temperature To Be Expected if Bond Between Spacer and Cladding Is Not Tight

Spacer Length (in.)	Cladding Temperature (°F) at Midpoint of Spacer for Radial Gap Between Spacer and Cladding of			
	0.0022 in.	0.0031 in.	0.0046 in.	0.0092 in.
1/8	1560	1580	1610	1675
3/16	1580	1610	1655	1745
1/4	1595	1630	1685	1810
3/8	1615	1660	1735	1905
1/2	1630	1675	1760	1965
3/4	1640	1695	1790	2030

Subsequent heat transfer tests have shown that the heat transfer coefficient at the spacer will be about 400 Btu/hr·ft^2·°F or greater because of the turbulence induced by the spacer. Also, since the spacer length has been set at 1/4 in. and the maximum diametral clearance

between the spacer and cladding will be about 0.055 in., a helium gap between the spacer and sleeve will not be serious.

An investigation was made of the temperature throughout an outer element near the exit end of an assembly. At this location the element is subject to the normal radial variation[4] and also to a rather sharp axial variation[5] due to flux peaking at the end of the rod. The heat generation rate as a function of position is shown in Figs. 2.2 and 2.3.

It was found that the axial gradients were essentially nil 2 in. from the end of the rod. It was also seen that the maximum temperature variation in the steel end cap was about 50 to 175°F above the coolant temperature. The temperature of the magnesium oxide spacer varied from 200 to 800°F above the ambient temperature, and the UO_2 reached a temperature of about 2200°F above that of the coolant. The rod temperatures are highest, of course, on the side of the rod where the thermal flux is highest. A three-dimensional representation of the temperature field at the exit end of an EGCR fuel rod is shown in Fig. 2.4.

The temperature variations of the surface of the stainless steel cladding are shown in Fig. 2.5. All temperatures shown are the surface temperature less the gas temperature. The curve labeled 0° represents the position facing the graphite sleeve (the highest flux region) and the curve labeled 180° is the position facing the central fuel rod. It may be seen that there is very little axial peaking of temperature (about 6°F) caused by the neutron flux peak near the end of the rod. Peripheral variations at any axial location do not exceed 80°F.

Structural Investigations

Study of Fuel Cladding Behavior Under Arbitrary Temperature Distributions

The initial studies[6,7] of the deflections and stresses in the fuel element cladding have been summarized. The studies have included shells

[4] GCR Quar. Prog. Rep. Sept. 30, 1959, ORNL-2835, p 12.
[5] Personal communication, R. E. Heineman (HAPO) to C. A. Preskitt, ORNL.
[6] GCR Semiann. Prog. Rep. June 30, 1959, ORNL-2767, p 26.
[7] GCR Quar. Prog. Rep. Sept. 30, 1959, ORNL-2835, p 24.

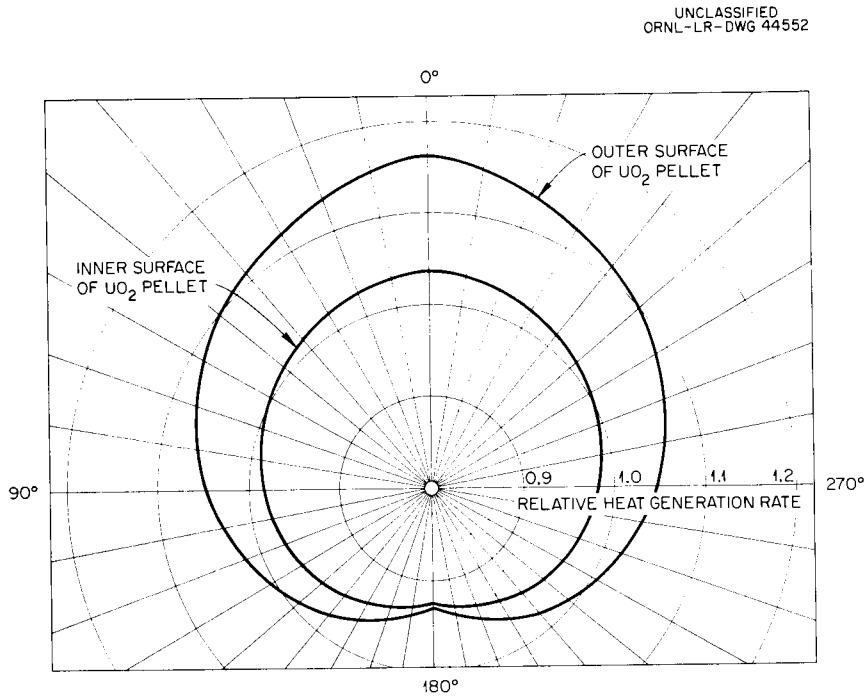

Fig. 2.2. Angular and Radial Variation of Heat Generation Rate in an Outer Element Near the Exit End of a Fuel Assembly.

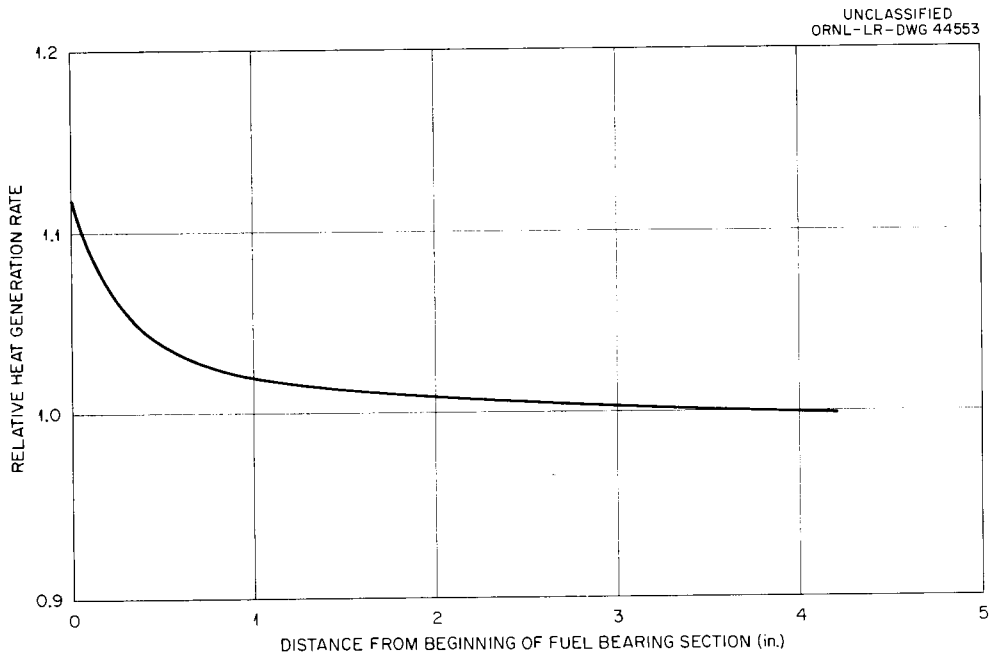

Fig. 2.3. Axial Variation of Heat Generation Rate in an Outer Element Near the Exit End of a Fuel Assembly.

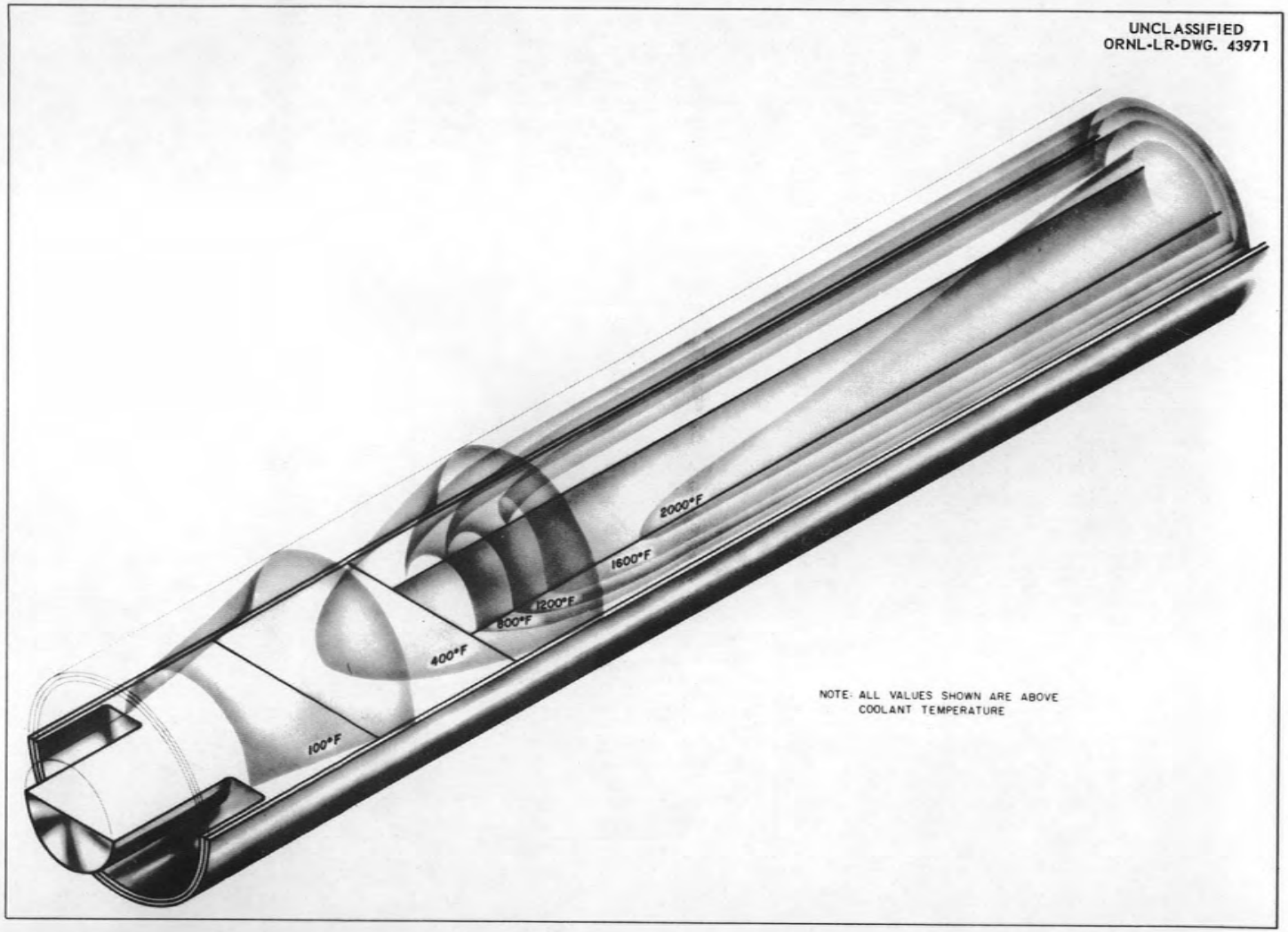

Fig. 2.4. Three-Dimensional Temperature Structure at the Exit End of an EGCR Fuel Rod.

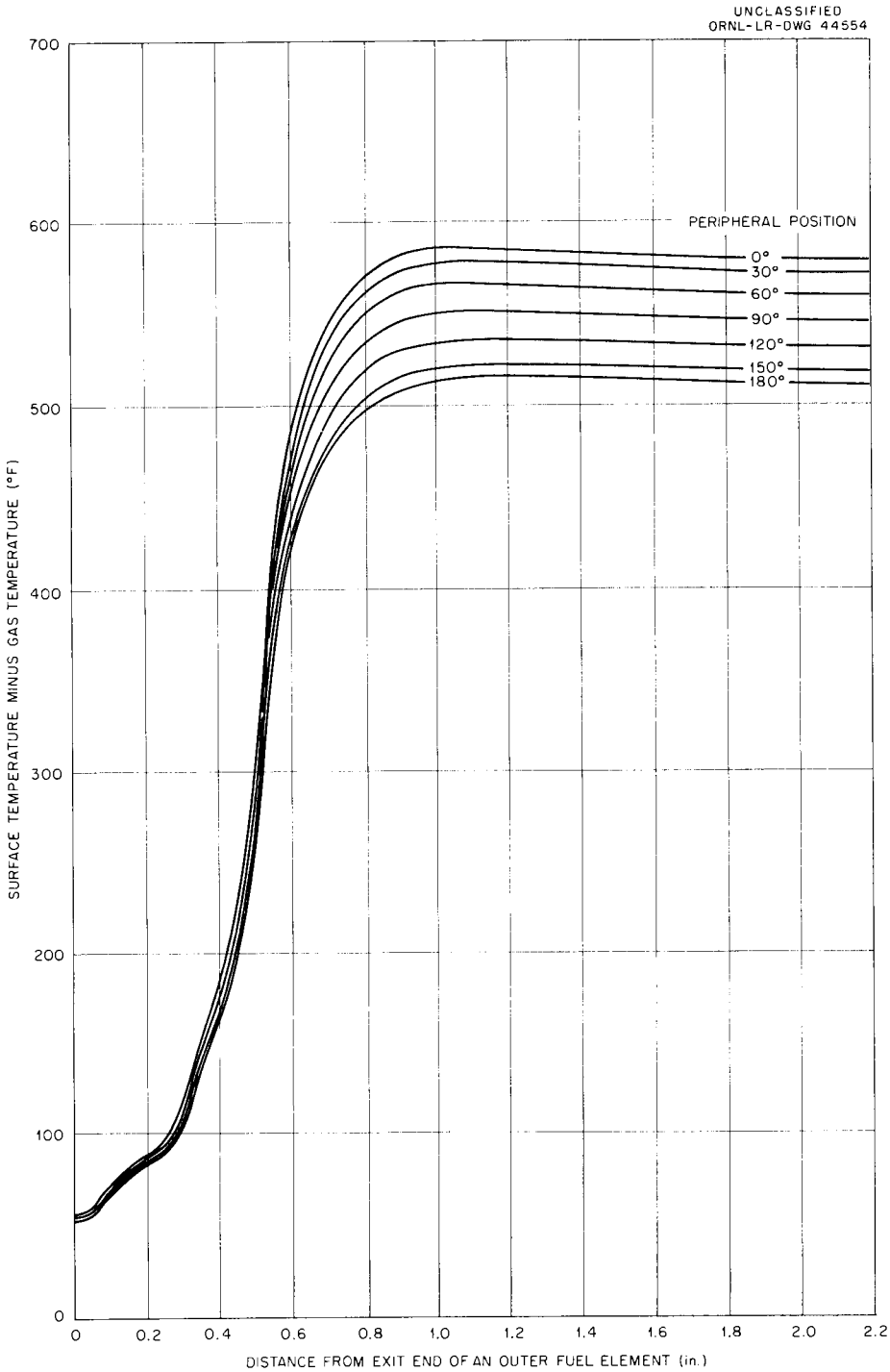

Fig. 2.5. Surface Temperature as a Function of Distance from Exit End of an Outer Fuel Rod for Various Peripheral Positions.

with the temperature distributions listed in Table 2.2. The last two functions of Table 2.2 are forms of the generalized equation

$$t = t_0F(b \cos \theta + c \sin \theta + d \sin 2\theta) \quad , \tag{1}$$

which was selected for representing profiles obtained from the heat transfer experiments. Here, t_0, b, c, and d are arbitrary constants, F is a function of the dimensionless axial coordinate $y = x/L$, θ and x are the angular and axial coordinates, and L is the length of the tube.

Table 2.2. Temperature Functions Used in Cladding Analyses

Temperature Function	Remarks
$t = t_0F \cos \theta$	The temperature is linear with respect to the 0 to 180° diameter and constant along the length
$t = t_0F(0.5 + \frac{\theta}{\pi})$; $0 \leq \theta \leq 180°$	The temperature is linear along the circumference and constant along the length
$t = t_0F \cos 3\theta$	The temperature is constant along the length and the circumferential temperature profile is that of a three-leaf rose
$t = t_0 \cos (\theta + 2\pi y)$	The temperature is linear along a reference diameter which rotates one revolution along the length of the shell
$t = t_0F(0.0632 \cos \theta - 0.4969 \sin \theta + 0.162 \sin 2\theta)$	The temperature is constant with length
$t = t_0y(0.0632 \cos \theta - 0.4969 \sin \theta + 0.162 \sin 2\theta)$	The temperature is linear with length

Subsequently, the following temperature distributions were included in the investigations:

$$t = t_0(0.5 \cos \theta + 2.0 \sin 2\theta) \tag{2}$$

and

$$t = t_0 \cos\theta \begin{pmatrix} 0 & 0 \leq y \leq 0.375 \\ \sin \dfrac{y - 0.375}{0.25} \pi & 0.375 \leq y \leq 0.625 \\ 0 & 0.625 \leq y \leq 1.0 \end{pmatrix} \qquad (3)$$

The function given in Eq. 2 is another form of the one given in Eq. 1. The maximum diametral temperature differential in this case occurs along the 0 to 180° diameter, and the maximum temperature occurs at an angle θ of approximately 42.5°. The results are being analyzed primarily to determine the plane of bowing. In the cases examined previously, the bowing has been in the diametral plane containing the maximum temperature difference.

The second function, Eq. 3, gives a distribution that is representative of the axial temperature variation caused by the central spacer in the resistance-heated-tube heat-transfer experiment.[8] Hence, only the changes in displacements and stresses caused by the spacer are evaluated using Eq. 3; the total results are obtained by superposition.

The lateral displacement, w, for the second case is in excellent agreement with the results from elementary beam theory, which yields the following expressions:

$$w = \frac{\alpha\, \Delta t\, L^2}{a} \frac{0.5}{\pi} y \qquad 0 \leq y \leq 0.375$$

$$w = \frac{\alpha\, \Delta t\, L^2}{a} \left(\frac{0.0625}{\pi^2} \sin\beta + \frac{0.25}{\pi} y + \frac{0.09375}{\pi} \right) \qquad 0.375 \leq y \leq 0.5 \qquad (4)$$

In these equations, α is the coefficient of thermal expansion, Δt is the maximum diametral temperature difference, a is the radius, and

$$\beta = \frac{y - 0.375}{0.25} \pi \quad .$$

---

[8] GCR Quar. Prog. Rep. Sept. 30, 1959, ORNL-2835, p 54.

For most practical cases, the maximum stresses corresponding to the temperature function in Eq. 3 can be summarized by the following expressions:

$$\left.\begin{array}{l}\text{axial membrane stresses} = \sigma_m = -0.21\ E\alpha t_0 (h/a)^2 \cos\theta \sin\beta \\ \text{axial and circumferential bending stresses} = \sigma_B = -0.746\ E\alpha t_0 (h/a) \cos\theta \sin\beta\end{array}\right\} \begin{array}{l} 0.375 \leq y \leq 0.625, \\ \text{otherwise, } \sigma = 0\end{array} \quad (5)$$

where h is the thickness of the shell and the other quantities are those previously defined.

Tests of Metal-Clad Graphite Bodies

The first test of a stainless-steel-clad graphite body[9] was completed. In this test, the specimen was mounted in a helium-filled furnace in which the pressure was held constant at 300 psig. A vacuum of approximately 30 in. Hg existed inside the metal envelope at the beginning of the test. The clad assembly was heated from room temperature to 600°F at the lower end and 1300°F at the top. Steady-state conditions, with a linear temperature variation along the length of the unit, were achieved in 12 hr and were held for 36 hr. The cooling phase of the cycle required 6 hr.

At the end of the first cycle, the specimen was removed from the furnace in order to replace two thermocouples which had failed. An examination of the element revealed cracks in the cladding. The vacuum gage for indicating the pressure inside the metal envelope was found to be defective, and, since it did not signal rupture of the cladding, it was not possible to determine when the first crack or cracks developed.

The element is shown in Fig. 2.6. The largest crack is along the helical groove near B in the figure; it is shown again in Fig. 2.7. This was the only crack along a groove. A crack was found along the axial wrinkle that was formed at the time the cladding was forced into the grooves in the graphite. It lies in the region of A in Fig. 2.6 and is shown in Fig. 2.8. Although these were the major regions of failure, there were indications of others at various positions along the axial wrinkle.

---

[9] GCR Quar. Prog. Rep. Sept. 30, 1959, ORNL-2835, p 36.

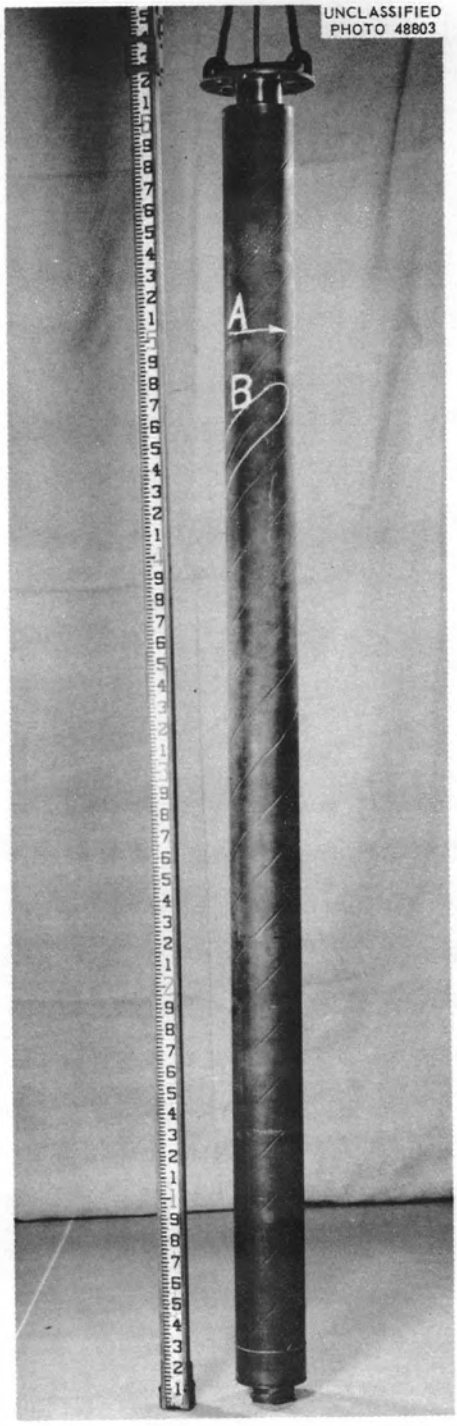

Fig. 2.6. Metal-Clad Graphite Body Showing Cracks along Helical Groove at B and at A.

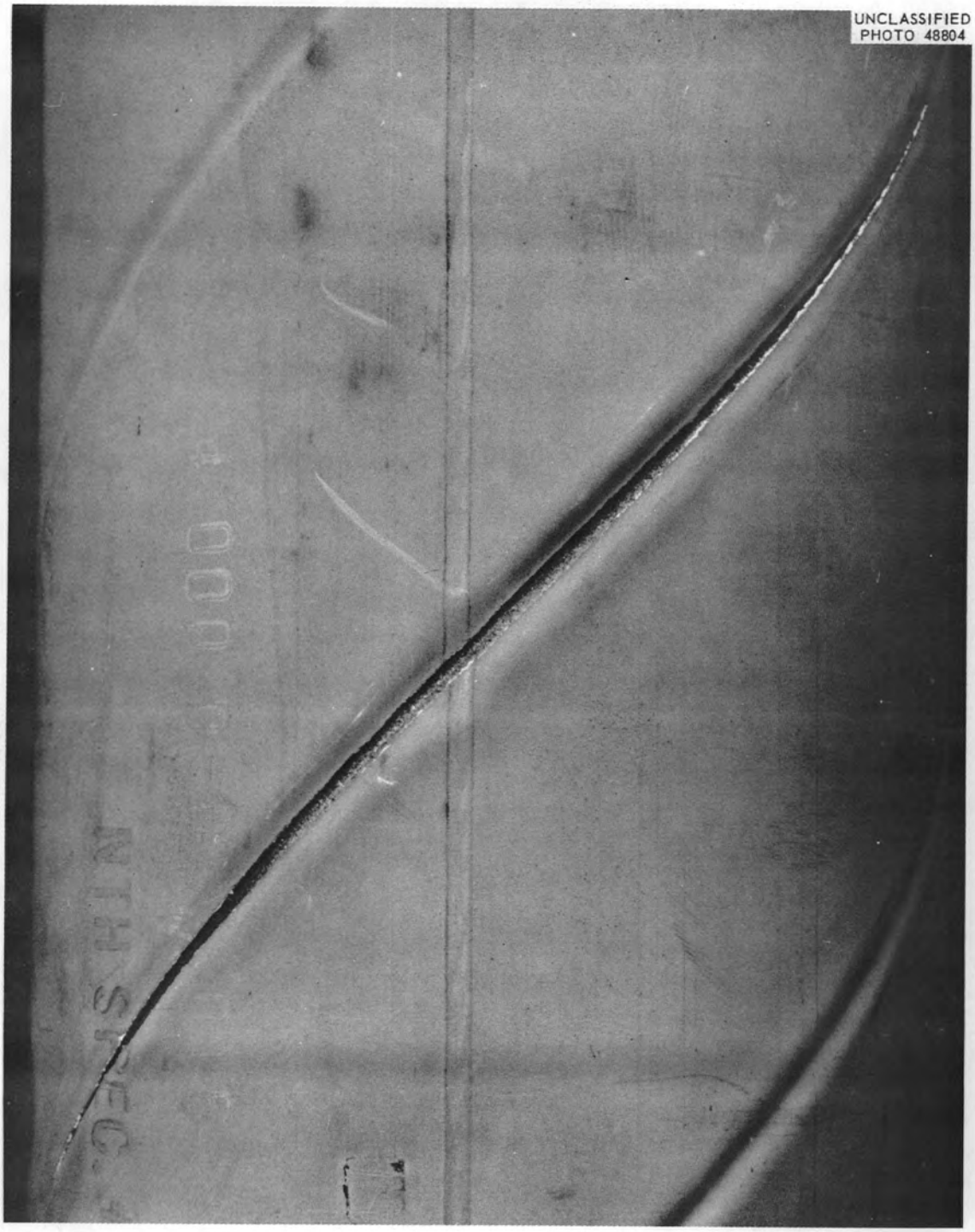

Fig. 2.7. Enlarged View of Crack at B in Fig. 2.6.

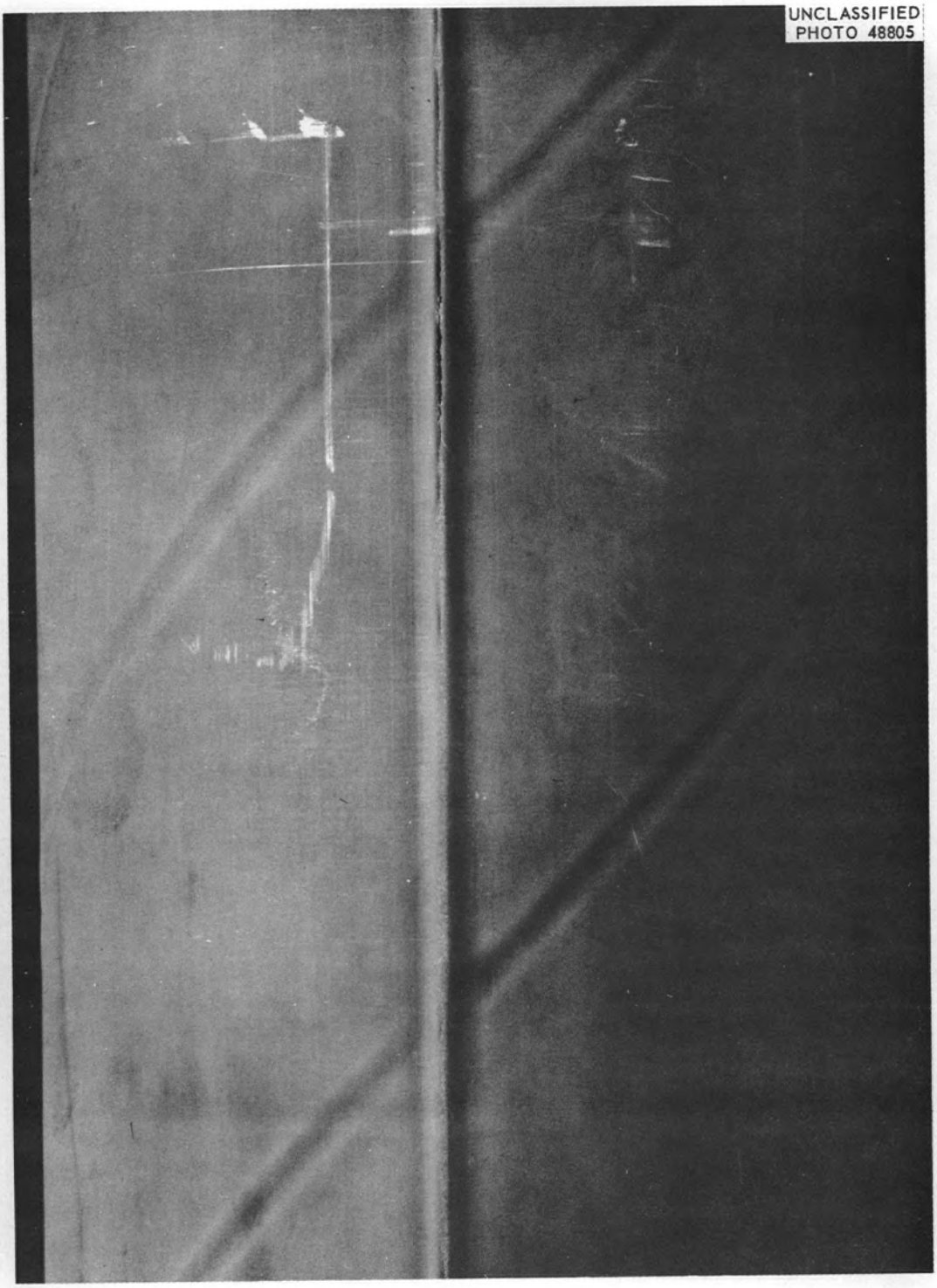

Fig. 2.8. Enlarged View of Cracks at A in Fig. 2.6.

It is evident that the matched helical grooves in the graphite and metal cladding did not adequately accommodate the different dimensional changes of the two materials, and rupture occurred near the high-temperature end where the difference was greatest. However, no detectable changes in either the number of wrinkles or their patterns were caused by the thermal cycle.

Coolant Channel Flow Adjustment and Pneumatic Load Sensing by EGCR Charge Machine

The analyses of a variety of EGCR operating conditions have demonstrated that the effects on fuel capsule surface temperatures of the various flux patterns which can be predicted are serious enough to require either a reduction in reactor power for some conditions or an adjustment of the coolant flow through individual fuel channels. Transient and long-term operating conditions attendant upon installation or removal of experimental assemblies are examples of the situations to which reference is made. The present design of the EGCR permits adjustment of coolant flow in individual fuel channels by the relatively cumbersome process of removing the orifice-fitted bottom dummy assembly and the six fuel assemblies from the selected channel and replacing the bottom dummy assembly with a new one fitted with an orifice of the required size.

A study of this problem has led to a design concept for a new bottom dummy fitted with an adjustable nozzle and a design for a new ram head for the flexible fuel ram of the charge machine that would be capable of adjusting the nozzle in place in a fuel channel. The proposed design also incorporates in the fuel ram head a pneumatic load-sensing device to replace the much more cumbersome fuel column weighing device presently proposed. The load-sensing device functions to assure the operator that one or more fuel assemblies has not jammed and remained unsupported in a fuel channel during fuel removal.

Procedures for Decontamination of Charge and Service Machines

An experimental program for the development of methods for decontaminating the gas-cooled reactor charge and service machines has been started. Two phases of the problem being explored are the determination of the amount and nature of the contamination to be expected and the development and testing of decontaminating agents which have a suitably low corrosion rate on possible materials of construction.

The contamination of metals by volatile fission products diffusing out of irradiated UO_2 at high temperature will be studied by interposing metals in the helium gas stream in in-pile experiments. Room-temperature studies will also be made of specimens contaminated by helium that has passed over UO_2 under irradiation in the ORR. Equipment for these studies is under construction.

Contamination of metals by irradiated UO_2 in fine powder form like that which would probably be blown into the charge and service machines after a fuel element rupture is being simulated under rigorous conditions by coating metals with finely powdered UO_2 and UO_3 in liquid suspension, drying, sealing in a capsule, and irradiating in the ORNL Graphite Reactor. The irradiated capsule is then heated at 300°C, while still sealed, for several hours. After radioactive and thermal cooling until the capsule can be handled and opened, the metal pieces are removed and scanned by a scintillation spectrometer. Decontamination tests are then made, with the progress of decontamination being followed by a broad-range GM survey meter and by a spectrometer.

One capsule has been irradiated in which the oxide was UO_3 and the metal specimens were carbon steel, type 347 stainless steel, and type 2S aluminum. After 6 hr of irradiation and 5 hr of cooling, the gamma radiation from 0.45 g of depleted uranium was 10 r at 3 in. After 5 days of cooling the radiation was only 100 mr at contact. Thus a high degree of "decontamination" can be expected from cooling alone when time is available. The oxide was readily dissolved by boiling the metals in a solution of 1 ml of concentrated HNO_3 in 1 liter of water. The

corrosion rates were 0.12, <0.001, and 0.007 mil/hr for carbon steel, type 347 stainless steel, and type 2S aluminum, respectively. Gamma decontamination was poor, however; the decontamination factors were 1, 2, and 3, respectively.

Further tests will be made with enriched UO_2. Decontamination by steaming and spraying with various reagents will be evaluated as soon as the apparatus is available.

EGCR Hazards Evaluations

Core Levitation in the EGCR in Case of Main Coolant Pipe Failure

Rupture of the main exit coolant pipes in the EGCR would result in a rapid blowdown of the main reactor coolant that could lead to an excessive lifting pressure differential across the core. If this force is sufficiently large, the graphite stack could be lifted and/or the fuel elements and the control rods could be blown out. If the graphite stack were lifted, subsequent derangement of the graphite blocks could make later insertion of the control rods impossible.

An analysis was therefore performed to estimate the extent of the core damage in case of double-ended and single-ended coolant pipe failures.[10] A double-ended failure is one that exposes an area equal to that of two pipe ends. A single-ended pipe failure is taken as one that exposes an area to flow of one-half that of a double-ended failure. The reactor cooling system was idealized as being split into six volumes, with flow resistances between the volumes. The six volumes consisted of the upper plenum and the lower plenum of the main pressure vessel, with the core as the resistance, and each of the two steam generators split into two volumes, upper and lower, separated by the whole steam generator gas-side flow resistance. Six nonlinear first-order differential equations were written describing a mass balance around each volume as a

[10] M. H. Fontana, Core Levitation in the EGCR in Case of Main Coolant Pipe Failure, ORNL CF 59-8-2 (Aug. 4, 1959).

function of time after the pipe breaks. The ORNL Reactor Control Analog Computer facility was then employed to solve the equations and thus obtain the pressure drop across the core as a function of time. This pressure drop was then used to calculate the attendant displacement of the core. Various values of blower resistance were used because of the difficulty of predicting blower response to pressure surges.

It was found that a double-ended pipe failure would cause a pressure differential across the core of 35 to 42 psi in about 0.1–0.2 sec after the break. This could result in vertical displacement of the core of from 4.5 to 15 ft if it were free to do so. A single-ended failure would cause a pressure differential of from 14 to 21 psi, depending on the behavior of the blowers. The vertical displacement of the core would be from 0.05 ft for the case of no coolant flow prior to the break to ~0.2 ft for the case in which the blowers continue to operate. The true value lies somewhere between these extremes. In all cases, the period during which a lifting force exists is only about 0.4 sec, but the impulse is sufficient to damage the core.

It is obvious that the levitation of the core as described above must be prevented, although it is not obvious how this may best be accomplished. Consideration is being given to several proposals, including (1) quick closing valves, (2) core bypass relief valves, (3) a core design to accommodate such forces, and (4) preventing the occurrence of such an extreme accident.

Pressure and Temperature in the EGCR Experimental Loop Cell in Case of Accidental Release of Main Reactor Coolant

The EGCR is designed so that eight separate experimental loops pass through the core, the main pressure vessel, and individual equipment cells external to the containment shell. The cells are constructed of steel-lined concrete designed to hold a pressure of 12 psig, which is sufficient to contain the loop coolant in case of a piping failure. Loss of the loop coolant could, however, result in overheating of the test specimen and the adjacent piping. Along with the collapsing pressure of

the main core coolant, this could lead to failure of the loop within the core and expulsion of the main coolant into the experimental cells.

This occurrence would cause the cell pressure to rise rapidly to above the design point unless relieved. Since the loop cooling gas could be highly contaminated, it is imperative that it be contained. This will be accomplished by installing blowout disks to vent the experimental cell atmosphere into the containment shell in the event the cell pressure exceeds 12 psig.

In the analysis of this situation,[11] a double-ended pipe failure was assumed both within the core and the equipment cell, because this is clearly a worst case. The cell pressure and temperature and the blowout area required to vent the flow into the containment shell were calculated with the use of an IBM-704 machine. The key results are summarized in Table 2.3. With flow restrictions placed in the lines, the required blowout disk area can be obtained with one 28-in.-dia disk or two 19.8-in.-dia disks per equipment cell.

---

[11]M. H. Fontana, Pressure and Temperature in the EGCR Experimental Loop Cell in Case of Accidental Release of Main Reactor Coolant, ORNL CF 59-10-76 (Oct. 20, 1959).

Table 2.3. Results of Loop Accident Analysis

Condition*	Time to Rupture Disk Actuation (sec)	Rupture Disk Area** (ft^2)	Peak Cell Pressure (psia)	Peak Cell Temperature (°F)
1	0.4	8.63	26.7	305.7
2	0.8	4.29	26.7	304.4

*Condition 1: double-ended failure in both the core and the equipment cell.

Condition 2: same as condition 1 except for 3.3-in.-dia orifice placed in both lines at junction with containment shell.

**Based on discharge coefficient of 0.95. The true area required is found by scaling the effective discharge coefficient for the particular kind of blowout disk employed.

3. EXPERIMENTAL INVESTIGATIONS OF HEAT TRANSFER AND FLUID FLOW

Resistance-Heated-Tube Heat-Transfer Experiment

Data obtained previously[1] in the study of heat transfer in the septafoil geometry showed an unexpected skewness in the circumferential temperature profiles which, it was speculated, was associated with the flow entrance configuration. Since it is the purpose of this investigation[2] to develop thermomechanical stability criteria for the tubes in a seven-tube cluster, the precise knowledge of the temperature distributions for the base condition (tubes restrained to the design position at the mid-plane) is of major importance. Thus the existence of a rotational velocity component at the channel entrance introduces a serious complication in relation to the interpretation of succeeding experiments with bowed tubes. A considerable effort has been made during the past months to understand this situation and to correct the condition. As a result of this work (described in detail in the following section on mass-transfer experiments), the experimental channel was modified to include the most promising of the entrance arrangements studied. Heat-transfer tests were then resumed.

Initial data (designated series 2) on the mean inside surface temperature of the peripheral tube in the No. 2 position[1] are given in Table 3.1 for 12 axial locations ranging from the channel inlet to the outlet and are compared with previous results (series 1). The over-all mean heat flux for this series of runs was 6700 Btu/hr·ft^2, with a flow rate of 2160 lb/hr. The air inlet temperature was 63°F, and the average axial temperature rise was 66.5°F. The lower inlet temperature (of the order of 45°F less than in earlier experiments) derives from the use of a new air supply; the original rotary blower[3] has been replaced by a

---

[1] GCR Quar. Prog. Rep. Sept. 30, 1959, ORNL-2835, p 54-63.

[2] GCR Semiann. Prog. Rep. June 30, 1959, ORNL-2767, p 75.

[3] GCR Semiann. Prog. Rep. Dec. 31, 1958, ORNL-2676, p 26.

Table 3.1. Axial Variation in Mean Inside Surface Temperature of Tube 2

L/d_e	Mean Inside Surface Temperature (°F)	
	Series 1	Series 2
0	248	262
5	322	272
7.5	339	290
10	359	301
15	382	319
17.9	381	325
20	302	238
22.5	347	278
25	380	317
30	418	356
35	441	387
38	446	394

plant instrument-air line capable of supplying up to 4000 lb/hr of dry air at 90 psig. There is some question as to the validity of the temperature value at the channel inlet; this will be rechecked in the near future. The data obtained with the new entrance configuration are in reasonable agreement with the earlier results, as shown in Fig. 3.1. The lower surface temperatures of the series 2 experiment arise from (1) a lower air inlet temperature, as mentioned above, and (2) a somewhat higher Reynolds modulus (77,000 as compared with 67,600 for series 1).

Circumferential temperature profiles have not been completed for all seven tubes at the same axial position; thus, a complete comparison of the two sets of data with respect to skewness is not possible. For tube 2 at the $L/d_e = 17.9$ elevation, the circumferential temperature distributions for series 1 and 2 are compared in Table 3.2 and Fig. 3.2. The general pattern for series 2 appears to be somewhat more in agreement with the expected profiles. There is an indication of minima in the region 100 to 120 deg and 250 to 275 deg (ideally these should

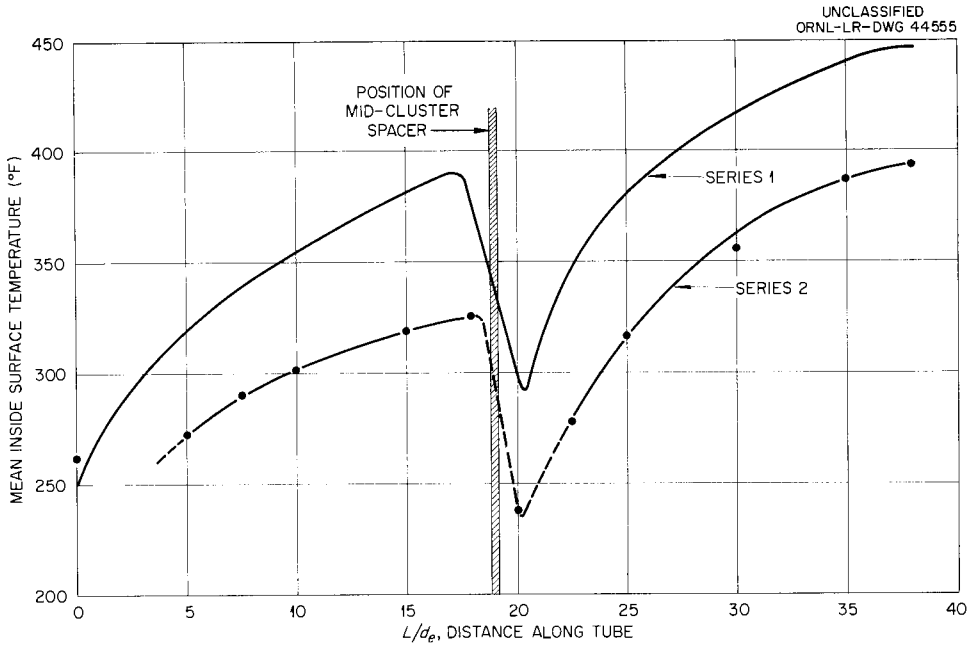

Fig. 3.1. Axial Variation of the Mean Inside Surface Temperature of Peripheral Tube 2.

probably appear at 120 and 240 deg). The primary maximum, anticipated at 180 deg, occurs at 150 deg; the secondary maxima (60 and 360 deg) appear at 80 and 280 deg, respectively. The over-all result is a strong indication of the dependence of the circumferential temperature distribution on the inlet conditions. A profile at the $L/d_e = 35$ position (near the cluster outlet) is given in Fig. 3.3; the continued clockwise rotation of the pattern is apparent. Note, however, that all the anticipated maxima and minima are in roughly the expected locations. This observation of the continuing development of the temperature profiles along the cluster length points up the postulate advanced previously[1] that the entire cluster lies within the thermal entrance region.

The local heat-transfer coefficients have been estimated based on the assumption that the air temperature varies linearly along the cluster length and is uniform in any plane perpendicular to the direction of flow,[1] and the results are presented in Fig. 3.4. For the region downstream of the central spacer, the asymptotic (established flow) value of the heat-transfer coefficient is 26 $Btu/hr \cdot ft^2 \cdot °F$.

Table 3.2. Circumferential Variation in Inside Surface Temperature of Tube 2 at $L/d_e = 17.9$

Angular Position[a] (deg)	Temperature[b] (°F)	
	Series 1	Series 2
0	5.5	1.6
20	11.2	5.3
40	15.6	11.5
60	20.7	14.6
80	21.5	16.5
100	25.8	16.8
120	29.6	19.5
140	31.3	23.0
160	29.7	23.2
180	23.8	22.6
200	18.1	21.3
220	15.1	19.5
240	11.8	17.7
260	7.5	14.7
280	5.0	12.9
300	1.8	1.5
320	0	11.5
340	1.2	0

[a]The angular position on the tube surface was chosen such that the 0-deg point on a peripheral tube was on the side adjacent to the central tube (corresponding to the points of closest approach of the tubes to each other) and was measured in a clockwise direction facing downstream, that is, in the direction of flow. The 0-deg location on the central tube was matched to the 0-deg position for tube 5.

[b]Listed in °F above the minimum surface temperature for the tube.

Mass-Transfer Measurements

Previous isothermal mass-transfer studies[1] indicated that the surface temperature asymmetries observed in the heat-transfer experiments might be due, in part, to nonuniformities in the flow through the septafoil cluster. Therefore, a systematic investigation of the effect of minor changes in the entrance geometry on mass transfer in the model-3

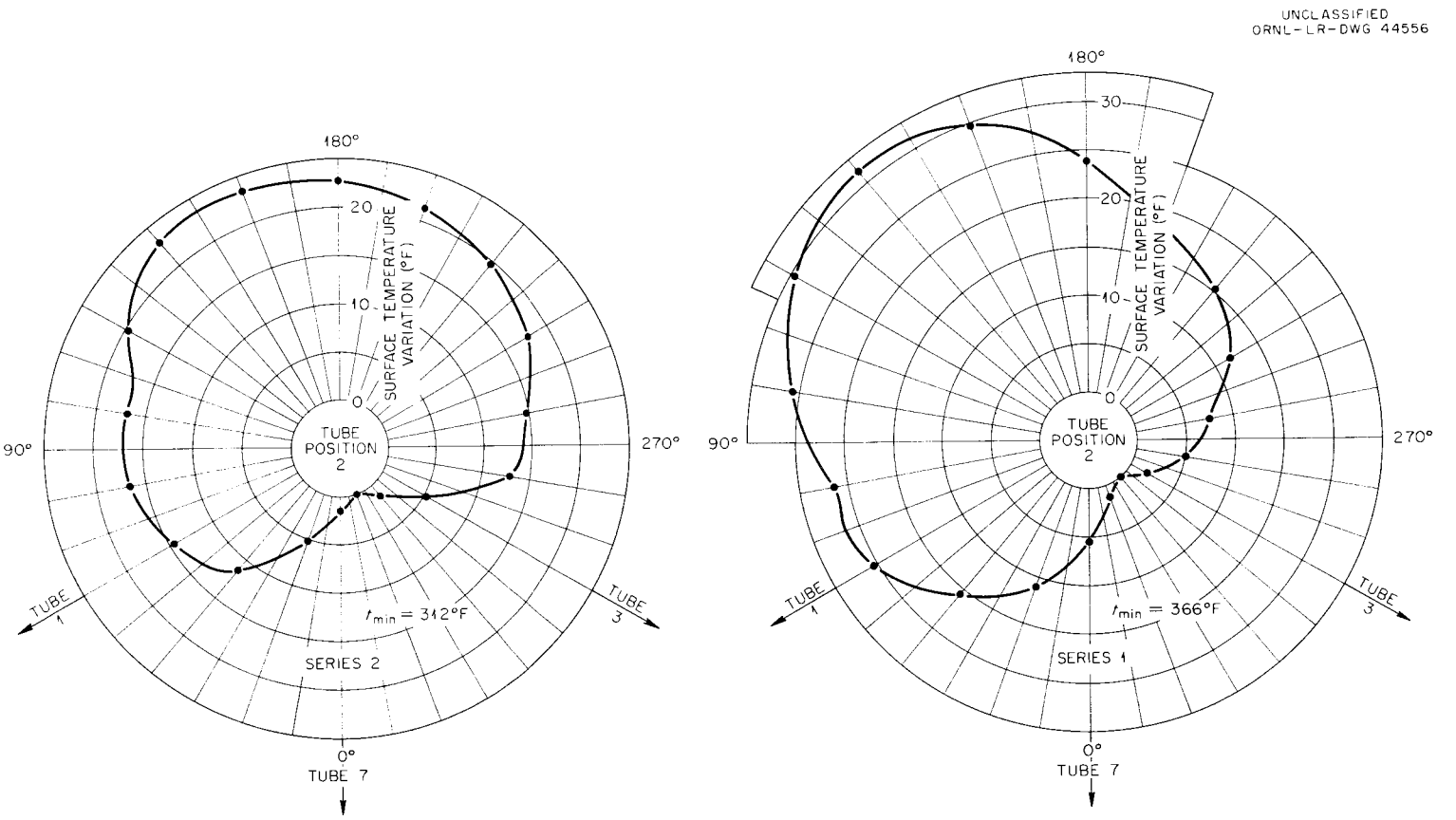

Fig. 3.2. Comparison of Circumferential Temperature Profiles from Series 1 and Series 2 Experiments; Peripheral Tube 2 at L/d_e = 17.9 Level.

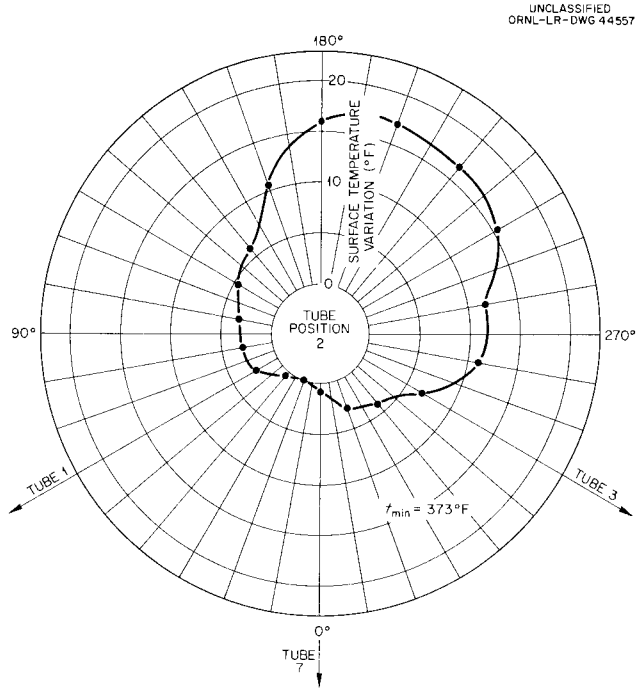

Fig. 3.3. Circumferential Temperature Profile for Peripheral Tube 2 at L/d_e = 35 Level; Series 2.

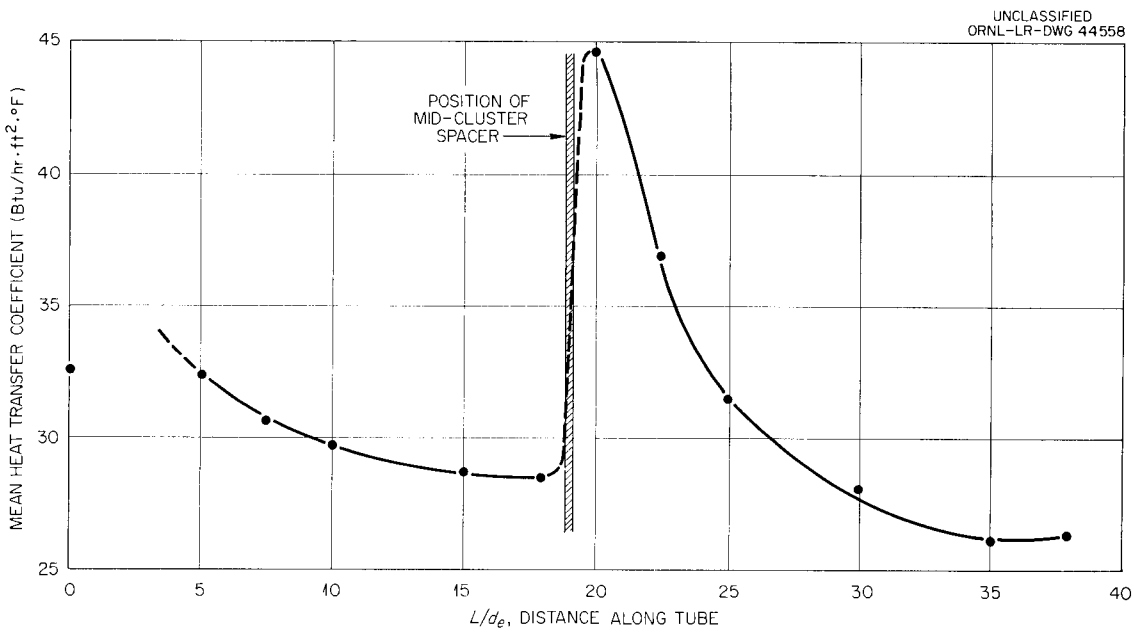

Fig. 3.4. Axial Variation of the Mean Heat-Transfer Coefficient for Peripheral Tube 2; Series 2.

heat-transfer apparatus was initiated. Following a series of tests with various entrance arrangements, it was established that a set of three coaxial screens (see Fig. 3.5) located within the inlet plenum were of maximum effectiveness in reducing the rotational component of the entrance flow. This rotational aspect of the flow probably arises from the right-angle entrance to the upper plenum. Flow instabilities (such as non-uniform separation) in the plenum inlet diffuser will lead to swirl flow in the plenum itself. The concentric screen concept is an attempt to alleviate this condition by introducing sufficient flow resistance at the channel inlet to equalize the pressure distribution in the plenum.

Three cotton threads that extended about 10 in. into the channel were cemented to the central weir at positions radially opposed to peripheral tubes 2, 4, and 6 to indicate the flow at the channel inlet. Deflection of the threads was observed through the Pyrex wall of the test unit. Entrance configurations which visually appeared to generate straight flow were then studied in detail by the mass-transfer technique. The best arrangement of screens and baffles, as mentioned above, was that shown in Fig. 3.5. This arrangement consisted of a central weir 5 in. in diameter and 3 1/8 in. in height (item 1 in Fig. 3.5) that was concentric with the septafoil and which created a 7/8-in.-wide gap between the weir and the top of the inlet plenum chamber. The central weir was surrounded by three coaxial stainless steel screens (16 × 16 × 0.023 in.), with diameters of 5 1/8 in., 6 1/4 in., and 7 1/2 in., that extended the full height of the plenum chamber (items 2, 3, and 4 of Fig. 3.5). A curved baffle plate (item 5 of Fig. 3.5) of plenum height was installed contiguous with the outermost screen and was positioned directly opposite the plenum inlet. In the final configuration, the width of this baffle was 3 in. The effects of various orientations and widths of this baffle on the channel flow were studied visually. As may be seen from Table 3.3, slight changes in the positioning or width of the baffle strongly affected the flow distribution in the channel.

Two mass-transfer tests were made with the 3-in.-wide baffle diametrically opposite the plenum inlet. The results are shown in

Table 3.3. Angular Displacement of Flow Direction Indicating Strings for Various Widths and Orientations of Plenum Baffle

Thread Location (Adjacent to Tube No.)	Baffle Width (in.)	Thread Deflection (deg)[a]				
		Rotation of Baffle from Centerline of Plenum Chamber				
		1-in. CCW[b]	1/2-in. CCW	Centered	1/2-in. CW[b]	1-in. CW
2	4	<5 CCW	5 CCW	5 CCW		
4	4	10 CCW	5 CCW	5 CCW		
6	4	10 CW	5 CW	10 CW		
2	3 1/2	0		0		
4	3 1/2	0		5 CCW		
6	3 1/2	10 CW		0		
2	3		0	0	0	
4	3		0	0	5 CCW	
6	3		5 CW	<5 CW	0	
2	2 1/2	<1 CW	0	0	0	1 CW
4	2 1/2	<5 CCW	<1 CCW	5 CCW	<1 CW	1 CCW
6	2 1/2	5 CW	<1 CW	<1 CW	<1 CW	1 CW
2	2	<1 CCW	0	1 CW		
4	2	5 CCW	1 CCW	1 CCW		
6	2	5 CW	5 CW	5 CW		

[a]All angles are measured looking in the direction of flow.

[b]CCW indicates counterclockwise and CW indicates clockwise.

Fig. 3.6 (mass transfer runs 1 and 2) for the peripheral tube in the No. 2 position at the $L/d_e = 17.9$ level. The Reynolds modulus, based on the free-flow area perpendicular to the channel axis, was of the order of 68,000. After completion of the second mass-transfer run, the Pyrex channel was accidentally broken. It was replaced, and a third test was made to determine whether the slight dimensional differences between the channels had a significant effect on the mass-transfer pattern. The results are presented as mass-transfer run 3 in Fig. 3.6. Heat-transfer experiments were then resumed, and the circumferential variation in the heat-transfer coefficient was calculated, based on a uniform air temperature. The results of the calculations are compared in Fig. 3.6 with the results of the mass-transfer experiments.

The mass-transfer data of Fig. 3.6 indicate that the use of concentric screens within the inlet plenum has not been effective in eliminating the nonuniform flow characteristics associated with the model-3 heat-transfer apparatus. The mass removal pattern of run 1 shows that slightly counterclockwise rotating flow exists near the channel mid-plane (forward stagnation point at 330 deg). On the other hand, run 3 suggests clockwise rotating flow with a forward stagnation point at 30 deg. For run 2, the flow appears to be parallel to the longitudinal axis of the tube. Two possible explanations for the cross flow can be advanced: (1) general swirl in the flow associated with the entrance configuration and (2) radially outward transfer of fluid from the inner to the outer flow passages, as dictated by the relative friction losses in the two flow regions. If the latter is the dominant mechanism, patterns of the type observed for run 2 should result for all tubes at all levels; unfortunately, data are not now available to check this. An attempt is being made to analytically estimate the magnitude of such radial flow. At this time, however, it appears that the major effect is associated with the entrance, as discussed above. The profiles agree, in general, with those observed in an earlier experiment[4] in which a helical flow

[4] GCR Semiann. Prog. Rep. June 30, 1959, ORNL-2767, p 80-91; see also J. L. Wantland and R. L. Miller, Heat Transfer in Septafoil Geometries by Mass-Transfer Measurements, ORNL CF 59-6-9 (June 1959).

UNCLASSIFIED
ORNL-LR-DWG 44559

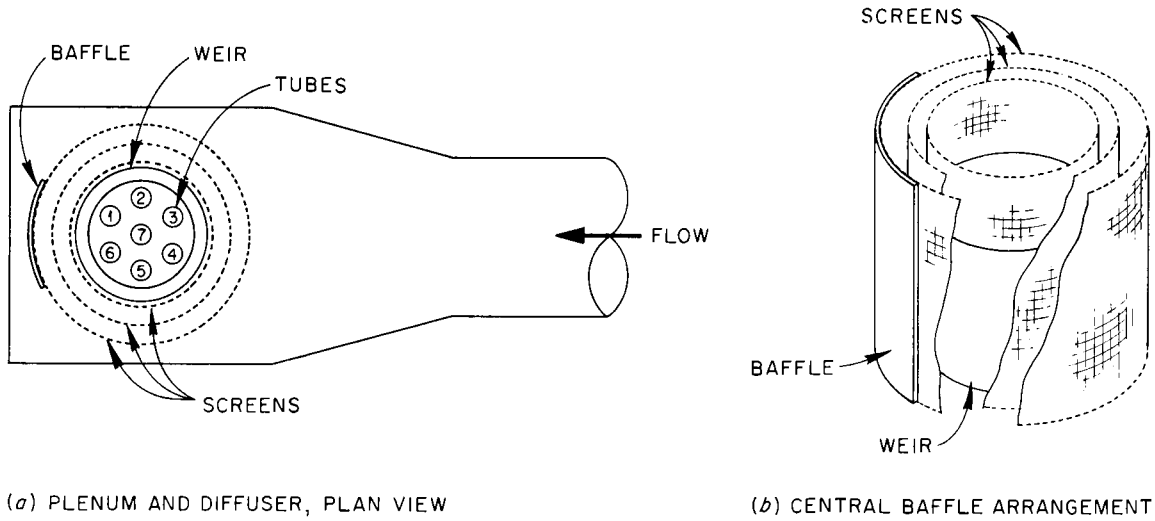

Fig. 3.5. Schematic Diagram of the Modified Inlet Plenum Chamber of the Model 3 Experimental Heat-Transfer Apparatus.

UNCLASSIFIED
ORNL-LR-DWG 44560

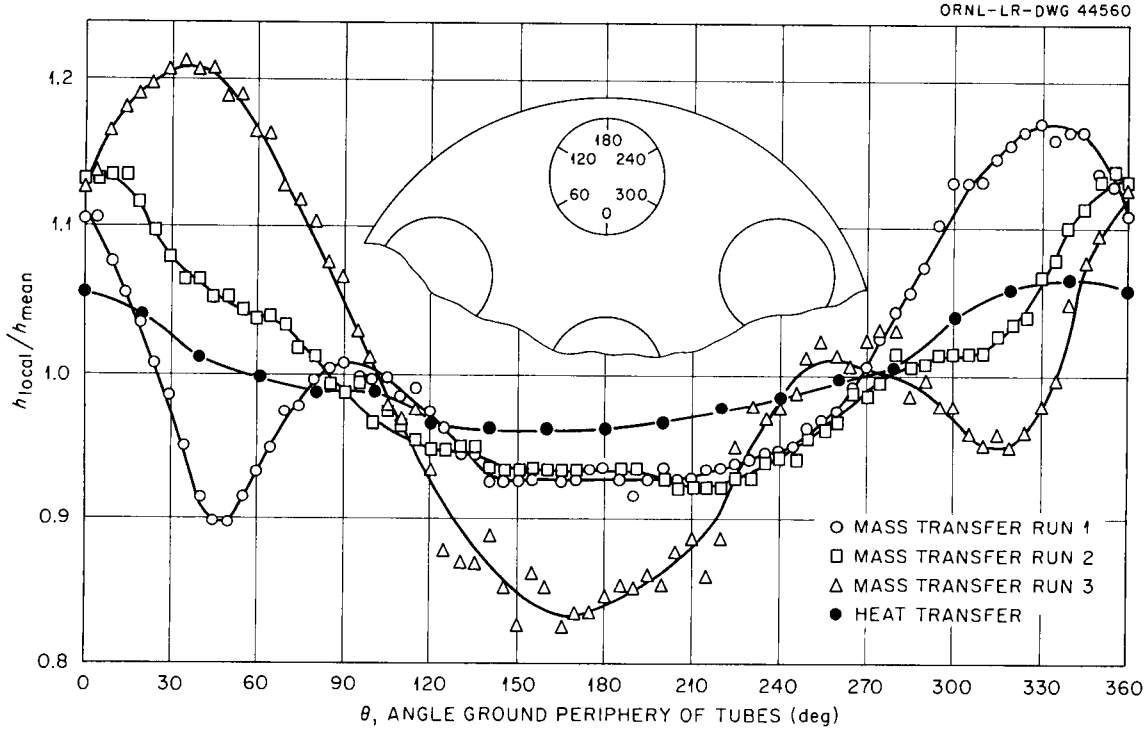

Fig. 3.6. Comparison of Mass Transfer and Heat Transfer in the Model 3 Experimental Heat-Transfer Apparatus with the Modified Inlet Plenum Chamber; Tube 2, $L/d_e = 17.9$, $N_{Re} \cong 68{,}000$.

was intentionally generated in the channel. It is planned to make further modifications in the entrance section, particularly by introducing a set of screens into the inlet diffuser, following conclusion of the present series of heat-transfer runs.

The results of mass-transfer run 1, presented in Fig. 3.6, have been replotted in Fig. 3.7 taking the peak in the h_{local}/h_{mean} curve as an indication of the forward stagnation point in the flow. For flow perpendicular to a cylinder, the diameter drawn through the stagnation point will define an axis of symmetry. The replot of the data of run 1 emphasize this feature (note that in Fig. 3.7a the angular displacement from the 0-deg position is measured in a clockwise direction, while in Fig. 3.7b the measurement is in a counterclockwise direction). The asymmetry (in magnitude rather than in general shape) of the two halves of the profile is believed to be due to the effect of the channel wall on the right-hand side of the flow. This conclusion is borne out by an examination of the data for run 3 in which the forward stagnation point is at 30 deg; it is noted that the patterns are reversed from those of Fig. 3.7. Heat-transfer coefficient distributions similar to those of Fig. 3.7a have been observed by Zapp[5] and by Giedt[6] for flow perpendicular to single circular cylinders over a Reynolds modulus (based on cylinder diameter) range of 39,000 to 219,000. The coefficient was found to decrease smoothly from a maximum at the forward stagnation point to a minimum in the vicinity of 90 to 95 deg. Between this point and about 110 deg, the coefficient increases sharply; this is ascribed to a laminar-to-turbulent transition in the boundary layer. As the turbulent boundary increases in thickness, the heat-transfer coefficient again falls until (at about 140 deg) the flow separates from the cylinder. The coefficient then increases again in the wake region following the separation point. The curves of Fig. 3.7 follow this description closely. At

---

[5]G. M. Zapp, M. S. Thesis, Oregon State College (1950); see also Kundsen and Katz, Fluid Dynamics and Heat Transfer, p 496-501, McGraw-Hill, New York, 1958.

[6]W. H. Giedt, Trans. ASME 71, 375 (1949).

low values of the Reynolds modulus, the transition to a turbulent boundary layer does not occur; and the circumferential heat-transfer coefficient profile shows only the single minimum corresponding to flow separation (at 80 deg from Zapp's[5] results and in the vicinity of 120 to 130 deg from the data of Eckert and Soehngen[7] for very low Reynolds moduli). It is difficult to state a cross-flow Reynolds modulus for the model 3 apparatus (a low value is probably the better estimate). The question this raises concerning the profiles of this study can be answered, however, by another observation of Zapp[5] in which it was noted that the laminar-to-turbulent transition was a function of the percentage of turbulence in the fluid stream. The effect of an increased turbulence level was not only to increase the local heat-transfer coefficient over most of the cylinder, but also to bring about a transition from a laminar to a turbulent boundary layer at a lower Reynolds modulus. The turbulence level in the model-3 apparatus is probably high.

A system for studying the heat transfer in the vicinity of the mid-cluster spacer of the EGCR fuel element is being assembled. The apparatus will consist of two full-scale fuel-element bundles of EGCR Title I design arranged consecutively within a 3-in.-ID Plexiglas channel. The upstream cluster will function to establish flow distributions equivalent to those in the reactor for the succeeding "active" unit. Each of the rods of the second, or active, cluster will contain a 12-in.-long naphthalene mass-transfer section, as previously described,[4] either immediately preceding or following the mid-cluster spacer. It will be possible to study spacers of various design and the effect of relative rotational orientation of the two bundles. A profilometer capable of giving more accurate and rapid measurements of local mass removal is being constructed. This profilometer will use a small differential transformer as its sensing element. The transformer output will then be amplified and recorded by a Sanborn unit. The rod will be rotated

---

[7]E. R. G. Eckert and E. Soehngen, Trans. ASME 74, 343 (1952).

by a constant speed motor. The movable core of a second differential transformer will ride on a fine-toothed gear to record simultaneously the angular position. The primary sensor will also be able to move longitudinally in predetermined steps to enable recording of mass-removal profiles at as many as eight positions along the 12-in. coated length.

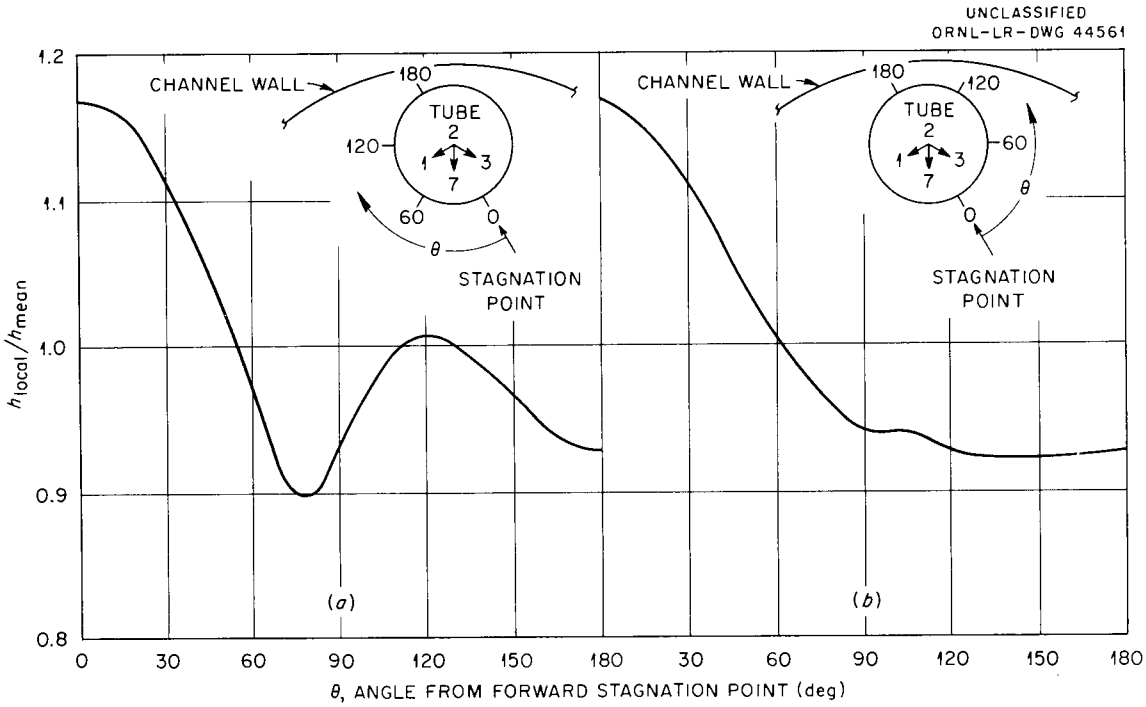

Fig. 3.7. Circumferential Variation in the Local Heat-Transfer Coefficient Ratio as Calculated from Mass-Transfer Run 1, Series 2; Tube 2 at L/d_e = 17.9 Level.

Velocity Distribution in Septafoil Channels

Measurement of the velocity profiles in septafoil fuel-element clusters using the apparatus previously described[8] has continued. The tubes were spaced to give an inner-to-outer ligament ratio of 2:1 (γ = 2), and the Reynolds modulus was maintained at approximately 52,000.

[8]GCR Quar. Prog. Rep. Sept. 30, 1959, ORNL-2835, p 63-69.

Data have been obtained at five additional L/d_e levels (4, 14, 23, 31.2, and 39.7). The results reported earlier were obtained at $L/d_e = 50$. A typical set of profiles at $L/d_e = 23$ are given in Fig. 3.8, and, as may be seen, agreement with the $L/d_e = 50$ results is reasonable. A slight counterclockwise rotation of the pattern is again evident. About a 4% difference in maximum velocities between tubes in the outer flow region was also observed. While the location of the maximum velocity regions appears to be constant, the velocity magnitudes show some scatter. There are also some discrepancies in the boundaries of the high velocity areas at the various levels. Analysis and interpretation are proceeding in an attempt to rationalize the data.

The uncertainties and scatter in the preliminary data have manifested the need for more accurate spacing of the tubes in the cluster and a more precise knowledge of the location of the Pitot probe. A new set of spacers and associated equipment for accomplishing this have been fabricated. It is planned to redetermine the velocity profiles at the

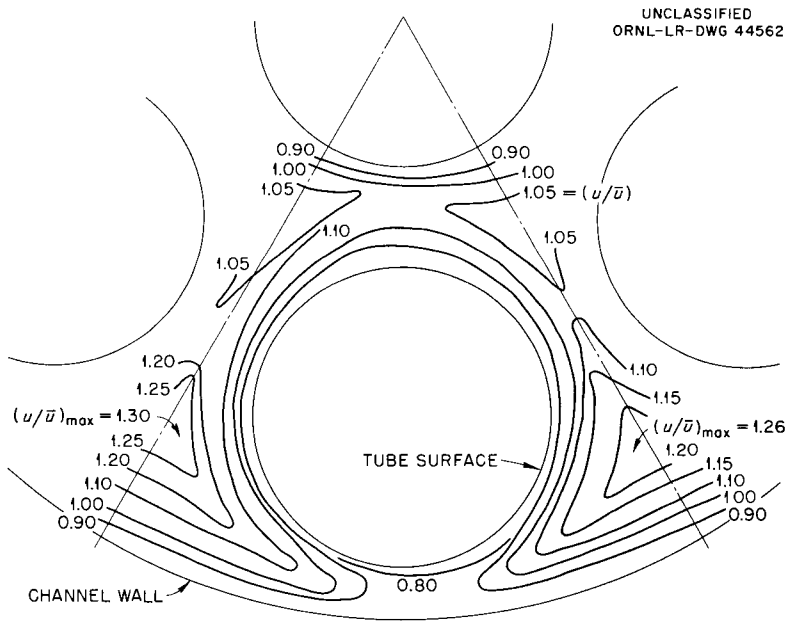

Fig. 3.8. Measured Velocity Distribution Between Tubes in a Septafoil Channel; $L/d_e = 23$; $N_{Re} \cong 52{,}000$, $\gamma = 2$.

six axial locations indicated above in the near future. In view of the demonstration of cross flow by the heat-transfer and mass-transfer studies described in the preceding sections, the determination of the flow direction within the cluster will be considered.

Part 2. Materials Research and Testing

4. METALLURGY

Fuel Materials Development

Fabrication of UO_2

The conversion process for producing the highly sinterable UO_2 powder required for optimum fabrication has been refined to the point where the reproducibility is generally good, particularly when stable processing conditions are maintained during conversion of a large amount of material. Currently, development work is directed toward establishing conditions for recycling material from the fabrication process.

In addition to the material used for process development, eight batches of oxide powder of various enrichments were produced for use in fabricating specimens for irradiation tests. By suitable control of the fabrication process, it has been possible to produce prototype-size pellets to within ±0.3% of reference dimensions.

Work is also in progress to prepare bushings of MgO and ZrO_2 for use as insulators in high-temperature irradiation experiments. Prefabrication test work of stabilized ZrO_2 has shown that heating subsequent to sintering causes a change in dimensions. Test work is in progress to establish the temperature and time required for complete dimensional stability of these bodies. A study is also in progress to determine the compatibility of ZrO_2 in contact with UO_2 and Inconel, as planned in these irradiation experiments.

Thermal Conductivity of UO_2

An apparatus for measuring thermal conductivity by radial heat flow under steady-state conditions has been completed, and a test run is being conducted with Armco iron as the standard. An extensive data file on the thermal conductivity and related physical properties of UO_2 has been compiled, and data analyses are being carried out. The data are summarized in Fig. 4.1.

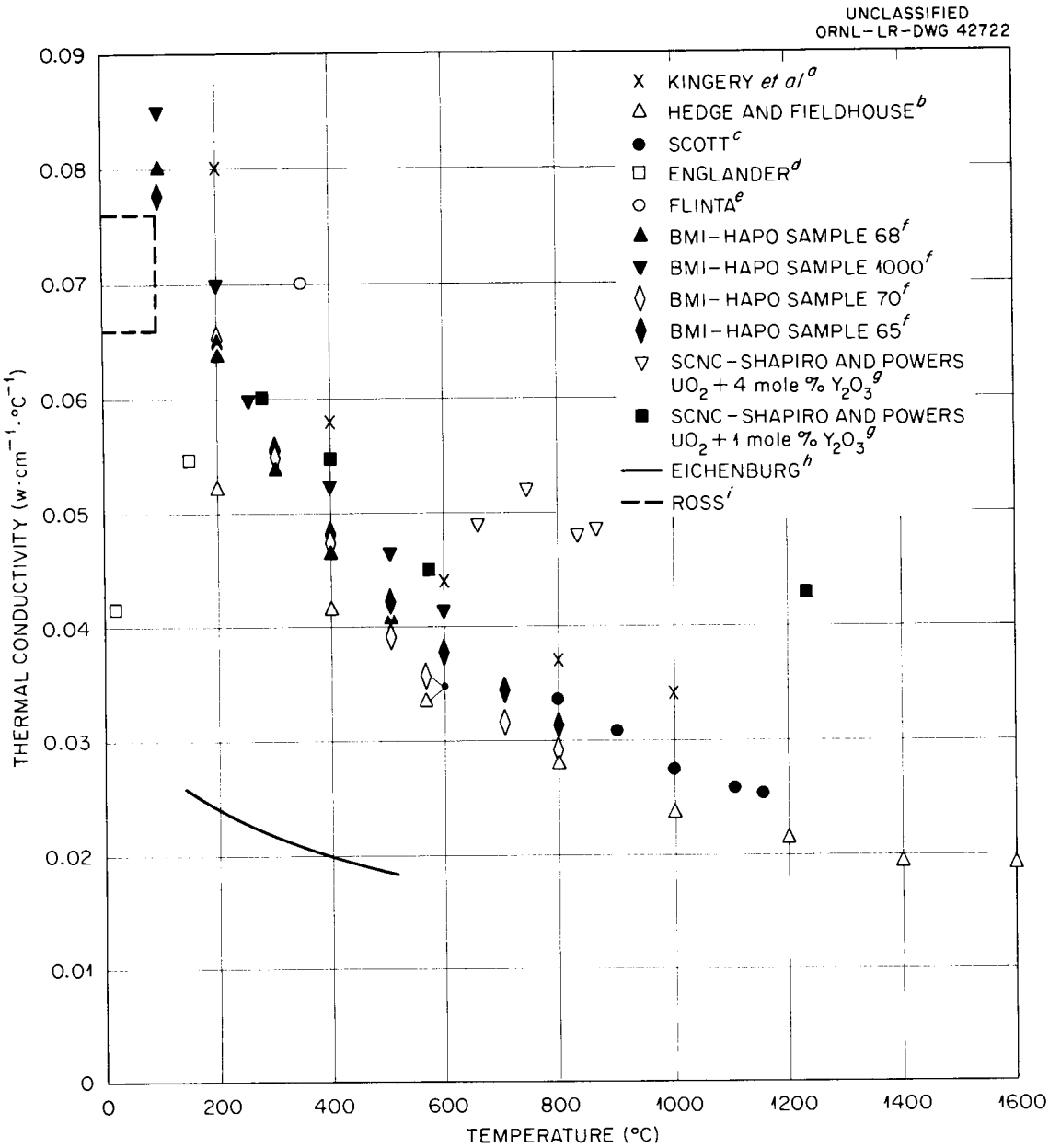

Fig. 4.1. Compilation of Reported Thermal Conductivities of UO_2, Extrapolated Linearly to Theoretical Density. The references are: (a) J. Am. Ceram. Soc. 37(2), 107–110 (1954). (b) AECU-3381; G022D3, Armour Research Foundation Report (Sept. 1956). (c) AERE-M/R-2526 (1958). (d) CEA-79 (June 1951). (e) TID-7546, Book 2, p 516–525 (Mar. 1958). (f) BMI-1315, p 7–9 (Feb. 1959). (g) SCNC-296, p 28. (h) WAPD-200 (Sept. 1958). (i) CRFD-817, AEC of Canada, Ltd. (to be published).

High-Temperature Compression Testing of UO_2

Compression testing of UO_2 bushings has been continued according to the method described previously.[1] Sintered UO_2 bushings were compressed axially in a graphite die at temperatures up to 1800°C and pressures of 1000 and 5000 psi. The load was applied after reaching the test temperature and held constant for 1 hr. The results are summarized in Table 4.1.

Table 4.1. Results of Compression Tests of UO_2 Bodies

Test Temperature (°C)	Pressure (psi)	Change in Height (%)	Condition of Bushings After Testing
1200	1000	+0.04	Unchanged
1500	1000	-0.06	Unchanged
	5000	-0.57	Surface slightly oxidized
	5000	-1.70	Fused to UO_2 spacer
1800	1000	+0.63	Badly oxidized
	5000	-26.0	Fused to spacer
	5000	-50.0	Fused to spacer

The specimens of UO_2 were high-density pellets of near-stoichiometric composition, such as those fabricated for the prototype fuel irradiation program. From the data it is evident that, even at 1500°C, the material will support a substantial load without rapid deformation. At 1800°C, however, the high-density UO_2 bodies became relatively weak and plastic, as was expected. Specimens are being prepared for studying the properties of these pellets at intermediate temperatures.

Mechanical Behavior of Encapsulated UO_2

The dimensional stability and mechanical behavior of UO_2 in a type 304 stainless steel capsule under the thermal conditions predicted for

[1] GCR Semiann. Prog. Rep. June 30, 1959, ORNL-2767, p 102.

the EGCR are being studied. The apparatus is shown schematically in Fig. 4.2. The effect of thermal cycling and thermal gradients across the UO_2 pellets on the dimensional stability of the UO_2 will be studied at temperatures up to 3500°F in this apparatus. Initial tests were completed in which the temperature gradient from the center of the element to the capsule wall was measured at temperatures up to 2000°F in a helium atmosphere. The data showing the temperature drop across a 0.706-in.-dia heated capsule at steady-state conditions are given below:

Maximum Pellet Inner Surface Temperature (°F)	Capsule Wall Temperature (°F)	Temperature Gradient (°F)
500	446	54
750	665	85
1000	855	145
1250	1025	225
1500	1190	310
1750	1315	435
2000	1485	515

The radial clearance between the UO_2 pellet and the stainless steel capsule may be observed in this apparatus by means of low-voltage radiography. The measurement technique was established in a model setup of the apparatus in which increments of clearance as small as 0.001 in. could be detected at room temperature.

The mechanical strength of a UO_2 fuel element at elevated temperature may be predicted from the results of this study. Experimental data on the flow of heat will be used to calculate the effective thermal conductivity of UO_2 as a function of temperature. Dimensional and temperature measurements will be used to calculate the effective thermal coefficient of expansion. In addition, the increase in surface area of the UO_2 as a result of thermal treatment in this experiment will be measured.

Fission-Product-Release Studies

An apparatus has been constructed for measuring the rate of fission-product release from UO_2 pellets. The apparatus is illustrated

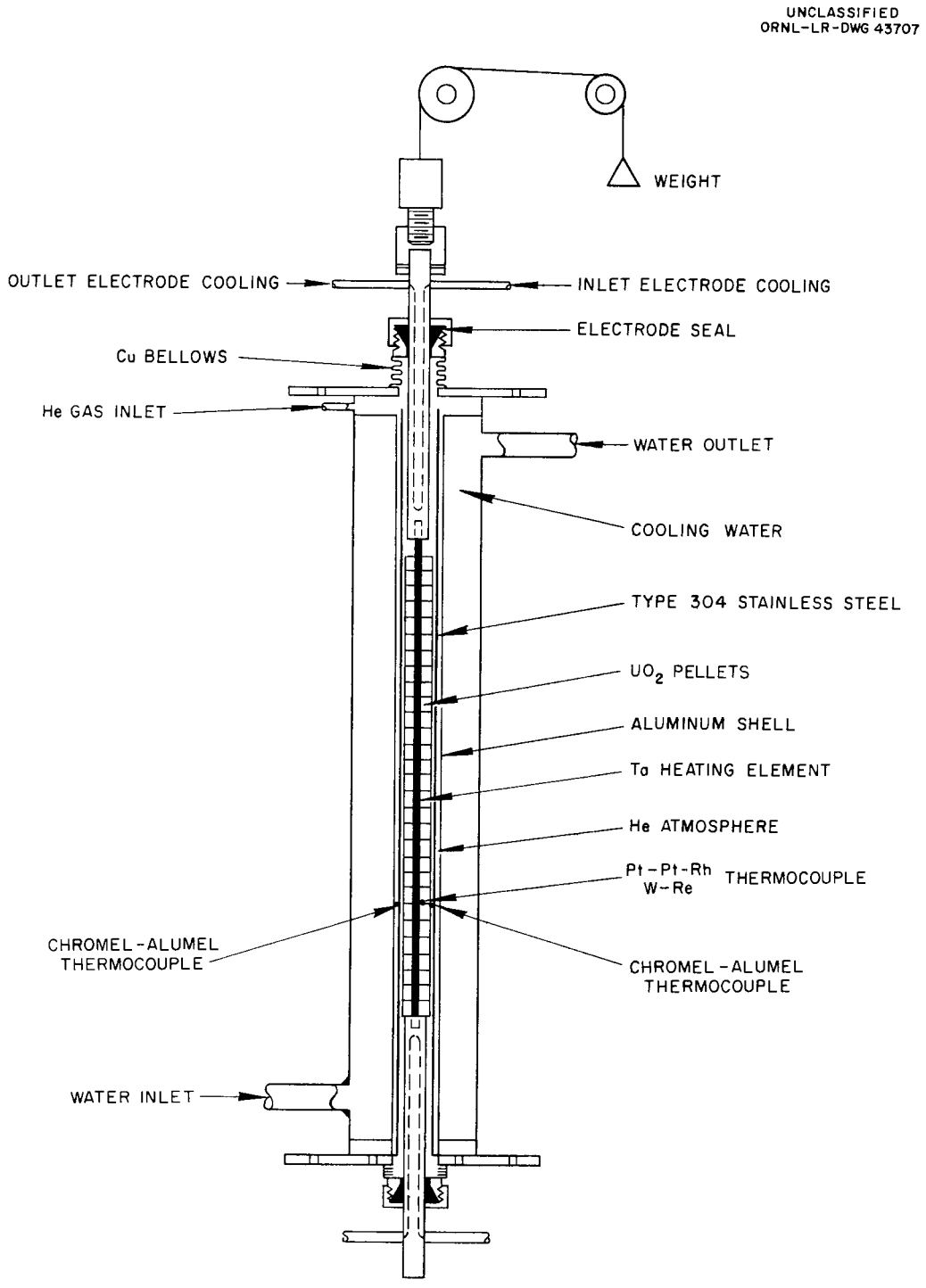

Fig. 4.2. Apparatus for Determining the Dimensional Stability and Mechanical Behavior of UO_2 Pellets in a Type 304 Stainless Steel Capsule.

schematically in Fig. 4.3. To obtain the specimens, small pieces of UO_2 pellets, ranging in size from 1 to 10 g, are irradiated at low temperatures for periods of one to five days at a flux of 10^{12} neutrons/cm^2·sec. After a suitable decay period, the diffusion coefficient, D', for release of gaseous fission products is determined at various temperatures by the method developed by Eichenberg et al.[2]

To obtain the desired data, a sample is placed in the tantalum bucket shown in Fig. 4.3 and raised into the furnace chamber. The system is then evacuated and flushed with high-purity helium, and the tantalum susceptor is heated by induction to the desired temperature, as determined by a calibrated optical pyrometer. When the desired temperature is attained, the sample is raised into the center of the furnace by means of a winch and chain, and purified helium is passed over the sample at a rate less than 50 cm^3/sec (STP). The volatile fission products which are released are carried by the helium sweep gas through a heated charcoal trap, which removes I^{131}, and into a collection bulb containing activated charcoal at -196°C. The xenon and krypton are absorbed on the surface of the activated charcoal. A second charcoal trap is included in the system to provide a method of determining whether all the fission gases have been trapped in the collection bulbs.

Samples of absorbed fission gas are removed from the system by sealing off the Pyrex tubes leading into the collection bulbs. Analyses for Kr^{85} or Xe^{133} are made by means of a calibrated gamma-ray spectrometer. Parallel trains are incorporated in the system so that as many as 12 samples of fission gas may be collected from a single specimen of UO_2. After a series of runs the UO_2 sample is removed, and the burn-up is determined by analytical methods.

The optical pyrometer and optical system of the apparatus were carefully calibrated so that the true UO_2 temperature could be determined. Corrections for absorption and reflection of light in the optical system

---

[2]J. D. Eichenberg et al., Effects of Irradiation on Bulk Uranium Dioxide, WAPD-183 (Oct. 1957).

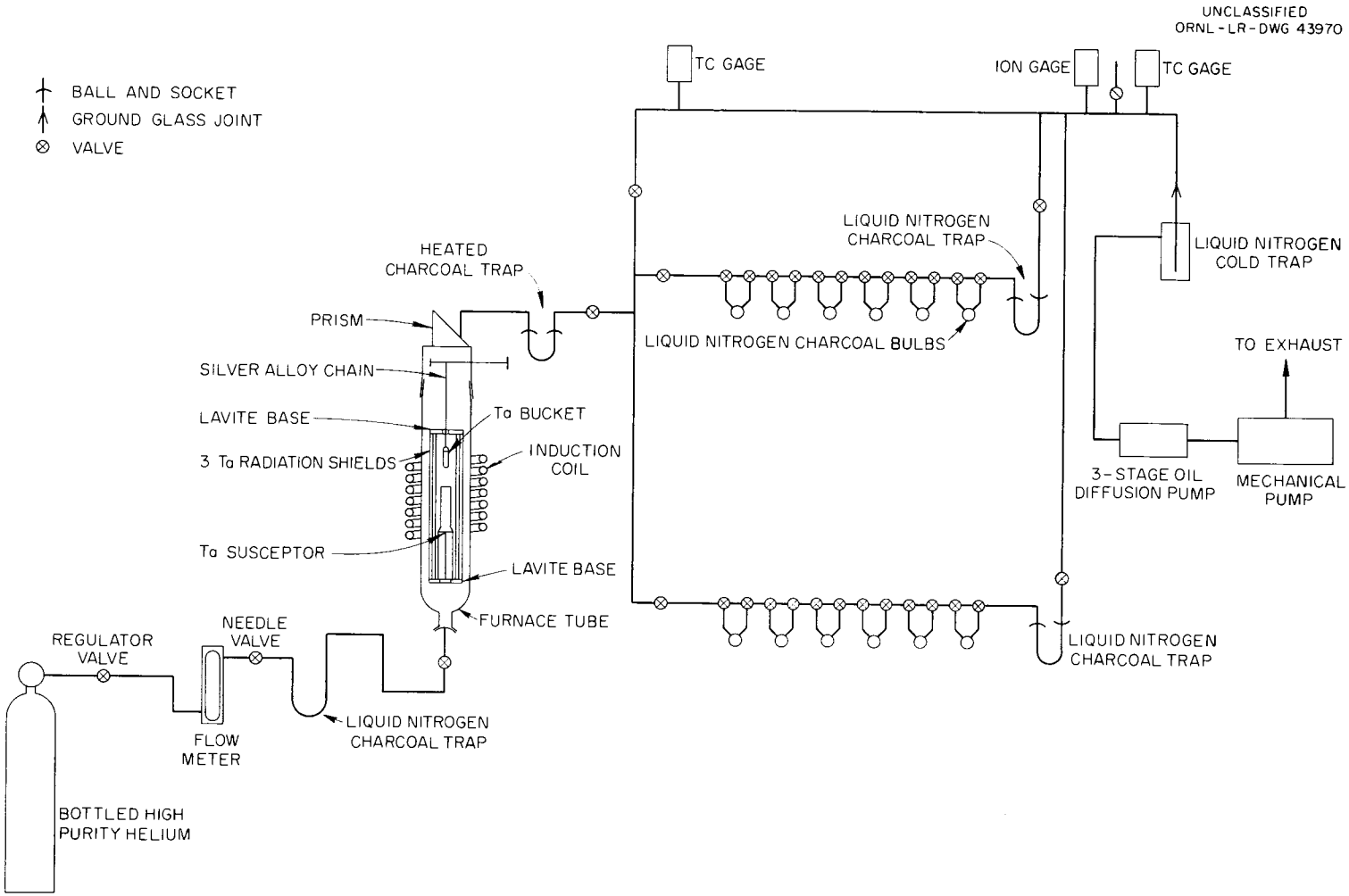

Fig. 4.3. Fission-Gas Collection Apparatus

were found to increase linearly from a value of 18°C at a true temperature of 1000°C to 78°C at a true temperature of 2000°C. Additional calibration runs were conducted by melting of nickel, iron, and platinum in the furnace. Good agreement between the observed and reported melting points were found.

One sample of UO_2 has been studied to date. This sample was a piece weighing 1.3 g that was taken from a 95% dense pellet of UO_2 enriched to 2% U^{235} that had been irradiated in the LITR for 332 hr at a flux of 6×10^{11} neutrons/cm^2·sec. Following irradiation, the sample was placed in storage for 14 months. Fission gas samples have been collected for runs of 1 hr at 1400°C and 1650°C but have not yet been analyzed.

Structural Materials Evaluation

Gas-Metal Reaction Studies

The reaction rates between type 304 stainless steel and small partial pressures of CO and CO_2 in vacuum and in flowing argon are being studied, as well as the effect of stress on the reaction rates. The all-glass thermal-convection loop described previously[3] is being used for these studies.

Test runs were made to determine whether a constant CO-to-CO_2 ratio could be maintained. These preliminary tests indicated that manometric control of the CO_2 concentration was not feasible and that the amount of CO in metastable equilibrium with CO_2 and activated charcoal was an order of magnitude lower than predicted. These results are in agreement with the theory of the formation of an oxide on carbon[4] at temperatures of about 660°C.

Subsequent tests showed that the CO_2 concentration could be maintained at prescribed levels by decomposing calcium carbonate at elevated temperatures. The apparatus is being modified to include this feature,

---

[3] GCR Quar. Prog. Rep. Sept. 30, 1959, ORNL-2835, p 82.

[4] H. W. Davidson, "Graphite for Nuclear Reactors," General Electric Company Atomic Energy Review, March 1958.

and a third furnace is being installed to convert the resulting CO_2 to CO.

Effect of Gas Concentration. Experiments were conducted to determine the effect of the CO_2 concentration on the rate of reaction with type 304 stainless steel at 1400°F. Pure CO_2 generated by decomposing $CaCO_3$ was passed over 0.002-in.-thick tubing at pressures of 10 and 100 μ. The data obtained from these experiments are presented in Table 4.2. These

Table 4.2. Weight Gains of Type 304 Stainless Steel Tubing in Low-Pressure CO_2 at 1400°F

Exposure Time (hr)	Weight Gain of Steel Specimen (mg/cm^2)	
	In CO_2 at Pressure of 10 μ	In CO_2 at Pressure of 100 μ
50	0.09	0.09
100	0.13	0.12
150	0.21	0.14
200	0.23	0.16
250	0.24	0.18

data are to be compared with the results of previous tests at 1500°F in which argon at 1 atmosphere was used as the carrier gas for the CO_2. In CO_2 at a partial pressure of 1000 μ the specimen weight gain was 0.109 mg/cm^2 and in CO_2 at a partial pressure of 6000 μ the weight gain was 0.117 mg/cm^2.

The data of Table 4.2 indicate that the CO_2 concentration and/or the presence of an inert gas such as argon have little effect on the reaction rates under the conditions described. These results are in agreement with the concept that concentration has no significant effect on the reaction rate in the presence of an oxide film when diffusion through the film is the rate-controlling process. In this case, exposure of type 304 stainless steel to CO_2 results in the formation of an adherent, magnetic, oxide film which is green-black in color.

The rate of carburization of type 304 stainless steel in argon with small partial pressures of CO is also being studied. Results obtained thus far indicate that no change occurs in the total amount of carbon absorbed by unstressed specimens when the partial pressure is varied from 1 to 5% of 1 atm. This conclusion is based on the average carbon analysis. However, significant differences in the weight changes as a function of the partial pressure were found at any given time during the 500-hr testing period.

Effect of Stress. It was previously reported[5,6] that extensive carburization occurs during creep testing of type 304 stainless steel in CO and CO_2. Examination of numerous creep-rupture specimens has shown that stress greatly accelerates the rate of carburization in CO. A sample taken from the shoulder of a specimen where the stress was fairly low had a carbon content of 0.14%, while a specimen from the gage length contained 0.95% C. These values are averages for a cross section and hence are not the maximum carbon content. The high carbon values which can be obtained under cyclic stress conditions are indicated below. Samples were taken at increments of ~0.007 in. from a 0.75-in.-OD, 0.060-in.-wall tube that had been cycled for 133 hr at 1500°F to a stress of 6500 psi with a cycle frequency of 1 hr. The effect of such high carbon content on the ductility of this material has not been determined.

Depth of Layers from Surface (mils)	Carbon Content (%)
1–7	1.27
7–14	1.34
14–21	1.31
21–28	1.02
28–35	0.76
35–42	0.56
42–49	0.46
49–56	0.36

[5] GCR Semiann. Prog. Rep. June 30, 1959, ORNL-2767, p 109.

[6] GCR Quar. Prog. Rep. Sept. 30, 1959, ORNL-2835, p 85.

Loop Failures. The importance of gas-metal reaction in the performance of high-temperature devices was illustrated by a recent series of loop failures. A low-pressure thermal-convection loop scheduled for a 5000-hr test at 1400°F failed in the type 316 stainless steel sidearm because of the oxidation shown in Fig. 4.4. The catastrophic oxidation was caused by pockets of stagnant air between the insulation and the piping. This failure illustrates the rapid high-temperature oxidation which may occur with certain alloys containing molybdenum. Severe oxidation also occurred on other parts of the loop where Sauereisen porcelain cement had been used near the thermocouples. On completion of a test run in another low-pressure loop, an examination revealed that in areas where Sauereisen cement had been used oxidation had occurred to such an extent that the loop had to be scrapped.

Another such incident was the failure of a high-pressure thermal-convection loop after 18 hr of operation at 1400°F. The point of failure was in the hottest portion of the sidearm in the heat-affected zone of a plug weld. The entire section of pipe had bowed, and catastrophic oxidation had occurred around the weld, although no Sauereisen cement had been used. It is felt that the oxidation reduced the effective wall thickness of the pipe, which then deformed and caused undue stress on the weld. The loop was repaired by replacing the section of pipe, and it was put back into operation. However, failure by catastrophic oxidation occurred in the new section of type 316 stainless steel pipe after less than 200 hr at 1400°F.

Implications of Test Results. Both oxidation and carburization have been observed in all types of tests. The fact that no carburization of stainless steel specimens has been noted in large-scale engineering tests (see Chap. 6, this report) is understandable, since the laboratory tests have demonstrated that the presence of ferritic steels in the same system as the austenitic steels results in preferential carburization of the ferritic material. When the austenitic steels are tested singly, however, carburization occurs quite readily. The laboratory tests also show that although the presence of an oxide film on the metal surface

Fig. 4.4. Point of Failure of 2-in. Sched-40 Type 316 Stainless Steel Pipe by Catastrophic Oxidation in a Low-Pressure Thermal-Convection Loop Operating at 1400°F.

tends to delay the process to some extent, it will not prevent carburization.

Much of the information from the engineering tests cannot be correlated with the laboratory experiments or related to service conditions because of the variations in the constituents outgassed from the graphite. The significance of these variables is revealed by the marked changes which occur with changes in surface area of metal in comparison with the volume of graphite present. Some of the experimental difficulties may be resolved by the introduction of the small-scale gas purification system in the forced-convection loops (see Chap. 6, this report).

Mechanical Properties of Structural Materials

Investigations of the properties of type 304 stainless steel as a container material for UO_2 fuel pellets have continued. The experimental program has included tube-burst testing, studies of the effect of mid-plane spacers, thermal cycles, creep-buckling tests, and creep tests in various gaseous environments.

Tube-Burst Tests. Failure of an EGCR fuel capsule may occur if the release of a large percentage of the fission gas from the UO_2 produces pressures in excess of 300 psi or if an accident occurs that leads to the loss of the coolant pressure. An investigation of the effect of differential pressure, temperature, and environment on the time-to-rupture of seamless, 0.020-in.-wall, type 304 stainless steel capsules is therefore in progress. Some results obtained in air were reported previously,[7,8,9] and the plot of time-to-rupture vs tangential stress presented in Fig. 4.5 summarizes the data obtained thus far.

Results have also been obtained from four in-pile tube-burst tests of type 304 stainless steel. The in-pile data, as shown in Table 4.3, fall within the normal scatter band for rupture in out-of-pile tests.

---

[7] GCR Semiann. Prog. Rep. Dec. 31, 1958, ORNL-2676, p 81–85.

[8] GCR Semiann. Prog. Rep. June 30, 1959, ORNL-2767, p 103–105.

[9] GCR Quar. Prog. Rep. Sept. 30, 1959, ORNL-2835, p 75–77.

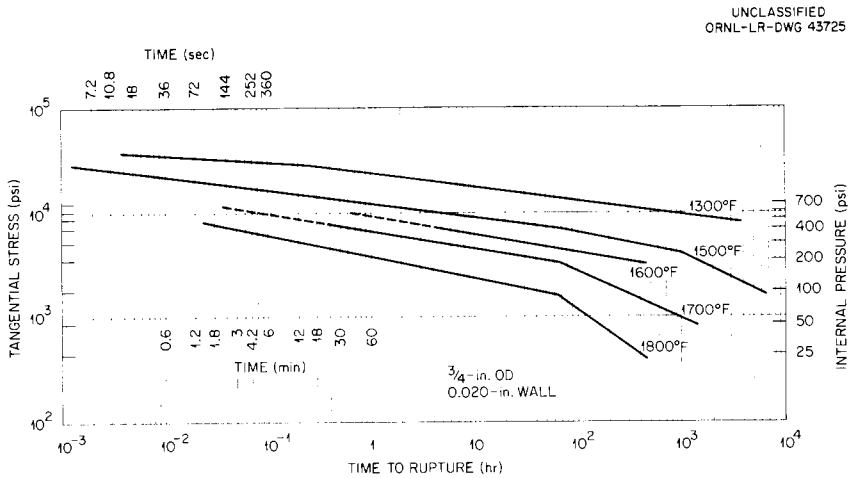

Fig. 4.5. Tube-Burst Data for As-Received Type 304 Stainless Steel Tubing Tested in Air.

Table 4.3. Comparison of Results of In-Pile and Out-of-Pile Tube-Burst Tests of Type 304 Stainless Steel at 1500°F in Air

	Stress (psi)	Time to Rupture (hr)
Out-of-Pile Test	4000	~870
	5000	~540
In-Pile Test		
Specimen 7–3	4000	895
Specimen 9–6	4000	673
Specimen 9–7	5000	337
Specimen 9–8	5000	518

Although this is very encouraging, the data are limited to one temperature and two stress conditions. Therefore, it appears premature to conclude that the creep or rupture properties of type 304 stainless steel are unaffected by irradiation. As a matter of fact, the effects of irradiation may not be known until the EGCR is operated, since no additional in-pile tests of stainless steel are planned at present.

Thermal-Cycling Tests. For a typical scram of the EGCR, it has been estimated that the temperature transient of the cladding material will be of the order of 600 to 800°F at the rate of 100°F/min. A maximum of 100 cycles of this type can be predicted during the life of a fuel element. In order to determine the behavior of a capsule operating under these conditions, a cycling test was conducted using a 6-in.-long tubular specimen (type 304 stainless steel, 0.800-in.-OD × 0.020-in. wall) which had been previously collapsed around UO_2 pellets. After 75 cycles between 1000 and 1600°F at a rate of 100°F/min, the specimen length was found to have increased by 0.07% and the diameter by 0.13%. Additional cycling tests will be conducted with long hold times at the higher temperature, in addition to other tests at a cycle rate of 250°F/min for 10 cycles.

Effect of Mid-Plane Spacers on Creep Buckling. The investigation of the effect of spacers brazed to the capsule material has continued. Central spacers with and without fins (0.825-in.-OD excluding fins) were brazed to type 304 stainless steel tubular specimens (3/4-in.-OD × 0.020-in.-wall thickness) previously filled with inserts to obtain a cold diametral clearance of 0.010 in. The specimens were then subjected to an external pressure of 300 psi at 1800°F. After 44 hr at these conditions, examination of a specimen without fins indicated that the tube wall had collapsed around the inserts in a uniform manner. Measurements of the specimen revealed that the diameter of the tube was 0.009 in. less than the original dimension, while the diameter of the spacer was reduced only by 0.005 in.

A second specimen with a finned spacer was examined after 15 hr under the same condition, and it was found that uniform collapse of the tube wall had occurred. The diameters of both the tube and spacer were 0.010 in. less than originally. In this case the reinforcement of the tube wall by the spacer was not sufficient to prevent collapse.

Creep Buckling of Loop Materials. It is anticipated that the experimental loops in the EGCR will be subjected periodically to an external pressure of 300 psi at elevated temperatures. Such a condition

can lead to collapse of the wall due to creep buckling. Since the information available on creep buckling is limited, a program has been initiated to establish failure criteria. Tests at 1200°F on small-size tubes with equivalent ratios of wall thickness to diameter are also to be performed to produce a more complete set of data. The effects of variable wall thickness and concentricity will be explored. Equipment is being constructed and testing will begin shortly.

Environmental-Creep Testing. Creep-rupture tests of type 304 stainless steel have been conducted in air and in pure gaseous environments, including He, CO, CO_2, N_2, H_2, and A. As reported previously,[10] CO and CO_2 carburized type 304 stainless steel during tests at 1500°F. As a result, the creep curve exhibits a decreasing strain rate that asymptotically approaches zero in a 1000-hr test. A set of curves summarizing the general environmental effects found to data are shown in Fig. 4.6. Hydrogen is the only gas which appears to adversely affect the creep properties when compared with the base-line data obtained in argon.

Despite the fact that argon and helium are both inert gases, there has been some question as to whether creep data obtained in argon were

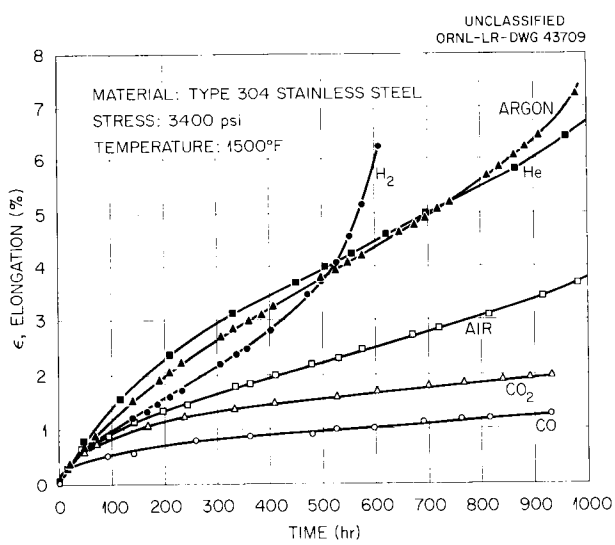

Fig. 4.6. Summary of Data on Creep of Type 304 Stainless Steel at 1500°F and a Stress of 3400 psi.

[10] GCR Quar. Prog. Rep. Sept. 30, 1959, ORNL-2835, p 85.

truly representative of the behavior of type 304 stainless steel in helium. Therefore, a test was run in a helium environment under conditions of stress and temperature similar to previous tests in argon. The results are presented in Table 4.4 and in Fig. 4.6. As may be seen, no significant differences exist between the two sets of data. Unless further evidence of chemical inertness is required, no additional tests will be run in helium.

Table 4.4. Results of Creep Tests of Type 304 Stainless Steel at 1500°F Stressed at 3400 psi

Environment	Time to Indicated Strain (hr)			Time to Rupture (hr)	Strain at Rupture (%)
	1%	5%	7%		
Argon	78	705	960	1001	7.8
Helium	60	696	1010	1123	7.7
Air	110			*	

*Test discontinued at 1005 hr; the strain at that time was 3.8%.

Pressure-Vessel Steel Tests. A study has been initiated of the brittle fracture characteristics of various pressure vessel steels, both in the as-fabricated condition and after service under nuclear irradiation. Techniques have been developed within the past few years for predicting a safe minimum operating temperature above which brittle fracture should not occur, but this temperature usually increases when the steel is exposed to a fast neutron (>1 Mev) dose greater than 10^{18} neutrons/cm^2. The problem is further complicated in that welding introduces weld filler metal and a heat-affected zone.

A welded 4-in.-thick plate of ASTM type SA-212, grade B steel has been procured for this study, and tests have been conducted on specimens in the as-received condition. The rolling direction was determined by macroetching specimens from one of the corners of the plate. Macroetching also revealed that the surface of the plate was

less porous and contained fewer inclusions than the interior of the plate.

Transverse and longitudinal drop-weight specimens from the outer surface of the plate were tested, and the nil-ductility transition (NDT) temperature was determined to be approximately 15°F. No significant difference between the NDT temperatures in the longitudinal and transverse directions could be detected.

Charpy V-notch impact specimens oriented transverse to the rolling direction and with the notch normal to the plane of the plate were machined from the surface of the plate, and a conventional impact-strength study of these specimens was made. As part of a subcontract at Rensselaer Polytechnic Institute, data were obtained from tests on longitudinal Charpy V-notch specimens from the same plate. The data from both types of specimens are presented in Fig. 4.7.

Below -20°F, the longitudinal and transverse impact curves are similar, with the lognitudinal 10-ft-lb transition temperature occurring at -20°F. Above -20°F, the two curves diverge, with the longitudinal specimen exhibiting greater impact energies than the transverse specimen. At the NDT temperature of approximately 15°F, the standard longitudinal Charpy V-notch energy is about 23 ft-lb, whereas the transverse energy is about 14 ft-lb.

Standard Charpy V-notch specimens from the type SA-212, grade B parent plate were thermally cycled at Rensselaer Polytechnic Institute to produce synthetic weld heat-affected zones (corresponding to energy inputs of 50 kilojoules per inch of weld). Specimens cycled to 1400°F (simulating conditions just above the Ac_1 line or the iron-carbon phase diagram) exhibited an improvement in the impact properties, as shown in Fig. 4.8. However, specimens cycled to 2400°F (simulating conditions near the fusion zone) caused the curve of impact energy to shift to higher temperatures, with a large decrease in absorbed energy in the ductile portion of the curve. The effect of the cycling temperature on the 10-ft-lb transition temperature is shown below. Additional Charpy V-notch specimens are being thermally cycled to determine the influence of intermediate peak temperatures.

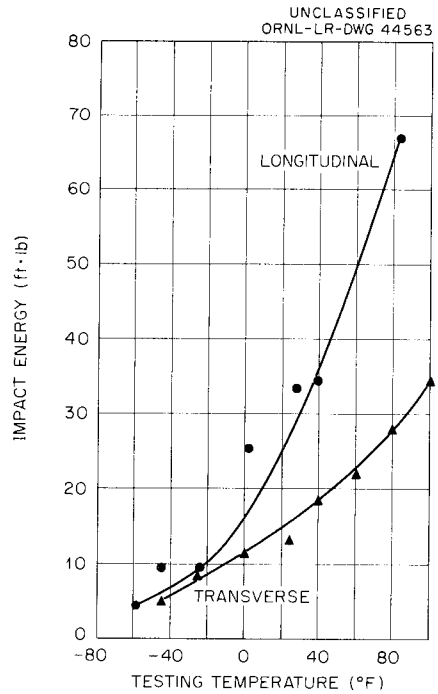

Fig. 4.7. Charpy V-Notch Impact Strength Data for ASTM Type SA-212, Grade B Steel. Specimens oriented with notch normal to face of plate in longitudinal and transverse directions.

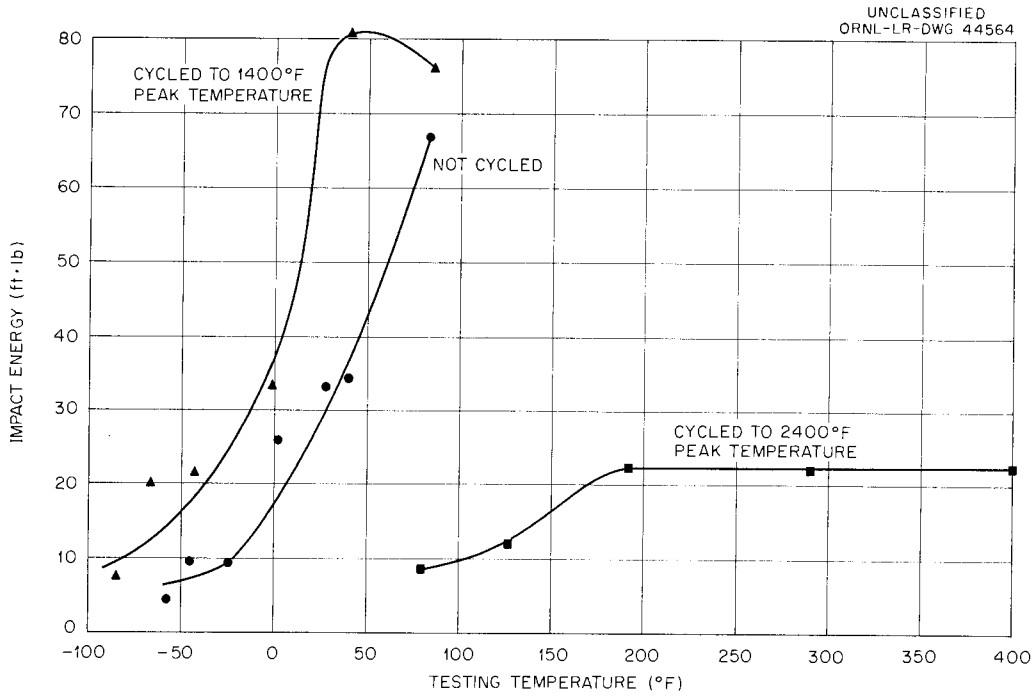

Fig. 4.8. Charpy V-Notch Impact Strength Data for ASTM Type SA-212, Grade B Steel Longitudinal Specimens Cycled to 1400 to 2400°F Peak Temperatures.

Peak Temperature (°F)	Temperature Corresponding to 10-ft-lb Energy Absorption (°F)
Not cycled	-20
1400	-80
2400	+100

Manufacturing and Inspection Methods

Fabrication of Title I EGCR Fuel Elements

In order to obtain information regarding the influence of manufacturing variables on the procedures to be employed in constructing EGCR fuel elements, the pilot plant fabrication of 50 elements was undertaken. The fabricability of the Title I design will be evaluated during this pilot run, and various modifications of the design will be checked. The cost and availability of the components will be ascertained, and the labor involved in the various steps in fabrication and inspection will be determined. It will then be possible to obtain realistic fuel fabrication costs for the reactor.

Procurement specifications were prepared for the following components of the fuel element: (1) type 304 stainless steel capsule tubes, (2) mock fuel pellets of mild steel, (3) top end caps, (4) bottom end caps, (5) mid-plane helical spacers, (6) top spiders, (7) bottom spiders, (8) graphite support sleeves, (9) magnesium oxide pellets. These specifications, as adapted from existing materials specifications or as written, were issued and orders were placed with commercial vendors for the various components. At the same time, quotations were obtained on quantities of each item sufficient for a reactor loading.

Partial shipments of all components, except top and bottom spiders, are on hand, and fabrication of the elements is under way. Jigs and fixtures for welding and brazing the elements were prepared, including (1) a loading jig for inserting stacked lengths of fuel into the capsule, (2) a semiautomatic rotary positioner for end-cap welding in the inert atmosphere welding chamber, (3) jigs for aligning the hanger assembly,

(4) mid-plane spacer brazing fixtures, and (5) a rotary positioner for handling final welds upon insertion of the fuel element into the graphite sleeve.

A fabrication schedule was established, but the late delivery of components has put the expected completion date somewhat behind schedule. Arrangements are being made for production inspection of completed fuel elements.

Purity of Atmosphere in Fuel Capsules. The gas contained in the EGCR fuel capsules is currently specified as helium of 99.9% purity in order to provide optimum heat transfer. The conventional method for insuring an atmosphere of this purity involves making the final closure weld of each fuel capsule in an inert-atmosphere chamber which has been filled with helium of the required purity. Since manufacturing operations under these conditions have several limitations and tend to be slow and expensive, other techniques for fabrication have been studied. One technique consists of loading the capsule in the inert-atmosphere chamber, pressing the end plugs in place, and fitting a latex rubber guard over the unwelded end. The element is then removed from the chamber and welded in air utilizing conventional techniques.

Preliminary experiments were conducted to determine the degree of purity which could be maintained in the capsule as a function of elapsed time before welding. Simulated fuel capsules with one end fitted with a vacuum-type valve were loaded with dummy fuel slugs, sealed with an end cap, and covered with a rubber guard. These specimens were then welded outside the chamber after various elapsed time intervals, and the internal contamination was determined by mass spectrometer analyses of gas samples. The composition of the internal atmosphere was found to change approximately as shown in Fig. 4.9, indicating that this technique is unsuited for maintaining an atmosphere of high-purity helium in the capsules. It is therefore planned to make the final closure welds within the inert-atmosphere chamber.

Component Evaluation. Nondestructive evaluation of the components and assembled units is being accomplished during the pilot plant

fabrication of fuel elements. Most of the components were produced in accordance with recommended inspection procedures, and the evaluation should provide essential data on the adequacy of the proposed inspection program for the EGCR fuel elements. The nondestructive tests being used in evaluating the various components are itemized in Table 4.5.

Table 4.5. Tests Used in Evaluating Fuel Element Components

Component	Nondestructive-Testing Technique	Condition Investigated
Capsule	Eddy current	Flaws
	Fluorescent penetrant	Flaws
	Visual	Flaws
	Pulse-echo ultrasonic	Flaws
	Resonance ultrasonic	Wall-thickness
	Air gage	Inside-diameter
End caps and spacers	Fluorescent penetrant	Flaws
Spiders	Fluorescent penetrant	Flaws
	Radiography	Flaws
Graphite sleeves	Eddy current	Flaws
Capsule-closure weld	Helium leak testing	Flaws
	Fluorescent penetrant	Flaws
	Radiography	Flaws

Thus far, evaluation has been completed on partial shipments of capsule tubing, end caps, and spacers by all the indicated techniques. In addition, helium leak testing has been accomplished on a few bottom closure welds. Results to date indicate that all the tubing is rejectable by the eddy-current technique, as was noted at the tube manufacturer's plant; about 2% has been rejected by dye-penetrant inspection; approximately 10% is over size in the wall thickness by amounts from 0.0003 to 0.0006 in.; and about 3% of the tubing fails to meet the dimensional tolerance on the inside diameter. Most of this latter discrepancy is localized at the extreme end of the tubes and is probably

the result of rough handling or slight distortion when cutting to length. No rejectable defects have been detected by the other inspection methods.

Graphite-Sleeve Inspection. An investigation has been conducted to determine the test parameters for the eddy-current inspection of graphite sleeves for the EGCR fuel elements. These sleeves are 3 in. ID, 5 in. OD, and about 29 in. long. Because of the 1-in.-thick wall it was necessary to choose a combination of external encircling coil and internal bobbin coil to insure adequate inspection of both the inner and outer surfaces of the sleeve. The internal and external coils used in the work are shown in Fig. 4.10.

A reference standard was prepared with longitudinally milled notches 0.010 in. wide that varied in depth from 0.050 to 0.250 in. on the outer surface and 0.050 and 0.100 in. on the inner surface. This reference standard was used in calibrating the instrumentation. Sensitivity adequate to detect 0.100-in.-deep simulated cracks on both surfaces was demonstrated by the respective internal and external coils. Inspection of the graphite sleeves for the pilot production of fuel elements will give additional evaluation of the technique.

Inspection of Capsule Closure Welds. Work is continuing toward the development of radiographic techniques for inspecting the fuel capsule closure welds. One of the problems has been that the 0.200-in.-dia hanger pin makes the alignment of the radiation source and the radiographic film very difficult. The orientation illustrated in Fig. 4.11 is being considered. The geometrical interference produced by the separation between the film and the weld should be small enough to ignore in comparison with the size of the minimum detectable defect.

Another possible solution is the use of a masking technique which would permit radiography of the closure weld through the interfering pin, as illustrated in Fig. 4.12. Preliminary tests with this technique indicate that the size of the minimum detectable defect would not be increased by the additional material. This technique would offer the advantage of reduced radiation scatter and undercut and would simplify

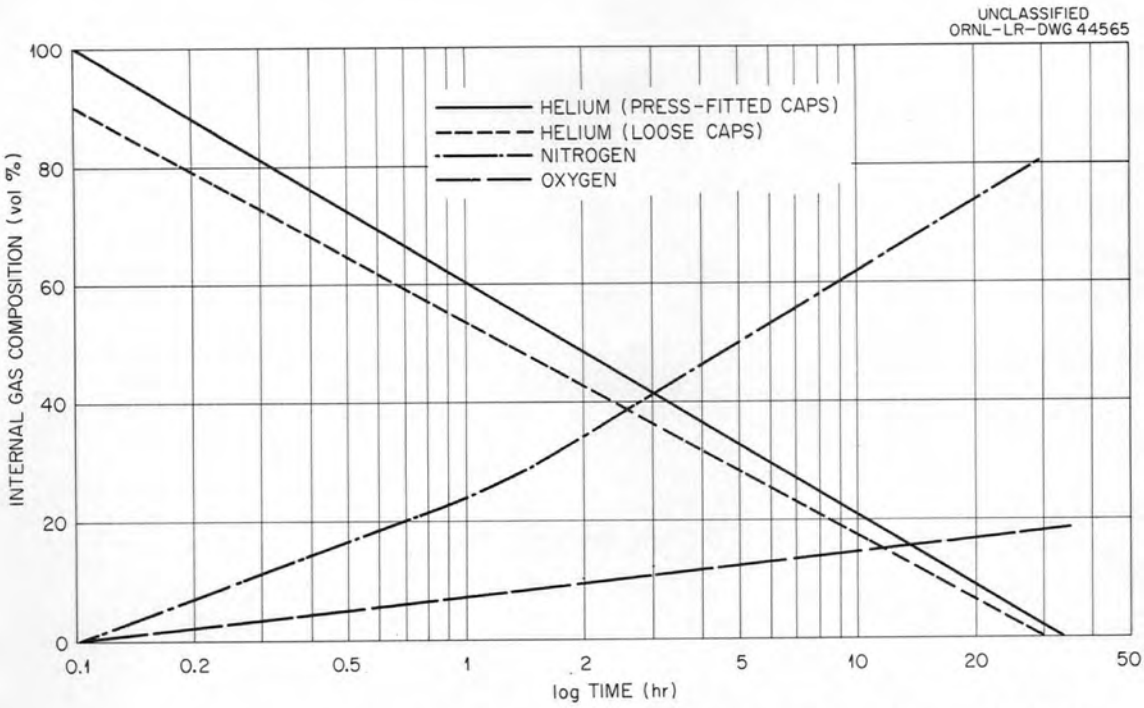

Fig. 4.9. Change in Composition of Internal Atmosphere of Fuel Capsule as a Function of Elapsed Time Before Welding.

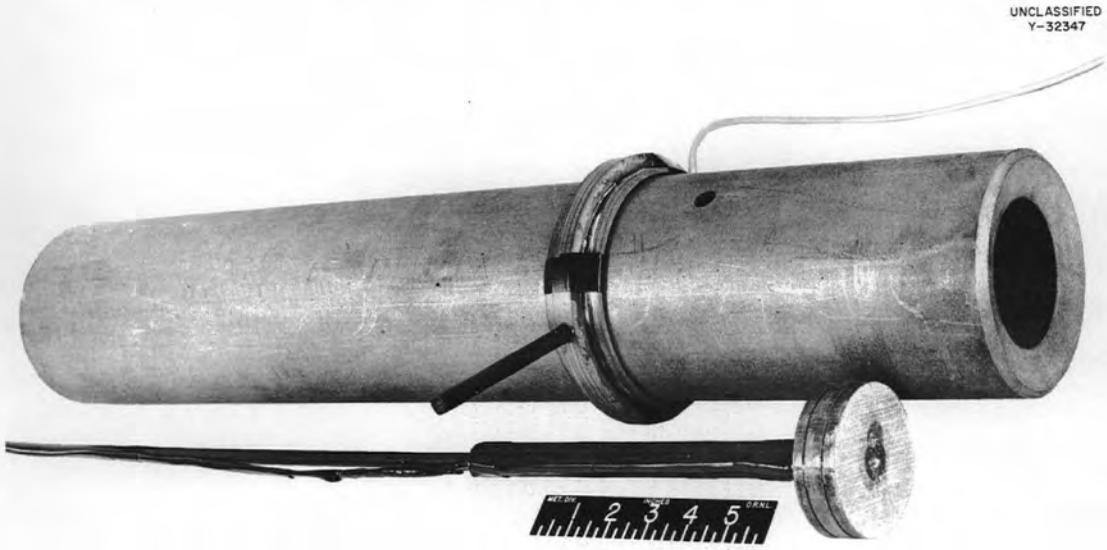

Fig. 4.10. Internal and External Coils Used for Inspection of Graphite Sleeves.

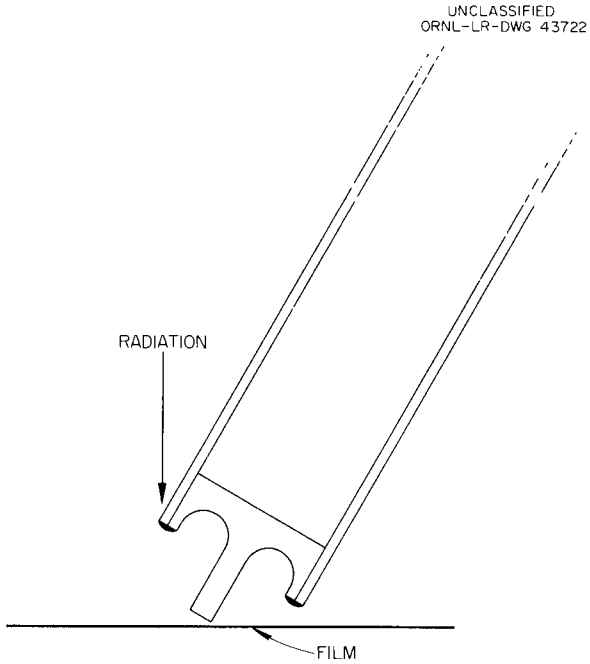

Fig. 4.11. Possible Orientation for Radiographic Inspection of Capsule-Closure Welds.

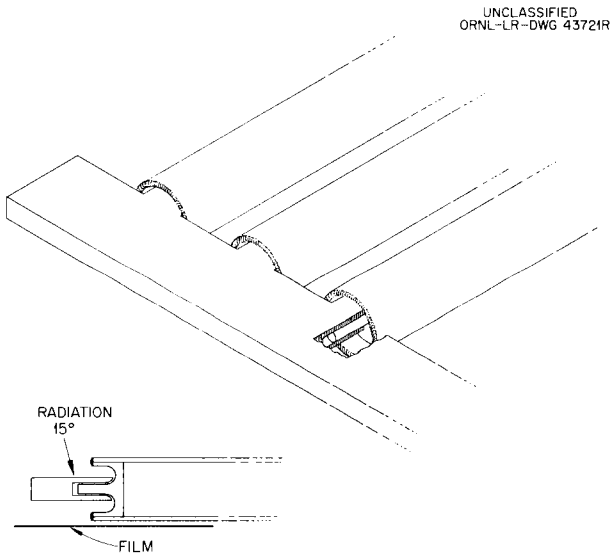

Fig. 4.12. Masking Technique for Radiographic Inspection of Capsule-Closure Welds.

the preparation of written procedures, whereas the first technique may offer higher contrast because of the thinner section of metal. Further study will be required to determine the optimum technique.

Helium Leak Detection. Evaluation of the "Procedure Specification for Helium Leak Testing of Gas-Cooled Reactor Fuel Capsules," RMIS-8, has been started in conjunction with the assembly of Title I fuel elements. Twenty-nine closure welds on fuel capsules have been inspected and found to be leaktight.

Welding of Ferritic Steels to Austenitic Stainless Steels

A proposed program for a dissimilar-metal welding study has been prepared, and samples of type SA-212, grade B carbon steel (to A-300 specification), Croloy (2 1/4% Cr–1% Mo), and type 304 stainless steel have been ordered. Delivery of material has been delayed as a result of the steel strike; however, small amounts of 1-in.-thick SAE-type 1020 carbon steel and type 316 stainless steel were obtained for preliminary investigations. A quantity of developmental nickel-base welding electrode (International Nickel Company BP-85) which has been recommended for the welding of dissimilar metals for high-temperature cyclic service was also obtained.

Several weld-test plates were prepared, with the welding being performed in the 1G (flat) position. The electrode is considered to have excellent operating characteristics, and flux removal from the weld bead poses no problem. Radiography of the welds indicated that porosity and flux entrapment were insignificant. Side-bend, tensile, radiographic, and metallographic studies have been made in accordance with procedures specified by Section IX of the ASME Boiler and Pressure Vessel Code, and the results have shown the welds to be satisfactory. A tentative welding procedure specification was prepared to cover the joining of type 1020 carbon steel to stainless steel in the range of thickness of 3/8 through 2 in. in the 1G position only.

Joints of SAE-type 1020 steel welded to type 304 stainless steel were prepared to test the compatibility of welding alloys with the

outgassing products of graphite. Type 304 stainless steel and carbon steel plates, 1/4 in. thick, were welded together using "Inco weld A," "Inco 62," and type 308 filler wires. Tensile specimens were then machined from the plates for testing in the component materials compatibility tests.

Reactor Vessel Penetrations

Burst-Slug Detection Tubes. A procedure is being developed for joining the burst-slug detection (BSD) tubes to the pressure shell. A mockup assembly (BSD-1) was fabricated, as shown in Fig. 4.13, to determine whether adequate welding-torch accessibility was available. It was apparent that manipulation could be improved materially and that

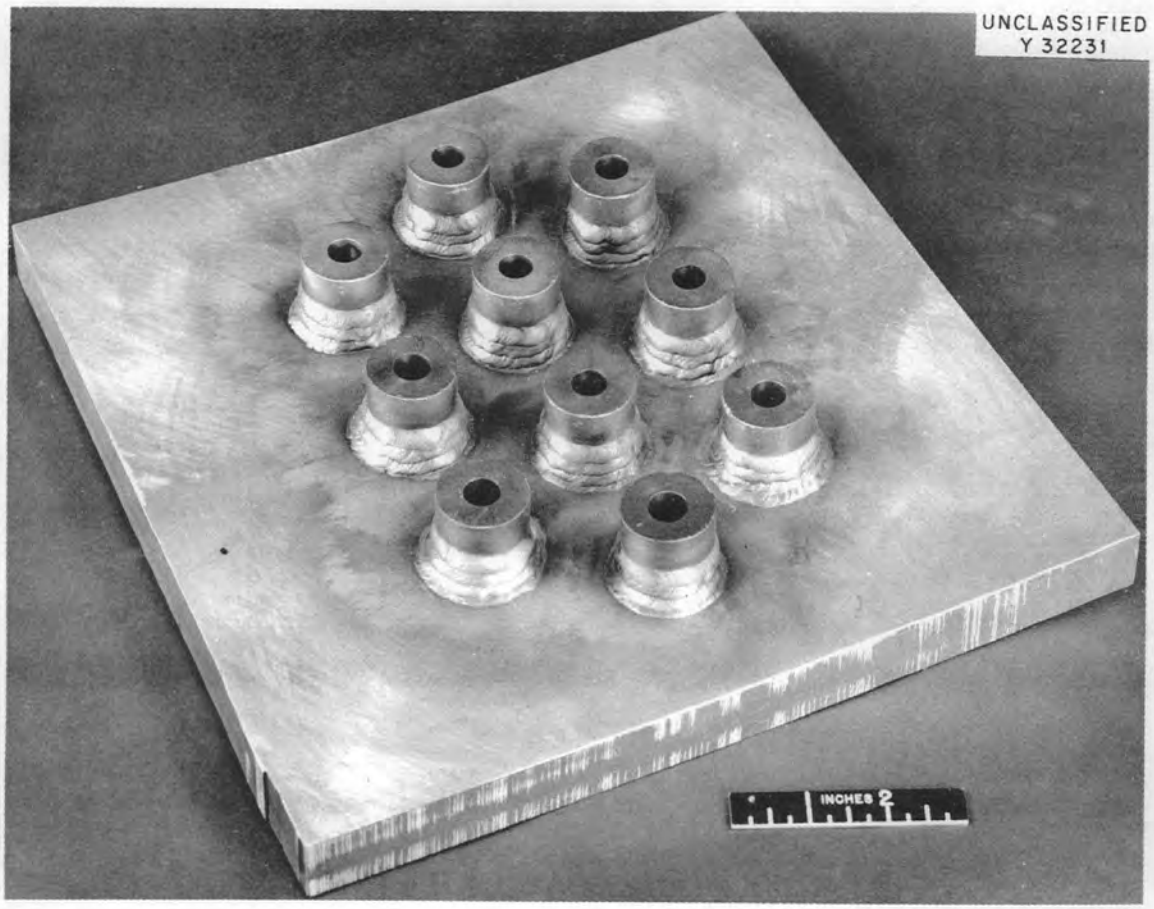

Fig. 4.13. Mockup BSD-1 of Welds for Burst-Slug Detection Tubes.

fewer weld passes would be necessary if the nozzle wall thickness was decreased. Consequently a mockup (BSD-2) is being fabricated with which ten transition nozzles will be welded to a 1-in. stainless steel plate, with the welding being performed in the horizontal (2G) position. The 7/16-in.-ID, 3/8-in.-wall nozzles are beveled at each end for welding. Each nozzle will be bored to 1/2 in. ID to permit entry of the BSD tubes after it has been welded to the plate. Fillet welds of the BSD tubes to the transition nozzles will then be made in the 5G position. Sample joints of each type have been prepared and are being examined metallographically.

Thermocouple Attachment. Components have been machined and experimental joints prepared to determine the suitability of various procedures for attaching the EGCR thermocouples to the pressure shell. The individual joints are being investigated prior to the construction of a mockup in order to evaluate the weld quality attained with different techniques. Several samples are being examined metallographically.

Inspection of Pressure Vessel Welds

About 11 linear feet of weldment in 4-in.-thick, type SA-212, grade B, steel plate has been completely inspected using ultrasonic techniques. The evaluation was carried out to develop adequate inspection techniques, as well as to determine the quality of the weldments. These test weldments were of three different types, as described in the previous report.[11] The 3-ft section of weld prepared in the overhead (4G) and downhand (1G) positions contained more and larger discontinuities than the other weldments. The largest discontinuities presented reflections equivalent to those from a standard having a diameter of 1/8 in. Examination of selected sections from these weldments is being carried out to confirm the results of the inspection. Some difficulty was experienced with the reflection obtained from the edge of the bead reinforcement. This difficulty may be remedied by (1) removing the reinforcement, (2) establishing

[11] GCR Quar. Prog. Rep. Sept. 30, 1959, ORNL-2835, p 96–99.

the size of acceptable discontinuities such that the signal from a rejectable defect will exceed that from the reinforcement, or (3) ignoring signals in the immediate vicinity of the reinforcement. Quality requirements and economic considerations will determine which of the three alternatives is most acceptable.

Beryllium Investigation

Reactions of Beryllium with Gases

Studies were initiated to determine the maximum permissible temperatures for exposure of beryllium in (1) low concentrations of CO_2, CO, CH_4, H_2, and H_2O in pressurized helium and in (2) pressurized CO_2 with impurities of CO, H_2O, H_2, and CH_4. The estimated maximum content of each impurity is 0.1 vol %.

An apparatus was constructed for investigating the reaction of beryllium with CO_2, using a sensitive manometer to monitor the reaction. Beryllium sheet 0.020 in. thick was carefully polished and exposed to CO_2 at an initial pressure of 200 mm Hg at 700°C. The weight gain of the sample after 200 hr was 1.1 mg, whereas a weight gain of only 3 μg was predicted based on manometric data and the assumption that the reaction was

$$4Be + CO_2 \rightarrow 2BeO + Be_2C \ .$$

Mass-spectrographic analyses of the residual gases in the reaction chamber and the two standard bulbs are presented in Table 4.6.

Examination of the reaction film of the specimen by electron-diffraction revealed no compounds other than BeO. Thus it may be concluded that the reaction under these condition is

$$Be + CO_2 \rightarrow BeO + CO \ .$$

Table 4.6. Composition of Residual Gases from Reaction of Beryllium with CO_2

Component	Amount in Reaction Bulb (%)	Amounts in Standard Bulbs (%)	
		Bulb No. 1	Bulb No. 2
H_2	0.9		
H_2O		0.1	0.1
CO and N_2	35.9	1.3	1.3
O_2	<0.1	0.5	0.4
A	0.3	0.3	0.3
CO_2	62.8	97.9	97.9

Additional experiments will be performed to investigate the effect of CO on the reaction.

Evaluation of Beryllium Tubing

One of the principal defects noted in beryllium tubing by radiographic inspection is the presence of high-density inclusions. These are largely surface inclusions of mild steel that formed during the extrusion operation. Since these inclusions cause considerable interference with the inspection techniques, they must be removed by selective dissolution in concentrated sulfuric or nitric acid. All tubing is currently being cleaned by this method before inspection.

Pulse-echo ultrasonic inspections of the tubing are made to determine the condition of the inner surface. One large crack that extended nearly through the wall from the inside was detected by this method.

Joining of Beryllium

Studies are continuing in an effort to develop techniques for joining beryllium. These studies include fusion welding, high-temperature brazing, and diffusion bonding. The welding studies have been confined to investigations of techniques for joining machined end caps to extruded tubes with the use of an edge-weld joint design. The inert-arc welding process has been used with both direct and alternating welding currents.

All specimens fabricated thus far have exhibited extensive porosity, but the use of alternating current and a copper chill ring appears to minimize this condition. It is believed that base-metal contamination is at such a level that the porosity presently found in the weld zone is, in part, caused by these impurities. This assumption has not yet been verified.

Brazing. Screening tests are in progress of brazing alloys for joining beryllium for service up to 700°C. The alloy systems listed below are being studied:

Ag–Ti–Be	Cu–Ti–Zr–Be
Ag–Zr–Be	Pd–Ti–Al–Be
Pd–Ti–Be	Cu–Ti–Be
Pd–Al–Be	Cu–Zr–Be
Ag–Ti–Zr–Be	

Buttons (10 g) of several of these compositions are being prepared, and flowability determinations and metallographic examinations on vacuum-brazed T-joints will be conducted. Of the compositions tested thus far, the 49 wt % Ti–49 wt % Cu–2 wt % Be alloy appears to be quite promising. This alloy exhibits excellent flowing and wetting properties on beryllium. The joint integrity appears to be good if the brazing cycle is controlled so that the time at the brazing temperature is minimized. A cross section of a brazed beryllium T-joint is shown in Fig. 4.14.

Since the fabrication of in-pile tube-burst specimens requires that a stainless steel tube be joined to one end cap in order to pressurize the specimen, an experimental joint between beryllium and stainless steel was made. A tube of type 430 stainless steel was joined to a beryllium end cap using the 49% Ti–49% Cu–2% Be brazing alloy and was found to be leaktight. A longitudinal section of this joint is shown in Fig. 4.15, and a magnified view of the joint showing both interfaces is presented in Fig. 4.16. Aging and thermal-cycling tests are presently being conducted on similar joints of this type.

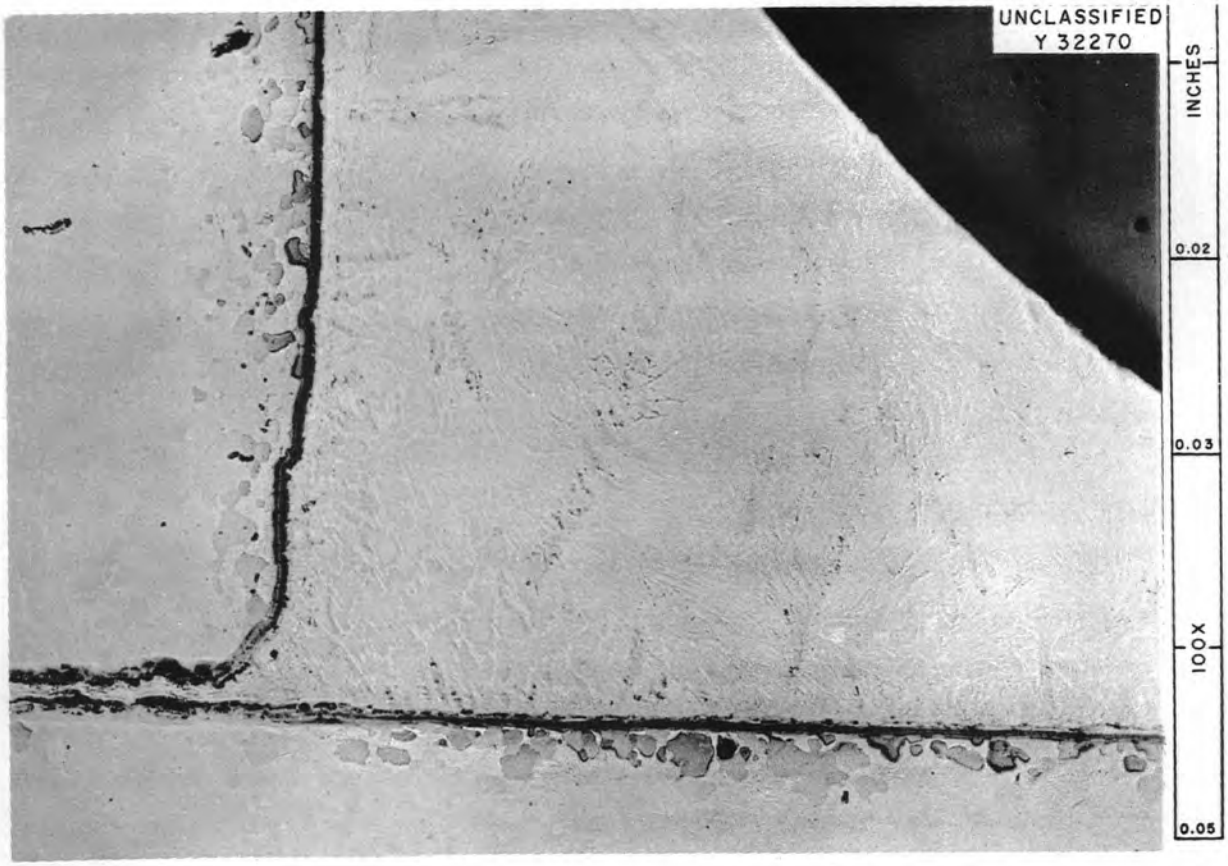

Fig. 4.14. Beryllium T-Joint Made With 49 wt % Ti–49 wt % Cu–2 wt % Be Alloy. Unetched.

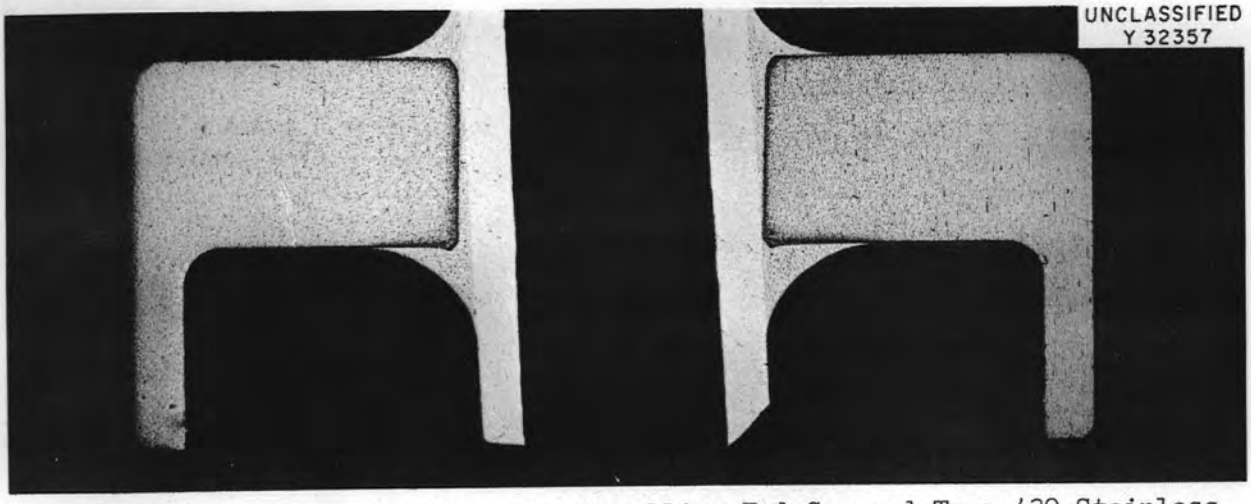

Fig. 4.15. Cross Section of a Beryllium End Cap and Type 430 Stainless Steel Tube Brazed with 49 wt % Ti–49 wt % Cu–2 wt % Be. 6.5 X. Unetched.

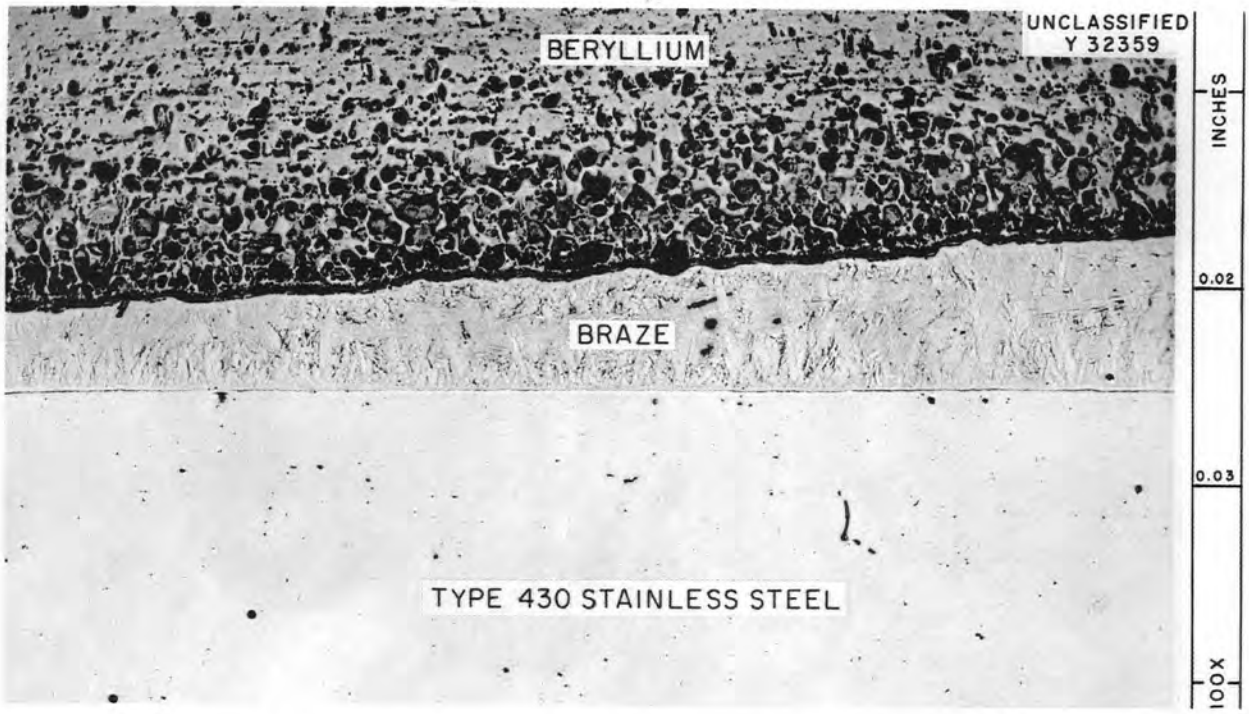

Fig. 4.16. Enlarged Section of Fig. 4.2 Showing the Interfaces Between the Braze and the Two Base Metals. Unetched.

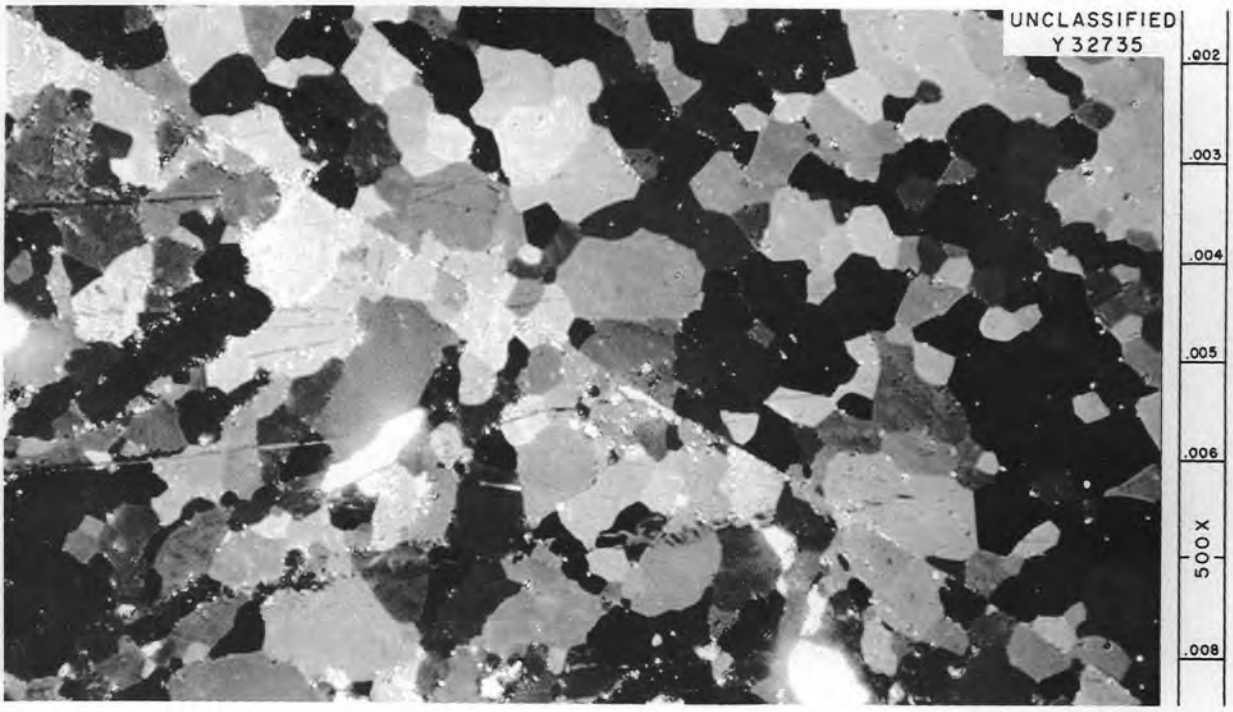

Fig. 4.17. Diffusion Bond of Beryllium After 24 hr at 1000°C. Polarized light.

Diffusion Bonding. The molybdenum apparatus and the technique discussed in the previous report[12] are being used to make diffusion bonds that are being evaluated under various conditions of time and temperature. A section of a diffusion bonded specimen heated from 24 hr at 1000°C in the molybdenum jig is shown in Fig. 4.17. The bonding interface shows slight deformation and occasional grain growth across the original boundary. Additional leaktight diffusion bonds have been made by heating for 2 and 4 hr at 1100°C. These joints are being examined metallographically.

---

[12] GCR Quar. Prog. Rep. Sept. 30, 1959, ORNL-2835, p 100.

5. IN-PILE TESTING OF COMPONENTS AND MATERIALS

Fuel Element Irradiation Program

Irradiation of the first set of eight full-size (diameter only) single fuel rod specimens has been completed in the ORR and one capsule has been removed from the ETR. Postirradiation examinations of most of the fuel assemblies from these experiments have been started. A second set of eight capsules has been installed in the ORR and four additional units are in the ETR, bringing the total being irradiated to 18. Five fuel stringers irradiated in the GETR loop were removed for examination, and all were observed to be defective because of faulty installation and/or improper loop operation. Since time will not permit the fabrication, irradiation, and examination of additional fuel assemblies at the GETR within the EGCR fuel procurement schedule, use of this loop has been discontinued.

Full-Diameter Prototype Fuel Capsules

ORR Experiments. Irradiation in the ORR of the eight experimental capsules described previously[1] was completed on October 31. Following withdrawal, the units were moved to the west pool of the reactor and readied for transfer into the ORR south hot cell. The operating data for this group of experiments are summarized in Table 5.1. The relationship of the temperature of capsule 0-2 to the heat barrier gas composition (0.008-in. gas annulus) when adjusted with mixtures of helium-nitrogen and helium-argon is shown in Fig. 5.1.

A second set of eight capsules that are essentially duplicates of the group 1 capsules was inserted in the reactor on November 29 and irradiation commenced with reactor operation cycle 19 on December 3. A revised flow diagram of the control system for these experiments is

[1] GCR Quar. Prog. Rep. Sept. 30, 1959, ORNL-2835, p 104.

Table 5.1. Summary of Operating Data for Full-Diameter Prototype Capsule Irradiations in the ORR

Starting date: 4/11/59
Ending date: 10/31/59
Reactor power generation during irradiation: ~70,000 Mwhr

	Capsule Number							
	0-1	0-2	0-3	0-4	0-5	0-6	0-7	0-8
Reactor position	P-8, P-9	P-8	P-7, P-8	P-7	P-3	P-2, P-3	P-2	P-1, P-2
Perturbed thermal flux, neutrons/cm^2·sec	8.8×10^{12}	8.9×10^{12}	10.0×10^{12}	11.4×10^{12}	11.1×10^{12}	9.2×10^{12}	9.4×10^{12}	8.1×10^{12}
Number of pellets	12	12	12	12	12	12	11	11
Pellet density, % of theoretical								
Bulk								
Maximum	94.99	94.80	95.08	94.99	95.17	94.26	96.44	96.35
Minimum	94.26	93.71	94.35	94.17	93.71	93.71	95.62	94.17
Average	94.68	94.17	94.80	94.62	94.17	94.07	95.99	95.26
Immersion								
Maximum	97.45	98.18	97.54	97.22	98.18	98.45	96.81	96.81
Minimum	96.90	97.72	96.99	97.08	97.72	97.45	96.63	95.53
Average	97.33	97.90	97.27	97.33	97.99	98.18	96.72	96.17
Pellet enrichment, % U^{235}	4.03	4.03	4.03	4.03	4.03	4.03	3.052	3.052
Oxygen-to-uranium ratio	2.0287	2.0365	2.0287	2.0287	2.0365	2.0365	2.0008	2.0227
Pellet diameters (cold), in.								
Inside (average)	0.3248	0.3233	0.3247	0.3254	0.3234	0.3233	0	0
Outside (average)	0.7064	0.7060	0.7063	0.7065	0.7061	0.7060	0.7060	0.7061
Radial clearance, UO_2—clad, in.								
Maximum	0.0029	0.0030	0.0029	0.0027	0.0031	0.0031	0.0031	0.0031
Minimum	0.0016	0.0020	0.0018	0.0019	0.0020	0.0016	0.0021	0.0020
Total power, Btu/hr·ft	24,800	24,900	28,100	31,900	31,900	25,700	25,900	22,300
Total heat flux, Btu/hr·ft^2	134,200	134,700	152,000	172,600	172,600	139,000	140,100	120,600
Burnup (calculated)								
Total, Mwd/MT	1678	1697	1900	2158	2102	1752	1369	1186
Rate, Mw/MT	11.50	11.63	13.02	14.79	14.41	12.01	9.38	8.13
Irradiation time, days (normalized to operation at 20 Mw)	145.8	145.8	145.8	145.8	145.8	145.8	145.8	145.8
Typical irradiation conditions[a]								
Temperature at outer surface of cladding, °F								
Design	1300 ± 50[b]	1600^{+0}_{-50}[c]	1300 ± 50	1300 ± 50	1600^{+0}_{-50}	1600^{+0}_{-50}	1300 ± 50	1600^{+0}_{-50}
Highest	1406	1576	1348	1370	1578	1558	1410	1528
Lowest	1240	1430	1188	1250	1272	1340	998	1446
Average	1323	1514	1301	1324	1450	1475	1248	1501
Pressure on outer surface of cladding, psig	297	295	296	291	294	294	294	290

[a] As of 7 a.m. on 10/13/59.

[b] Average temperature to be indicated by the six thermocouples.

[c] Highest temperature to be indicated by the thermocouples.

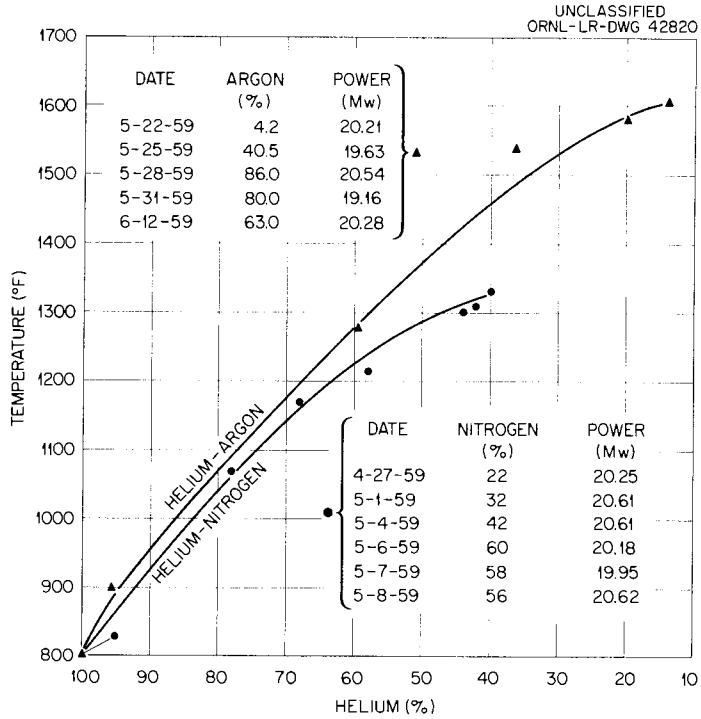

Fig. 5.1. Relationship of Temperature of Capsule O-2 to Composition of Heat Barrier Gas.

shown in Fig. 5.2. A new method has been provided for passing the temperature-control gas through the capsule, but otherwise the revisions are minor. To reduce possible temperature fluctuations resulting from bypassing of the temperature-control gas, the mixed gas is now introduced at the top of the capsule and bled out from the bottom. For group 1 capsules, gas was introduced at the top, channeled in a helical path to the bottom and back to the top, where it exited from the capsule. Also, removal of the channelling wires which also served as spacer wires permits a considerable reduction in the amount of annulus spacer wire needed and increases the over-all thermal resistance. This, coupled with an increase in the annulus gap from 0.008 to 0.012 in., makes it possible to operate the four high-temperature capsules at 1600°F with a helium-nitrogen gas mixture. A helium-argon mixture had been used previously. The other four capsules have been similarly modified but will be tested at 1300°F as before.

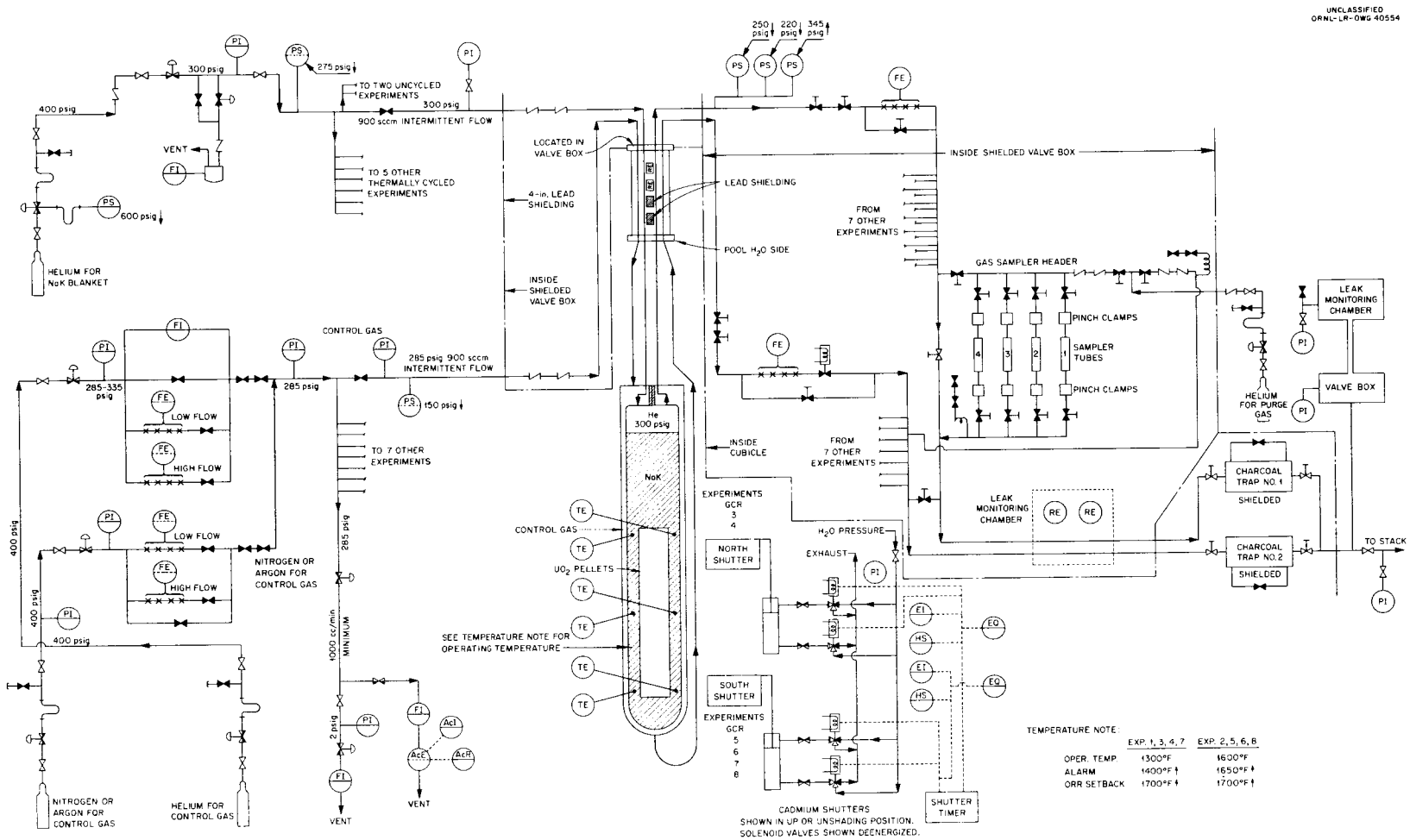

Fig. 5.2. Revised Flow Diagram for Irradiation Tests of Full-Diameter EGCR Prototype Fuel Elements in the ORR.

ETR Experiments. The first ETR capsule, designated E-1, was removed from the reactor on October 19 after achieving a total burnup of 1005 Mwd/MT. During most of the irradiation period the capsule was at the design surface temperature of 1300°F, although lower temperatures were experienced at the outset. The fuel pellet can was removed from the assembly in the MTR hot cell and shipped to the General Electric Company Laboratory at Vallecitos, California, for detailed examination. Visual inspection in the MTR cell showed the capsule to be in good condition; however, photographs revealed a slight change in the appearance of the cladding at the interfaces between pellets.

The six experimental assemblies installed in the ETR during July continue to operate satisfactorily, except for periods of low-temperature operation. It has been necessary to move the in-pile units repeatedly to obtain the desired neutron flux because of flux changes due to other ETR experiments. Four additional capsules have been installed and a fifth is completed and ready for the next cycle.

Reduced-Size Prototype Capsules

Following extensive modification of the GETR loop facility, one reactor cycle (3 weeks) of satisfactory loop operation was achieved with gas temperatures maintained at approximately 800°F. Helium leakage continued to be a problem but was sufficiently reduced to permit continued operation. Prior to the startup of this reactor cycle, it was necessary to replace the facility tube gasket for fuel stringer 1-2. This operation required lifting the stringer a few inches. Following replacement of the gasket, it was found that the fuel stringer could not be lowered into operating position, and therefore the assembly was removed for examination. It was observed that the fuel cans had warped badly and that most of the thermocouples were detached. It was then revealed that a temperature excursion had occurred on May 16 in which fuel temperatures were in excess of the recorder range, 1600°F. Further investigation showed that the fuel stringers had been seated on the bottom of the facility tubes rather than suspended from cables as designed. This

permitted the thermocouple sheaths to apply a column load to the fuel stringers through thermal expansion when exposed to the high gas temperatures. One or both of these factors are believed to be responsible for the fuel stringer damage. Stringers 1-3 and 1-1, which were on opposite sides of stringer 1-2, were also removed for examination and found to be damaged, although less severely. It was also apparent from the operational data that all thermocouples on fuel stringer 1-4 had become detached. Fuel stringer 1-5, which was installed just prior to discovery of the damaged elements, appeared to operate satisfactorily throughout the October reactor cycle, although it also had not been properly installed. Upon removal from the loop, distortion was found which indicated that improper installation was the principal cause of damage.

There is not now sufficient time available for the fabrication, irradiation, and examination of a new set of stringers prior to the date for specification of the EGCR fuel. Accordingly the General Electric Company was requested on November 3 to remove the facility tubes from the reactor for temporary storage and to place the loop in standby condition pending its disposition.

The fourth attempted experimental calibration of fuel stringer thermocouples was unsuccessful because of failure of the calibration thermocouples and defective fabrication of the electrical heater. Accordingly, although fuel stringer 1-5 was irradiated at an estimated temperature of 1300°F, an uncertainty of approximately 100°F exists in the temperature. The estimated burnup for this fuel stringer is less than 400 Mwd/MT. Fuel stringer 1-4 reached an estimated burnup of 700 Mwd/MT, and stringers 1-1, 1-2, and 1-3 reached 500 Mwd/MT.

Miniature Capsule Fission-Gas-Release Experiments

Irradiation of UO_2 pellets in fission-gas-release experiments has been extended to temperatures of 3400°F. A new capsule with a depleted UO_2 ceramic insulating bushing around the UO_2 fuel has been designed and fabricated for use in a series of experiments to extend the irradiation temperature range to higher values. Test capability with the new

capsules should be greater than 4000°F, and it is hoped that the thermometry can be extended to this range.

With the exception of the temperatures given for experimental assembly L-16abx, which had tungsten-rhenium thermocouples in both ends, the central void temperatures listed in Table 5.2 were measured with platinum-platinum-10% rhodium thermocouples in the "a" sample and tungsten-rhenium thermocouples in the "b" sample. It has been found that platinum-platinum-10% rhodium thermocouples with BeO insulation will operate for an extended period of time at temperatures up to 2850°F; however, drifts in emf's equivalent to approximately 50 to 80°F per day are present above temperatures of about 2200°F. The experimental assemblies combing tungsten-rhenium thermocouples, BeO insulation, and a tantalum sheath also show drifts in emf's, but to a much lesser extent (about 5 to 10°F per day), at temperatures up to 3400°F. To exclude the fission gas atmosphere from the junction of a platinum-platinum-10% rhodium thermocouple, a tantalum sheath was swaged over the BeO insulation containing the thermocouple wires. Three thermocouples of this design were used, and all failed either during the initial heatup or shortly thereafter. X-rays of similar assemblies indicated that the cause for failure probably resulted from twisting and kinking of the wires during fabrication.

Agreement between the tungsten-rhenium thermocouples and the platinum-platinum-10% rhodium thermocouples during the first few hours of operation is very good. However, for service at temperatures greater than 2200°F for extended periods of time, the tungsten-rhenium thermocouples are superior. Only one Chromel-Alumel thermocouple has failed while operating at a temperature of 1300°F. These thermocouples are very dependable and have not shown drifts in emf relative to each other.

The cladding on experimental assemblies L-10ab and L-21ab failed. The fission products thus released from both capsules were contained in the offgas system, and the experimental assemblies were removed from the reactor without incident. The cause for these cladding failures is unknown, since the stress calculations indicated values within the allowable code limits.

Table 5.2. Operating Conditions for Miniature Capsules Irradiated in the LITR

Experimental Assembly No.	UO_2 Density (% of theoretical)	UO_2 Enrichment (% U^{235})	Central UO_2 Temperature (°F)		Date Installed in LITR	Date Removed From Reactor
			"a" Capsule	"b" Capsule		
L-7abx	95	20	(a)	2950	9-22-59	In-pile
L-10ab	95	20	2450	3000	8-18-59	9-22-59[b]
L-11ab	85	20	2460	2850	7-7-59	In-pile
L-16ab	95	30	1810	2040	6-16-59	9-21-59
L-16abx	95	30	2860	3400	9-29-59	11-2-59
L-17abx	95	30	3100	3300	9-9-59	10-13-59
L-18abx	85	30	2860	3180	7-7-59	10-13-59
L-20abx	75	15			8-18-59	8-18-59[c]
L-21ab	95	10	1500	1650	8-11-59	10-6-59[d]
L-22ab	95	10	1400	1600	11-10-59	In-pile[e]

[a]Thermocouple failed during initial heatup.

[b]Cladding failed; assembly removed from reactor shield 9-25-59.

[c]Leak found at thermocouple joint during startup; assembly removed from reactor shield 8-25-59.

[d]Cladding failed; assembly removed from reactor shield 10-13-59.

[e]Fuel encapsulated in helium.

As indicated by the absence of increases in central fuel temperatures at thermal neutron doses between 3×10^{16} and 3×10^{20} neutrons/cm^2, the thermal conductivity of UO_2 does not appear to change with radiation. Better values of this parameter will be obtained after installation of rotometers and additional thermocouples in the cooling air stream so that a heat balance can be obtained.

Advanced Fuel Elements

A series of irradiation experiments has been initiated to evaluate graphite-clad fuel elements consisting of UC_2 in a graphite matrix. The test specimens are enriched to obtain acceleration of burnup and high central temperatures with reduced dimensions for convenience in testing. Test fuel pieces are 1 in. in diameter and 1 1/2 in. long. The effects of irradiation on chemical and dimensional stability of the fuel and cladding and the migration of fission products through the structure are to be studied. Heat generated in the fuel is dissipated to water from a stainless steel capsule in which high fuel surface temperatures are obtained by the thermal resistance of a gas annulus between the graphite and the container wall. Two fuel pieces are assembled in an instrumented tandem arrangement, as shown in Fig. 5.3. Low-density carbon was used to obtain thermal insulation in the supports at the capsule ends which accurately center the fuel in the stainless steel jacket. Dobule containment for released fission gases is provided by the outer aluminum can which is shrink-fitted over the stainless steel in the heat transfer area and is grooved to provide extended surface in the cooling water stream. The large helium-filled volume in the stainless steel can minimizes the concentration of the fission gases, which would otherwise increase thermal resistance and consequently fuel temperatures during irradiation. Temperatures are measured at three positions opposite the center of each matrix, 120° apart, and at the midpoint of the graphite cladding. The emf's of the six type 316 stainless steel-sheathed MgO-insulated Chromel-Alumel thermocouples are monitored by three temperature recorders, two of which provide reactor control. The specified

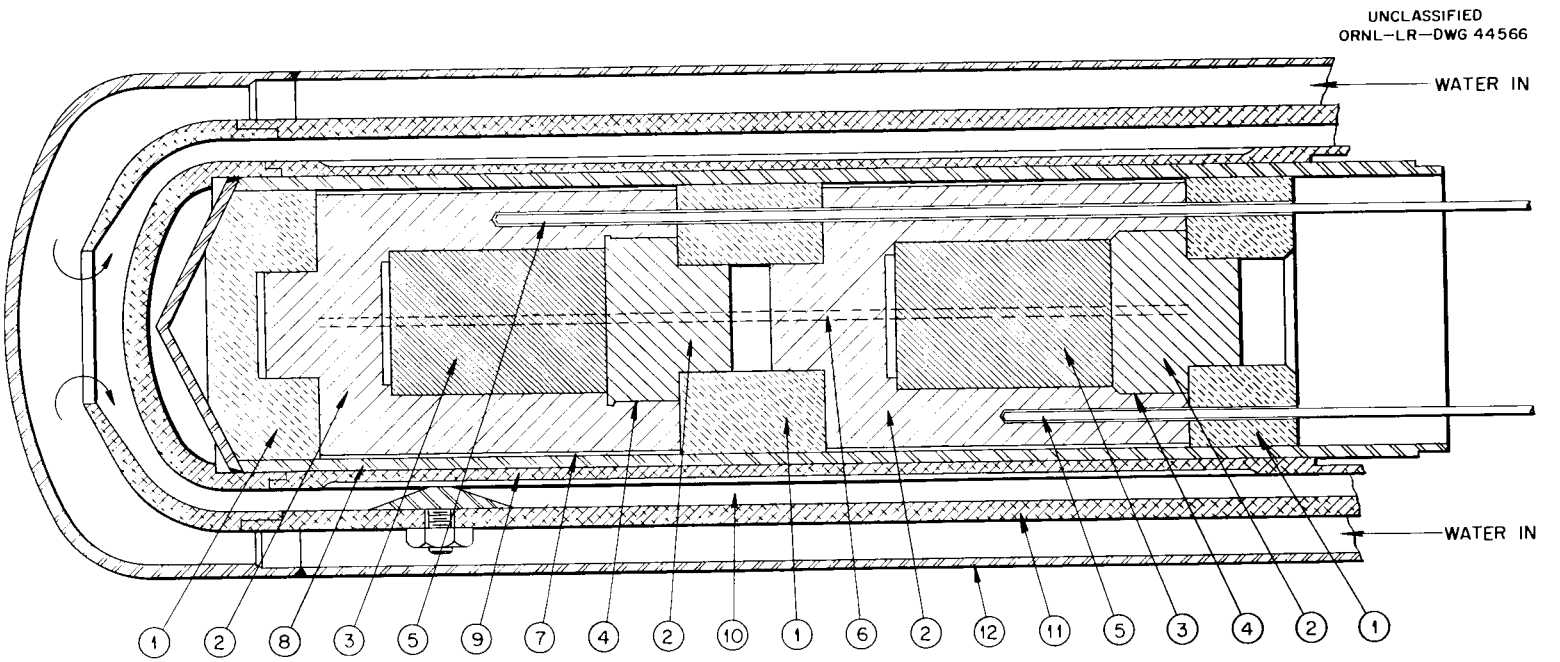

1. POROUS CARBON-60
2. R-0020-TYPE GRAPHITE
3. U^{235}-FUELED GRAPHITE MATRIX
4. GRAPHITE THREADS SEALED WITH Si–SiC
5. TYPE 316 STAINLESS STEEL-SHEATHED MgO INSULATED CHROMEL-ALUMEL THERMOCOUPLES (THREE 120° APART PER MATRIX)
6. FLUX MONITOR WIRES 120° APART ALONG FULL LENGTH OF BOTH MATRICES
7. HELIUM GAS GAP, 0.010 in.
8. INNER CONTAINMENT VESSEL, TYPE 304 STAINLESS STEEL
9. OUTER CONTAINMENT VESSEL, 6061 ALUMINUM (WITH LONGITUDINAL GROOVES)
10. 1/8-in. WATER FLOW ANNULUS
11. WATER FLOW DIVIDER, 6061 ALUMINUM
12. OUTER WATER JACKET, TYPE 304L STAINLESS STEEL

Fig. 5.3. Experimental Assembly for Irradiation of Graphite-Clad Fuel Elements.

operating temperature is 1600°F, with overtemperature protection set at 1650°F. The capsule is designed as a replaceable element in a beam hole shield plug. Temperature control is effected by moving the entire assembly in the flux gradient of the beam hole to change the heat generation rate. The first experimental assembly, identified as ORNL-48-1, is now being irradiated in the MTR HB-3 facility. Instrumentation, control, and handling equipment constructed for the molten-salt loop experiments operated previously have been utilized.

The fuel pieces and graphite for the first experiment were supplied by the National Carbon Company and were machined and assembled to fit the ORNL capsule. Dimensions, fuel loading, and density, as well as thermal flux, heat generation, and temperature data for the first experiment are given in Table 5.3. The fuel is typical of that proposed for advanced gas-cooled reactors, but available type R-0020 graphite instead of high-density graphite was used for encapsulation to initiate the first test during a period when suitable irradiation facilities were available. Uranium enrichments were chosen to give 1500 to 1600°F indicated temperatures for each fuel piece; however, the flux gradient apparently is steeper than predicted, and the rear fuel piece operates at 1300 to 1400°F.

Instantaneous Fission-Gas-Release Experiment

An experimental assembly is now being irradiated that contains two thin plates of high-density UO_2 with thermocouples sandwiched between them, as well as thermocouples on the outer surfaces. The assembly is air cooled, and the fission power is varied by inserting or withdrawing the assembly from the reactor lattice. Helium is passed over the fuel to entrain released fission gas. This experiment was described in detail previously.[2]

The gas emerging from the trap system is at a comparatively high level of activity and produces a complex gamma spectrum. Some products, presumably daughters of krypton and xenon, plate on the surface of the

[2] GCR Quar. Prog. Rep. Sept. 30, 1959, ORNL-2835, p 113.

Table 5.3. Conditions of First Experimental Irradiation of Graphite-Clad UC_2 Fuel in Graphite Matrix Experiment ORNL-48

	Forward Pellet No. 85	Rear Pellet No. 91
Pellet characteristics		
Diameter, in.	0.9969	0.9965
Length, in.	1.4687	1.4682
Volume, cm^3	18.766	18.764
Bulk density, g/cm^3	1.887	2.017
U^{235} enrichment		
Weight, g	3.1476	6.1822
Concentration, g/cm^3	0.1677	0.3295
Total weight of element, g	35.4107	37.8407
Estimated thermal flux, neutrons/$cm^2 \cdot sec$	4.6×10^{13}	1.9×10^{13}[a]
Fission heat, w/cm^3	270	300
Gamma heat, w/cm^3	4.70	2.80
Pellet heat, w	5065	5630
Total heat, w	6310	6326
Central pellet temperature, °F	3355	3616
Temperature of interface between graphite cladding and pellet, °F	1705	1796
Temperature at middle of graphite wall, °F		
Design	1525	1600
Average at start of test	1570	1310
Temperature at outer surface of graphite wall, °F	1389	1456
Temperature at inner surface of stainless steel capsule, °F	417	428

[a]Estimated from operating temperature.

counting chamber. This produces a high background which must be subtracted from the gas activity measurements. The background is measured directly upon purging of the counting chamber with pure helium. Measurements have been hampered by unstable behavior of the gamma spectrometer. Because of drift and nonlinearity, quantitative measurements have not

yet been possible. The single-channel analyzer requires 7 1/2 min for a spectrum scan. In addition to gamma energies, the half life of a component gas must be measured in order to identify the isotope. When gas is trapped in the counting chamber for a half-life measurement, many components vanish between one scan and the next. It is hoped that a 200-channel spectrometer will overcome some of these difficulties.

Neutron Flux Measurements

To determine the ratio of released to retained fission gas on a steady-state basis, it is necessary to know the neutron flux inside the fuel assembly at the time of equilibrium. An argon-activation method has been developed to determine this value. The system consists of an argon supply, pressure regulator, throttle valve, oxygen removal system, and a flowmeter. It is attached to the helium sweep system so that argon can replace the helium as a sweep gas. Because the volume of the fuel container is large compared with that of the positioning tube, the argon is activated by the neutron flux which produces the fission power. Argon-40 is the only significant isotope of argon, and it has a 1/v cross section with no resonance energy capture peaks. Argon-41 has a 1.8-hr half life and emits a single 1.3-Mev gamma ray. The argon is in the neutron flux less than 1 min, so the activation is directly proportional to the neutron flux and the time exposed to the flux.

At a constant flux (determined by temperature equilibrium) the flow rate of the argon can be varied, and a series of activity measurements can be obtained. The activity consists of fission-product activity and A^{41} activity. The fission product activity at a constant sweep gas flow rate is a function of fuel power and temperature only, so, at a given flux and temperature, this activity is a constant. Varying the flow rate of the argon produces no measurable temperature change of the fuel. The argon activity will vary with flow rate, and when equilibrium conditions are attained the combined activities can be expressed as $A_f + A_a = A$ (measured), where A_f is the activity of the fission products and is a known function of flow rate and A_a is the activity of the argon and is

a known function of flow rate and a known function of the flux. When A_f and A_a are corrected for the known function of flow rate to some arbitrary standard, an equation with two unknowns (the fission product activity and the flux) is obtained. Since each measurement results in a different equation, with the activity of the fission products a constant, a simultaneous solution of the equations eliminates the activity contribution of the fission product. Since all equations should yield the same flux, this method reveals the precision of the measurement as well as the flux. Preliminary flux measurements made with the use of this method were reproducible to within 10%.

UO_2 Thermal Conductivity Determinations

The thermal conductivity of a plate with uniform internal power generation and no edge losses can be determined from the expression

$$\Delta T = \frac{L^2 Q}{2K} ,$$

where Q is the power generated per unit volume, L is the half thickness of the plate, K is the thermal conductivity of the plate, and ΔT is the temperature across the plate. The plates being used in these experiments are 0.032 in. thick and are 4% enriched in U^{235}. The flux depression across the fuel will be small, and uniform power generation can be assumed. The edge losses can be neglected because of the large ratio of surface area to edge area. The temperature drop is measured by thermocouples located opposite each other between the plates and on the outer surface. Therefore, since the plates have known thicknesses, the thermal conductivity could be determined if the power were known. By measuring the neutron flux, the power could be calculated if the gamma heating were small compared with the fission heating. This suggests that if a fuel-bearing material with a known thermal conductivity were used in this facility, the neutron flux could be measured by argon activation, and the gamma heating could be determined by subtracting the fission power from the measured power. A relation between neutron flux and gamma heating could be established in this manner.

Any change in thermal conductivity can be detected by temperature measurements. If the temperature of the surface of the assembly which contains the fuel is a constant (for a given cooling air flow), then the power generated within the assembly is a constant. If the temperature inside the fuel sandwich remains a constant with time under these conditions, then the thermal conductivity of the material has not changed with time. The relation of the temperature inside the fuel to the temperature of the surface of the assembly is shown in Fig. 5.4. The

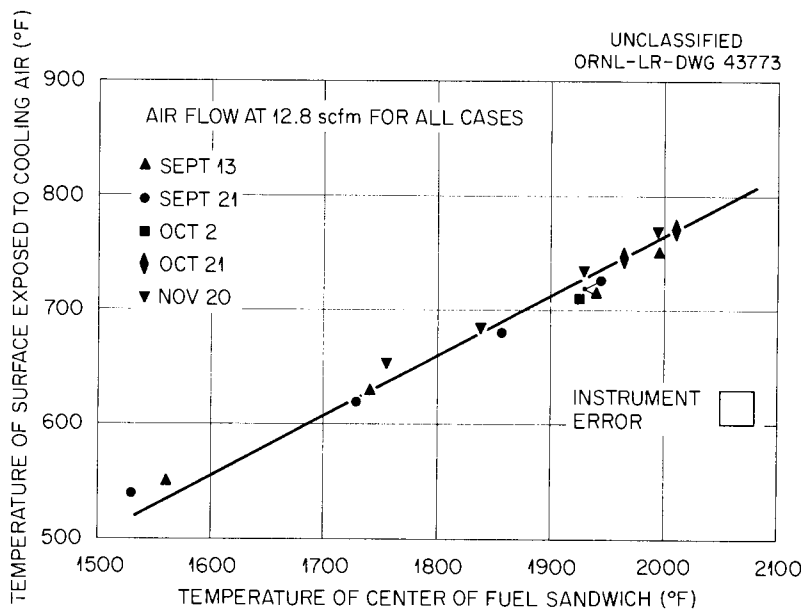

Fig. 5.4. Surface Temperature vs Fuel Temperature.

apparent shift of the November 20 points is probably due to a recalibration of the recorder monitoring the assembly surface temperature. This recorder was shifted to read 20°F higher on November 3, while the recorder for the central temperature needed no correction. Under any circumstance, the recorders are only accurate to 1% of scale reading, or to 30°F for this case. No change in thermal conductivity greater than 15% (the instruments limits) has been observed in a two-month period. The flux is estimated to be 1.2×10^{20} neutrons/cm^2.

When argon is substituted for helium as a sweep gas, the temperature of the fuel increases because of the lower thermal conductivity of the argon. Since the power remains a constant, any change in temperature

differential between the inside and outside of the fuel is a direct consequence of thermal conductivity change. In this manner, the relation of thermal conductivity to temperature may be established. In the 500 to 900°C range, the change in thermal conductivity agreed (to within instrument limits) with the relation given by Kingerly for UO_2 to 95% theoretical density:

$$\frac{K}{K_0} = e^{-1.207\ T \times 10^{-3}} ,$$

where T is temperature in degrees Kelvin.

Examinations of Irradiated Capsules

Miniature Capsules

Dimensional and Density Changes. Comparisons of UO_2 specimens before and after irradiation have shown a correlation between initial bulk density and changes in structure and dimensions. Examinations of the specimens described previously[3] have revealed no change in dimensions of pellets from capsule UO_2-1-1, which were 96% dense UO_2 and were irradiated to 4000 Mwd/MT at 1760°F. On the other hand, capsules L-3a and b, which contained UO_2 of 75% bulk density and which were irradiated to 5000 Mwd/MT at ~3000°F, showed 6 to 8% decreases in dimensions of the pellets. The length of pellet 10-4 in capsule L-3b changed from 0.2500 to 0.2360 in. The outside diameters of pellets 10-10 and 10-12 of capsule L-3a changed from 0.154 to 0.142.

As maybe seen from the data of Table 5.4, comparisons of pre- and postirradiation densities of pellets do not give indications of dimensional changes. The postirradiation immersion density measurements are made by utilizing a vacuum impregnation technique and subsequent immersion in CCl_4. Since the change in immersion density is small compared with the change in bulk density, postirradiation bulk density measurements are planned for the future. Immersion in mercury will be used as a means for obtaining the volume measurement.

[3] GCR Quar. Prog. Rep. Sept. 30, 1959, ORNL-2835, p 117.

Table 5.4. Effect of Irradiation on Density of UO_2 Pellets

Capsule No.	Pellet Density Before Irradiation		Pellet Immersion Density After Irradiation (g/cm^3)
	Immersion Density (g/cm^3)	Bulk Density (% of theoretical)	
L-1a	10.6	92.7	10.7
b	10.6	93.9	10.7
L-2a	10.2	84.9	9.5
b	10.1	84.4	10.3
L-4a	10.6	92.1	10.5
b	10.6	93.3	10.4
L-6a	10.5	73.6	10.5
b	10.5	74.2	10.5
L-14a	10.5	94.1	9.9
b	10.5	95.4	10.0

Changes in bulk densities have been apparent in ceramographic photographs taken before and after irradiation, as shown by the pellets from capsule L-6b in Fig. 5.5. No pattern of differential grain growth as a result of temperature variations in the pellets has been noted (Fig. 5.6). Photographs of 95 and 85% dense pellets irradiated in the LITR are shown in Figs. 5.7, 5.8, and 5.9. There were pieces large enough for dimensional measurements even in the 85% dense material.

Fission Gas Release. Two isolated cases of very high fission gas release have been observed. Capsule L-3b evolved 19% of the Xe^{133} that was formed; it initially contained 75% dense UO_2 and 2400 ppm C, had an oxygen-to-uranium ratio of 2.12, and was irradiated to a burnup of 5000 Mwd/MT at ~3000°F. Capsule L-17 evolved 56% of the Xe^{133}; it contained 94.6% dense material and 400 ppm C, had an oxygen-to-uranium ratio of 2.04, and was irradiated to a burnup of 4000 Mwd/MT at ~3300°F. It is felt, however, that these data should not be taken seriously without corroborating tests.

Analyses for the stable, as well as the radioactive, isotopes have been completed for capsule L-3a (described above). The results show

UNCLASSIFIED
PHOTO 48921

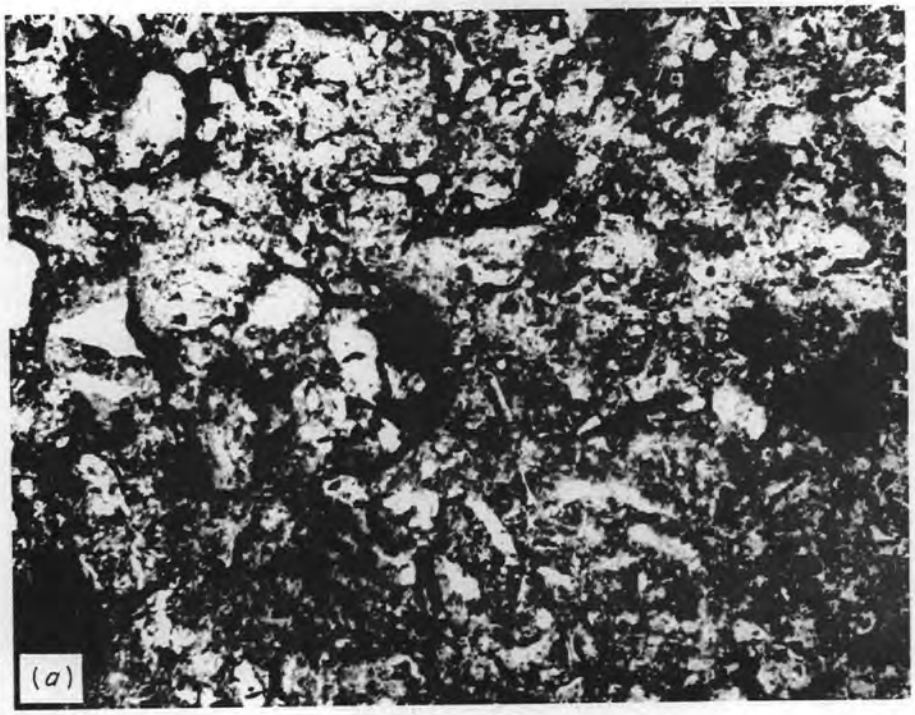

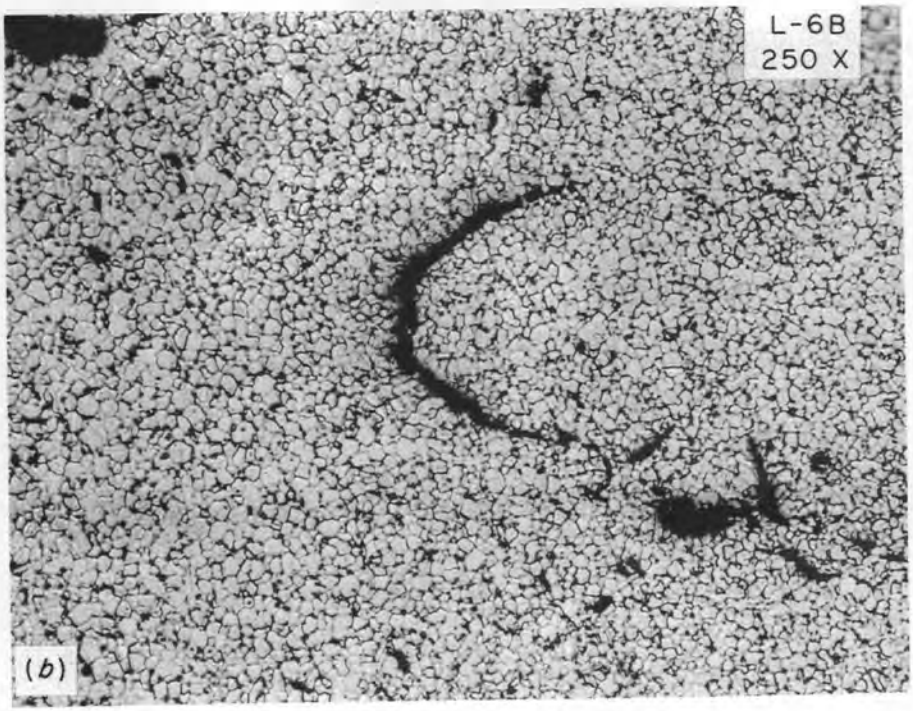

Fig. 5.5. (a) Unirradiated and (b) Irradiated UO_2 of 75% Bulk Density Showing Changes in Structure. Capsule L-6b before and after irradiation for 4000 hr at 2500°F in the LITR. Photographs made at the Vallecitos Atomic Laboratory. (b) 250X.

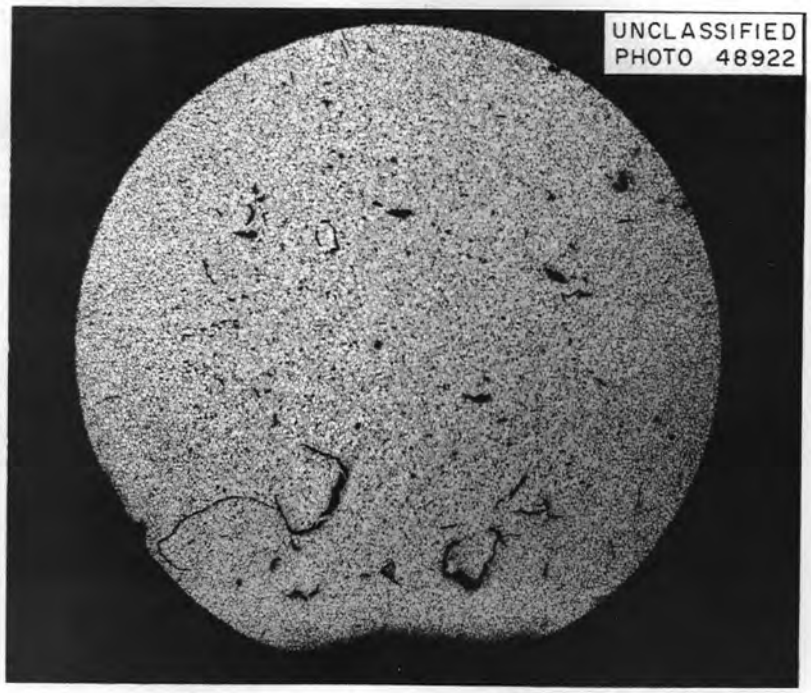

Fig. 5.6. UO_2 Pellet from Capsule L-6b Showing Absence of Differential Grain Growth. Capsule contained UO_2 of 75% bulk density and was irradiated for 4000 hr at 2500°F in the LITR. Photograph made at Vallecitos Atomic Laboratory. 75X.

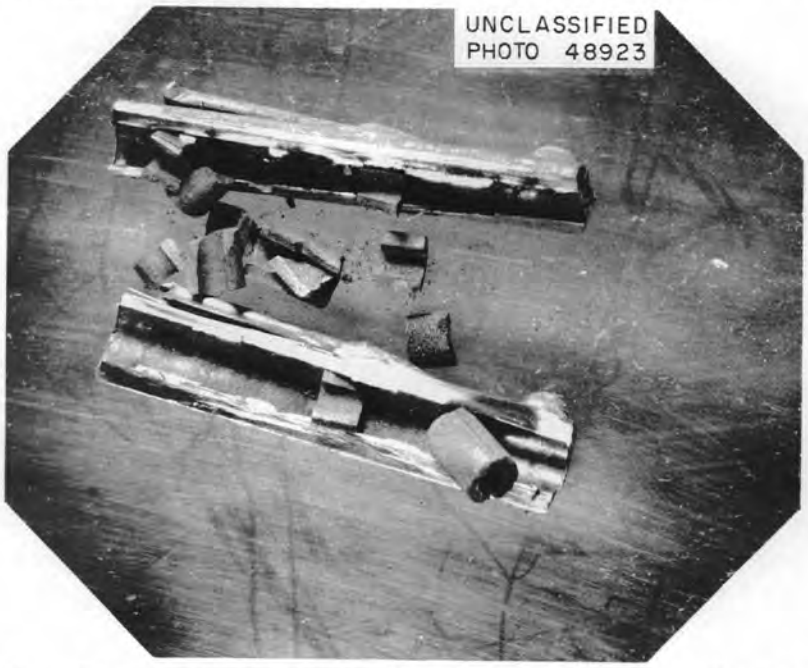

Fig. 5.7. Capsule L-3b, Which Contained 95% Dense UO_2 Pellets and Was Irradiated to 5000 Mwd/MT at 3000°F in the LITR. Note that some pieces were large enough for dimensional measurements. Photograph made at Vallecitos Atomic Laboratory.

Fig. 5.8. Additional Pellets from Capsule L-3. As in Fig. 5.7, note that some pieces were large enough for dimensional measurements. Photograph made at Vallecitos Atomic Laboratory.

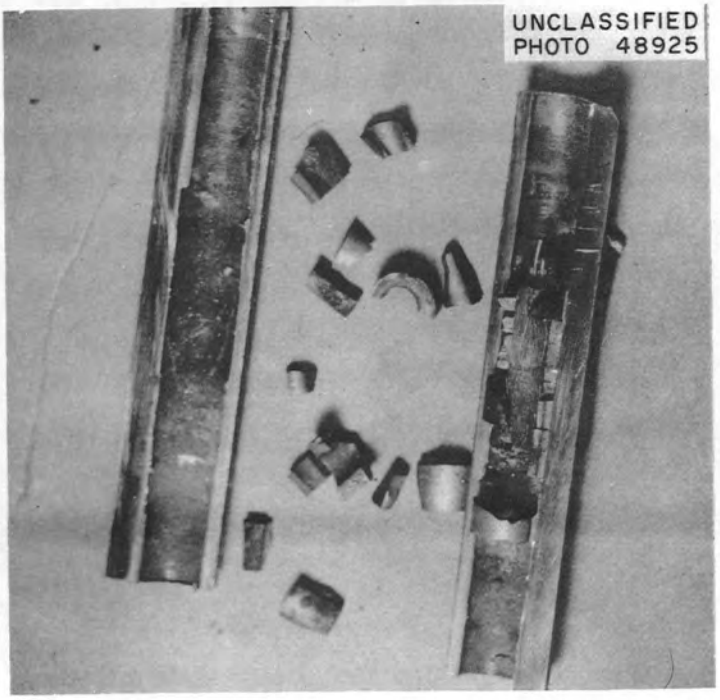

Fig. 5.9. Capsule L-8a, Which Contained 85% Dense UO_2 and Was Irradiated to 5000 Mwd/MT at 2600°F in the LITR. Note that, as in Figs. 5.7 and 5.8, some pieces were large enough for dimensional measurements. Damaged thermocouple may also be seen. Photograph made at Vallecitos Atomic Laboratory.

that roughly the same percentage of each isotope was evolved:

Isotope	Amount Evolved (% of that formed)
Kr^{83}	2.1
Kr^{84}	1.5
Kr^{85}	1.5
Kr^{86}	1.5
Xe^{131}	0.14
Xe^{132}	0.14
Xe^{133}	0.42
Xe^{134}	0.10
Xe^{136}	0.10

Burnup Analyses. In order to check the validity of the neutron fluxes determined by flux monitors on capsules UO_2-1-1, 1-2, and 2-1, it was decided to determine the fluxes by mass analyses of the uranium isotopes and plutonium. Since the atomic fractions of the various uranium isotopes (except U^{236}) do not change greatly with irradiations up to 10^{20} neutrons/cm^2, it was decided to send duplicate samples to the ORNL and Y-12 laboratories for mass spectrographic analyses in order to get some idea of the precision of the measurements.

Initially, samples were selected from small fragments of irradiated pellets returned to ORNL by the Vallecitos Atomic Laboratory after post-irradiation examination. It was recognized that these were not representative samples, so small fragments of unirradiated pellets were selected and subjected to the same decontamination procedures as the irradiated samples. Duplicate coded samples were prepared for each of the analytical laboratories.

The results of the various burnup analyses are presented in Table 5.5. Normally, results of a mass spectrograph analysis are given in atomic fractions which total one. The results listed under "atomic fraction" are derived from such measurements. Laboratory B stated that more precise results could be obtained from raw U^{235}-to-U^{236} peak-height ratios and presented the results listed as peak-height measurements. The Vallicitos Atomic Laboratory made fission-product cesium

Table 5.5. Burnup Analyses of LITR Capsules

Analytical Method	U^{235} Burnup (%)			Integrated Neutron Exposure (neutrons/cm^2)	
	Capsule UO_2-1-1	Capsule UO_2-1-2	Capsule UO_2-2-1	Capsule UO_2-1-1	Capsule UO_2-1-2
Atomic fraction				$\times 10^{19}$	$\times 10^{19}$
Laboratory A	4.47	5.18		6.35 ± 4.28	7.39 ± 4.17
Laboratory B	5.15	6.87		7.35 ± 1.44	9.90 ± 1.45
Peak height ratios (Laboratory B)	4.99	7.12		7.12 ± 0.69	10.30 ± 0.79
Cesium analyses (GEVAL)	5.00	6.72	0.466		
Co^{60} monitor calculations					
No flux depression	5.17	14.59	0.72	7.37	21.9
Average flux depression	3.44	9.88	0.51	4.86	14.5
Two times average flux depression	1.68	4.92	0.30	2.36	7.0

analyses as one of their postirradiation measurements, and their results are also given in Table 5.5. They did not state how the samples were obtained, but it is known that they did not use a complete pellet for analysis.

The measured burnup results agree fairly well and indicate that the UO_2-1-1 sample came from near the surface of the pellet and that the UO_2-1-2 sample came from near the inner surface of the pellet. It is apparently coincidental that the Vallicitos results agree so closely with the ORNL values, since different samples were used which presumably were not representative. For comparison, results obtained from flux monitor measurements are listed that are based on (1) no flux depression, (2) average flux depression obtained by the method of Dwork, et al.,[4] and (3) two times the average flux depression. The mass spectrometer results are not listed for UO_2-2-1 because the burnup was small, and the initial and final U^{236} atomic fractions were so small that changes in the U^{235}-to-U^{236} ratios were not significant.

The results of an error analysis of the neutron exposures derived from the mass spectrometer measurements are also presented in Table 5.5. Again, the results obtained from flux monitors are presented for comparison. It should be noted that the flux monitor for UO_2-1-1 was lost and that these results are based on earlier flux measurements at the same location. The error values are for the 95% confidence interval, or approximately two standard deviations. The results support the contention of Laboratory B that peak-height ratio measurements are more precise than absolute atomic fraction determinations.

GETR Capsules

All the capsules that were irradiated in the GETR have now been examined visually in the hot cells at the Vallecitos Atomic Laboratory. External inspections revealed that nearly all the thermocouples had

[4]J. Dwork, P. L. Hoffman, H. Hurwitz, Jr., and E. F. Clancy, Self-Shielding Factors for Infinitely Long Hollow Cylinders, KAPL-1262 (Jan. 10, 1955).

broken from the surfaces of the capsules and that the stringers were distorted to various degrees. The surfaces of the capsules were discolored and heat bands were visible. All stringers were photographed at different orientations, at high and low magnifications, in color, and in black and white.

The conclusion obtained from a study of the photographs is that the stringers had been subjected to an axial thrust from thermal expansion of the long bundle of sheathed thermocouples. This thrust, along with a high-temperature excursion, caused the welded and brazed connections between the thermocouples and the capsule cladding to break. The thrust was also responsible for the distortion of the capsules and the stringers, as shown in Fig. 5.10.

Dimensional measurements are now being made. The capsules will then be punctured, and gas analyses will be made if the pressure is high. Some capsules will be impregnated with plastic and then sectioned; others will be opened without plastic impregnation. The plastic-impregnated capsules will show the location and condition of the UO_2. Although the burnup in these capsules is too low to yield much radiation damage information on the UO_2, a few routine measurements will be made to determine whether early effects of thermal cycling can be detected. Density and metallographic measurements will be made, as well as other measurements indicated by the condition of the pellets.

ORR Capsules

The eight prototype EGCR fuel element capsules irradiated in the ORR have been disassembled in the ORR hot cell. Each pellet can has been carefully removed from the NaK container, examined, and photographed (see Fig. 5.11). All the capsules appeared to be in good condition, with no warping or collapsing evident.

Postirradiation examinations have been started that will include cladding dimensional measurements, gamma scans, a study of pellet fragmentation and structure, and measurements of density and fission gas release. Four of the capsules will be pierced in a closed container

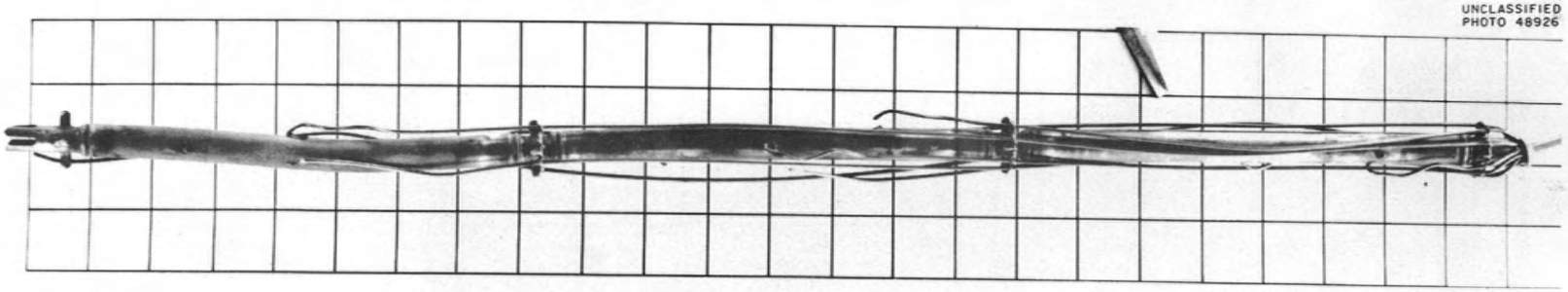

Fig. 5.10. GCR Fuel Element Stringer After Removal from GETR. Photograph made at Vallecitos Atomic Laboratory.

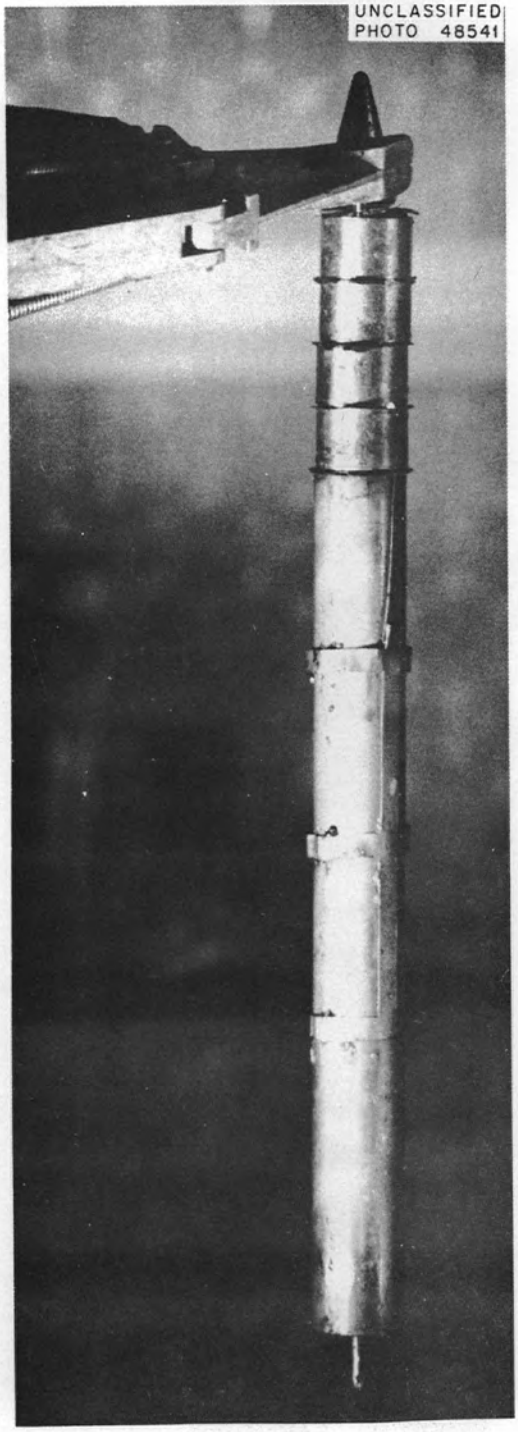

Fig. 5.11. A Typical ORR Capsule as Viewed Through the Hot-Cell Window. This capsule contains hollow pellets. The bands are monitor foils. The capsule begins below the four steel bushings seen at the top.

and heated to 1600°F to obtain a pressure vs temperature plot. This experiment will give the pressure in the fuel element from fission gases and other fission products that are volatile at this temperature under the same conditions as in the reactor.

Closed-Cycle-Loop Irradiation Facility in ORR

A capsule containing two ThO_2-UO_2 cylinders encased in siliconized silicon carbide-coated graphite had been irradiated for 440 hr at a 1500°F maximum cylinder temperature in the ORR closed-cycle-loop facility when high gas activity indicated a broken sample. The ThO_2-UO_2 test cylinders were 0.5 in. long, 0.5 in. OD and 0.25 in. ID and were composed of 95.5 wt % ThO_2 and 4.5 wt % fully enriched UO_2. They contained 0.43 g of U^{235} per cylinder. The fuel was fabricated at ORNL and was encased in graphite shells and coated with Si-SiC by the Minnesota Mining and Manufacturing Company. To determine coating continuity, the samples were submitted to a weight-loss test in a furnace at 1800°F for 400 hr prior to being accepted for in-pile testing. The capsule construction is shown in Fig. 5.12.

After the reactor had reached its operating power of 20 Mw, the capsule was lowered into the high flux zone while being cooled with nitrogen flowing at 30 scfm. This flow was reduced to 12 scfm to increase the temperature to 1500°F. Coolant pressure instability, caused by compressor unloading, cycled the coolant flow by approximately 0.5 scfm, which cycled the sample temperature 270°F. This cycling was stopped when a bypass escape valve was adjusted.

Fission gas leakage was evident from the onset of the test. Gas samples were collected after 144 and 336 hr of irradiation. Analyses of these gas samples revealed Xe^{133} and Xe^{135} in sufficient quantities to be detectable above other radioactive gases in the samples. High concentrations of these xenon isotopes plus other gases in the gas samples indicated that all fission gases escaping from the fuel were emitted into the coolant gas. This conclusion, based on gas sample analyses, is supported by coolant gas total activity measurements. The

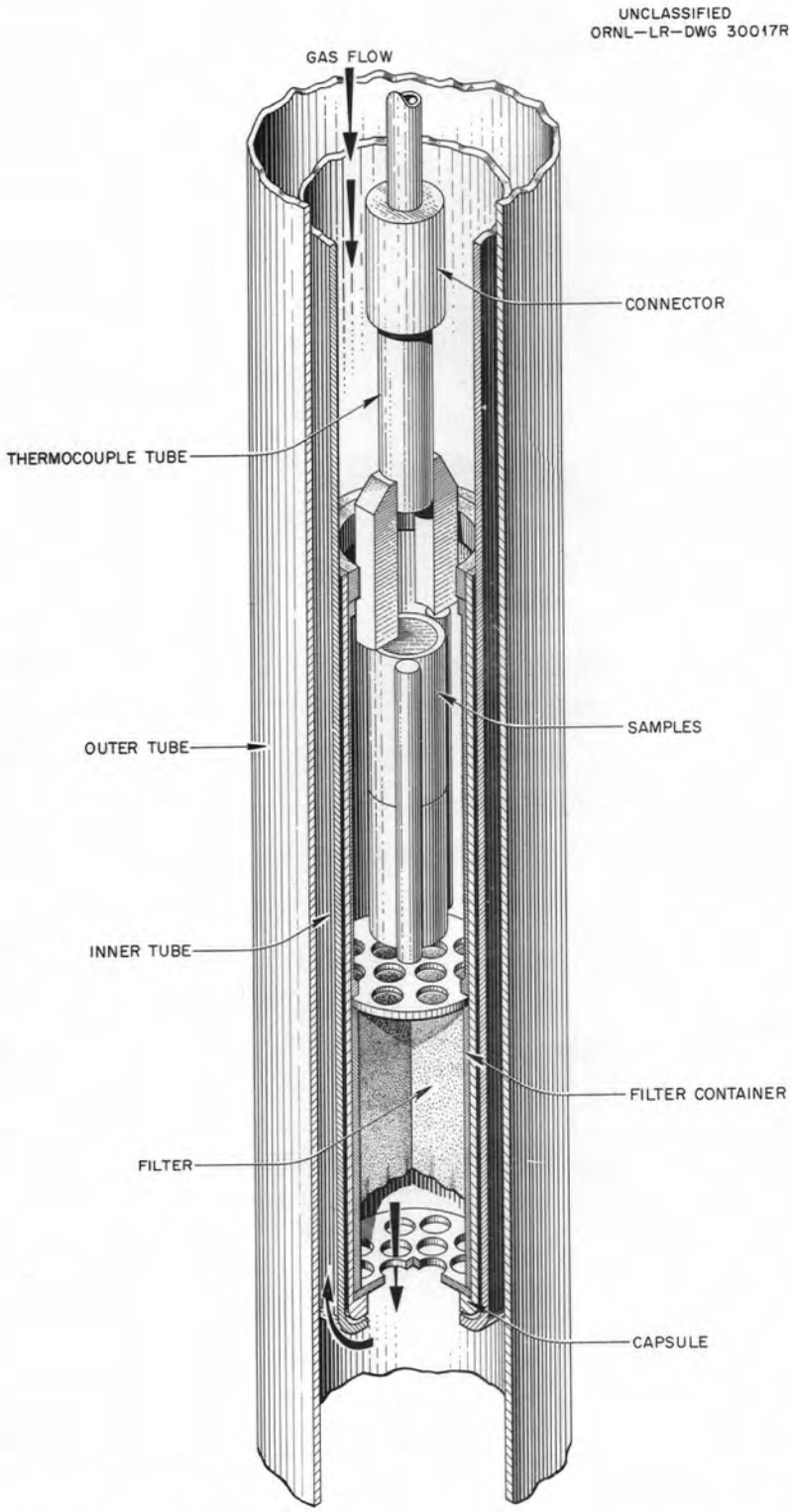

Fig. 5.12. Capsule for Irradiation of Coated-Graphite Encased Fuel Specimens.

total activity increased gradually during the test, until near the end of the test, when it increased rapidly and the test was terminated.

A major obstacle in providing this loop facility has been procurement and installation of a dry-lubricated gas pump having a tolerable packing leakage rate. The leakage rate of the present system is 2 scfh, and the system can operate only two weeks from the three standard gas cylinders at the supply manifold. At the end of each test the coolant gas is bled from the loop into the offgas system. To clean the gas, a charcoal trap has been fabricated and is being installed in the experiment offgas line.

It was found that radioactive materials had plated out on the loop exit leg and were especially concentrated at the main tube-to-pipe tee joint. To allow other experimenters access to the reactor top during down time, it was desirable to dispose of this plated activity by flushing the loop with water. Since water is destructive to the main gas filter, a flushing valve is being added to protect the filter.

The only samples now available for testing in this facility are $Cr\text{-}Al_2O_3$ bodies (solid cylinders, 0.75 in. long and 0.5 in. OD) fueled with UO_2 containing 0.5 g of U^{235} per cylinder. Three of these samples will be encased in the capsule being assembled for the next test. These capsules will be irradiated until higher priority specimens are available.

Radiation Effects on Structural Metals

Beryllium

One of the most serious potential problems to be evaluated in determining the usefulness of beryllium as a cladding material for gas-cooled-reactor fuels is the effect of gases produced within the metal by the (n,α) and the $(n,2n)$ reactions. The amounts of gas produced in beryllium[5] after exposure to a fast neutron (>1 Mev) dose of 10^{22} neutrons/cm^2 are shown in Table 5.6. The amount of gas produced in

[5]R. S. Barnes and G. W. Greenwood, The Effect of Gases Produced in Reactor Materials by Irradiation, A/Conf.15/P/29 (1958).

Table 5.6. Gases Produced in Beryllium and Uranium by Nuclear Reactions During Exposure to a Fast Neutron Dose of 10^{22} Neutrons/cm^2

Target Isotope	Reaction	Reaction Energy (Mev)	Threshold Energy (Mev)	Cross Section (barns)	Gases Produced	Ratio of Volume of Gas to Unit Volume of Metal After Exposure
Be^9	(n,α)	-0.64	0.71	0.050	He^4, H^3	5.7
	(n,2n)	-1.66	1.84	0.20	He^4	20
U	Fission	180	Slow	4.2	Xe, Kr	30

natural uranium metal is included for comparison. It is seen that significant quantities of gas are produced in the beryllium as a result of the nuclear reactions.

The effects of the xenon and krypton produced in uranium as a result of the fission process are well documented. Briefly, the following effects have been observed. As the uranium is irradiated at constant temperatures above approximately 450°C, the gases precipitate within the metal and small bubbles or voids are formed. These voids contain the gases xenon and krypton at pressures high enough to cause plastic deformation of the metal or vacancy condensation on the voids. By either of these processes the voids grow until equilibrium between the gas pressure and the restraining forces is obtained. Thus the apparent volume of the uranium metal increases; this phenomenon is referred to as swelling.

It is probable that an effect similar to that described above will occur as a result of the helium produced in beryllium. Ells and Perryman[6] and Rich et al.[7] have studied the effect of the helium produced in beryllium by postirradiation annealing of beryllium obtained from sections

[6]C. E. Ells and E. C. W. Perryman, "The Swelling of Beryllium from Neutron-Induced Gases," J. Nuclear Materials 1 (1959).

[7]J. B. Rich, J. B. Redding, and R. S. Barnes, "The Effects of Heating Neutron-Irradiated Beryllium," J. Nuclear Materials 1 (1959).

of an MTR shim rod. These investigators found that, at temperatures above approximately 600°C, the volume increase in beryllium containing 23 cm^3 of helium per cubic centimeter of beryllium would exceed 1%. Since beryllium is being considered as a cladding material, the effects of void formation on the ability of beryllium to contain the fission product gases and on its resistance to failure under thermal and mechanical stresses are more important than swelling.

Theoretical studies of the swelling of uranium have been reported at Harwell. Some success in predicting behavior under certain conditions of irradiation has been achieved. The general approach to the analytical problem involves the following assumptions: (1) the gases produced are insoluble in the metal, and (2) the gases precipitate in uniformly spaced bubbles identical in size.

In order to simplify the analysis, separate calculations must be made for the restraint of the swelling due to the strength of the material and the restraint due to the equilibrium between the gas pressure and surface tension. Since this equilibium requires that

$$p = \frac{2\gamma}{a_0} ,$$

where

p = gas pressure,
γ = surface tension,
a_0 = radius of bubble,

it is necessary, in order for the bubble to contain significant quantities of gas, that the bubble radius and the distance between the bubbles be small. The equilibrium between the gas pressure and the strength of the metal is not strongly dependent on the bubble size and the bubble spacing, so long as the difference between the spacing and the diameter of the bubble is large.

Enderly[8] has shown that the initial swelling of uranium on post-irradiation annealing can be represented by

$$x \ln \frac{1}{x} = k \frac{T}{Y} \quad ,$$

where

x = the fractional volume increase

k = constant which represents the amount of gas in the metal and the necessary conversion units to make the right side of the equation dimensionless,

T = temperature,

Y = yield strength at T.

On the other hand, bubble spacing and surface tension were used as criteria by Greenwood et al.[9] to develop an equation of the following form to represent the observed swelling:

$$x = k_2 \left(\frac{TL}{\gamma}\right)^{3/2} \quad ,$$

where

x = the fractional volume increase,

k_2 = constant which includes the gas constant and the amount of gas in the metal,

T = temperature,

L = distance between bubbles,

γ = surface tension.

In order to evaluate the applicability of this theoretical treatment to the study of beryllium, the extent of swelling expected at the

---

[8]J. A. Enderly, Plastic Flow and the Swelling of Gas Bubbles in Uranium, IGR-R/R 198 (Nov. 1956).

[9]G. W. Greenwood, A. J. E. Foreman, and D. E. Rimmer, The Role of Vacancies and Dislocations in the Nucleation and Growth of Gas Bubbles in Irradiated Fissile Material, AERE-R 2863 (1959).

conditions of the experiments conducted by Ells[6] was calculated. The calculated volume increase values are compared with the experimental values in Table 5.7. The yield strengths of beryllium used in the calculations were for unirradiated material, whereas the material used by Ells had a somewhat greater yield strength. The difference in yield strengths may account for part of the difference between the calculated and experimental values. The volume increase values tabulated from Ells' work were obtained after 1 hr at the indicated temperatures and were considerably greater after longer annealing periods.

The values of swelling calculated on the basis of restraint by surface tension are orders of magnitude greater than the experimentally determined volume increases. This large discrepancy is probably due, in part, to the assumptions necessary in the calculations. For instance,

Table 5.7. Swelling of Irradiated Beryllium Upon Postirradiation Heating

Annealing Temperature (°C)	Volume Increase (%)		
	Calculated from Yield Strength	Calculated from Surface Tension	Experimental Data from Ref 6
For Sample Containing 23 cm^3 of Gas Per Cubic Centimeter of Metal			
500	1.7	330	0.4
600	2.8	390	0.8
700	9.5		1
800			5
For Sample Containing 4.6 cm^3 of Gas Per Cubic Centimeter of Metal			
500	0.22	29	<0.1
600	0.40	35	0.12
700	1.0		0.4
800	3.7		1.3

the value used for the surface tension of beryllium was 500 dynes/cm, which may be low by a factor of 2. In addition, the bubble spacing was assumed to be 5×10^{-5} cm, a value which could be incorrect by an order of magnitude or more.

In view of the uncertainties in the properties of the irradiated beryllium, the swelling data calculated on the basis of yield strength are considered to be in reasonable agreement with experimental values. Further attempts will be made to treat the irradiation behavior of beryllium analytically. Also, irradiation studies have been initiated to determine the amounts of gas produced and the high-temperature mobility of the gas, to relate the void formation during irradiation to crystal orientation, grain size, and section thickness, and, finally, to determine the effect of neutron irradiation on the creep strength and permeability of beryllium.

The first phase of the test program consists of irradiating unstressed specimens at reactor coolant temperature and at elevated temperatures of 500, 600, and 700°C. The low-temperature irradiation will be followed by postirradiation annealing experiments designed to measure the amounts of gas released as a function of temperature and time at temperature and to observe the amount of void formation. A few specimens will be subjected to vacuum fusion analyses to accurately determine the total amount of gas formed during the irradiation. The amount of gas released from the beryllium during elevated-temperature irradiations will be measured either by collecting the gas contained in the capsule or by measuring the gas released during vacuum fusion of the irradiated specimen and deducting from the total the gas that was formed during the low-temperature irradiations. Density and dimensional measurements will be made and hardness and bend tests will be performed at various stages of the postirradiation examination. Metallographic examinations will be made to determine the amount and type of void formation as a function of neutron dosage, irradiation temperature, and/or annealing time and temperature.

For the low-temperature irradiations, 55 specimens will be mounted in an aluminum holder designed to fit into core position B-2 of the ORR. The specimens will be cooled by passage of the reactor cooling water directly across them. For the elevated-temperature irradiations, 22 specimens will be encapsulated in stainless steel and assembled in a gas-tight exposure can designed for insertion at core position B-8. The function of the capsule is to contain the gas released from the specimen at the elevated temperature. The capsules will operate in a helium atmosphere containing about 2% hydrogen. The hydrogen is included on the basis that it will diffuse into the preevacuated capsule and improve heat transfer from the beryllium to the stainless steel capsule. Each capsule has its own furnace for supplementary heat and its own temperature controller for continuous fine control. The specimen, capsule, and furnace for the high-temperature tests are shown in Fig. 5.13. A partially assembled mockup of the apparatus is shown in Fig. 5.14.

Designs of all the experimental parts and the associated equipment have been complete, and fabrication is under way. The specimen and capsule have been completed, and assembly of the in-pile apparatus will begin soon. Equipment for puncturing the capsules, for the annealing experiments, and for the vacuum fusion analyses is being designed. The other equipment needed for the postirradiation examinations is presently available and only minor modifications will be needed.

The second phase of the program will be stress-rupture tests of beryllium tubing and in-pile permeability tests in the absence of stress. Some of the problems in connection with the design of these experiments are fabrication of the beryllium tubing and joining of beryllium to itself and to other metals (see Chap. 4). The conditions of stress and temperature for these tests are dependent on the results of the first phase of the irradiation program and on the results of out-of-pile stress-rupture tests.

Steel

The observation of irradiation-induced property changes in pressure vessel steels has led to consideration of methods for removal of these

UNCLASSIFIED
RMG 2722

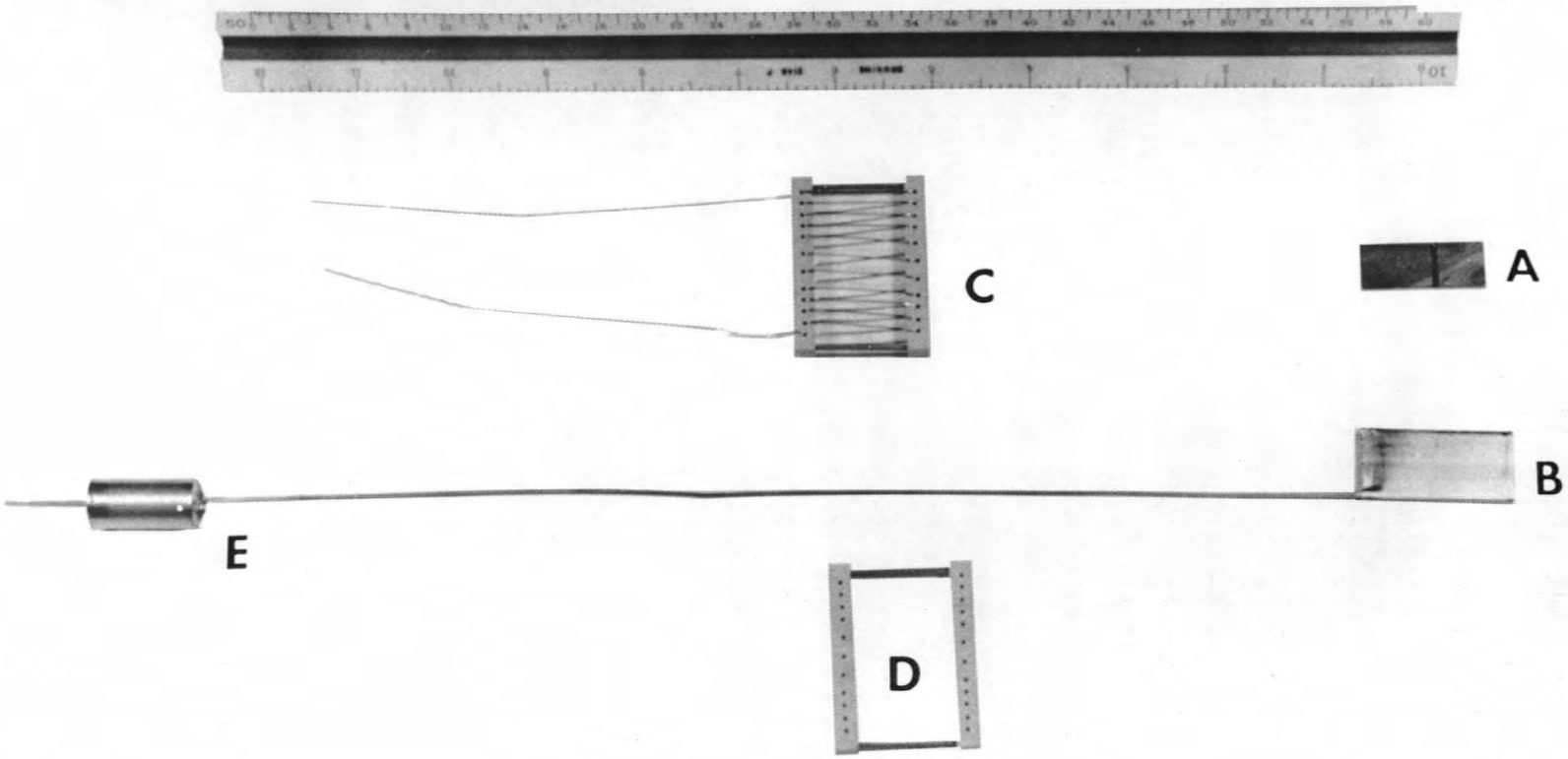

Fig. 5.13. Apparatus for High-Temperature Irradiation of Beryllium. Part A is the beryllium specimen. Part B is the specimen holder section of the stainless steel capsule. Part C is the furnace. Part D is the Lavite furnace form. Part E is the expansion chamber section of the capsule.

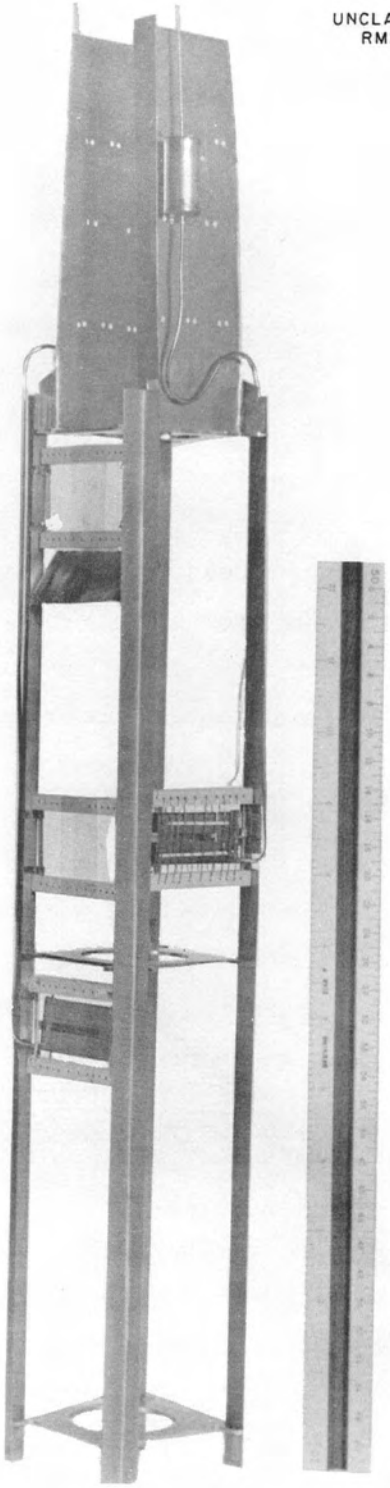

Fig. 5.14. Partially Assembled In-Pile Section of High-Temperature Beryllium Capsule Testing Apparatus.

effects in nuclear pressure vessels by periodic annealing. The effects of annealing an ASTM type 212A, grade B, carbon-silicon steel after exposure to reactor neutrons have been studied by making hardness measurements and by conducting notched-bar impact and tensile tests on specimens annealed at several temperatures.

The results[10] of hardness measurements on step-annealed Charpy V-notch specimens that had been irradiated and impact tested indicated that recovery started at about 500°F, was essentially complete at 900°F, and that specimens irradiated at 575°F did not anneal as readily as those irradiated at 140°F. Further hardness tests are in progress, with annealing time being used as a parameter in an attempt to determine some of the kinetics of the recovery process.

Tensile and impact specimens from a different heat of ASTM type 212A, grade B steel that had been irradiated in the ORR pool-side facility to a dose of 1 to 3×10^{19} neutrons/cm^2 at neutron energies greater than 1 Mev were given isothermal annealing treatments. The results of impact tests on these specimens are presented in Fig. 5.15 as percentage recovery of transition temperature at each annealing temperature. The annealing times were all 1 1/2 hr. The data were corrected for variations in fast-neutron exposure. An interesting feature of the data is the apparent anomaly in the temperature range 550 to 600°F. This is the temperature range in which a slight increase was observed in the hardness of step-annealed specimens in the first phase of this study.

The tensile test results also show several interesting features. The load vs elongation curves, Fig. 5.16, for specimens irradiated to 1.5×10^{19} neutrons/cm^2 and annealed at various temperatures show a progression of effects. The large preyield-point plastic strain for irradiated but unannealed specimens decreased with increasing annealing temperatures. The large difference between upper and lower yield points dropped to zero at an annealing temperature of 400°F and approached the

---

[10] R. G. Berggren *et al.*, *Solid State Div. Ann. Prog. Rep. Aug. 31, 1959*, ORNL-2829, p 213.

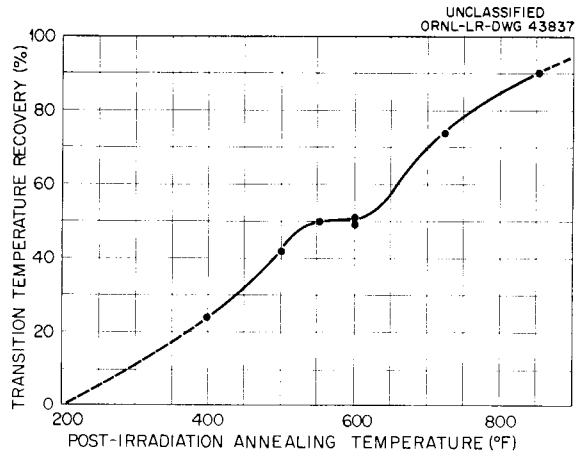

Fig. 5.15. Effect of Postirradiation Annealing for 1 1/2 hr on Transition Temperature Recovery of ASTM Type 212A, Grade B Steel.

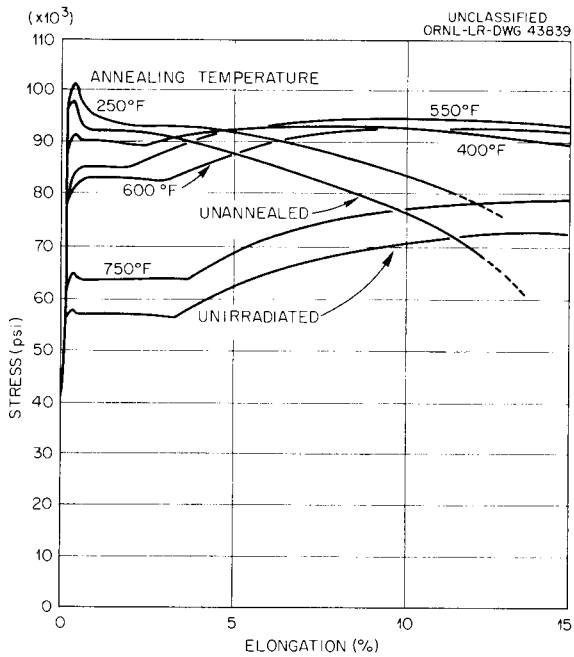

Fig. 5.16. Load vs Elongation Curves for Irradiated ASTM Type 212A, Grade B, Carbon Steel After Anneals at Various Temperatures for 1 1/2 hr.

value for the unirradiated material at annealing temperatures above 600°F. Work hardening was small or nonexistent at lower annealing temperatures but was recovered at higher annealing temperatures. Uniform elongation (strain before necking) was very small for low annealing temperatures and was recovered at higher annealing temperatures. Annealing at 750°F resulted in about 80% recovery from the irradiation-induced property changes. This progression of behavior changes is depicted in Fig. 5.17. Data are included in Fig. 5.17 for specimens irradiated to 3×10^{19} neutrons/cm^2 at neutron energies greater than 1 Mev, that is, twice the exposure of the specimens of Fig. 5.16. At 250°F, recovery is very small and may even be negative. Between 250°F and 400°F, slight recovery is observed. Increasing the annealing temperature to 465°F resulted in no further recovery. In the temperature interval between 465 and 500°F there was a decrease in yield stresses but an increase in ultimate strength, and the "drop-in-load" at yielding became zero. There was little or no change in recovery between 500 and 550°F. At 600°F, the usual type of yield point was observed. Above 600°F, the final stages of recovery were observed. It is apparent that the recovery processes vary considerably with temperature and that several mechanisms are involved. There may be as many as five stages of recovery in this particular steel.

The annealing recovery of a Swedish steel[11] that is similar to ASTM type 212A, grade B steel but of higher manganese content appeared to be much simpler than the above processes. The load vs elongation curves for this steel are shown in Fig. 5.18. While recovery seems to occur at lower temperatures for this steel, it should be noted that the yielding behavior after irradiation and annealing is not the same as it was before irradiation. This steel had shown little or no region of low work-hardening rate before irradiation. However, after irradiation and annealing at 750°F, there was a yield-point strain of several per cent

[11]Composition of Swedish 21-YY-Steel, Degerfors Jarnverks Ab, Heat M-6896: carbon, 0.13%; silicon, 0.34%; manganese, 1.66%; phosphorus, 0.011%; sulphur, 0.033%; chromium, 0.07%; nickel, 0.05%; copper, 0.15%; aluminum (soluble), 0.027%.

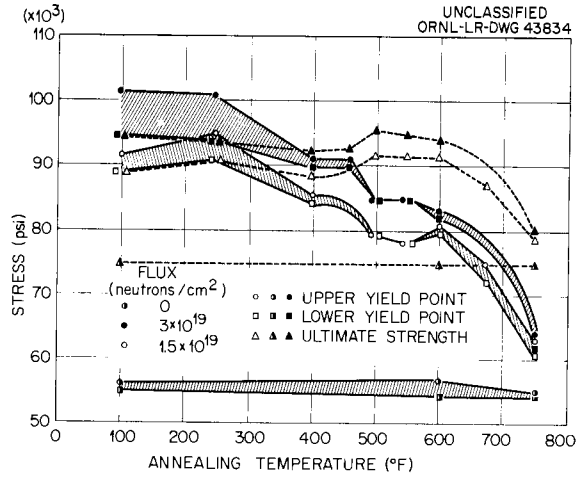

Fig. 5.17. Effect of Postirradiation Annealing on ASTM Type 212A, Grade B Steel on Recovery from Irradiation-Induced Property Changes.

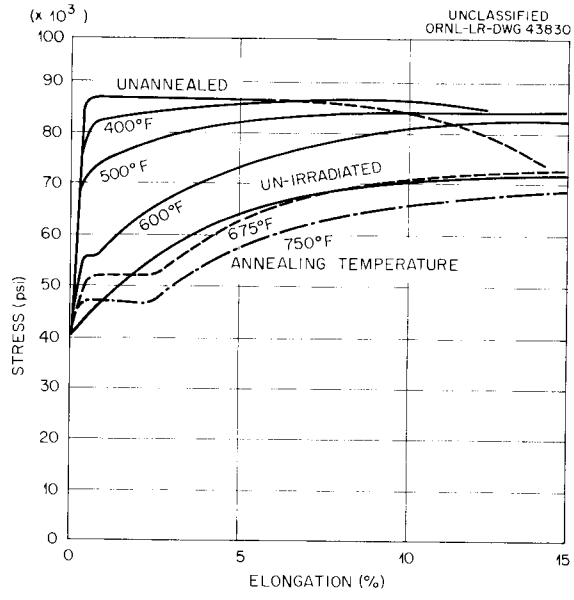

Fig. 5.18. Load vs Elongation Curves for Irradiated Swedish Steel 21-YY, Heat M-6896 After Anneals at Various Temperatures for 1 1/2 hr.

before work hardening became apparent. Thus this steel was not truly restored to the same condition as it had been before irradiation.

Annealing kinetics and processes are complex and vary for different steels. There is some evidence that the recovery behavior of a steel irradiated at an elevated temperature cannot be readily predicted from recovery data on steels irradiated at lower temperatures. Annealing may not restore all the preirradiation properties. Although annealing at temperatures of about 900°F may be required to accomplish nearly complete recovery of preirradiation properties, adequate or even superior properties may be obtained by partial recovery at lower temperatures. It is recognized that the 1 1/2-hr annealing periods used in this study were much shorter than would be practical for a reactor pressure vessel, and longer annealing times should be studied.

6. OUT-OF-PILE TESTING OF MATERIALS AND COMPONENTS

Materials Compatibility Tests

Additional test results have been obtained from out-of-pile tests designed to evaluate the corrosion behavior and structural stability of the EGCR fuel element assembly.[1-4] These tests have been run in static helium, in low-pressure and high-pressure thermal-convection loops, and in a forced-circulation loop.

Static Helium Tests

Tables 6.1, 6.2, and 6.3 list the operating conditions and results obtained in static-helium tests of type 304 stainless steel elements heated independently of the test container. The design of these tests was described previously.[3] All the tests were of 1000 hr duration, and all the test systems included AGOT graphite maintained at 1100°F. The temperatures of the independently heated specimens varied in the tests from 1500 to 1800°F. The specimens in tests 10, 11, and 12 were heated by internal calrods, while those in test 14 through 17 were heated by direct resistance. In addition to a heated specimen, the assemblies used for tests 12, 14, 15, 16, and 17 contained various iron-base alloy specimens located above the graphite assembly in a region where the temperature was approximately 1100°F.

The first two tests with heated elements, tests 10 and 11, although they were operated under similar temperature conditions, produced quite different test results.[3] This difference was attributed to a different surface area of metal in each test relative to the container and graphite volume. As a result, two tests have been run at every temperature level

---

[1] The ORNL Gas-Cooled Reactor Materials and Hazards, ORNL-2505, May 22, 1958, p 12–33.

[2] GCR Semiann. Prog. Rep. Dec. 31, 1958, ORNL-2676, p 138–146.

[3] GCR Semiann. Prog. Rep. June 30, 1959, ORNL-2767, p 180–190.

[4] GCR Quar. Prog. Rep. Sept. 30, 1959, ORNL-2835, p 125–132.

Table 6.1. Conditions and Results of High-Surface-Area[a] Static-Helium Tests of Type 304 Stainless Steel Heated Elements and AGOT Graphite Maintained at 1100°F

	Test 10	Test 16	Test 17
Design of heated element	Sleeve-type specimens; calrod heated	Tube-type specimens; direct-resistance heated	Tube-type specimens; direct-resistance heated
Element temperature, °F	Bottom sleeve, 1410–1460 Top sleeve, 1500	1480–1500	1580–1600
Surface area of heated element, cm^2	619	324	324
Volume of graphite, cm^3	21,000	21,000	21,000
Weight gain of heated element, mg/cm^2	Bottom sleeve, 2.9 Top sleeve[b]	42	(c)

[a]Surface area of stainless steel test vessel (not including heated element) = 81,000 cm^2.

[b]Sleeve was self-welded to holder.

[c]Weight change not measured because of conflicting reaction along inner surface.

Table 6.2. Conditions and Results of Low-Surface-Area[a] Static-Helium Tests of Type 304 Stainless Steel Heated Elements and AGOT Graphite Maintained at 1100°F

	Test 11	Test 12	Test 14	Test 15
Design of heated element	Sleeve-type specimens; calrod heated	Sleeve-type specimens; calrod heated	Tube-type specimens; direct-resistance heated	Tube-type specimens; direct-resistance heated
Element temperature, °F	Bottom sleeve, 1410–1475 Top sleeve, 1500	Bottom sleeve, 1550–1600 Top sleeve, 1600	1780–1800	1680–1700
Surface area of heated element, cm^2	619	619	324	324
Volume of graphite, cm^3	26,900	26,900	26,900	26,900
Weight gain of heated element, mg/cm^2	Bottom sleeve, 6.6 Top sleeve[b]	Bottom sleeve[b] Top sleeve[b]	4.7	0.37

[a]Surface area of stainless steel test vessel (not including heated element) = 17,300 cm^2.

[b]Sleeve was self-welded to holder.

Table 6.3. Weight Changes of Specimens Tested at 1100°F with AGOT Graphite in Heated-Element-Type Static-Helium Tests

Specimen	Specimen Weight Change (mg/cm^2)				
	Test 12	Test 14	Test 15	Test 16	Test 17
Type 304 stainless steel	0.073	0.084	0.052	0.018	0.022
Type 310 stainless steel	0.086	0.10	0.070	0.049	0.016
Type 316 stainless steel	0.093	0.15	0.021	0.025	0.023
Type 410 stainless steel	0.093	0.12	0.058	0.012	0.037
Type T-1 steel	0.64	0.23	0.87	-0.16	-0.056
Croloy (2 1/4% Cr)	0.48	1.51	0.76	-0.076	0.00
Croloy (3% Mo)	1.62	3.40	1.92	0.20	0.092
DB-2 (Fe-Cr-Al)	0.054	0.040	0.027	-0.042	0.028

of the series, one in which the surface area was equivalent to that used for test 10 and one in which the surface area was equivalent to that used for test 11. The ratio of the metal surface area to the graphite container volume was six times greater in tests patterned after test 10 (tests 16 and 17) than in the tests patterned after test 11 (tests 12, 14, and 15).

Results of the high-surface-area tests are summarized in Table 6.1. The heated element used in test 16 was held at approximately the same temperature as that used in test 10, although the element was heated by means of direct resistance in test 16 and by a calrod in test 10. The results were similar despite the differences in the method of heating. Both elements exhibited a silvery-gray, poorly adherent film on all surfaces that were at temperatures above 1460°F. The weight gain associated with this film was approximately 42 mg/cm^2 in test 16; no measurement could be made for test 10 because of self-welding of the test specimen to its holder. The heated specimen used in test 17 was held at 1580 to 1600°F and was also silvery in appearance, but it showed no evidence of a film or scale; rather, it had a deoxidized appearance. The weight change which resulted for this specimen was invalidated by a conflicting reaction which took place along the inner surfaces of the specimen. Ordinarily the inner surfaces of the heated tubes, which do

not come in contact with the test atmosphere, are protected by a pure argon cover gas, but contamination of the cover gas obviously occurred in this test.

Results of the tests of heated elements contained in systems with low surface areas are shown in Table 6.2. Specimens were exposed to helium in these tests at temperatures from 1500 to 1800°F. Despite differences in temperature, all the specimens were similar in appearance after the tests. Surface films which formed on the specimens were dark green to black, typical of spinel-type oxides, and were tightly adherent. Weight gains were generally less than for the specimens associated with higher metal surface areas. The weight gains ranged from 0.4 to 6.6 mg/cm^2, and there was no apparent correlation with temperature.

While the trends in weight gains among the heated elements are believed to be valid, it must be pointed out that the manner in which the weights are obtained is somewhat indirect. Because the specimens must be welded in place, it is necessary after a test to subdivide the specimens into accurately machined lengths and to determine the weight changes of each length. However, checks of the validity of this method of analysis have shown the errors to be encouragingly small, that is, considerably less than the order of weight gains which were obtained.

As previously mentioned, metal specimens in addition to the heated elements were included in all test systems described in Tables 6.1 and 6.2, except 10 and 11. These additional metal specimens were located above the graphite and were at essentially the same temperature as the graphite, that is, approximately 1100°F. The weight changes of these specimens are presented in Table 6.3. The weight gains of the specimens in the high surface area systems were smaller than the weight gain of the specimens in the low surface area systems. Other iron-base alloys also exhibited smaller weight gains in systems with high surface areas than in systems with low surface areas. In some cases, there were even weight losses.

Low-Pressure Thermal-Convection Loop Tests

Loop 9, which contained type TSF graphite, was terminated after successfully operating for 5000 hr at a test section temperature of

1400°F. Stainless steel specimens (types 304, 316, 310, and 410) which had been suspended in a graphite channel in the hot-leg section of the loop had a dark gray oxide film which was overlaid in some areas by silvery-gray or green films. The surfaces of low- and medium-alloy steels from the same location visually appeared shiny and free of oxide layers. However, under slight magnification, a silvery film composed of highly reflective platelets was evident. All samples are being subjected to x-ray and electron diffraction analyses.

The weight changes of these specimens are listed in Table 6.4, as well as the weight changes of specimens exposed for 1000 and 2000 hr under test conditions similar to those of test 9 (tests 1 and 3, respectively). As may be seen, weight gains of relatively small magnitude were incurred by the stainless steel specimens at all test intervals. The gains appear to increase very slightly as the test duration is increased.

The low- and medium-alloy steel exposed in test 9 displayed considerably greater weight gains over the 5000-hr test period than did the stainless steels exposed in this test. In contrast, the low- and medium-alloy materials exhibited effectively no weight gain after exposure for 1000 hr and, after 2000 hr, showed a weight loss. However, the pattern of this behavior is felt to be related more to differences in graphite outgassing properties among the tests than to differences in exposure time.

Table 6.4. Weight Changes of Metal Specimens Exposed to Helium at 1400°F in Low-Pressure Thermal-Convection Loops for 1000, 2000, and 5000 hr

Specimen	Specimen Weight Change (mg/cm^2)		
	1000-hr Test (No. 1)	2000-hr Test (No. 3)	5000-hr Test (No. 9)
Type 304 stainless steel	0.03	0.08	0.08
Type 310 stainless steel	0.08	0.07	0.11
Type 316 stainless steel	0.03	0.06	0.11
Type 410 stainless steel	0.00	0.18	0.12
Croloy (2 1/4% Cr)	0.01	-0.05	1.0
Croloy (3% Mo)		-0.10	3.6
T-1 steel	0	-0.04	1.0

Where conditions (including test duration) have been maintained exactly the same in static pot tests with TSF graphite, specimens of low- and medium-alloy steels in some cases have lost weight as a result of decarburization, but in other cases have shown weight gains as a result of oxidation. It has not been possible to establish just what factors in gas composition govern each type of behavior. Difficulties in pinpointing these factors arise because of the very rapid changes which occur in the test atmosphere during the initial test periods, which are the most significant insofar as gas-metal reactions are concerned. Tests with controlled atmospheres, which are scheduled for the immediate future, should aid considerably in clarifying these effects.

In addition to the samples suspended in the graphite channel, stainless and low-alloy steel samples were placed between the graphite logs used in test 9. Several of these samples were fused to the graphite surface, suggesting the growth of a carbide interface between the metals and graphite. The exact pressure on the samples is difficult to estimate, since the contact area is dependent on relative surface roughness of both the graphite and metal, a variable which is indeterminate. However, assuming complete contact, the pressures were between 50 and 100 psi. These samples have been submitted for metallographic and electron diffraction analyses. The cold leg of this loop showed no signs of carbon mass transfer as a result of the back reaction of CO to carbon.

As reported earlier,[4] test 8, which was scheduled for 5000 hr at 1400°F with AGOT graphite, was interrupted after 2754 hr because of a gas leak in the loop cold leg. All the iron-base alloy specimens used in this test showed weight gains several times larger than those found in preceding tests. These above-average weight gains were attributed to the high level of impurities (maximum total = 18.45 vol %) which existed in the loop. Examination of the cold leg of this loop also showed an appreciable amount of carbon mass transfer, which was explained by the extremely high CO concentration present in the helium used in test 8.

During this report period, most of the metallographic and analytical investigations were completed on the various specimens from test 8. The stainless steel specimens (types 304, 310, 316, and 410) showed a second phase precipitated throughout the specimen cross section, as illustrated for the type 310 stainless steel sample in Fig. 6.1. The phase was much

Fig. 6.1. Type 310 Stainless Steel After Exposure to Helium at 1400°F in Low-Pressure Thermal-Convection Loop Test 8. Etchant: electrolytic NH_4OH.

less prevalent in the type 304 stainless steel samples than in the other alloys and was similar in etching characteristics to sigma-phase, iron-chromium intermetallic material. In the type 310 stainless steel specimens, the presence of sigma-phase material was definitely established by x-ray diffraction. In spite of the rather positive evidence that the bulk of the second-phase material is sigma, chemical analyses of the specimens are being made to detect whether some carburization may also have occurred. There were two other areas where type 304 stainless steel was exposed in this test, namely, the simulated EGCR fuel element hangar and the fuel rod mockup.[1] These components had been utilized in

thermal-convection-loop test 6, as well as in test 8, and had accumulated a test exposure amounting to 3750 hr. The hangar was of particular interest because certain sections had been in direct contact with graphite at a temperature of 1400°F during the entire exposure period.

Metallographic examination of the hangar and fuel rod mockups showed surface and intergranular oxidation and a second phase precipitated throughout the structure (Fig. 6.2). In this case, however, the second

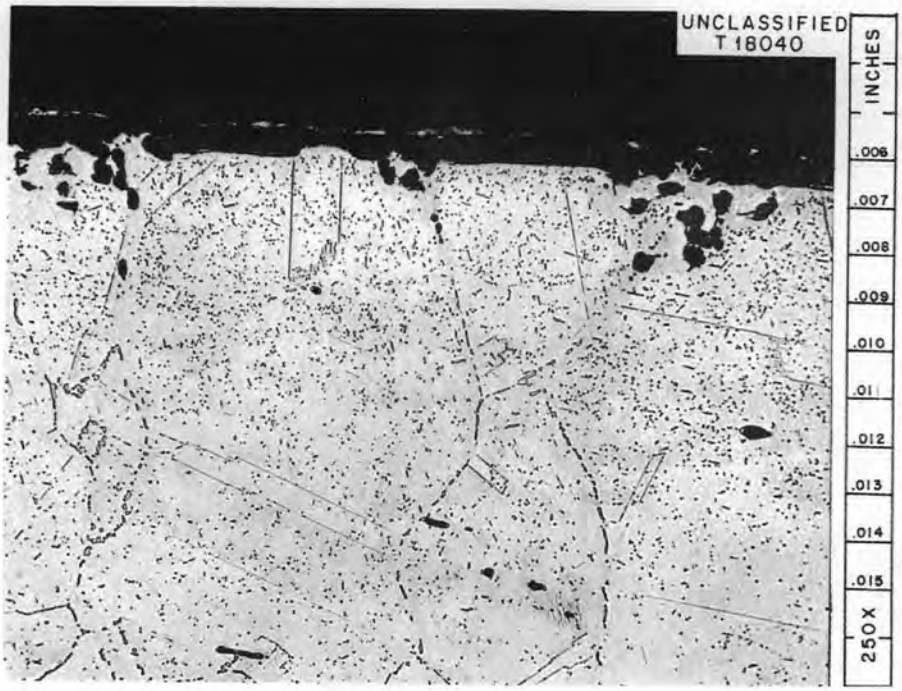

Fig. 6.2. Section of Type 304 Stainless Steel Hangar Rod Mockup After Exposure to Helium at 1400°F in Low-Pressure Thermal-Convection Loop Tests 6 and 8. Etchant: glyceregia.

phase existed only near the exposed surfaces and appeared to be carbides rather than sigma-phase material. Sections of these pieces are also being analyzed chemically to determine whether there was any noticeable rise in carbon content of the metal.

The low-alloy steel specimens exposed in test 8 were heavily oxidized along the exposed surfaces and were carburized throughout their entire 50-mil thickness. A carburized T-1 steel specimen from this test system is shown in Fig. 6.3. The presence of the lamellar eutectoid

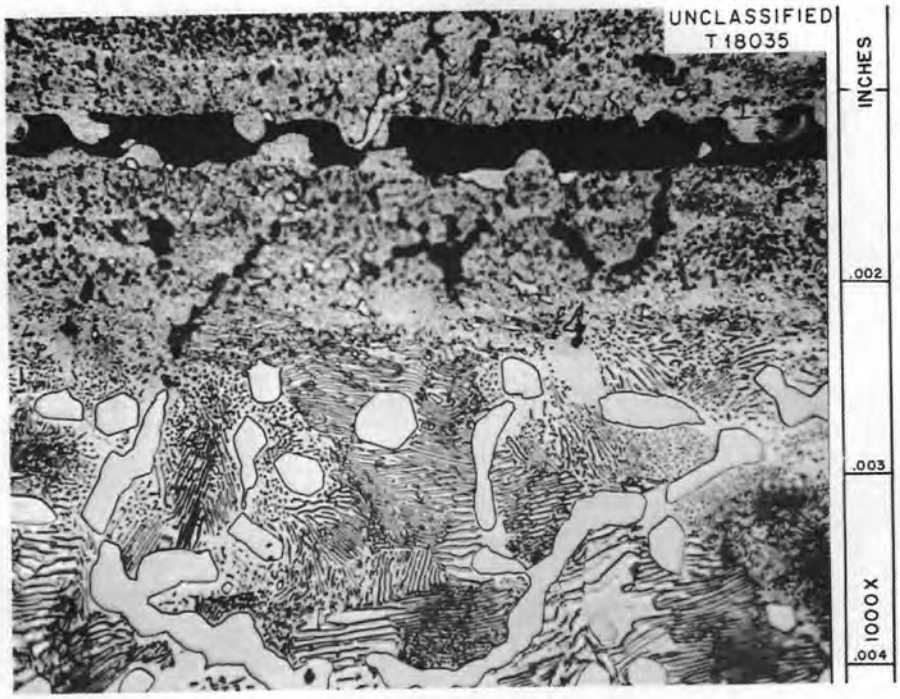

Fig. 6.3. T-1 Steel Specimen After Exposure to Helium at 1400°F in Low-Pressure Thermal-Convection Loop Test 8. Etchant: 2% nital.

structure (pearlite), along with massive carbides, indicates a carbon content greater than 0.8%. The as-received carbon content of this alloy was 0.1 to 0.2%. Mechanical testing of these specimens showed very marked reductions in ductility at room temperature and at 1400°F as a result of the heavy carburization.

Carburization of the stainless steel specimens used in test 8, if it occurred at all, was certainly much less extensive than the carburization resulting for the low-alloy steel specimens. The heavy carburization was not unexpected in the case of these low-alloy specimens in view of the high CO concentration during the test and the fact that the specimens were austenitic at the test temperature. However, a similar driving force existed for carburization in the case of the stainless steel specimens. A possible explanation for the lower rate or absence of carburization in the latter materials may be associated with the presence of a tightly adherent oxide film, which was evident on all stainless steel samples.

Low-pressure thermal-convection loop test 10 is undergoing initial graphite outgassing at a graphite temperature of 1100°F. This test system includes a type 304 stainless steel heated specimen similar to the specimens installed in the static-helium tests and an impurity addition system capable of adding H_2O, H_2, CO, and CO_2 to the gas stream. An on-stream gas chromatograph will provide continuous gaseous impurity monitoring (see later section of this chapter). The purpose of this test is to evaluate the compatibility of heated metal specimens with a helium atmosphere containing a controlled level of impurities.

High-Pressure Thermal-Convection Loop Tests

Operation of the third high-pressure thermal-convection loop, which contained AGOT graphite, metal test specimens, and an EGCR fuel element assembly mockup, was terminated after 500 hr of operation with a test section temperature of 1225°F and a system pressure of 325 psig. The appearance of the metal specimens after the test was similar to the appearance of the specimens used in test 1A, which was run under the same conditions as test 3 but for 1000 hr.[4] The stainless steels showed tightly adherent, irridescent surface films, while the low-alloy steels showed loosely adherent, silvery-gray films. The weight changes of these specimens are presented in Table 6.5. Again the results are similar to those obtained from test 1A, which have been included in Table 6.5 for comparison purposes. In both tests the stainless steels gained less than 1.0 mg/cm^2, while the low- and medium-alloy steels gained in excess of 6 mg/cm^2.

The cold leg of this loop was inspected for possibility of carbon mass transfer during test and showed no detectable deposit.

Test system 2, containing AGOT graphite and a dummy fuel element assembly, has completed 4500 hr of operation with a test section temperature of 1225°F and a system pressure of 325 psig.

Test system 4, which contained AGOT graphite, various iron-base alloy specimens, and a fuel element assembly with four rods loaded with UO_2 pellets was terminated after 16 hr at 1400°F and 325 psig. Termination

Table 6.5. Weight Changes of Metal Specimens Exposed to Helium at 1225°F for 500 and 1000 hr in High-Pressure Thermal-Convection Loops Containing AGOT Graphite

Specimen	Specimen Weight Gain (mg/cm^2)	
	1000-hr Test No. 1A	500-hr Test No. 3
Type 304 stainless steel	0.09	0.06
Type 310 stainless steel	0.11	0.07
Type 316 stainless steel	0.12	0.06
Type 410 stainless steel	0.25	0.14
Croloy (2 1/4% Cr)	7.61	8.61
Croloy (3% Mo)	(a)	13.45
T-1 steel	8.13	6.24
DB-2 (Fe-Al-Cr)	0.07	0.00

[a]Scale spalled from specimen.

followed the occurrence of a leak in the heat-affected zone of a plug weld at the entrance to the test vessel. Failure appeared to be associated with catastropic oxidation of the 316 stainless steel tube comprising this section.

Forced-Circulation Loop Tests

The third forced-circulation loop, which contained AGOT graphite, various iron-base alloy specimens, and a dummy fuel element assembly, completed 1000 hr of operation with a test section temperature of 1400°F and a gas velocity of 300 ft/sec through the fuel element assembly. During the test, several of the wires supporting the metal specimens broke loose, and the mechanical interaction among the specimens made it impossible to use weight change data as a measure of the degree of metal reaction.

A small-scale gas purification system of the type proposed for use at the EGCR[5] has been designed and is currently being fabricated for

[5]F. A. Anderson, Proposed Helium Purification System for the Experimental Gas Cooled Reactor (EGCR), ORNL-2819 (Oct. 2, 1959).

evaluation in conjunction with forced-circulation-loop test 4. The system includes a catalytic converter containing Girdler type G-43 catalyst for converting H_2 and CO to H_2O and CO_2, a cooler-condenser and Silica-Gel absorber for removing H_2O, and a molecular-sieve absorber for removing CO_2. The effectiveness of this system will be evaluated by use of the process stream gas chromatograph currently in operation on the low-pressure thermal-convection loop.

Evolution of Gases from Graphite

The experimental results of studies of the degassing behavior of a number of different graphites and the experimental techniques used in these studies have been reported previously.[6-8] Data previously reported[6] that related to the volume of gases evolved by National Carbon Company AGOT graphite (AGOT-III, ORNL designation) upon being heated to 1000, 1400, and 1800°C by means of induction heating showed that about three-fourths of the total volume was evolved at 1000°C and that only a very small amount came off above 1400°C. Furthermore, the volume evolved at 1000°C when induction heating was used was found to be roughly twice that measured at comparable temperatures attained by external resistance heating. These observations suggested that the discharge noted in the quartz tube used in the induction heating assembly might be promoting the evolution of the gases. Specimens of AGOT-III graphite were therefore degassed under conditions that minimized the occurrence of the discharge to ascertain whether this was the cause of the behavior noted. The main difference in the operating conditions was that the evolved gases were held over the graphite specimen for about 30 min after 1000°C was reached instead of being pumped off continuously. After the 30-min holding period, the specimen temperature was dropped to ~900°C; the

---

[6] GCR Semiann. Prog. Rep. Dec. 31, 1958, ORNL-2676, p 147.

[7] GCR Semiann. Prog. Rep. June 30, 1959, ORNL-2767, p 190.

[8] GCR Quar. Prog. Rep. Sept. 30, 1959, ORNL-2835, p 133.

gases were pumped off; and the temperature was raised slowly to 1000°C to avoid discharging. The temperature was held at 1000°C until the rate of evolution of the gases was very low, and the temperature was then raised slowly to 1400°C, with continuous pumping; held at 1400°C for a specified time; and then raised slowly to 1800°C. By this procedure, it was possible essentially to eliminate the visible discharge, and this method has been used routinely for all studies reported here. The results (Table 6.6) obtained with this method of operation are similar to those found earlier for AGOT-III. The total volume of gases evolved was ~70 cm^3/100 cm^3 of graphite. Approximately 80% of this volume came off at 1000°C, and only ~2 cm^3/100 cm^3 of graphite was evolved above 1400°C. Of the gases evolved at 1000°C, some 90% came off in the 30-min period in which the gases were held over the graphite at a sufficiently high pressure to prevent discharge. Thus, it would appear that the large fraction of the total volume of gases evolved at 1000°C with induction heating is not dependent upon the accelerating effect of the discharge. Further evidence of this behavior can be obtained from the results given in Table 6.7, which also were obtained using the conditions described above to minimize the appearance of a discharge.

Samples from different bars of graphite taken from a furnace load of Great Lakes Carbon Company R-1HLM graphite were received and evaluated for gas content. This type of graphite is under consideration for use as sleeve material in the EGCR. A 2-in. sample (4 × 4 in. in cross section) was cut from each of 6 different bars, and specimens either 1 1/2 in. in diameter and 2 in. long or 1 1/4 in. in diameter and 1 in. long were cut from the samples. The apparent density of the various specimens ranged from 1.58 to 1.70 g/cm^3.

The results of the degassing studies of these specimens are presented in Tables 6.6 and 6.7, where the numerals in the first column refer to the particular sample (bar) from which the specimen was machined and the letters indicate specimens from the same sample (bar). In several instances, the gases were lost after sampling and the composition data are incomplete. The volumes evolved are included, however, for

Table 6.6. Volume and Composition of Gases Evolved by Great Lakes Carbon Company R-1HLM Graphite Specimens 1 1/2 in. in Diameter and 2 in. Long at 300, 600, and 1000°C

Sample No.	Temperature (°C)	Time (hr)	Gas Volume (cm^3/100 cm^3 of graphite)	Gas Constituents													
				H_2		Hydrocarbons		H_2O		CO_2		Mass 28		N_2		CO	
				Vol %	cm^3	Vol %	cm^3	Vol %	cm^3	Vol %	cm^3	Vol %	cm^3	Vol %	cm^3	Vol %	cm^3
1-A	300	4.0	0.6	1.0		6		66	0.4	10	0.1	14	0.1	6		8	
	300	15.5	0.1	Not analyzed													
	600	6.0	5.9	1.1	0.1	5	0.3	13	0.7	21	1.3	59	3.5	0.4		59	3.5
	600	16.0	1.4	1.3				1		19	0.3	78	1.1	0.7		77	1.1
	1000	0.25	20.8	12	2.4			2	0.4	4.6	1.0	82	17.1	0.3	0.1	82	17.0
	1000	6.5	15.1	33	4.9			2	0.3	0.2		66	10.0	2	0.2	64	9.8
	Total		43.9		7.4		0.3		1.8		2.7		31.8		0.3		31.4
1-B	300	5.0	0.7	0.9		9		71	0.5	8	0.1	11	0.1	5		6	
	300	12.0	0.2	Not analyzed													
	600	7.0	4.7	3.9	0.2	11	0.5	28	1.3	21	1.0	36	1.7	0.5		35	1.7
	1000	6.0	22.1	Sample lost													
	1000	5.0	0.1	Not analyzed													
	Total		27.8														
2-A	300	5.5	0.4	Not analyzed													
	600	17.5	3.5	4.2	0.1	11	0.4	27	0.9	41	1.4	17	0.6	6	0.2	11	0.4
	1000	9.5	18.6	31	5.8	4	0.7	4	0.7	14	2.6	47	8.7	3	0.5	44	8.2
	Total		22.5		5.9		1.1		1.6		4.0		9.3		0.7		8.6
2-B	300	5.0	0.7	0.8		2		67	0.5	2.3		23	0.2				
	600	13.0	5.1	Sample lost													
	1000	6.5	28.5	Sample lost													
	Total		34.3														
3-A	300	17.0	0.7	2.0				34	0.2	9	0.1	55	0.4	49	0.4	6	
	600	28.5	4.5	5.7	0.3	16	0.7	6	0.3	46	2.1	25	1.1	11	0.5	14	0.6
	1000	23.5	19.4	42	8.2	3	0.7	2	0.5	9	1.7	42	8.1	3	0.6	39	7.5
	Total		24.6		8.5		1.4		1.0		3.9		9.6		1.5		8.1
3-B	300	5.5	0.4	1.7		7		69	0.3	11		12	0.1	6		6	
	600	15.0	4.3	8.6	0.4	17	0.7	27	1.1	20	0.9	28	1.2	1		27	1.2
	1000	6.0	24.8	27	6.7					3	0.8	69	17.2	1	0.3	68	16.9
	Total		29.5		7.1		0.7		1.4		1.7		18.5		0.3		18.1

Table 6.6 (continued)

Sample No.	Temperature (°C)	Time (hr)	Gas Volume (cm^3/100 cm^3 of graphite)	Gas Constituents													
				H_2		Hydrocarbons		H_2O		CO_2		Mass 28		N_2		CO	
				Vol %	cm^3	Vol %	cm^3	Vol %	cm^3	Vol %	cm^3	Vol %	cm^3	Vol %	cm^3	Vol %	cm^3
4-A	300	5.5	0.6			6		66	0.4	10	0.1	18	0.1	12	0.1	6	
	600	18.0	4.6	4.5	0.2	12	0.5	26	1.2	23	1.1	33	1.5	3	0.1	30	1.4
	1000	19.0	22.5	37	8.4	3	0.6	4	0.8	7	1.6	50	11.2	1	0.1	49	11.1
	1000	8.0	2.0	69	1.4							31	0.6	1	0.1	30	0.5
	Total		29.7		10.0		1.1		2.4		2.8		13.4		0.4		13.0
4-B	300	17.0	0.8	2.0		4.0		67	0.5	5	0.1	22	0.2	19	0.2	2	
	600	7.0	2.8	5	0.1	13	0.4	29	0.8	25	0.7	25	0.7	5	0.1	20	0.6
	600	4.0	0.2	Not analyzed													
	1000	11.0	18.3	28	5.0	1.6	0.3	1.4	0.3	7	1.3	62	11.3	2	0.4	60	10.9
	1000	1.0	0.2	Not analyzed													
	Total		22.3		5.1		0.7		1.6		2.1		12.2		0.7		11.5
5-A	300	2.0	0.9	0.9		1.6		79	0.7	4		9	0.1	8	0.1	1	
	300	16.0	0.1	Not analyzed													
	600	5.0	2.6	3.4	0.1	12	0.4	35	0.9	24	0.6	25	0.6	2		23	0.6
	600	19.0	0.7	Not analyzed													
	1000	21.0	25.9	28	7.3	1.5	0.4	0.8	0.2	2.5	0.6	67	17.4	0.6	0.1	66	17.3
	1000	5.0	1.7	Not analyzed													
	Total		31.9		7.4		0.8		1.8		1.2		18.1		0.2		17.9
5-B	300	11.0	0.6	3.1		3.0		73	0.4	4.6		16	0.1	14	0.1	2.0	
	600	6.5	4.8	6	0.3	29	1.4	32	1.5	12	0.6	20	1.0	5	0.2	15	0.8
	600	4.5	0.3	Not analyzed													
	1000	18.0	28.6	31	8.9	4.5	1.2	2.9	0.8	5	1.5	56	16.0				
	1000	1.5	0.2	Not analyzed													
	Total		34.5		9.2		2.6		2.7		2.1		17.1				
6-A	300	6.0	0.7	Sample lost													
	600	12.0	3.5	6	0.2	14	0.5	29	1.0	24	0.8	26	0.9				
	1000	10.5	18.8	36	6.8	3	0.6	2	0.3	6	1.1	53	10.0	1	0.2	52	9.8
	Total		23.0		7.0		1.1		1.3		1.9		10.9				
6-B	300	7.0	0.9	1.3		11	0.1	72	0.7	6	0.1	9	0.1				
	300	16.0	0.2	Not analyzed													
	600	7.0	6.5	7	0.5	20	1.3	27	1.8	18	1.2	28	1.8				
	600	4.0	0.4	Not analyzed													
	1000	13.0	40.6	24	9.6	0.9	0.4	1.1	0.4	2.8	1.1	72	29.1				
	1000	3.5	2.0	Not analyzed													
	Total		50.6		10.1		1.8		2.9		2.4		31.0				

Table 6.7. Volume and Composition of Gases Evolved by Great Lakes Carbon Company R-1HLM Graphite Specimens 1 1/4 in. in Diameter and 1 in. Long at 1000, 1400, and 1800°C

Sample No.	Temperature (°C)	Time (hr)	Gas Volume (cm^3/100 cm^3 of graphite)	Gas Constituents													
				H_2		Hydrocarbons		H_2O		CO_2		Mass 28		N_2		CO	
				Vol %	cm^3	Vol %	cm^3	Vol %	cm^3	Vol %	cm^3	Vol %	cm^3	Vol %	cm^3	Vol %	cm^3
1-C	1000	7.5	41.2	32	13.2			1	0.4	1.4	0.6	66	27.2	1	0.4	65	26.8
	1400	6	10.6	5.6	0.6			0.3		1.2	0.1	93	9.9	1	0.1	92	9.8
	1800	3	0.2	9.3		0.5				0.2		88	0.2	34	0.1	54	0.1
	Total		52.0		13.8				0.4		0.7		37.3		0.6		36.7
2-C	1000	2	31.7	19	6.1			1.4	0.4	2.4	0.8	77	24.4	2	0.6	75	23.8
	1000	3	3.4	Not analyzed													
	1400	3.5	5.1	19	1.0			2.8	0.1	0.8		77	4.0	16	0.8	61	3.2
	1800	3.5	0.8	15	0.1					0.2		80	0.6	71	0.5	9	0.1
	Total		41.0		7.2				0.5		0.8		29.0		1.9		27.1
3-C	1000	5.5	44.1	27	11.9			0.9	0.4	1.3	0.6	71	31.3	0.4	0.2	70	31.1
	1400	6	13.7	9	1.3	0.1		0.3		1.3	0.2	89	12.2	0.5	0.1	88	12.1
	1800	2.5	0.8	Not analyzed													
	Total		58.6		13.2				0.4		0.8		43.5		0.3		43.2
4-C	1000	6	44.3	27	11.8	0.5	0.2	2	0.9	0.7	0.3	71	31.3	0.8	0.3	70	31.0
	1400	2	13.1	11	1.4	0.2		0.4		0.7	0.1	88	11.5	0.2		88	11.5
	1800	1.5	0.1	Not analyzed													
	Total		57.5		13.2		0.2		0.9		0.4		42.8		0.3		42.5
5-C	1000	2	54.9	26	14.3							74	40.6	1	0.5	73	40.1
	1000	6	6.8	39	2.6			1.4	0.1	0.5		60	4.1	2	0.1	58	4.0
	1400	9	13.8	Samples lost													
	1800	3	3.7	Samples lost													
	Total		79.2														
6-C	1000	2	61.1	21	13.1	0.2	0.1	0.2	0.1	0.3	0.2	78	47.6				
	1000	9	15.3	33	5.0	0.3		0.3		0.8	0.1	66	10.1				
	1400	14	22.2	19	4.2	0.2		0.6	0.1	1.0	0.2	78	17.4				
	1800	5	2.3	96	2.2							4.3	0.1				
	Total		100.9		24.5		0.1		0.2		0.5		75.2				
6-D	1000	3	65.9	25	16.2	0.2	0.1	0.8	0.5	0.2	0.1	74	48.8				
	1000	2	3.0	32	1.0			0.8		1.6		66	2.0				
	1400	17	24.0	6	1.4	0.2				1.7	0.4	92	21.9				
	1800	10	8.1	93	7.5	0.7	0.1			0.2		4.4	0.4				
	Total		101.0		26.1		0.2		0.5		0.5		73.1				

comparison. The most striking aspect of the data of Tables 6.6 and 6.7 is the large variation in the gas content of the different specimens examined. For example, a comparison of the volumes of gases evolved by specimens from the various samples (bars) when heated to 1000°C by external resistance heating shows a range from ~23 to ~50 $cm^3/100\ cm^3$ of graphite. This same range also exists for the two specimens machined from sample 6, indicating that the gas content is not only extremely variable from sample to sample but also for specimens machined from the same sample. A range of gas contents from ~41 to ~100 $cm^3/100\ cm^3$ of graphite was found for specimens machined from the various samples when degassed at 1800°C using induction heating. Duplicate tests have been completed only for sample 6. The results are in good agreement, but, as previously noted, duplicate specimens from this sample gave very poor agreement when degassed at 1000°C by external resistance heating. It may be noted that the relative compositions of the gases evolved approximate those found for the various AGOT graphites previously examined in that the sums of the volumes of CO_2 + CO evolved exceed the volume of H_2 in all cases. The average of these widely divergent volumes approximates the volume previously found for AGOT graphite at 1000°C using external resistance heating, as well as at 1800°C using induction heating. It is unfortunate that the values for the gas content of the samples examined vary so widely. Any estimate of the gas content of a large number of bars of this graphite would necessarily be reduced to a probable value somewhere within a wide range.

No systematic study of the rates of evolution of gases by graphite has been made during the period. The examination of the Great Lakes Carbon Company samples is to be concluded shortly, and then modifications are to be made in the equipment so that rate studies can be started.

Transport of Gases Through Graphite

Several constant-pressure experimental tests of the diffusion of helium and argon through graphite at 28°C have been completed. The experiments are the first of a series designed to determine the apparent

interdiffusion coefficients of noble gases in reactor-grade graphites.[9] Prior to these diffusion experiments, graphite characterization parameters were determined for the material from which the diffusion septum was fabricated (Speer No. 1 graphite). Graphite parameters and septum dimensions based on the results of porosity and permeability measurements are presented below:

Open porosity (with helium)	17.8 vol %
K_0 (with helium)	2.23×10^{-6} cm
B_0 (with helium)	9.64×10^{-11} cm^2
Tortuosity factor	1.73
Septum shape	Cylindrical
Inside diameter	0.5 in.
Outside diameter	0.8 in.
Exposed surface length	4 in.
Effective area-to-length ratio	135.8 cm

The experimental procedures and calculations involved in establishing these parameters are discussed in detail in refs 10, 11, and 12. The permeability measurements are shown on Fig. 6.4.

The diffusion experiments were carried out by streaming helium past one face of the septum while streaming argon past the other. The entering sweep gases were pure and at the same pressure. The diffusion-rate constants for argon, for example, were obtained through a knowledge of the argon concentration in the effluent helium stream and the helium effluent rate. Since the gas was not recycled, it was necessary to

---

[9]H. L. Weissberg and A. S. Berman, Diffusion of Radioactive Gases Through Power Reactor Graphites, ORGDP-KL-413 (April 6, 1959).

[10]C. G. Rall, H. C. Hamontre, and D. B. Taliafferro, Determination of Porosity by a Bureau of Mines Method, USBM, RPI-5025 (July 1953).

[11]Standard Procedure for Determining Permeability of Porous Media, API Code No. 27, 2nd Edition, American Petroleum Institute, Division of Production, Dallas, Texas, 1942.

[12]J. M. Hutcheon, B. Longstaff, and R. K. Warner, "The Flow of Gases Through a Fine-Pore Graphite," p 259 in Industrial Carbon and Graphite (London Conference, September 24-26, 1957, Society of Chemical Industry, 1958.

employ low sweep velocities (Reynolds number <10) in order to keep the diffused gas concentrations at measurable values. A complete description of a similar experiment may be found in the literature.[13] Average values of the diffusion experiment results are presented in Table 6.8

One of the primary objectives of the initial experiments was to establish the mechanism or mode of noble gas diffusion through a graphite environment. In many cases, a diffusion mechanism can be determined through interpretations of pressure-dependence plots of the diffusion coefficients. If diffusion occurs in relatively large-diameter pores, the over-all mechanism should be classical in nature and be characterized by equal coefficients for each gas. Plots of the diffusion coefficients vs reciprocal pressure should decrease linearly as the pressure is increased. If Knudsen and/or surface diffusion effects are involved (flow through small pores), the coefficient for each gas will differ and be independent of pressure. The curves shown on Fig. 6.5 suggest that both types of mechanisms contribute to the over-all diffusion process encountered in the present experiments.

The magnitudes of the experimental diffusion rates were much lower than those anticipated through preliminary calculations, which were based on a diffusion model suggested by Carman,[14] the characterization parameters

[13] E. Wicke and R. Kallenbach, Kolloidzchr. 97, 135 (1941).

[14] P. C. Carman, Flow of Gases Through Porous Media, p 79, Academic Press, New York, 1956.

Table 6.8. Apparent Diffusion Coefficients for Helium and Argon Through Speer No. 1 Graphite at 28°C

Pressure (atm)	Diffusion Coefficients (cm^2/sec)		Number of Determinations
	Helium	Argon	
	$\times 10^4$	$\times 10^4$	
1.61	30.3	9.1	2
2.00	24.5	6.1	8
3.00	18.4	4.2	6

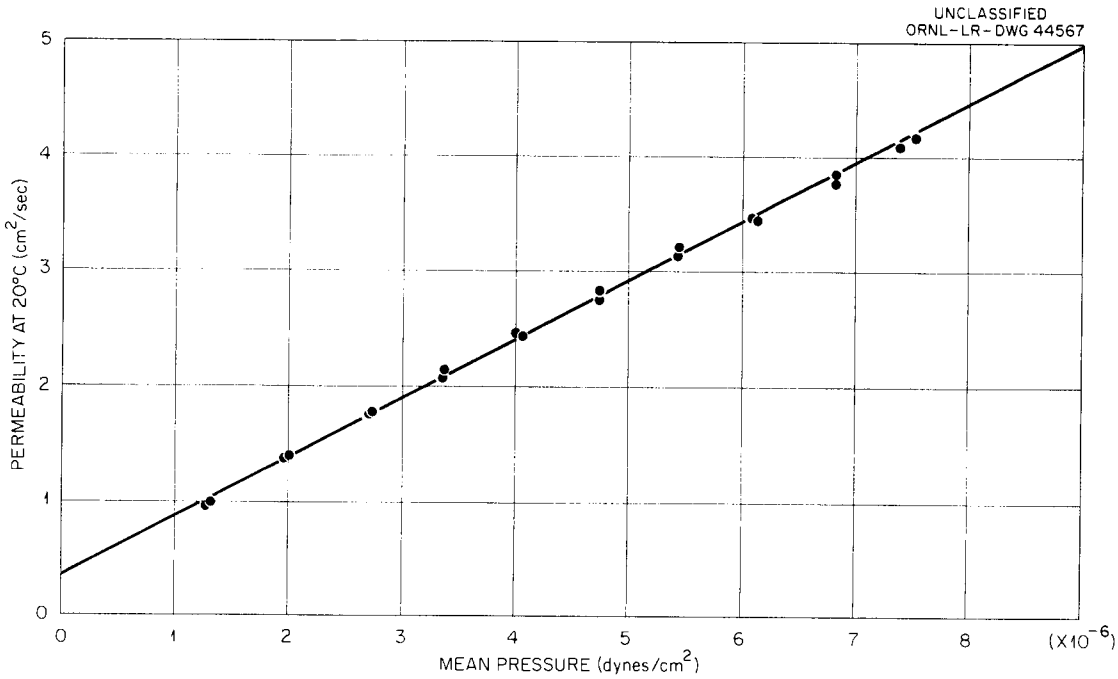

Fig. 6.4. Helium Permeability of Speer No. 1 Graphite

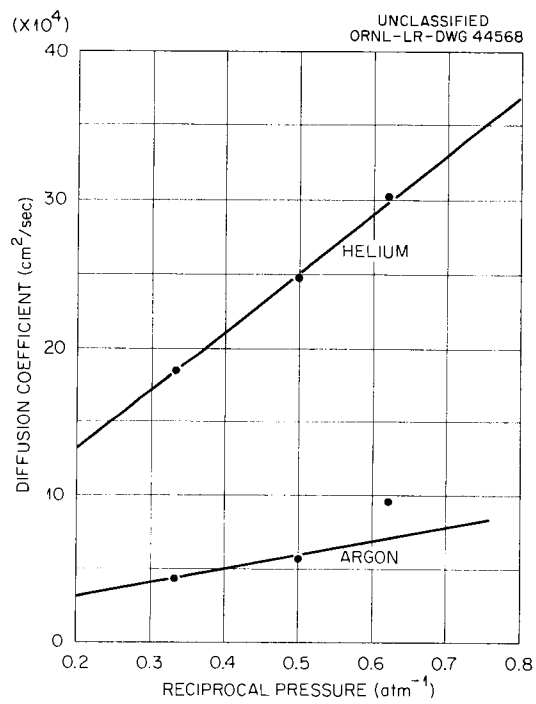

Fig. 6.5. Apparent Diffusion Coefficients for Argon and Helium in Speer No. 1 Graphite at 28°C.

given above, and the classical helium-argon diffusion coefficients.[15] For example, at one atmosphere and 28°C, the classical helium-argon coefficient is 8.1×10^{-1} cm^2/sec, the model value for argon in helium is 4.8×10^{-2} cm^2/sec, and the extrapolated experimental values are 8.8×10^{-4} cm^2/sec for argon and 4.4×10^{-3} for helium.

It is felt that the coefficients obtained to date are not completely reliable because of the possible existence of mass transfer films at the graphite surfaces. This might explain the low values obtained. Future work will be focused on attempts to eliminate these and other difficulties regarding the diffusion-rate measurements.

Cesium in EGCR Fuel Capsules

Investigations of the chemistry of cesium that will be significant in the GCR program are required because of the high fission yield of cesium, 18.6%.[16] The two important considerations related to this high yield are the form cesium will take and the effect of the cesium on the cladding. The form the cesium will take can be inferred from the thermochemical data for oxides supplemented by an intuitive treatment of the diffusion of cesium and other metallic fission products through UO_2.

The existence of cesium as an oxide or metal is primarily dependent on the distribution of the two oxygens made available from each fissioned atom. Tables giving the free energies of oxide formation[17] indicate that other fission products which occur in high yield (Zr, La, rare earths, Y, Sr, Ba, Mo) form more stable oxides than Cs_2O, and these other fission products would be effective in taking up all the available oxygen under equilibrium conditions. Furthermore, it is unlikely that

---

[15] J. O. Hirschfelder, C. F. Curtiss, and R. B. Bird, Molecular Theory of Gases and Liquids, p 539, 578–80, Wiley, New York, 1954.

[16] J. O. Blomeke and M. F. Todd, U-235 Fission Product Production as a Function of Thermal Neutron Flux, Irradiation Time, and Decay Time, ORNL-2127, Pt. 1, Vol. 1, p 35.

[17] J. P. Coughlin, Heats and Free Energies of Formation of Inorganic Oxides, U. S. Bureau of Mines Bulletin 542 (1954).

cesium would be oxidized by UO_2. In addition, any available oxygen in the gas space would react preferentially with the cladding at reactor temperatures.

Diffusion considerations also mitigate against cesium oxide formation. The temperature at which the diffusion and solid state reactions usually begin to occur is approximately one half the melting temperature in degrees absolute. For UO_2 the Tammann temperature is about 1500°K (2240°F). Since the temperature in the pellets is expected to exceed the Tammann temperature, it is likely that the UO_2 ionic lattice is fairly "loose." This implies that the fission products would not have too much difficulty forming their respective oxides. From cation size considerations, cesium, being the largest cation, would probably diffuse through the solid lattice at a slower rate than the much smaller Zr^{4+}, Mo^{4+}, Ba^{2+}, Sr^{2+}, Y^{3+}, and the trivalent rare earth ions, again making it difficult for cesium to obtain oxygen for compound formation.

Thus from thermochemical and crude diffusion considerations it would seem that cesium metal is the most likely form of the cesium fission product. As burnup of the fuel progresses, much of the cesium would vaporize from the solid into the cooler vapor space. When enough cesium gets into the vapor to exert a partial pressure equal to that exerted by liquid cesium at the same temperature, condensation will occur. The vapor pressures to be expected will be a function of the lowest temperature within each fuel rod. Some of these vapor pressures[18] are given below:

Temperature		Pressure (atm)
°K	°F	
900	1161	0.49
1000	1341	1.2
1100	1521	2.3
1200	1701	4.4
1300	1881	7.1

[18] O. Kubaschewski and E. U. Evans, Metallurgical Thermochemistry, p 324, 2nd ed., Wiley, New York, 1956.

In order to investigate the effect of cesium metal on stainless steel and to confirm the lack of reactivity with UO_2, a simple vapor pressure experiment was carried out in a stainless steel vessel containing 40 g of UO_2 and 1/2 g of cesium metal. In the temperature range 350 to 550°C, the vapor pressures measured were equal to those of cesium metal alone. Pressures at higher temperatures could not be measured with the apparatus available. However, the temperature of the vessel was raised to 700°C and maintained there for 17 hr. The temperature was then lowered to 524°C, and the vapor pressure was again found to be that of cesium metal. Examination of the container and its contents revealed that some Cs_2O had formed but not on surfaces of UO_2 chips, which is interpreted to mean that cesium reacted with residual oxygen present in the inert gases used in the dry box and vapor pressure experiment. Lathe shavings from the inside of the vapor pressure vessel were analyzed for cesium and found to contain 1 wt % cesium. There are at least two possible reasons for the cesium in the stainless steel. The first, alloy formation, would not be expected based on the lack of analogous alloying properties of other alkali metals. A second and more plausible reason is that cesium, with some cesium oxide and structural metal oxides acting as wetting agents, spread and adhered on the stainless steel surface. Some of this cesium was retained in an oxidized form on the surface after handling in a noninert atmosphere. The fact that cesium was found in the shavings suggests that further research into the compatibility of cesium with stainless steel is necessary.

Measurement of High Temperatures

Attachment of Thermocouples for Measurement of Surface Temperatures in High-Velocity Cooling Gas

The investigation of factors influencing the accuracy of thermocouples attached to metal surfaces in high-velocity cooling gas was continued. Preliminary experimental results were reported previously on the effects of gas pressure, identity of coolant gas, thickness of

coolant channel, and surface heat flux.[19] Studies of these factors have been continued. Additional experimental work has been conducted to determine the effect of the length of exposed thermocouple lead wire near the thermocouple junction. Theoretical calculations are being made, with the use of the Oracle, of the heat transfer in a thermocouple junction regarded as a cooling fin. The results of these calculations will be used to correlate the experimentally measured corrections for thermocouples attached in coolant streams.

The effect of absorption by windows of various types on the measurement of temperature by an optical pyrometer was experimentally determined. Windows of various glass materials and of various thicknesses were interposed between an optical pyrometer and a target heated to temperatures ranging from 750 to 1000°C. Window-absorption corrections of 3 to 7 degrees were required for Pyrex, plate glass, and quartz windows from 1/16 in. thick to 1/4 in. thick. Apparently, reflection is the mechanism contributing most strongly to loss of radiation, and absorption of radiation by the glass material is relatively unimportant, as evidenced by the insensitivity of the effect to window thickness. Optical pyrometers are used in the work on attachment of thermocouples to determine the actual surface temperature for comparison with the temperature indicated by the thermocouples. Quartz windows have been used in the past in this work, and the corrections applied have been consistent with the results presented here.

Equipment and Techniques for High-Temperature Thermocouple Studies

Work is continuing on the use of small high-temperature furnaces for thermocouple studies. The tungsten-ribbon furnace has been operated up to the melting point of the tungsten. Because of the difficulty in measuring the temperature of the ribbon accurately by optical means, attempts are being made to obtain black-body conditions in the test region. The ribbon furnace is thought to be less desirable from this

[19] GCR Quar. Prog. Rep. Sept. 30, 1959, ORNL-2835, p 146.

standpoint than tube or helix furnaces. A technique has been developed for winding self-supporting helices from tungsten wire or rod of 0.040 to 0.125 in. in diameter. The helices have performed satisfactorily, and the furnace has been operated for a short time at over 2800°C without failure. The furnace operates in a vacuum or on inert atmosphere, but traces of water or oxygen in the atmosphere are thought to be the cause of slow oxidation of the tungsten.

Equipment has been assembled to check the abnormal drifts in Chromel-Alumel thermocouple readings obtained at 1000°C in a previous investigation when the thermocouples were exposed to particular environmental conditions. At present, experiments are under way to determine the reproducibility of test data when using commercially available wires. In order to show significant trends it will be necessary to accumulate more data than was previously available. Therefore, the tests under way include larger numbers of thermocouples, and all variables are being controlled as completely as possible. It is expected that the increased accuracy of measurements and control of variables will result in smoother data which will show without doubt whether there are drift trends caused by atmospheric conditions.

Stability of Rhenium-Tungsten Thermocouples

Tests on rhenium-tungsten thermocouples at temperatures from 1500 to 2000°C have been continued. The outputs of thermocouples were measured for various temperatures determined by an optical pyrometer. The calibration curves of the thermocouples appeared to be constant with duration of exposure of the thermocouple at 1800°C up to 64 hr, within experimental error. The reproducibility of results obtained between 1000 and 1600°C was better than between 1600 and 2000°C. The thermocouples being tested consisted of a rhenium and a tungsten wire 0.010 in. in diameter in a beryllium oxide insulator. Additional tests are being run to improve the reproducibility of results. The furnace is being improved with a tungsten heater rather than a tantalum heater and a larger power supply so that these tests can be extended to higher temperatures.

Arrangements were made for an IBM-704 computing program to process the experimental data obtained in thermocouple calibration experiments. The program selects the curve which fits the experimental points, determines the statistical variance of the curve, evaluates a series of such curves, and tests the data for significance of correlation with selected parameters, such as duration of exposure at high temperatures and duration of exposure to neutron flux. The program has been completed and will be used to analyze thermocouple calibration data obtained in this work.

Effects of Radiation on Thermocouples

Calculations of the amounts of impurities produced in thermocouple materials by transmutation reactions were continued. Arrangements were made for an IBM-704 computer program to calculate the amounts of impurities as a function of neutron exposure time and flux for any material. The program has been completed and will be used to determine the composition of thermocouple alloys after exposure to neutron flux.

Six Chromel-Alumel thermocouples which were irradiated in the MTR for 5500 hr in connection with a fused-salt capsule experiment are available for postirradiation examination. A special shearing tool was prepared and shipped to the MTR to permit removal of the experimental assembly at the conclusion of the tests without the thermocouple damage that normally occurs. The calibration curves of these thermocouples will be determined in hot cells at ORNL.

Postirradiation examination of irradiated thermocouples will indicate any permanent change in thermocouple calibration. It is possible that transient changes will occur, however, which will persist only while the thermocouple is being exposed to radiation. To provide information on this point, it is desirable to calibrate thermocouples during irradiation. To do this, a standard must be available which is not affected by radiation. Various standards have been considered for this purpose, including boiling sodium metal at a controlled vapor pressure and radiation pyrometers of various types. Methods for use of both of these standards are, however, quite complex. Melting-point standards

could be used in-pile with very little complexity. Of particular interest as a melting point standard are the fused-salt mixtures developed in connection with the molten-salt reactor program. The experience obtained in in-pile testing of fused-salt capsules makes the design of an in-pile thermocouple melting-point calibration experiment straightforward. The results of these in-pile experiments have indicated that fused salts are not affected appreciably by radiation. It is planned to install a fused-salt capsule with a thermocouple well in it and to determine the thermocouple output at the melting point of the fused salt before, during, and after irradiation to determine whether there is any transient effect of radiation.

Purification of Cooling Gases

Measurement of Fission Gas Retention by Adsorbers

Methods of measuring krypton adsorption on various adsorbents in the presence of other gases and at very low krypton equilibrium pressures have been studied, and consideration has been given to the potential hazard resulting from oxygen adsorption on charcoal at low temperatures. Measurements have been made of krypton retention by a series of experimental activated carbons.

Measurements of dynamic fission gas retention by adsorbers at very low temperatures, for example, the temperature of liquid nitrogen, are usually rather inconvenient because of the very long retention times involved, even for small quantities of adsorbent. Consequently, an effort is being made to develop a method for determining equilibrium adsorption of krypton on adsorbents in the presence of other gases at very low krypton pressures ($\sim 1\ \mu$). Such data will permit the estimation of dynamic retention of fission gases. The method utilizes circulation of mixtures of krypton and other gases and the measurement of the krypton pressure by beta counting with Kr^{85} as the tracer. A fair quantity of data has been obtained, all at -183°C, but the results are thus far

somewhat erratic. However, it is anticipated that the erratic tendency can readily be overcome by minor modifications in the method and that useful and reliable basic data will be obtained.

Calculations have been made pertaining to the potential hazard which exists when oxygen is adsorbed on charcoal at low temperatures. This hazard will vary considerably according to conditions such as quantity of charcoal in adsorber, charcoal temperature, oxygen concentration in carrier gas, nature of carrier gas, etc. The calculations are based on the adiabatic heat of reaction of oxygen with charcoal or the combustible component of the carrier gas and on enthalpies as a function of temperature for charcoal and the associated gases. The mechanism by which the reaction might be initiated is not apparent, but because of radiation and thus possible ozone formation, consideration of possible reactions does appear to be warranted. The increase in charcoal temperature that would result from the reaction would cause desorption of the adsorbed gases and a consequent increase in pressure. While each adsorber system would require individual analysis, it has been calculated that oxygen concentrations as low as a few parts per million in the inlet gas of an adsorber for an extended period of time could give rise to a potentially hazardous situation.

As part of a more or less continuous program for testing newly available adsorbents with respect to fission gas retention, dynamic adsorption coefficients or k values for krypton have been measured by the usual method[20] for a series of experimental activated carbons supplied by the National Carbon Company. These materials, all 6/14 mesh, were prepared from the same base material and differ only in the degree of activation. Helium was used as the carrier gas, and the adsorbent temperature was 24°C. The results are presented in Table 6.9 along with those for Columbia G activated carbon, 8/14 mesh, which has been used extensively in work connected with removal of fission gases

---

[20]W. E. Browning, R. E. Adams, and R. D. Ackley, Removal of Fission Product Gases from Reactor Off-Gas Streams by Adsorption, ORNL CF 59-6-47 (June 11, 1959).

Table 6.9. Dynamic Adsorption Coefficients for Krypton on Activated Carbons at 24°C with Helium Carrier Gas

Activated Carbon Designation	Activity (%)*	Carbon Bulk Density (g/cm^3)	Adsorption Coefficient	
			cm^3 of Kr per g of C	cm^3 of Kr per cm^3 of C
Experimental				
200	0	0.804	0.5	0.4
205	12.7	0.737	37.9	27.8
210	30.3	0.658	49.9	32.8
203	44.5	0.608	42.1	25.5
204	59.5	0.553	52.1	28.6
201	78.3	0.428	50.2	21.6
Columbia G	58	0.55	63.4	34.6

*The exact meaning of this quantity was not defined for the experimental materials. The customary definition is: weight per cent CCl_4 adsorbed at 25°C from dry air saturated with CCl_4 at 0°C.

from other gases.[20] In Table 6.9, the dynamic adsorption coefficients are expressed in cubic centimeters of krypton per cubic centimeter of charcoal, in addition to the customary cubic centimeter of krypton per gram of charcoal because a fairly wide range of charcoal densities was encountered. The results indicate that none of the experimental materials are as good as Columbia G activated carbon for krypton adsorption under these test conditions and that further tests will be required to establish the optimum degree of activation.

Removal of Coolant Impurities by Oxidation with Copper Oxide

The impurities to be removed from the helium coolant of a high-temperature gas-cooled power reactor include chemically active gases such as H_2, CO, H_2O, and CO_2, which could cause corrosive attack, and gaseous or solid fission products, which would create contamination hazards. In a review of the literature on the behavior and properties of copper oxides, it has been found that one of the simplest procedures for removing CO, H_2, and hydrocarbons from chemically inert gases such as helium is oxidation to CO_2 and H_2O. These two gases will be present

in the EGCR helium coolant and must be removed, in any case, for example, as by sorption. Oxidation with CuO is a standard procedure in gas analysis. It might also be possible to remove the impurities by oxidation with oxygen gas, using a catalyst such as palladium. In either case the excess oxygen in the gas returning to the reactor would have to be removed completely to prevent oxidation of the graphite moderator.

The use of a bed of copper oxides in the coolant purification system would provide for control of the oxygen concentration of the helium leaving the purification system, which would not be possible with commerical catalytic oxidizers. Temperatures between 1000 and 1200°F in the bed would be optimum for oxidation of CO and H_2 and would be satisfactory for the oxidation of Cu_2O to CuO by oxygen. If both CuO and Cu_2O were present in a bed maintained between 1000 and 1200°F, the exit concentration of O_2 should be below 1 ppm and CO and H_2 would be very low. While simple batch operation is the best way to avoid excessive O_2 concentrations in the exit gas, continuous operating schemes appear to be promising with respect to reducing the bed size and avoiding regeneration systems.

Mechanism of Oxidation with Copper Oxides. Copper oxides with copper-to-oxygen ratios of between 1 and 2 consist of two-phase mixtures of CuO and Cu_2O crystals which have been observed physically.[21,22] A quadruple point is reported for CuO–Cu_2O–O_2–molten oxides at 390 mm Hg and 1484°F.[21] Measured values of equilibrium O_2 pressures (Fig. 6.6) are represented by the equation[21]

$$\log P = -\frac{13216}{T} + 12.35 \quad ,$$

where T is in degrees Kelvin for the temperature range 1173 to 1355°K and P is the absolute pressure in mm Hg. The dissociation constants or

[21]F. H. Smyth and H. S. Roberts, J. Am. Chem. Soc. 42, 2582-2607 (1920).

[22]B. Reuter and X. Schroder, Z. anorg. u. allgem. Chem. 277, 146-55 (1954).

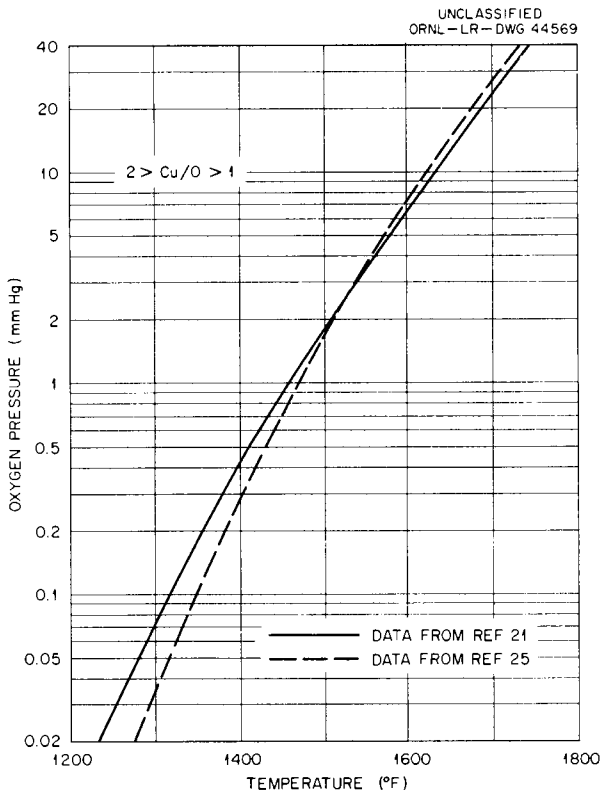

Fig. 6.6. Equlibrium Oxygen Pressures vs Temperature for the System $CuO-Cu_2O-O_2$.

equilibrium oxygen overpressures have been confirmed by thermodynamic data, such as emf measurements.

The oxidation of CO and O^{18} tracer in CuO has been studied.[23] When the feed was a mixture of gaseous CO and O_2 at 300°C, no O^{18} appeared in the CO_2 product. Thus, in this reaction, reduction of Cu_2O did not occur, although both the reactions

$$2CuO + CO \rightarrow CO_2 + Cu_2O$$

$$2Cu_2O + O_2 \rightarrow 4CuO$$

are rapid at 300°C. A stepwise oxidation of Cu_2O containing O^{18} tracer, followed by a partial stepwise reduction with H_2, gave equal O^{18}

[23]G. Y. Turovskii and F. M. Vainshtein, Doklady Akad. Nauk USSR 78, 1173-5 (1951).

concentrations in the water obtained from various steps. This result indicated that the mechanism did not involve only a small number of active points which were repeatedly reduced to Cu_2O and oxidized to CuO.

During an exchange of O_2 gas with CuO containing O^{18}, the exchange in 4 hr was 7% at 400°C, 11% at 500°C, and 22% at 600°C.[24] One author reports an induction period for the reduction of CuO by H_2 and concludes that the reduction rate is controlled by the absorption of H_2 on the oxide surface.[25]

While oxidation of CO and H_2 by CuO is rapid at 250 to 300°C, CH_4 does not react unless temperatures of 550 to 700°C are used.[26] The oxidation of methane is promoted by CuCl or by other oxides such as V_2O_5, NiO, CoO, or MnO.

Activation energies for various oxidation-reduction reactions of CuO to Cu_2O are:

13.3 kcal/mole for the reduction of Cu_2O with H_2 (ref 25),
13.8 kcal/mole for reduction of CuO with H_2 (ref 25),
49.0 kcal/mole for release of O_2 from CuO (ref 25),
13 kcal/mole for oxidation of CO by air with CuO catalyst (ref 27),
6.5 kcal/mole for oxidation of CO by air with a 75 mole % CuO—25 mole % Cr_2O_3 catalyst (ref 27).

The 75 mole % CuO—25 mole % Cr_2O_3 mixture has a higher equilibrium oxygen pressure than pure CuO and is more effective for oxidizing organic matter. Various other important thermodynamic data[28,29] are given in Table 6.10.

---

[24] J. A. Allen and I. Lauder, Nature 164, 142-3 (1949).

[25] E. P. Tatievskaya and G. I. Chufarov, Bull. Acad. Sci. USSR Classe Sci. Tech., 1005-14 (1946).

[26] L. F. Marek and D. A. Hahn, The Catalytic Oxidation of Organic Compounds in the Vapor Phase, The Chemical Catalog Co., New York, 1932.

[27] G. Rienäcker, Z. anorg. Chem. 258, 280-95 (1949).

[28] F. D. Rossini et al., Selected Values of Chemical Thermodynamic Properties, U. S. National Bureau of Standards, Circular 500.

[29] Jih-Heng Hu and H. L. Johnston, J. Am. Chem. Soc. 75, 2471-3 (1953).

Table 6.10. Thermodynamic Data for CuO and CuO_2

Quantity	Unit	Value for	
		CuO (s)	Cu_2O (s)
ΔH_f°	kcal/g-mole	-37.1	-39.84
ΔF_f°	kcal/g-mole	-30.4	-34.98
S°	cal/°K·g-mole	10.4	24.1
C_p°	cal/°K·g-mole	10.6	16.7

For the reaction

$$2CuO\ (s) \rightarrow Cu_2O\ (s) + 1/2\ O_2\ (g)\ ,$$

the free energy change is given by[29]

$$\Delta F^\circ = (33{,}550 - 0.95\ T \ln T + 0.00375\ T^2 - 22.340\ T)\ \text{cal/g-mole}\ .$$

Gas Purification Applications. Equilibrium O_2 pressures (Fig. 6.6) indicate the maximum O_2 pressure in a gas leaving an isothermal bed of mixed copper oxides and determine the maximum allowable bed temperatures for gas-cooled reactor applications. For the proposed coolant system pressure of 300 psia (15,500 mm Hg), a bed temperature of about 1500°F results in a 0.01% O_2 gas stream and 1200°F results in 1 ppm O_2. Temperatures of 1000°F or higher are desirable to insure rapid oxidation of the various oxidizable components, although CO and H_2 would be rapidly oxidized at any temperature above 500°F.[25,26]

Regeneration conditions should be selected for rapid oxidation of Cu_2O while avoiding a high equilibrium O_2 pressure. A temperature range of 1000 to 1200°F appears to be optimum.

The reaction and the thermodynamic changes at 298°K in the bed are:

$$2CuO\ (s) + CO\ (g) \rightarrow CO_2\ (g) + Cu_2O\ (s) \qquad \Delta H = -33.3\ kcal,\ \Delta F = -35.7\ kcal,\ \Delta S = 7.1\ eu$$

$$2CuO\ (s) + H_2\ (g) \rightarrow H_2\ (g) + Cu_2O\ (s) \qquad \Delta H = -23.4\ kcal,\ \Delta F = -28.8\ kcal,\ \Delta S = 17.2\ eu$$

$$Cu_2O\ (s) + 1/2\ O_2\ (g) \rightarrow 2CuO\ (s) \qquad \Delta H = -34.4\ kcal,\ \Delta F = -25.7\ kcal,\ \Delta S = -27.8\ eu$$

From the heat capacities of the reaction products and helium, about 1 vol % $CO + H_2$ would result in a 100°F temperature rise in gas stream. Oxidation of Cu_2O with pure O_2 would raise the bed temperature until the equilibrium O_2 pressure and the actual oxygen pressure over the CuO-Cu_2O were the same.

The properties of the CuO-Cu_2O system would permit several combinations of conditions and gas purification procedures. In a simple batch system, a bed of CuO would be converted to Cu_2O during oxidation of CO and H_2. The bed would be removed from the gas stream before all the CuO had been reduced, and the reduced material would be reconverted to CuO by oxygen in a heated gas stream. In a simple continuous system, oxygen would be added continuously and the CuO bed would act as a catalyst and a reservoir to supply any oxygen deficiency or react with any excess. In a cyclic continuous system, alternating periods of no O_2 addition and excess O_2 addition would be used, with the times being controlled by the bed temperature profiles.

The simple-batch scheme gives the least chance of return of uncombined O_2 to the reactor. However, it requires a regeneration system, including gas preheating, bed cooling, and purge gas discharge, and requires the largest equipment and inventory of coolant gas and copper oxides. The simple-continuous scheme probably requires the smallest volume of copper oxides, but this volume would be much larger than the volume of a more efficient catalytic oxidizer. However, if the relative amounts of CuO and Cu_2O could be measured, the presence of both would insure against release of excess oxygen or unoxidized gases, which is

not the case with conventional oxidation catalysts. The cyclic-continuous scheme provides a measure of the amounts of CuO and Cu_2O in the bed at any time. When starting with a CuO bed and no oxygen addition, there would be a region at the bed entrance with a sharp temperature rise due to the heat of reaction of CuO with H_2 and CO. This region would progress down the bed as CuO was converted to Cu_2O. When this higher temperature region reaches a preselected point, oxygen in excess of that necessary to oxidize the CO and H_2 in the gas would be added to the gas feed to the bed. There would be a region of sharp temperature rise resulting from oxidation of gases at the bed entrance and a second region progressing down the bed resulting from oxidation of Cu_2O by excess O_2. When the second region approached the preselected point, the flow of oxygen would be shut off and the cycle repeated.

While the simple-continuous and cyclic-continuous schemes are compatible with the known properties of copper oxides, no experimental data on the operation of such systems are available. These two modes of operation will be tested at reactor temperature and pressure.

Analyses of UO_2 Fuel Pellets

A study of the reliability of data on the analysis of UO_2 fuel pellets was initiated in an effort to establish methods of analysis that will serve as standards in the evaluation of chemical tests for the acceptability of UO_2 fuel pellets for reactor use. The determinations of most importance at present are the oxygen-to-uranium ratio and the carbon, fluorine, iron, and nitrogen contents.

Oxygen-to-Uranium Ratio

The reliability of the measurement of the oxygen-to-uranium ratio is presumed to be extremely critical in evaluating the lifetime of a given fuel element. Ratios greater than 2 reveal the presence of oxygen, presumably as UO_3, in excess of that combined as UO_2. Ideally, direct measurement of the "excess oxygen" should be made. A possible approach to this determination is to reduce the UO_3 with hydrogen at a high

temperature. The product of the reaction is water, which can be measured at low concentrations with a high degree of precision and accuracy. A definite limitation of this approach is the possibility that the UO_3 is inaccessible to the hydrogen, that is, it is surrounded by UO_2, which is not reducible with hydrogen. Hence, low results would occur. To avoid this, the UO_2 sample must be finely divided. The process of reducing UO_2 to sufficiently small particles could conceivably produce some oxidation to UO_3, again leading to erroneous results.

Another method for determing "excess oxygen" is to analyze for hexavalent uranium, assuming that all excess oxygen is present as UO_3. This is done by the polarographic technique after dissolving the sample of UO_2 in H_3PO_4 under an inert atmosphere. Complete protection of the solution of uranium (IV) is absolutely necessary to avoid air oxidation. This method is rather widely used[30,31] at the present time.

In another widely used method, the UO_2 is oxidized to U_3O_8, and the actual change in weight is compared with the calculated change in weight. This method is best carried out with the use of the thermogravimetric balance. An admitted weakness of this approach is the questionable stoichiometry of U_3O_8. The precise determination of total uranium has also been used to calculate oxygen-to-uranium ratios.

A new reagent, $KBrF_4$, has recently become available for the direct determination of total oxygen in UO_2. From a statistical evaluation of this method, a relative standard error of 0.5% has been established that is based on duplicates. Since total uranium can easily be determined to this order of precision, the calculated oxygen-to-uranium obtained by this approach has much inherent reliability. A careful evaluation of these various techniques is being made to decide upon a particular method that will be of widest usefulness.

---

[30] Anal. Chem. Div. Ann. Prog. Rep. Dec. 31, 1958, ORNL-2662, p 33.

[31] R. M. Burd and G. W. Goward, The Polarographic Determination of Hexavalent Uranium in Uranium Oxides. The Determination of Oxygen/Uranium Ratios, WAPD-205.

Carbon

The determination of carbon in UO_2 is ordinarily made satisfactorily by combustion in oxygen in an induction furnace. The evolved CO_2 is automatically measured conductometrically. The reliability of low carbon values (<100 ppm) is affected greatly by the magnitude of the "blank," that is, the amount of carbon in the crucible used to ignite the sample plus the carbon in the accelerator, usually iron or tin that is needed to aid ignition and combustion of the sample. This "blank" is ordinarily at least three times greater than the amount of carbon in the sample and sometimes nearly 10 times as much. To overcome this effect, a change in procedural detail was tried and tested. Instead of adding a known weight of sample to a known weight of accelerator, igniting, and then subtracting a blank due to that amount of accelerator, the crucible and accelerator are burned until all the carbon is removed. The melt is allowed to cool, and the sample, along with a small amount of tin accelerator, is returned to the crucible. The crucible is again heated slowly and the carbon in the sample is determined. The blank due to this method is small (less than 10 ppm) and constant to within ±2 ppm. This method requires somewhat more time for completion, but the precision on a standard iron sample shows a coefficient of variation of less than 4%. For UO_2 the result of a single analysis is reproducible to within 20%. A possible explanation for this difference in precision is the heterogeneity of the carbon in the UO_2 pellets.

Fluorine, Iron, and Nitrogen

Standard methods already in use have proven entirely satisfactory for the determination of fluorine, iron, and nitrogen.

Automatic Continuous Analysis of Helium from Test Loops

The system for the continuous monitoring of contaminants in the helium atmosphere of the low-pressure thermal-convection loop has been assembled, tested, and calibrated and is now in service, as mentioned in

a preceding section of this chapter. This system, which was described previously,[32] consists of a manifold of 1/8-in. sample lines designed to deliver representative samples from the test loop to a Greenbrier Chromamatic 112 process-gas chromatograph and to a Consolidated Electrodynamics Corp. moisture-monitor. The analyses of most immediate importance are obtained from the chromatograph.

The chromatograph is furnished in two sections: an analysis section, which contains the components for sampling operations and for seperation and detection of the contaminants H_2, CO_2, O_2, N_2, CH_4, and CO, and a control section, which contains electrical components for the generation of programing signals and the attenuation of signals from the detector for presentation of analytical results directly in terms of conventional concentration units. The control section has been installed adjacent to the control panel of the test facility, while the analyzer section has been located near the test loop to minimize the length of sample lines.

A simple flow diagram for the analyzer section is presented in Fig. 6.7. In order to obtain sufficient stability for the desired measurements it was necessary to effect minor modifications and repairs in the analyzer section. These changes included the elimination of leaks from the system, the substitution of a more sensitive needle valve for the restrictor in the dual-column-valve bypass, and the elimination of void space in the fittings to the dual-column valve to reduce flow perturbations which occurred when the valve was actuated.

The precision obtained with the improved apparatus for determinations at the 1000-ppm concentration level is illustrated in Fig. 6.8. A single analysis in spectrum form is shown in the upper section of the figure, and a recording of a series of repeated analyses of a five-component standard sample is reproduced below in bar-graph form. For the bar-graph recording the signals from the detector are attenuated so that full-scale recorder deflection corresponds to 1000 ppm of CO_2, O_2 (absent from sample), CH_4, and CO, and 2000 ppm of H_2 and N_2. The precision of

---

[32] GCR Quar. Prog. Rep. Sept. 30, 1959, ORNL-2835, p 153.

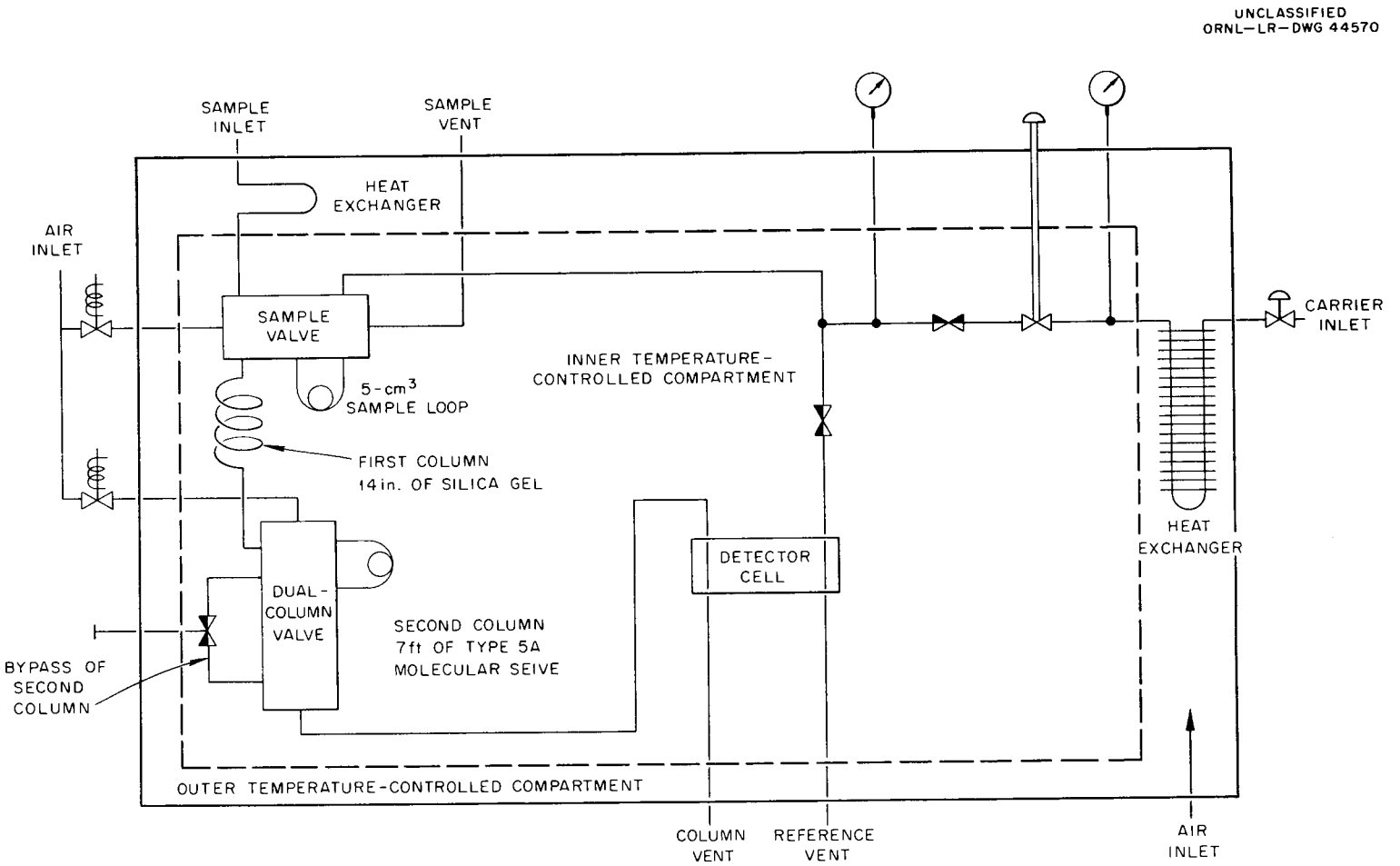

Fig. 6.7. Schematic Flow Diagram of Greenbrier Chroma-Matic 112 Chromatograph.

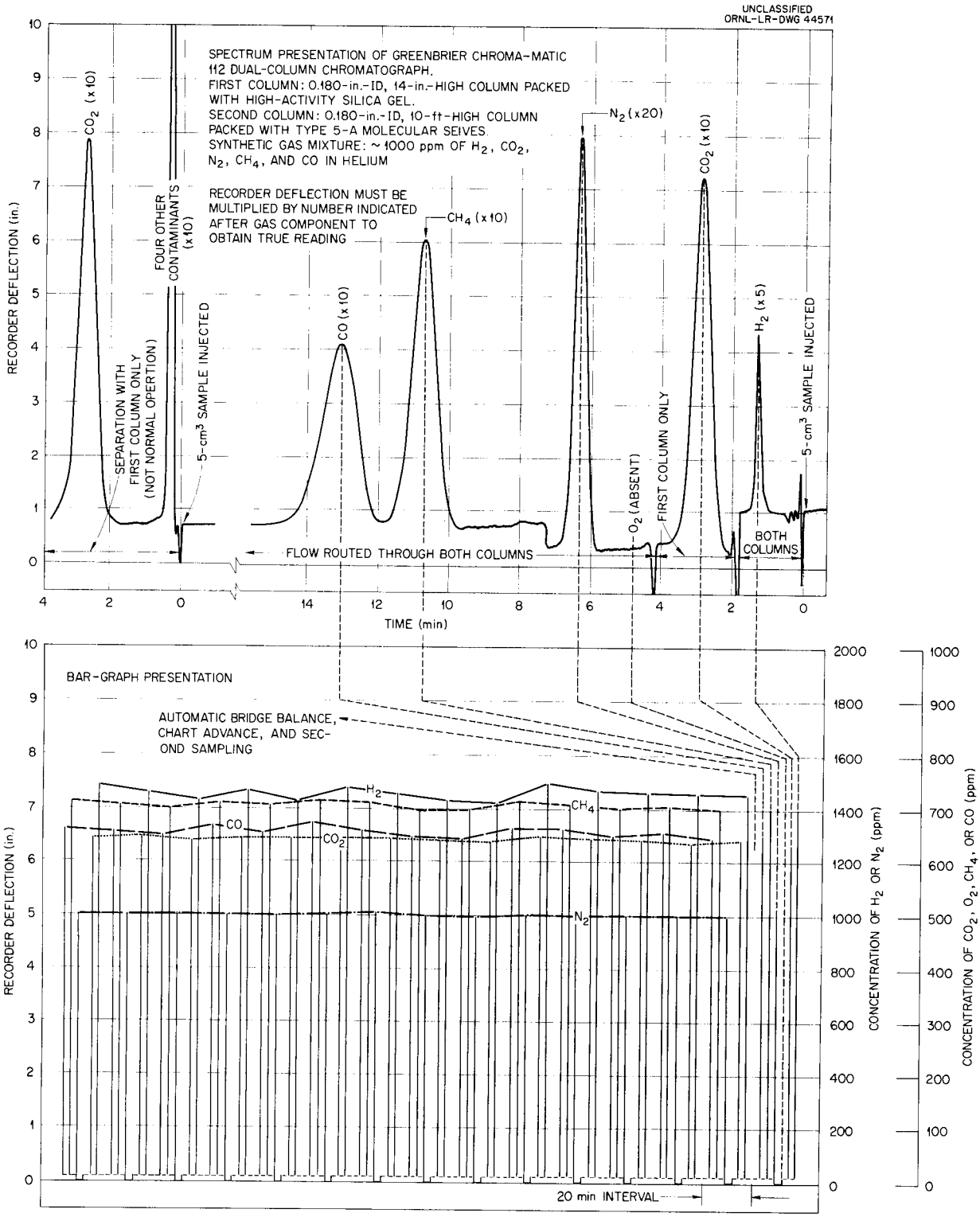

Fig. 5.8. Chromatographic Analysis of a Synthetic Gas Mixture.

the determination of each constituent, except H_2, is about 2%. The precision of the determination of hydrogen is somewhat poorer because of its lower sensitivity and consequent lower attenuation factor and because of base-line perturbations which follow sampling and occasionally persist throughout the interval in which hydrogen is recorded. Improved precision in the determination of hydrogen can be obtained by the addition of a special detector for the measurement of hydrogen.

Typical results of analyses carried out during preliminary operation of the test loop are shown in Fig. 6.9. In these analyses the precision suffered as a result of base-line variations which were introduced by contamination of the system with the condensable impurities that were evolved during the initial heating of the graphite in the test loop and by variations in the temperature of the control section which was opened frequently to change sensitivity ranges. Precision comparable to that obtained in the analyses of standard samples is expected as steady-state operation is approached. The effect of base-line variations on the measurement of the components present in low concentration is illustrated by the analyses of methane, which was present in concentrations of only about 50 ppm. The apparent negative concentrations of O_2 and N_2 indicate that the concentration of these components in the carrier gas was greater than that in the sample. These errors are not of significance in this experiment and can be eliminated by the incorporation of a purification system in the carrier gas line.

The chromatographic system appears to be entirely satisfactory for monitoring concentrations during compatibility tests in which concentrations of specific contaminants will be at a level of 1000 ppm or greater, since full-scale deflections corresponding to concentrations as low as 100 ppm can be obtained for all components except H_2. With certain minor modifications in the electrical components and flow control system, the sensitivity can probably be increased by an order of magnitude, if necessary. The precision of the measurements does not suffer even when the flow rate is reduced to as low as 5 cm^3/min. For a 20 cm^3/min flow rate the response of the system to changes in composition is more rapid

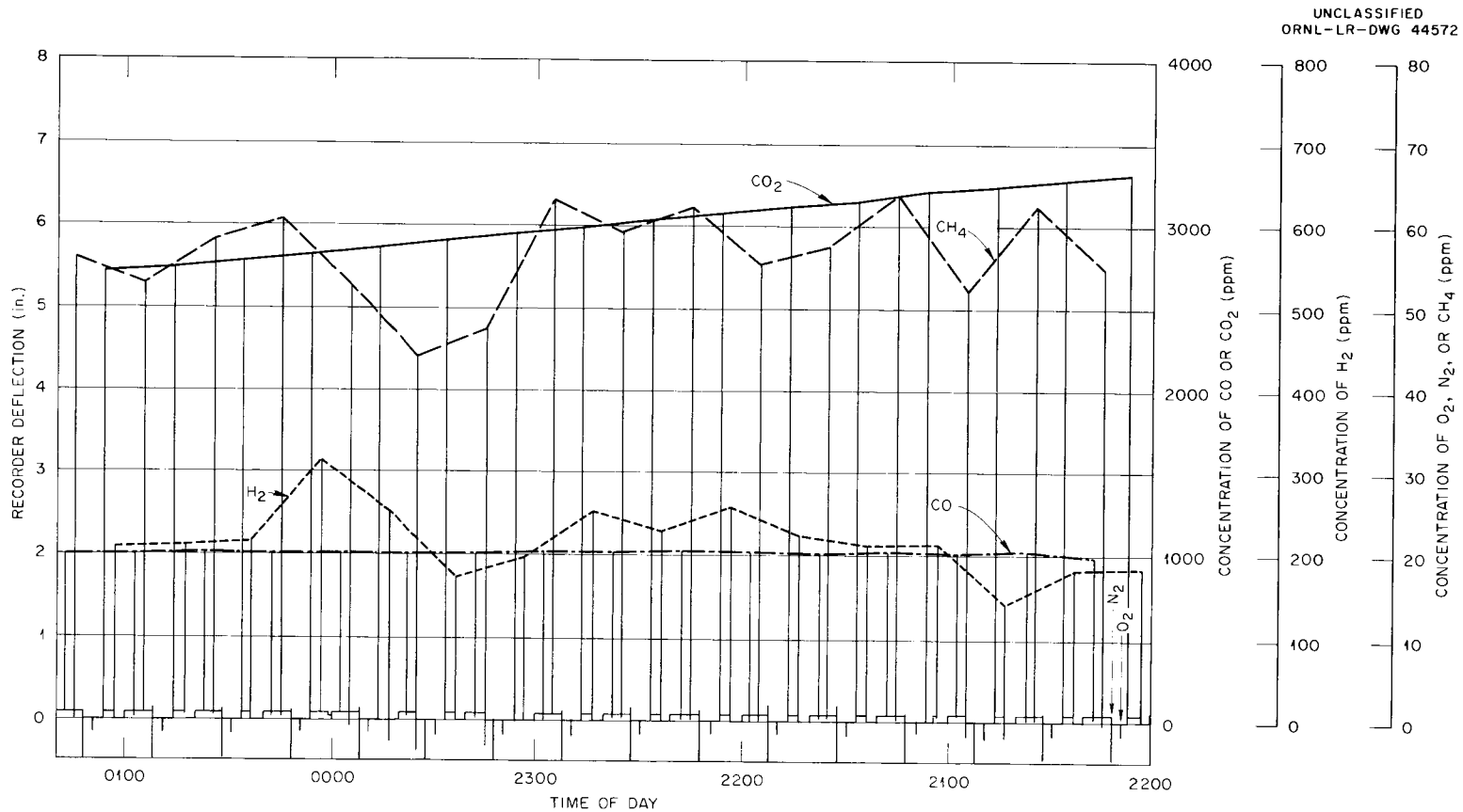

Fig. 6.9. Typical Chromatographic Analysis of Helium from Low-Pressure Thermal-Convection Loop.

than the diffusion of the contaminant additions through the test loop. Calibrations have remained constant to within ±5% during the first week of operation despite contamination introduced during startup operations.

The determination of water has been less satisfactory. The response of the moisture monitors has been slow as a result of holdup in sample lines, and there is some indication that contaminants in the helium affect the accuracy of the measurements. Since the proposed water-injection test can be deferred until the end of the compatibility test, it is not necessary to delay the experiment. During the interval of the compatibility tests, an improved moisture-sampling system is being installed and further laboratory tests of the moisture monitors are being carried out.

7. DEVELOPMENT OF TEST LOOPS AND COMPONENTS

ORR-Gas-Cooled In-Pile Loops

GCR-ORR Loop No. 1

The design of GCR-ORR loop No. 1 is complete, except for the fuel element design and some special tools. Design work on the reactor installation, auxiliary systems, and instrumentation is proceeding satisfactorily. Work is presently complete or under way on the utilities lines, control room layout, compressor cubicle, and loop supports. Procurement procedures have been initiated on some auxiliary components. Fabrication of the control room panels is well under way. The enrichment calculations and detailed design for the flux-monitoring test to be performed in the ORR are also complete.

All parts for the heater, cooler, in-pile section, and thermocouple calibration test piece are on hand. Thermocouples, gas taps, and insulation are being installed, and final assembly and welds are being made. Remaining work on the loop proper includes fabrication of the transfer station, regenerator section, and compressor piping.

The thermocouple calibration test design is complete, and the facility is under construction. This test will utilize the reactor loop heater and cooler and a test section which mocks up the temperature and flow conditions of the reactor loop in-pile section. The test will permit evaluation of the thermocouple error caused by impingement of the gas stream on the fuel cladding thermocouples. A performance check on the heater and cooler will also result.

A preliminary analog computer simulator study of the loop control system has been completed,[1] and the minor changes indicated were incorporated into the control scheme. A second study is to be made that will be based on the 3/4-in.-OD fuel rod which will be used in the initial tests; the preliminary study was based on a 1-in.-OD fuel rod.

---

[1]S. J. Ball, Preliminary Analog Computer Study of the Gas-Cooled ORR In-Pile Loop No. 1, ORNL CF 59-10-6 (Oct. 5, 1959).

The loop heater, which utilized a bundle of 13 electrical cartridges to attain a rated output of 60 kw, is shown in Fig. 7.1. The cooler, shown in Fig. 7.2, is of the bayonet type. It utilizes a mixture of air and water as the coolant to accommodate a wide range of cooling loads.

GCR-ORR Loop No. 2

A flow diagram of GCR-ORR loop No. 2 is shown in Fig. 7.3, and a plan view of the installation at the ORR is shown in Fig. 7.4. The design concept of the loop provides that all components, including the test fuel element, be individually accessible for replacement and examination. Such an arrangement will permit observation of the deposition of fission products released by the fuel, evaluation of the effectiveness of bypass and in-line filtration, and a determination of the feasibility of decontamination in place. Means will be available for indirect manipulation of the fuel test section and shield plug for changing fuel elements. Normal maintenance operations will be performed directly, at a controlled activity level 12 hr after loop shutdown not to exceed 250 mr/hr. The equipment cell will meet all requirements for secondary containment and safety shielding for the entire loop system.

EGCR Experimental Loops

Eight permanently installed experimental loops are to be constructed as an integral part of the EGCR. The experimental loop facilities are to comprise eight through-tubes in the EGCR core, with associated equipment cells, control room, waste disposal, and offgas facilities, as shown in Fig. 7.5.

Four of the through-tubes have nominal outside diameters of 5 in. and the other four tubes have nominal outside diameters of 9 in. The four larger tubes are equally spaced at the perimeter of the core, whereas the four smaller tubes are located near the center of the core, as shown in Fig. 7.6.

Nozzles are provided in the upper and lower pressure vessel head to accommodate the through-tubes which extend from the lower biological

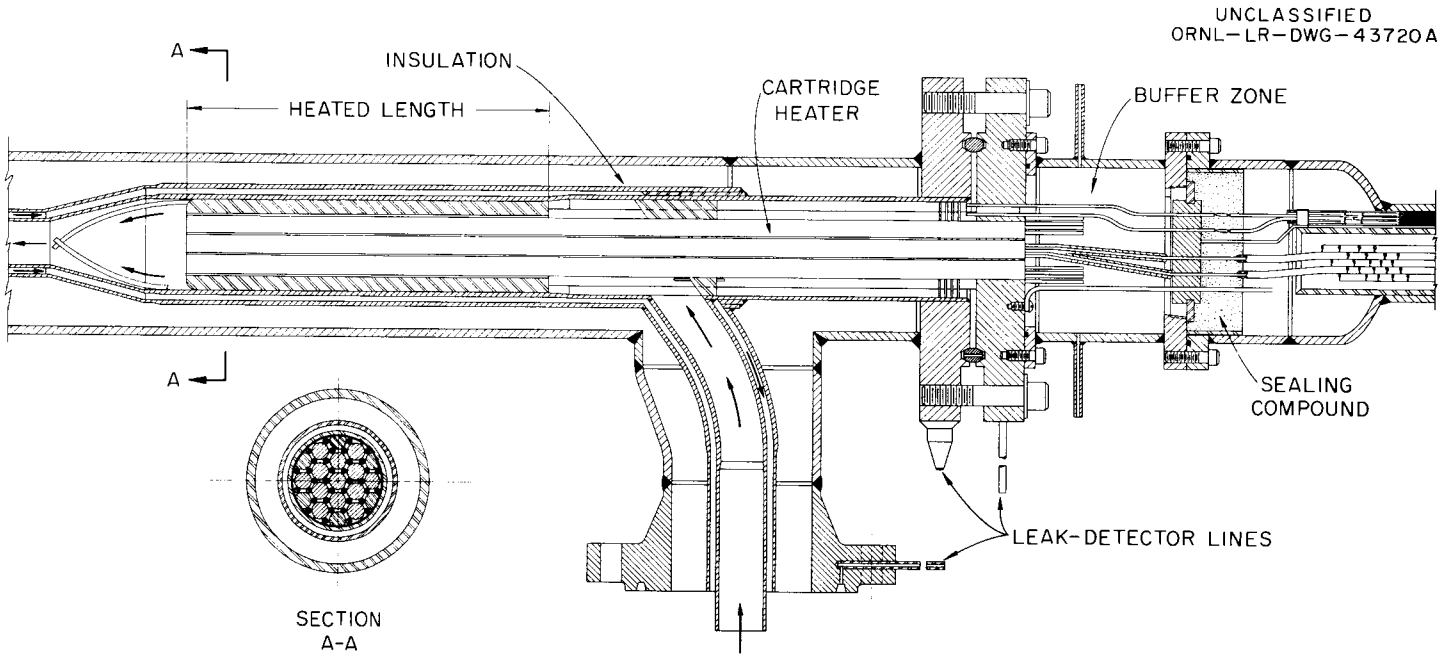

Fig. 7.1. GCR-ORR Loop No. 1 Heater.

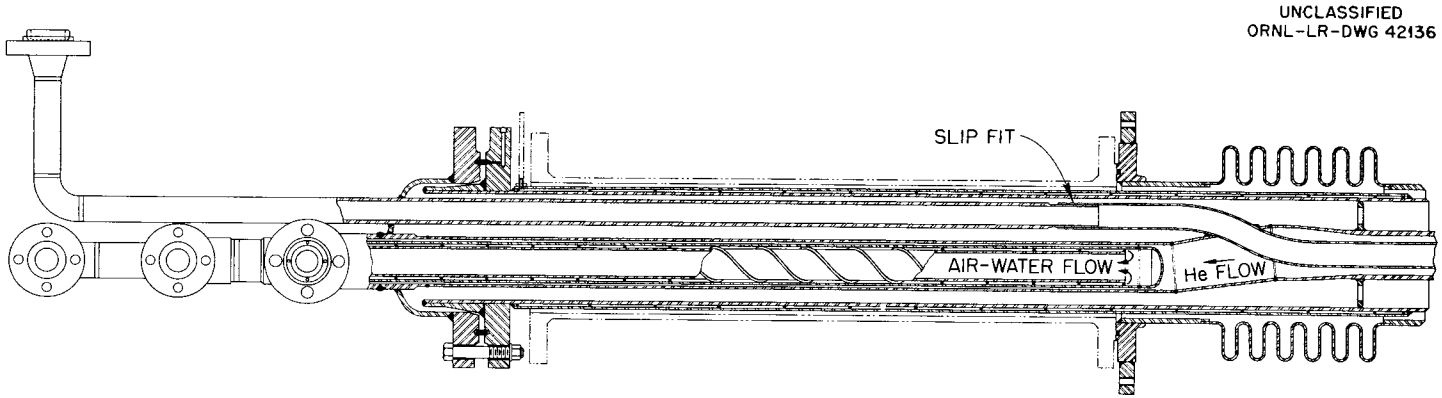

Fig. 7.2. GCR-ORR Loop No. 1 Cooler.

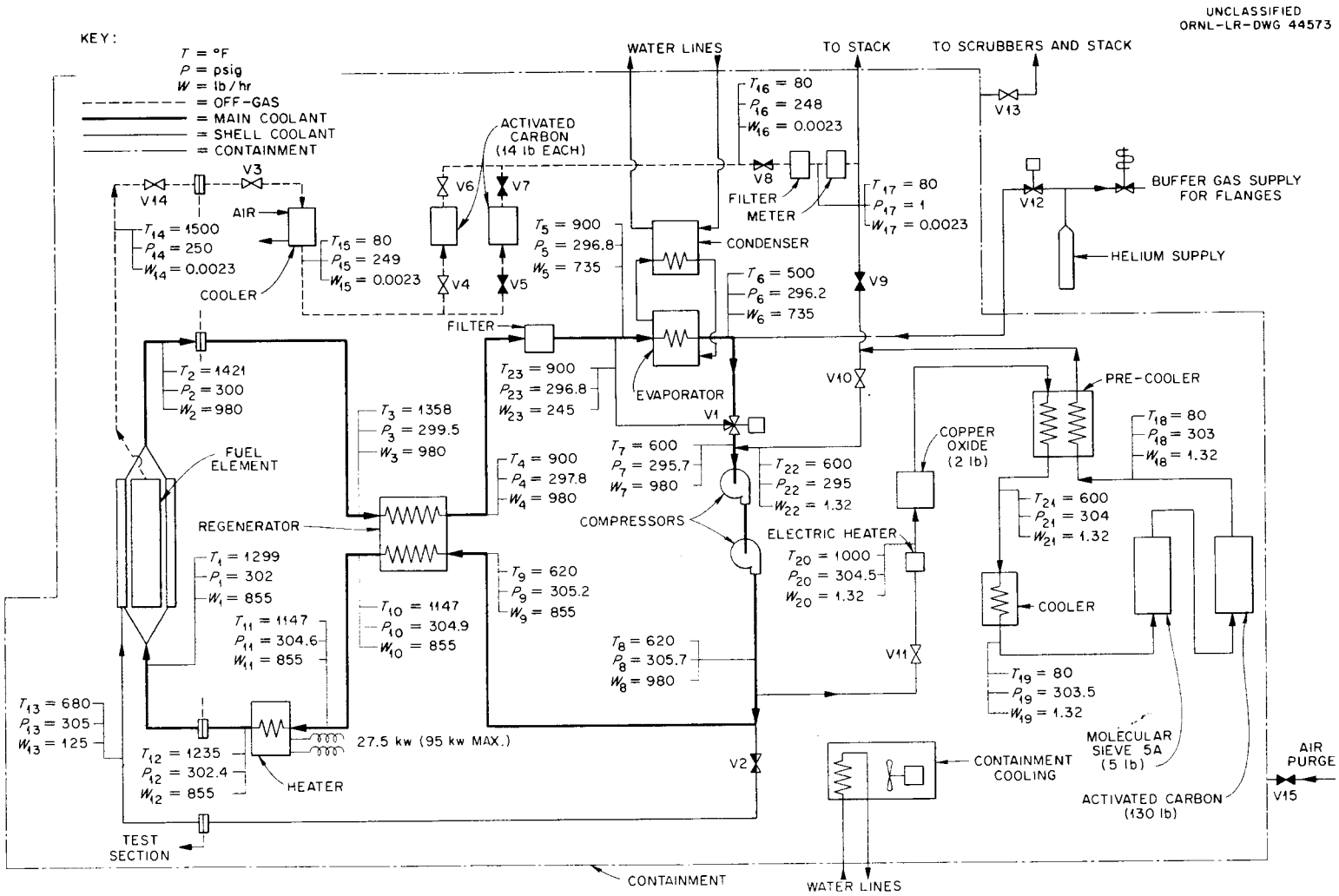

Fig. 7.3. Flow Diagram of GCR-ORR Loop No. 2.

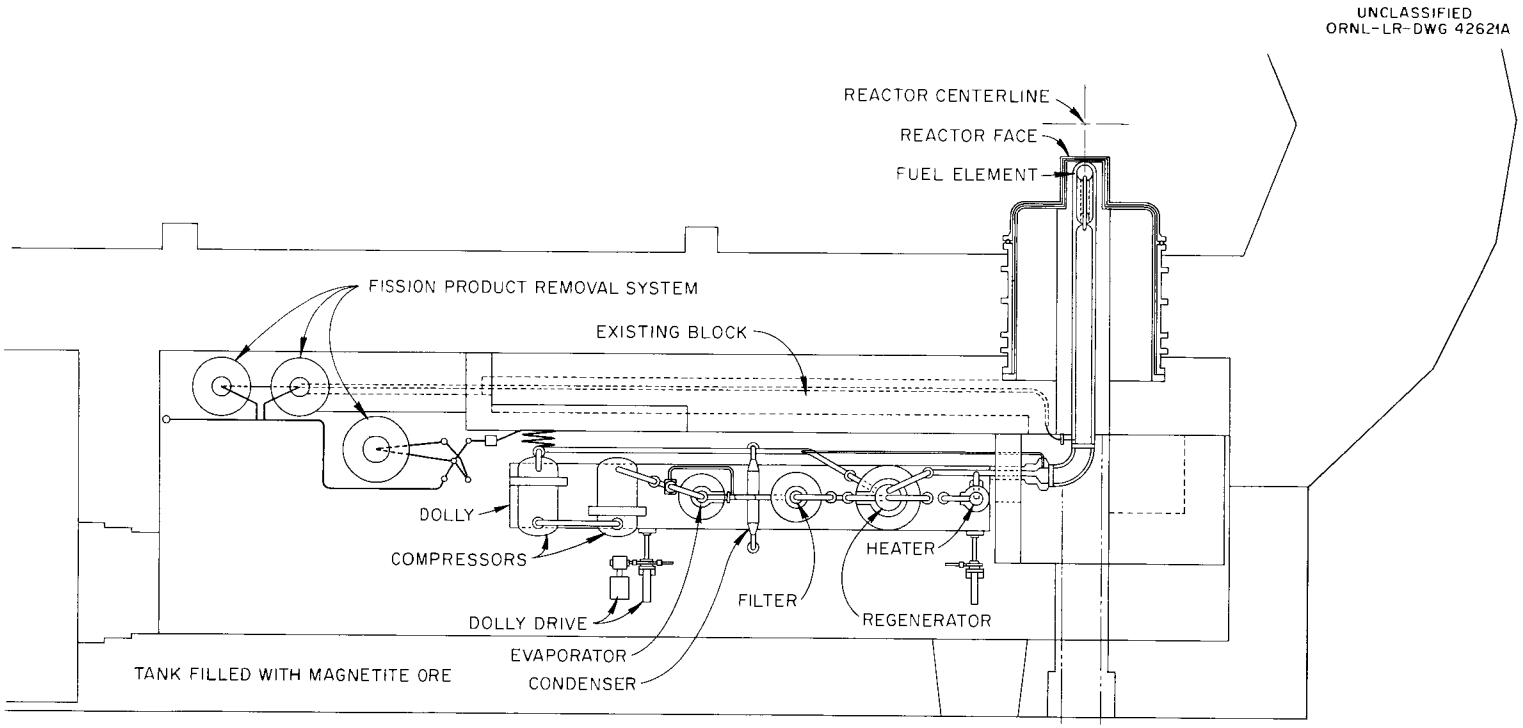

Fig. 7.4. Preliminary Layout of GCR-ORR Loop No. 2.

UNCLASSIFIED
ORNL-LR-DWG 40845A

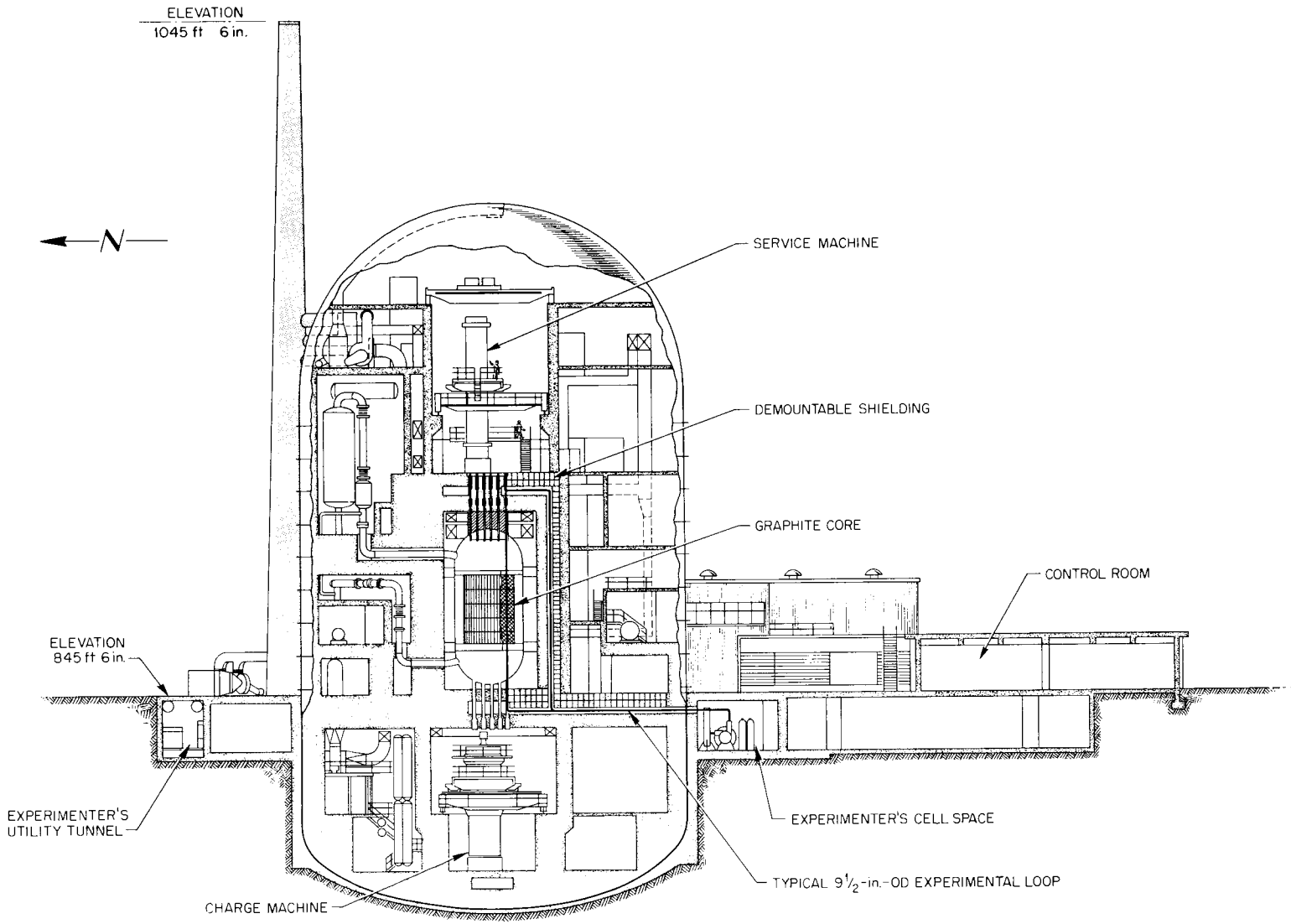

Fig. 7.5. Section View of EGCR Building Showing Experimental Facilities.

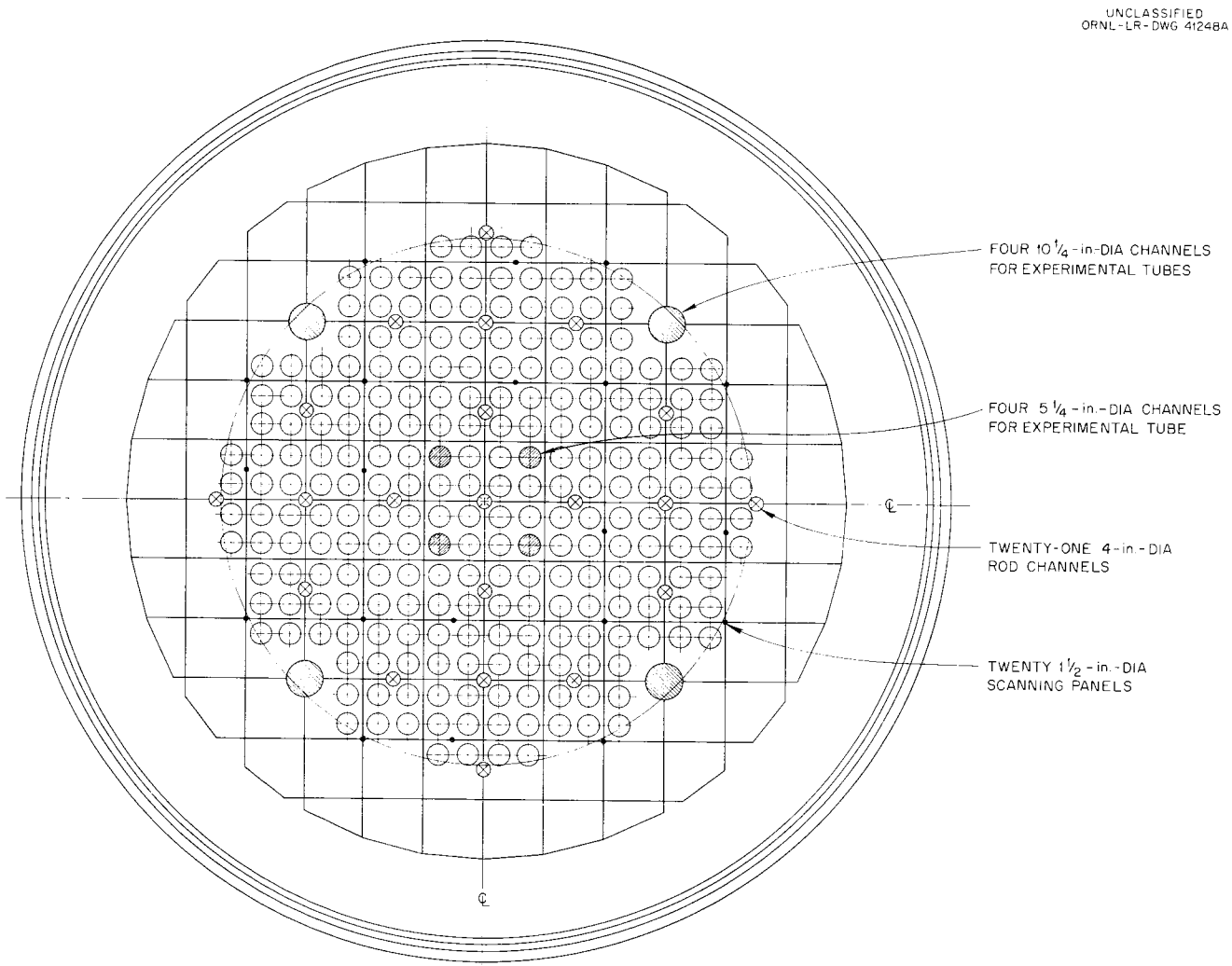

Fig. 7.6. Plan View of EGCR Core.

shield to the top of the upper biological shield for an over-all length of approximately 72 ft. Coolant circulates through the in-pile section in an upward direction, exits from the through tube at a tee located in the upper biological shield, passes through a downcomer in the side biological shield, and flows to the equipment area. The inlet piping is located in the lower reactor biological shield and extends from the equipment area to the lower end of the through tube.

An equipment area of 7000 ft^2 is provided adjacent to and outside of the reactor containment vessel in a semicircular arrangement, with the roofs of the cells at ground level, as shown in Fig. 7.7. The equipment area is divided into individual cells, each with a pressure-tight enclosure. Concentric piping is used between the reactor vessel and the equipment cell to provide double containment for the entire external loop system. Data recording and control instrumentation for each loop is located in a centralized area adjacent to the reactor control room.

During normal operation of a loop, coolant gas will enter the in-pile section at a nominal temperature of 600°F and a pressure of 500 psia and will exit from the in-pile section at a temperature of 1050°F; however, the loops are designed to accommodate a maximum inlet temperature of 950°F and loop pressures up to 1000 psia. The maximum power output for any loop will be 1.5 Mw.

The loops are designed to use helium and carbon dioxide as the coolant media; however, one of the loops will be designed for cooling with hydrogen.

Sample removal will probably be accomplished by the reactor service machine, which is mounted in the containment vessel above the upper biological shield. If it is feasible, this operation will be performed while the reactor is at power.

Mechanical Joint Service Testing

Commercially available mechanical joints have been specified for the EGCR experimental tubes, and double-gasketed, gas-buffered, mechanical

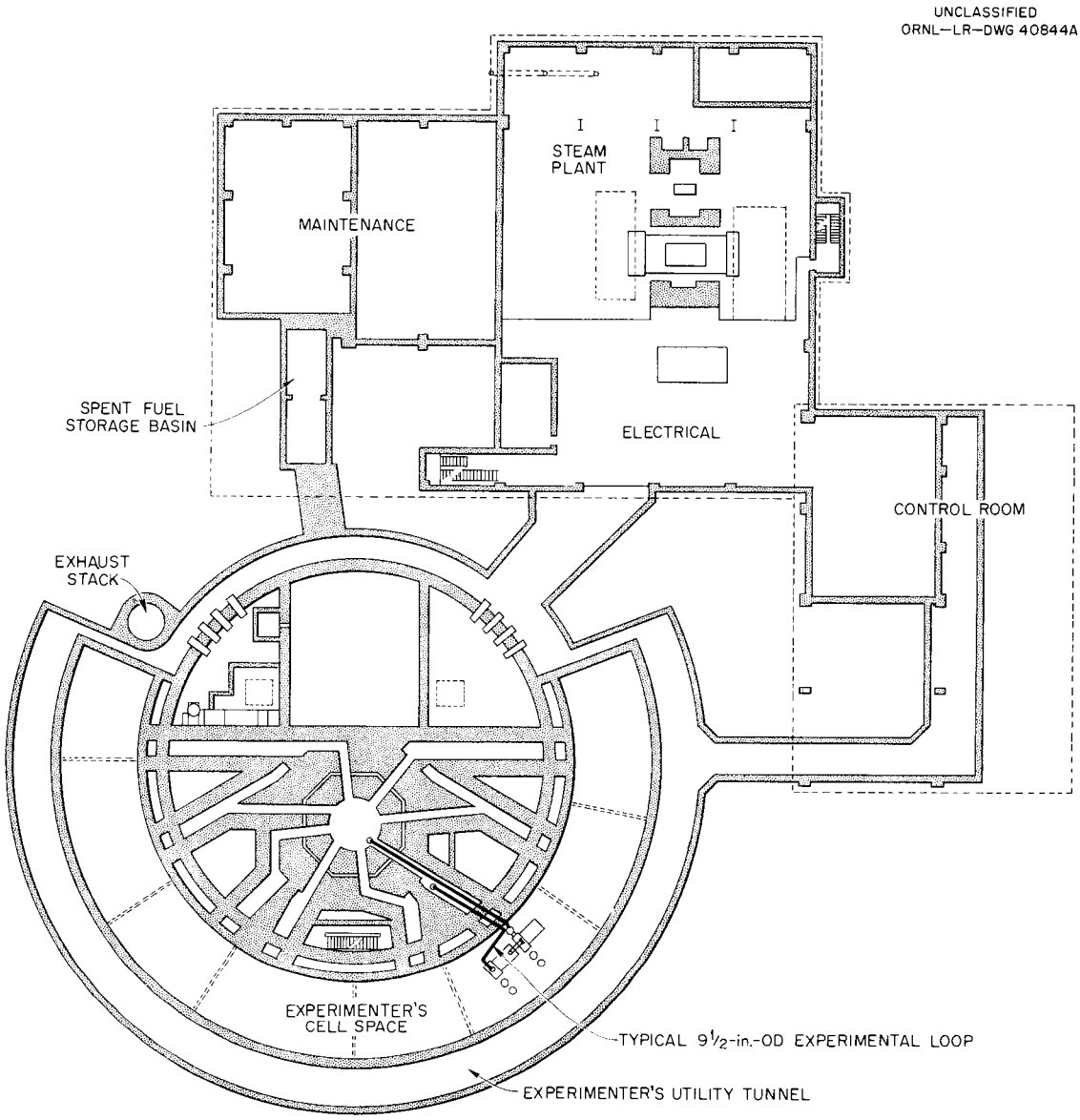

Fig. 7.7. Basement Floor Plan of EGCR Building Showing Roofs of Experimental Cells at Ground Level.

joints are being considered for applications in other experimental loops. Therefore proof tests are planned to evaluate Marman Conoseal mechanical joints similar to those specified for the EGCR and gas-buffered mechanical joints proposed by Marman and other vendors.

Two 10-in. and five 2 1/2-in. type 304 stainless steel Marman Conoseal joints have been ordered for testing. These joints will be evaluated at reactor operating temperatures and pressures and will be exposed to thermal cycling and pressure cycling. Initial test operations will include thermal cycling between ambient temperature and 500°F and pressure cycling between atmospheric pressure and 375 psig. The apparatus for testing a 10-in. Conoseal joint is shown in Fig. 7.8. During testing the joint will be continuously monitored for leakage with a mass spectrometer helium leak detector.

A preliminary evaluation was completed of an available 2 1/2-in. Inconel Conoseal joint by using type 321 stainless steel gaskets. Leakage was measured with a Consolidated Engineering Co. Model 24-102 helium leak detector. The following tabulation summarizes the results of this evaluation:

Number of closures	11
Total hours of hot operation	355
Total hours at 500°F and 375 psig	280
Total hours at 1000°F and 300 psig	24
Total thermal cycles from 500°F to ambient temperature	25
Total pressure cycles from 375 psi to atmospheric pressure	15
Torque required for first closure, in.-lb	45
Torque required for tenth closure, in.-lb	250
Leakage rate first closure, cm^3/sec	1.1×10^{-10}
Leakage rate tenth closure, cm^3/sec	1.1×10^{-10}
Leakage rate eleventh closure, cm^3/sec	2×10^{-4}

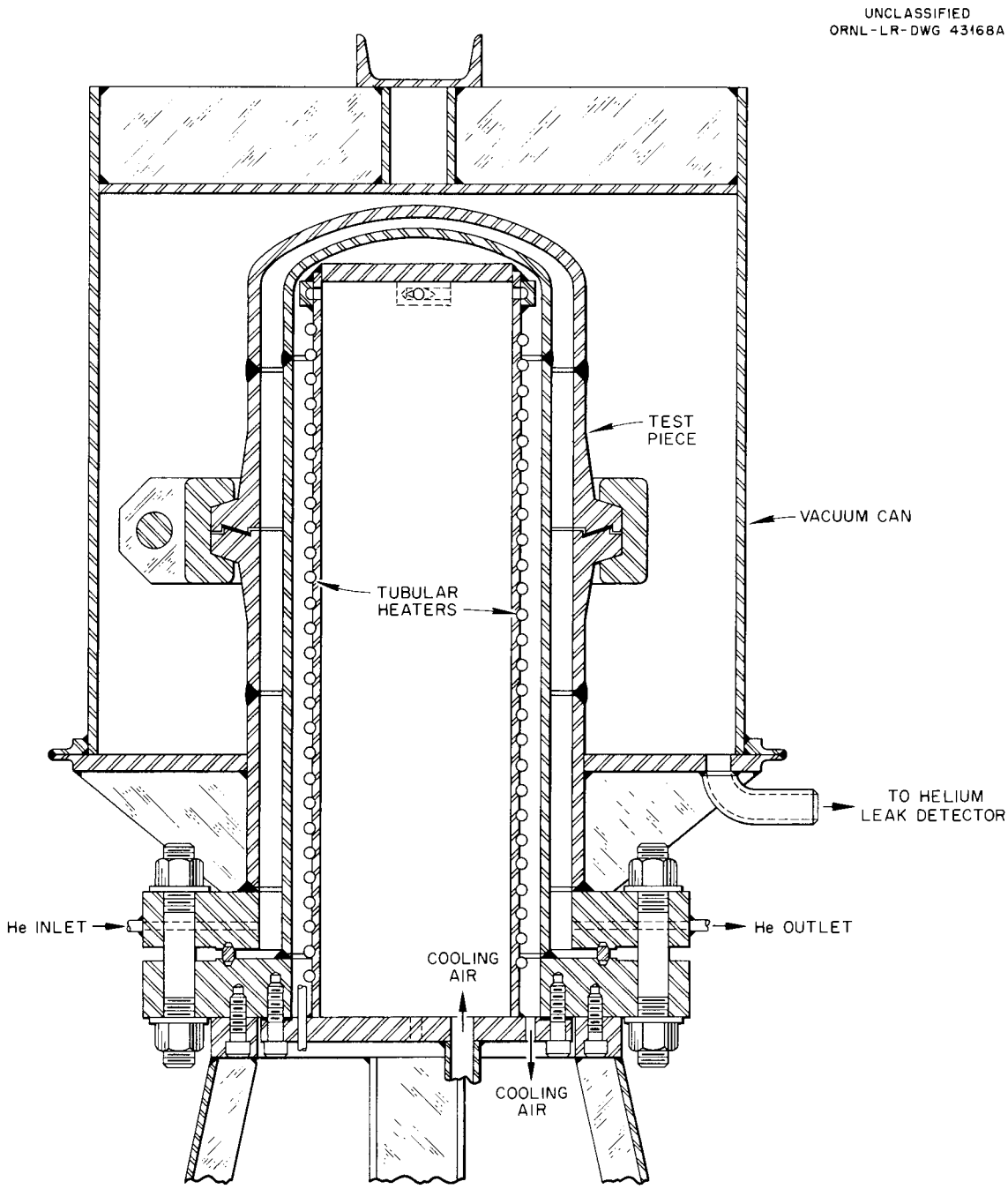

Fig. 7.8. Test Apparatus for Evaluating Mechanical Joints Under Thermal Cycling and Pressure Cycling Conditions.

The use of a gasket material harder than the flange material is not recommended by the vendor, but Inconel gaskets were not readily available. Visual examination of the test piece indicated that the gasket ultimately had scored the flanges and prevented the joint from sealing.

Performance specifications were prepared for gas-buffered mechanical joints suitable for operation at 1500°F and 300 psig. Quotations on designs to meet these specifications were received from the DSD Manufacturing Company and Marman Division of Aeroquip Corporation. Five 2 1/2-in. joints will be obtained from each company for testing and evaluation.

Special Gas Compressors

Grease-Lubricated Centrifugal Compressors

The endurance test of the compressor described in the previous report[2] is continuing, with the compressor operating at 12,000 rpm in helium at 590°F and a 400-psig suction pressure. The accumulated operating time is more than 2495 hr, and there have been only limited shutdowns for minor repairs to the drive unit, which is a gasoline-driven generator.

Compressor performance data were rechecked at several impeller speeds at 400 psig and 600°F. Curves of head vs flow and impeller speed are presented in Fig. 7.9. The sharp drop-off of head at low flow conditions is attributable to the vaned diffuser of the compressor. The substitution of air coolant for water to maintain an operable bearing temperature was found to be inadequate. For continuous compressor operation at a suction temperature of 600°F, a constant supply of coolant water is necessary.

Regenerative Compressors

A prototype regenerative compressor[3] unit was installed in the high-temperature test loop to check the mechanical performance and to

---

[2] GCR Quar. Prog. Rep. Sept. 30, 1959, ORNL-2835, p 157.

[3] Ibid., p 159.

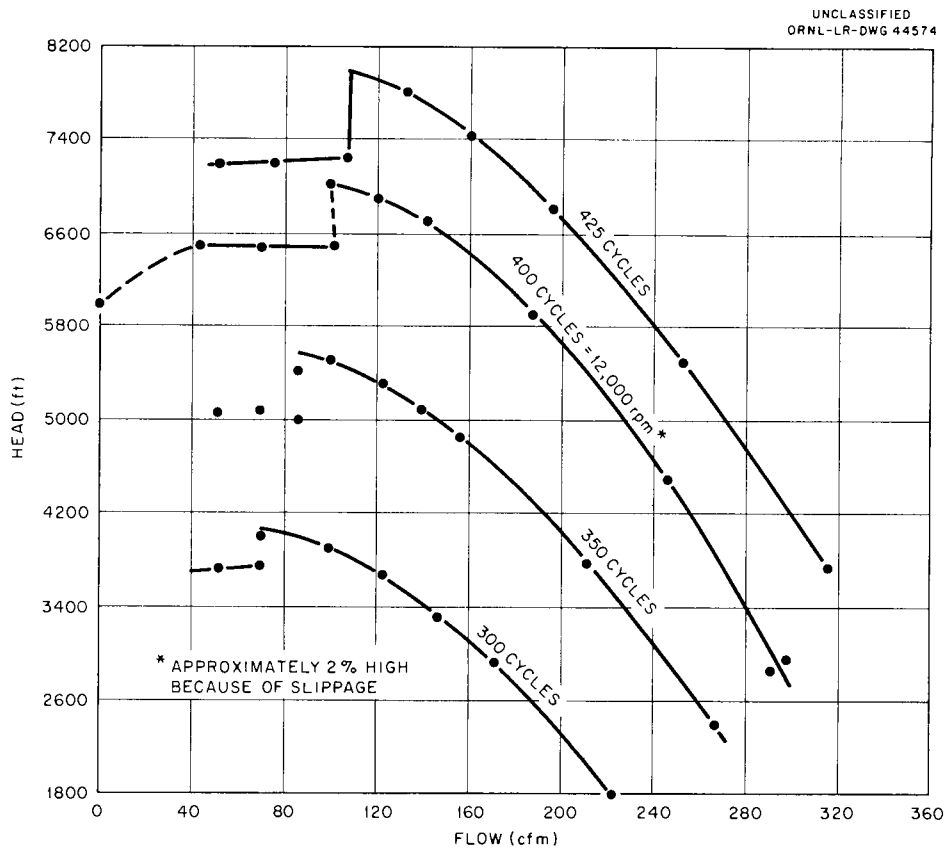

Fig. 7.9. Performance of Grease-Lubricated Compressor with Helium at 600°F and 400 psi.

obtain running-clearance and aerodynamic data at the desired operating conditions, that is, operation with helium at 400 psig and 600°F. The test of the prototype will provide design and operating criteria for the regenerative gas compressors to be used in ORR-GCR in-pile loop No. 2.

Several preliminary test runs were required before satisfactory running clearances were established. The capacitance probes indicated that both the inboard and outboard housings were subject to axial distortion from thermal effects that was compounded by mechanical restraint of the housings. Satisfactory compressor operation was attained after removing the outboard housing from the pilot diameter of the compressor support plate, modifying the thermal shield, applying stainless steel foil insulation at impeller end and compressor body, and adjusting the

impeller clearances (cold) to 0.007 and 0.025 in. outboard and inboard, respectively.

Analyses of preliminary performance data taken at several speeds (8,000 to 12,000 rpm) with helium at 380 psig and 580°F indicate that the prototype unit has adequate head-vs-flow capacity to meet the ORR-GCR in-pile loop compressor requirement. Additional tests are in progress to determine the effects of sudden pressure loss and/or temperature drop on compressor performance.

Compressors with Gas-Lubricated Bearings

The test journal (without the bearing) of the gas-bearing tester[4] was operated at a maximum speed of 24,000 rpm. Initial testing was delayed to permit modifications to the generator field windings to allow operation of the test unit at speeds as low as 6,000 rpm, with the voltage maintained proportional to the generator frequency. The bearing was then installed and operated for a period of 6 min at room temperature and a pressure of 200 psig. The unit loading was approximately 1.12 psi. The motor was stopped when metal-to-metal contact occurred between the bearing and the journal or the bearing positioner. No damage occurred to the bearing, and further testing is under way.

The design work on the loop for testing the Bristol-Siddeley compressor continued. Work was initiated on modifying an available throttling valve for use in the loop when it was found that no 3-in. bellows-sealed valves could be obtained commercially. Later, a valve was requisitioned from the Powell Valve Company. The flowmeter has been received from the vendor. A purchase order was issued for the 75-kva, 400-cycle, motor-generator set to be used with this loop. The gas control system design was completed, and a request for fabrication of the gas control cabinet was issued.

A report from Bristol-Siddeley Engines, Ltd., states that the compressor operated successfully at 1000°F and 900 rpm, but it has not been

[4]GCR Quar. Prog. Rep. Sept. 30, 1959, ORNL-2835, p 161.

able to reach the design speed of 15,050 rpm. A new shaft is being fabricated which should remedy the trouble and allow shipment of the compressor in January 1960.

Compressor for High-Temperature Electric-Motor Test System

The bearing actions of the rotary assembly of the compressor (GABE-1) to be used in the system being constructed for long-term tests of electric motors for high-temperature service were calculated to be 20.9 lb for the bearing farthest from the impeller and 22.7 lb for the other bearing. Checks to determine whether the difference in loading would affect the operating characteristics indicated that the effects would be negligible.

An independent check determined the capacity of the thrust bearing to be 338 lb, which may be compared with the 344 lb calculated here. The journal bearing was thought to be too heavily loaded, and it was suggested that the length-to-diameter ratio be increased from the present value of 0.5 to 1.0. However, the mass of the rotary element increases with an increase in bearing length at a rate which prevents a significant decrease in bearing loading. It is planned to calculate an angle of compressor inclination which will load the thrust bearing properly and yet reduce the static loading of the journal bearings as suggested.

Calculations were also made to determine the natural frequency of the rotary assembly in the axial direction as a function of the spring stiffness of the gas film. The limiting case would be for the rotary assembly in a vertical position. In this position the natural frequency was calculated to be 9700 rpm. This natural frequency will decrease as the angle of inclination approaches the horizontal and is considered sufficiently removed from the normal operating speed of 24,000 rpm for safety.

A request for bids for fabrication of the GABE-1 compressor was issued to ten companies on October 26, 1959, and two bids have been received. The low bid of $16,000 received from the A-Tool and Gage Company, Detroit, was accepted after a visit was made to the shop to assure the capability of the bidder to fabricate and measure the bearings to the precision required.

Compressors for ORR In-Pile Loop No. 2

A study of helium compressors to provide the necessary head-vs-flow requirements for ORR in-pile loop No. 2 was made. It was established that the compressors must produce a pressure head of 10 psi, minimum, at a helium flow rate of 153 cfm at inlet conditions of 310 psia and 600°F. This is equivalent to a mass flow rate of 0.278 lb/sec.

Preliminary performance data on the HECC-1[5] compressor indicated that it might be feasible to use two of these compressors in series to produce the required head and flow. More detailed performance data were obtained on HECC-1, and the required operating point for the ORR in-pile loop No. 2 compressors fell in the unstable operating range of the HECC-1.

The next approach considered was to design a new impeller and volute to be used with the existing HECC-1 motor and bearing design. Preliminary design calculations for the impeller and volute were completed.

A compressor capable of operating for periods of up to 10,000 hr without maintenance appeared to be highly desirable. The HECC-1 bearings are grease lubricated and have an expected life of only 3000 hr without maintenance. Further, the bearings and motor windings could be exposed to a relatively heavy radiation dosage in the ORR in-pile loop. Based on these requirements and on cost considerations, a specification has been prepared for purchase of helium compressors having self-acting gas bearings. Two compressors operating in series would be used to produce the required head. In the event one of the two compressors stopped because of a power failure or mechanical difficulty, the remaining compressor could continue to supply a reduced flow for emergency cooling.

Compressors for EGCR Experimental Loops

In an attempt to determine the availability of compressors for use with helium and carbon dioxide in the EGCR experimental loops, a preliminary inquiry was sent out to a number of compressor manufacturers in the United States, Great Britain, and Switzerland. The exact compressor

---

[5] GCR Quar. Prog. Rep. Sept. 30, 1959, ORNL-2835, p 160.

performance requirements for each loop were not available when the inquiry was released; however, sharp limitations on procurement time made it necessary to obtain all information possible from compressor manufacturers so that when the compressor requirements were known the time required for determining the number and arrangement of the compressors and for preparing specifications for procurement could be minimized.

The range of compressor operating parameters specified in the preliminary inquires was based on a compressor inlet gas temperature of 600°F at 300 to 1000 psia. Further engineering studies of the loop designs have indicated the desirability of operation without an economizer, so the compressor inlet temperatures may range from 600 to 900°F at 500 to 1000 psia.

The higher temperatures indicate that the available pressure rise per stage may be limited by the maximum allowable stress levels in the impellers. A study of disk stresses for various impeller peripheral speeds has been undertaken to determine these limitations. New estimates of the head-vs-flow requirements for each loop were established recently, and the data are being studied to determine tentatively the optimum arrangement of compressors in series or parallel to satisfy all anticipated test conditions.

It would be desirable to use the same compressors for carbon dioxide and for helium. Initial studies have shown that it may be difficult to obtain a motor having an adequate horsepower rating at the relatively low speeds required for operation with carbon dioxide that can also be operated at the much higher speeds needed for helium.

The very low gas contamination requirements for the loop, plus the probability that relatively high radiation levels may be present, indicate that the use of compressors with gas-lubricated bearings would be most advantageous. This would eliminate both contamination of the gas by oil vapors and deterioration of the oil by radiation.

Study of Back-Diffusion Through Labyrinth Seals

A study is being made of the phenomenon of back diffusion of buffer oil or water vapor (against the flow of helium) through labyrinth seals. The design of testing apparatus has been completed, and the apparatus is presently being fabricated. It is anticipated that assembly will be complete by mid-January 1960.

Previous reports in this series are:

ORNL-2500	Parts 1-4, issued April 1, 1958
ORNL-2505	Issued June 19, 1958
ORNL-2510	Issued September 18, 1958
ORNL-2676	Period Ending December 31, 1958
ORNL-2767	Period Ending June 30, 1959
ORNL-2835	Period Ending Sept. 30, 1959

INTERNAL DISTRIBUTION

1. G. M. Adamson
2. J. W. Allen
3. S. A. Beall
4. M. Bender
5. D. S. Billington
6. E. P. Blizard
7. A. L. Boch
8. C. J. Borkowski
9. W. F. Boudreau
10. G. E. Boyd
11. E. J. Breeding
12. J. C. Bresee
13. R. B. Briggs
14. C. E. Center (K-25)
15. R. A. Charpie
16. T. E. Cole
17. J. H. Coobs
18. J. A. Conlin
19. W. B. Cottrell
20. J. A. Cox
21. F. L. Culler
22. H. N. Culver
23. J. H. DeVan
24. L. M. Doney
25. D. A. Douglas
26. L. C. Emerson
27. L. B. Emlet (K-25)
28. E. P. Epler
29. H. L. Falkenberry
30. J. Foster
31. A. P. Fraas
32. J. H. Frye, Jr.
33. G. A. Garrett (K-25)
34. J. M. Googin (Y-12)
35. B. L. Greenstreet
36. W. R. Grimes
37. E. Guth
38. R. F. Hibbs (Y-12)
39. M. R. Hill
40. H. W. Hoffman
41. A. Hollaender
42. A. S. Householder
43. H. Inouye
44. W. H. Jordan
45. P. R. Kasten
46. C. P. Keim
47. M. T. Kelley
48. J. J. Keyes
49. R. B. Korsmeyer
50. J. A. Lane
51. S. A. Levin (K-25)
52. R. S. Livington
53. H. G. MacPherson
54. W. D. Manly
55. E. R. Mann
56. H. C. McCurdy
57. W. B. McDonald
58. H. F. McDuffie
59. C. J. McHargue
60. F. R. McQuilkin
61. H. J. Metz
62. A. J. Miller
63. R. S. Miller
64. J. G. Morgan
65. K. Z. Morgan
66. J. P. Murray (Y-12)
67. F. H. Neill
68. M. L. Nelson
69. L. G. Overholser
70. P. Patriarca
71. F. S. Patton (Y-12)
72. A. M. Perry
73. D. Phillips
74. M. E. Ramsey
75. P. M. Reyling
76. M. W. Rosenthal
77. A. F. Rupp
78. G. Samuels
79. H. W. Savage
80. A. W. Savolainen
81. J. L. Scott
82. O. Sisman
83. E. D. Shipley
84. M. J. Skinner
85. G. M. Slaughter
86. A. H. Snell

87. E. Storto
88. R. D. Stulting
89. C. D. Susano
90. J. A. Swartout
91. E. H. Taylor
92. D. F. Toner
93. D. B. Trauger
94. E. Von Halle (K-25)
95. C. S. Walker
96. J. L. Wantland
97. A. M. Weinberg
98. J. R. Weir
99. J. C. White
100. E. A. Wick
101. G. C. Williams
102. C. E. Winters
103. J. Zasler
104-107. ORNL – Y-12 Technical Library
Document Reference Section
108-177. Laboratory Records Department
178. Laboratory Records Department, ORNL R. C.
179-181. Central Research Library

EXTERNAL DISTRIBUTION

182-184. W. F. Banks, Allis-Chalmers Mfg. Co.
185-187. P. D. Bush, Kaiser Engineers
188. E. Creutz, General Atomics
189. Richard Kirkpatrick, AEC, Washington
190-191. H. Lichtenburger, General Nuclear Engineering Corp.
192. H. B. Rahner, Savannah River Operations Office
193. Donald Stewart, AEC, Washington
194. R. E. Watt, Los Alamos Scientific Laboratory
195-196. W. L. Webb, East Central Nuclear Group, Inc.
197. Division of Research and Development, AEC, ORO
198-774. Given distribution as shown in TID-4500 (15th ed.) under Reactors – Power category (75 copies – OTS)